The roles of SRSF6 in the alternative splicing response to hypoxia

Dissertation

zur Erlangung des Doktorgrades der Naturwissenschaften

vorgelegt beim Fachbereich Biowissenschaften (FB15) der Johann Wolfgang Goethe-Universität in Frankfurt am Main

Von Camila Freitas Stahl aus

Campo Grande, Brazil

Frankfurt 2019

(D 30)

vom Fachbereich der Biowissenschaften (FB15) der Johann Wolfgang Goethe Universität als Dissertation angenommen

Dekan: Prof. Dr. Sven Klimpel

Gutachter:

JunProf. Michaela Müller-McNicoll, Ph.D.

Dr. Kathi Zarnack

Datum der Disputation: 20.02.2020

Abbreviations

A	
APS	Ammoniumperoxodisulfate
AS	Alternative splicing
ASOs	Antisense oligonucleotides
ATP	Adenosine triphosphate
B	
BAC	Bacterial artificial chromosome
bp	Base pairs
BSA	Bovine serum albumin
C	
cDNA	Complementary DNA
CHX	Cycloheximide
circ	circular
circRNA	Circular RNA
CO_2	Carbon dioxide
$CoCl_2$	Cobalt chlorid
D	
DDR	DNA damage response
DMEM	Dulbecco's Modified
DMSO	Dimethyl sulfoxide
DNA	Desoxyribonucleic acid
dNTPs	Desoxyribonucleotide triphosphate
DSB	Double strand break
DTT	Dithiothreitol
E	
E. coli	*Escherichia coli*
EDTA	Ethylenediaminetetra- acetic acid
EJC	Exon junction complex
ESE	Exonic splicing enhancers
ESS	Exonic splicing silencer
F	
FW	Forward
G	
GFP	Green fluorescence protein
H	
h	hours
H2AX	H2A histone family member X
HRP	Horse radish peroxidase
I	
iCLIP	Individual nucleotide resolution cross linking and immunoprecipitation
IRES	internal ribosome entering sites
ISE	Intronic splicing enhancers
ISS	Intronic splicing silencer
K	
KD	Knock down
L	
LB	Lysogeny broth
lncRNA	Long non-coding RNA
M	
min	minutes
mM	Millimolar
mRNA	messenger RNA
N	
ncRNA	Non-coding RNA
nM	Nanomolar
NMD	Nonsense-mediated decay
NXF1	Nuclear export factor 1
O	
O_2	Oxygen
oligo(dT)	Oligo-desoxythymidine
ORF	Open reading frame

P

p53	Tumor protein 53
PAGE	Polyacrylamide gel electrophoresis
PABP	PolyA binding protein
PBS	Phosphate-buffered saline
PCE	Poison cassette exon
PFA	Paraformaldehyde
PHDs	Prolyl-4-hydroxylases
pre-	Precursor
PTC	Premature termination codon

R

RBP	RNA binding protein
RNA	Ribonucleic acid
RNA-Seq	RNA sequencing
RRM	RNA recognition motif
RRMH	RNA recognition motif homolog
RT	Reverse transcription
REV	Reverse

S

SDS	Sodium dodecyl sulfate
sec	seconds
siRNA	Small interfering RNA
snRNA	small nuclear RNA
snRNP	Small nuclear ribonucleoprotein
SRPKs	SR protein kinases
SRSF	Serine-, arginine-rich splicing factor
ss	Splice site

U

U2AF	U2 auxiliary factor
UTR	Untranslated region

W

WT	Wildtype

-

°C	degrees
µM	Micromolar

Index of contents

Abbreviations III
Index of Figures VII
Index of Supplementary Figures VIII
Index of Tables IX
Zusammenfassung X
1. Introduction 15
1.1. Deciphering the human genetic code 15
1.2. The messenger RNA (mRNA) life cycle 16
1.3. Pre-mRNA splicing 18
1.4. Alternative Splicing (AS) 21
1.5. SR proteins – essential alternative splicing regulators 30
1.6. The role of AS in stress conditions and upon DNA damage 36
1.7. Hypoxia 37
1.8. Hypoxia mimic 44
1.9. Hypoxia and AS 44
1.10. Hypoxia and HeLa cells 46
2. Objectives 47
3. Material and Methods 48
3.1. Materials 48
3.2. Programs and Databases 56
3.3. Methods 59
4. Results 77
4.1. Hypoxia causes differential expression of thousands of transcripts in HeLa cells 77
4.2. Hypoxia causes global changes in alternative splicing 79
4.3. Hypoxia changes the abundance of several circular RNAs (circRNAs) 82
4.4. Transcripts encoding SR proteins are differentially regulated in hypoxia 85
4.5. Hypoxia decreases SRSF6 protein level and alters its subnuclear localization 89
4.6. SRSF6 overexpression in hypoxia promotes formation of micronuclei and DNA damage 92
4.7. Identification of mis-regulated transcripts by SRSF6 overexpression in hypoxia using iCLIP 96
4.8. SRSF6 inhibits circRNA formation in normoxia and hypoxia 104
4.9. SRSF6 overexpression impairs *MALAT1* induction and *VEGFA165* splicing in hypoxia107 107

4.10. SRSF6 overexpression in hypoxia increases *MALAT1* accumulation in nuclear speckles 110
4.11. *MALAT1* depletion in hypoxia phenocopies SRSF6 overexpression and causes formation of micronuclei 112
5. Discussion 115
5.1. Gene expression and alternative splicing regulation in hypoxia 117
5.2. SRSF6 is downregulated in hypoxia through NMD 123
5.3. SRSF6 down regulation is essential for AS in hypoxia 125
5.4. SRSF6 modulates *MALAT1* levels and availability in hypoxia 129
5.5 SRSF6 overexpression in hypoxia protects cells from death due to DNA damage leading to micronuclei formation 130
6. Conclusions and outlook 133
7. References 135
8. Supplemental Figures 162
Acknowledgments ..... A
Erklärung und Versicherung ..... B
Curriculum Vitae C

Index of Figures

Figure 1. Simplified mRNA life cycle. 17
Figure 2. Protein composition of human spliceosomal snRNPs. 18
Figure 3.Overview of pre-mRNA splicing. 20
Figure 4. The different categories of AS events. 23
Figure 5. Three mechanisms of circRNA formation. 25
Figure 6. CircRNA functions. 26
Figure 7. Simplified NMD pathway. 29
Figure 8. SR proteins functions in constitutive splicing and AS. 30
Figure 9. Overview of the domain structure of canonical SR proteins (SRSF1-12). 31
Figure 10. The SR protein phosphorylation cycle. 33
Figure 11. *MALAT1* regulates splicing by moving SRSF1 from speckles to the chromatin. 35
Figure 12. HIF1α signaling pathway. 40
Figure 13. Angiogenesis and tumor metastasis. 42
Figure 14. Schematic of *MALAT1* KD experiment in normoxia and hypoxia. 63
Figure 15. Quantification and calculation of isoform fractions. 69
Figure 16. Quantification of GFP fluorescence with Fiji. 75
Figure 17. Hypoxia leads to global changes in gene expression. 78
Figure 18. Thousands of transcripts are alternatively spliced upon hypoxia. 79
Figure 19. Validation of cassette exon (CE) events in hypoxia. 81
Figure 20. circRNA formation is regulated in hypoxia. 84
Figure 21.*SRSF6* and *SRSF3* transcript levels are strongly decreased in hypoxia. 88
Figure 22. Hypoxia decreases SRSF6 protein levels and alters its nuclear localization. 91
Figure 23. SRSF6 regulation in overexpressing cell lines in normoxia and hypoxia. 93
Figure 24. SRSF6 overexpression promotes micronuclei formation and DNA damage. 95
Figure 25. Transcriptome-wide SRSF6 binding landscape in normoxia and hypoxia. ... 98
Figure 26. Changes in SRSF6 binding to regulated and flanking exons in hypoxia. ... 100
Figure 27. SRSF6 downregulation in hypoxia promotes exon skipping. 103

Figure 28. SRSF6 overexpression inhibits circRNA formation. 106
Figure 29. SRSF6 regulates *MALAT1* expression in normoxia and hypoxia. 109
Figure 30. SRSF6 overexpression sequesters *MALAT1* in nuclear speckles upon hypoxia.
..... 111
Figure 31. *MALAT1* KD phenocopies SRSF6 overexpression in the formation of micronuclei and aberrant nuclei shapes. 113
Figure 32. Mechanism of AS regulation by SRSF6 in hypoxia. 117

Index of Supplementary Figures

Figure S1. Validation of SRSF6 and SRSF4 cell lines. 162
Figure S2. SRSF6 protein level decrease in hypoxia. 163
Figure S3. SRSF6 over expression leads to micronuclei formation and DNA damage.
..... 164
Figure S4.Micronuclei formation in *MALAT1* KD cells. 165

Index of Tables

Table 1. Overview of circRNA functions. 27
Table 2. List of chemicals, solutions, enzymes and reagents. 48
Table 3. List of equipment. 50
Table 4. List of kits. 51
Table 5. Buffers and solutions recipes. 51
Table 6. Oligonucleotides used in PCR, qPCR and iCLIP assays. 52
Table 7. Antibodies used in Western Blot and Immunofluorescence assays. 55
Table 8. siRNAs and ASOs information.....64
Table 9. Taq PCR protocol and program. 69
Table 10. qPCR protocol and program. 70
Table 11. SDS-PAGE gel receipt 72

Zusammenfassung

Die Vorläuferform der eukaryotischen mRNA (prä-mRNA) durchläuft, eine Reihe von Prozessierungs-Schritte, die schließlich zu der Synthese einer „reifen“ und Exportkompetenten mRNA führt. prä-mRNA Spleißen ist ein essentieller Teilschritt dieser Reifung bei der intragene Sequenzen, sogenannte Introns, von der prä-mRNA entfernt werden, während Exons legiert werden. Das prä-mRNA Spleißen wird durch das Spleißosom katalysiert. Dieser Mega-Dalton Komplex, besteht aus fünf Sub-Komplexen, die sich wiederum aus katalytisch aktiven „kleinen nukleären Ribonukleinsäuren“ (snRNAs) und einer Vielzahl von proteinogenen Faktoren zusammensetzen. Diese Subkomplexe, bezeichnet als snRNPs (*small nuclear Ribonucleoprotein Particles*), binden die prä-mRNA an charakteristischen Sequenzen und richten die prä-mRNA durch eine Reihe von Konformations-Änderungen so aus, dass benachbarte Exons in Kontakt treten und über eine biochemische Ligations-Reaktion verbunden werden können.

Die Exon- bzw Intronerkennung der snRNPs wird durch zahlreiche Spleißfaktoren reguliert. Eine Proteinfamilie, die essentiell für die Regulierung des Spleißens ist, sind Serin/Arginin-reiche Proteine (SR-Proteine). Diese binden vorzugsweise an das 3‘ oder 5’ Ende von Exons, rekrutieren snRNPs und stimulieren dadurch die Exon-Inklusion. Durch diese Stimulierung können Spleiß-Events reguliert und gezielt spezifische Exons ausgeschlossen oder eingeschlossen werden. Dieser Prozess, der als alternatives Spleißen (AS) bezeichnet wird, tritt in 95% des menschlichen Transkriptoms auf und erweitert die Diversität eines Organismus, da verschiedene Transkripte von demselben Gen erzeugt werden können und folglich die Translation unterschiedlicher Proteine mit distinkten Funktionen ermöglicht wird.

Darüber hinaus verfügt die Zelle durch das AS über eine weitere posttranskriptionale Genregulationsebene, die insbesondere unter zellulären Stressbedingungen zur Expression von alternativen Protein-Isoformen von der Zelle genutzt wird. Eine in medizinischer Hinsicht besonders relevante Stressbedingung ist die sogenannte Hypoxie, die eine Sauerstoff-Unterversorgung von Zellen oder Gewebebereichen beschreibt. Hypoxie bzw. hypoxische Bereiche finden sich in

Krebszellen und treten in 90% aller soliden Tumoren auf. Als Teil der Hypoxie Stress-

Antwort, verfügt die Zelle über einen Adaptations-Mechanismus, der durch Hypoxieinduzierbare Faktoren (HIF) vermittelt wird. Diese Faktoren induzieren die Transkription zahlreicher Gene und stimulieren die Expression von Stressfaktoren, die an der zellulären Adaption der Hypoxie beteiligt sind. Einer dieser Faktoren ist der vaskuläre endotheliale Wachstumsfaktor A (VEGFA), welcher unter hypoxischen Bedingungen sekretiert wird und dadurch die Proliferation von

Endothelzellen, die Neubildung von Blutgefäßen und damit die Vaskularisation des hypoxischen Bereichs stimuliert.

Die zelluläre Anpassung ist jedoch nicht nur auf die transkriptionelle Regulation des HIF-vermittelten Hypoxie Signalwegs beschränkt, sondern wird auf multiplen Genexpressions-Ebenen reguliert. Obwohl bekannt ist, dass tausende Transkripte unter hypoxischen Bedingungen alternativ gespleißt werden, sind die Faktoren, die die zelluläre Stress-Antwort durch AS regulieren, sowie deren molekularer Mechanismus jedoch weitestgehend unbekannt.

Diese Arbeit umfasst die Identifizierung und Charakterisierung von AS Events, sowie den Einfluss und die Regulation von Spleißfaktoren auf AS unter hypoxischen Bedingungen. Hierzu führten wir globale Genexpressions- und AS-Analysen in HeLaKarzinomzelllinien unter Normoxie (21% O_2) und Hypoxie (0.2% O_2) durch und zeigen, dass 7962 Gene nach 24h Hypoxie unterschiedlich exprimiert werden. Über AS-Analysen konnten 4434 Transkripte identifiziert werden, die bei Hypoxie über AS reguliert sind. Dabei trat „Exon-Skipping“ als das am häufigsten auftretende AS-Events auf. Über PCR basierte Validierungs-Experimente konnten 5 regulierte Transkripte nachgewiesen werden. Dabei weisen Exon 3 und 4 in *BORA,* Exon 6 in *MDM4* und Exon 4-5 in *CSSP1* Exon-Skipping Events auf, während Exon-Inklusionen in *CEP192* Exon 28 und in der 3’UTR von *EIF4A2* validiert werden konnten.

Darüber hinaus wurde im Rahmen der AS-Analyse die Regulation des sogenannten „*backsplicings*“ bei Hypoxie untersucht. Im Gegensatz zum linearen
Spleißens, wird beim *backsplicing* das 5’Ende und das 3’Ende von Exons verbunden, was die Bildung von sogenannten zirkulären RNAs (circRNAs) zufolge hat. Obwohl nur wenige Funktionen dieser RNA-Klasse bekannt sind, wurde die Regulation von circRNAs während der Zell-Differenzierung sowie in diversen Krebszellen beschrieben. Dabei können circRNAs als microRNA- oder Protein-Schwämme fungieren oder dienen als Protein-Interaktion Plattform und regulieren dabei die Genexpression.

Zur Identifizierung von Hypoxie-regulierten circRNAs entwickelten wir eine stringente bioinformatische circRNA-Identifikations Pipeline und identifizierten 3.926 circRNAs in HeLa-Zellen. Über Validierungs-Experimente konnten 15 circRNAs nachgewiesen werden.

Mittels differentieller Genexpressionsanalyse identifizierten wir 22 hypoxieinduzierte circRNAs, von denen 7 (*exoZNF292, PLOD2, intZNF292, MTCL1, MAN1A2, SPECC1 und RTN4)* in Hinblick auf Hypoxie-induzierte Hochregulierung, sowie auf dessen Zirkularität validiert werden konnten. Da einige Studien zeigen, dass die circRNA

Formierung meist auf AS Events zurückzuführen ist, könnte die Zunahme von ExonSkipping Events bei Hypoxie die cirRNA-Hochregulierung erklären.

Da der Einfluss von Spleißfaktoren auf AS-Regulationen, sowie dessen molekularer Mechanismus bei Hypoxie weitestgehend unerforscht ist, untersuchten wir im Rahmen dieser Arbeit die Regulation von SR-Proteinen nach 24h Hypoxie. Dabei identifizierten wir SRSF6, als das am stärksten regulierte SR Protein mit einer mit einer
4-fachen Reduzierung der *SRSF6* mRNA und einer 40%igen Abnahme der
Proteinmenge. Um die Ursache dieser SRSF6 Reduktion zu verstehen, analysierten wir *SRSF6* Transkripte auf Hypoxie-induzierte Spleißänderungen. Dies ergab, dass es bei Hypoxie zur Inklusion eines alternativen Exons kommt, zwischen Exon 2 und 3 des *SRSF6* Transkripts. Dieses alternative Exon (PCE – *poison cassette exon*) enthält ein Abbruch-Kodon (PTC - *premature termination codon*). Diese Abbruch-Kodons destabilisieren Transkripte normalerweise und sie werden über den zytoplasmatischen Abbauweg NMD *(Nonsense-mediated decay)* abgebaut. Die Hypoxie-induzierte Hochregulierung und Stabilisierung dieser Isoform führt dazu, dass weniger proteinkodierende *SRSF6* mRNA gebildet wird und dadurch der SRSF6 Proteingehalt reduziert wird.

Darüber hinaus zeigen wir über Lokalisierungs-Experimente mittels konfokaler Mikroskopie, dass SRSF6 bei Hypoxie in nukleären Speckles lokalisiert sind. Da bekannt ist, dass SR Proteine innerhalb von Speckles Spleiß-inaktiv sind, wird SRSF6 über die Speckle-Lokalisierung in Hypoxie zusätzlich funktional reguliert.

Aktuelle Studien zeigen, dass SRSF6 und SRSF1 das Spleißen des Hypoxieinduzierten Transkripts *VEGFA* antagonistisch regulieren. SRSF6 stimuliert dabei die Inklusion des Exons 8b und die Erzeugung einer anti-angiogenen Isoform, während

SRSF1 bei Hypoxie aktiviert wird und dadurch die Exon-Inklusion 8a und damit die
Erzeugung einer pro-angiogenen Isoform fördert. Da erhöhte SRSF6 GenExpressionsraten mit einer gesteigerten Tumoraggressivität und schlechten Heilungschancen bei vielen Krebsarten korrelieren, fokussierten wir unsere Studien auf die Funktion von SRSF6 auf die AS Regulation bei Hypoxie.

Zur Untersuchung und Identifizierung von RNAs die von SRSF6 gebunden werden, führten wir UV Cross-linking and Immuno-Prezipitation Experimente (iCLIP) durch und verglichen das SRSF6 RNA-Bindemuster von HeLa Zellen unter normoxischen- und hypoxischen Bedingungen. Bei Betrachtung der iCLIP-Analyse stellten wir fest, dass SRSF6 durch die Bindung der *SRSF6* mRNA die Inklusion des PCEs und damit die Expression der NMD-

Transkriptisoform stimuliert und dadurch dessen Proteingehalt autoreguliert. Wird diese Autoregulation über eine SRSF6Überexpression überwunden und der SRSF6-Haushalt dysreguliert, hat dies direkte Auswirkung auf das AS-Muster von SRSF6 gebundenen Hypoxie-sensitiven Targets. So hat eine Überexpression von SRSF6 eine Verringerung von Exon-Skipping Events
(*MDM4, PAPOLA, SNAP25 und CHAF1A*) zufolge, was darauf hinweist, dass diese ASEvents direkt von SRSF6 reguliert werden.

Des Weiteren zeigen wir, dass neben der AS-Regulation von linearen Transkripten die verringerten SRSF6-Level bei Hypoxie auch die circRNA-Bildung vermehrt. Sowohl unter hypoxischen Bedingungen (*circPLOD2, circMTCL1, circMAN1A2, circRTN4*) als auch bei SRSF6 Depletions-Experimenten (circ*PLOD2*, circ*MTCL1*, circ*MAN1A2*, circ*RTN4*, circ*HIPK3*, circ*SRSF4*, circ*CPSF6*) konnte eine Zunahme von einigen circRNAs festgestellt werden. Interessanterweise zeigen unsere iCLIP Analysen, dass potentiell zirkularisierte Exons massiv von SRSF6 gebunden werden. Dieses Bindemuster, sowie SRSF6-Überexpressions-Experimente bei Hypoxie deuten darauf hin, dass die Bindung von SRSF6 an diese Exons die Exon-Inklusion in das lineare Transkript stimulieren und dadurch die Bildung von circRNA hemmen.

SR-Proteine binden an die lange nicht-kodierende lncRNA *MALAT1* in nuklearen Speckles. Aktuelle Studien haben gezeigt, dass *MALAT1* SRSF1 bindet und dabei das SR Protein zum Chromatin führt und dadurch das Spleißen von SRSF1-Targets, z.B. der der pro-angiogenen Isoform *VEGFA165a* fördert. Da die *MALAT1*-Expression sowie die Aktivität der lncRNA Hypoxie-sensitiv ist, untersuchten wir im Rahmen dieser Studie den
Einfluss von SRSF6 auf die *MALAT1* Expression und Funktion. Über quantitative PCRAnalysen konnten wir nachweisen, dass die *MALAT1* Regulation bei Hypoxie durch erhöhte SRSF6-Level gehemmt wird. iCLIP-Analysen zeigten, dass die Bindung von SRSF6 bei Hypoxie massiv erhöht wird, was darauf hindeutet, dass SRSF6 die *MALAT1* Funktionen bei Hypoxie hemmt.

Zur Untersuchung des Einflusses von SRSF6 auf die *MALAT1*-Aktivität bei Hypoxie führten wir Lokalisierungs-Experimente durch und visualisierten *MALAT1* mittels RNA-Fluoreszenz in situ-Hybridisierung. Dabei beobachteten wir, dass *MALAT1* bei einer Überexpression von SRSF6 in Hypoxie immobilisiert wird und in nuklearen Speckles zurückgehalten wird. Diese zu SRSF1 antagonistische Funktion spiegelt sich auch bei der AS Regulation von *VEGFA* wider, bei der eine SRSF6 Überexpression das IsoformVerhältnis in Richtung der *VEGFA165a* Isoform verschiebt.

Diese SRSF6 induzierte Dysregulation der Hypoxie Stress-Antwort ist jedoch nicht auf AS-Events beschränkt, sondern führt zu einer signifikanten Zunahme von zellulären DNA-Schädigungen, zu der Bildung abnormaler Nuklei-Formen, sowie zur Formierung von Mikronuklei. Diesen Phänotyp beobachteten wird ebenfalls in *MALAT1* Knockdown Experimenten, was darauf hindeutet, dass die Sequestrierung von *MALAT1* durch SRSF6 ein essentieller Faktor bei der zellulären Hypoxie Stress-Antwort und Chromosomen Segregation ist.

Im Zuge dieser Arbeit charakterisieren wir die Funktion von SRSF6 in der zellulären Hypoxie Stress-Antwort. Dabei zeigen unsere Ergebnisse, dass SRSF6 zum einen AS von multiplen linearen sowie zirkulären RNAs über eine direkte RNA-Bindung und zum anderen über eine *MALAT1* Sequestrierung in nuklearen Speckles indirekt reguliert. Da erhöhte SRSF6 Protein-Level zu einer Proliferation von Zellen mit DNASchäden, Destabilisierung von Chromosomen, sowie einer erhöhten Bildung von Mikronuklei führen, erklärt diese Studie zum Teil die pro-onkogene Funktion von SRSF6 in Krebs-Zellen mit erhöhter Tumoraggressivität.

1. Introduction

1.1. Deciphering the human genetic code

The human body is composed of around 37 x 10^{13} cells. Estimations based on cell morphology indicate that this number comprises around 200 different cell types (Bianconi et al. 2013). Although every cell type has its own specific characteristics and functions, they all carry the same genetic code. The genetic code contains all the information necessary for the development and survival of an organism. This information is stored in the desoxyribonucleic acid (DNA) in form of nucleic base sequences. Around 20 years ago, the Human Genome Project was initiated with the aim to decipher the human genetic code and in 2001 the first human genome assembly was published. Although a major amount of information was offered to the scientific community, it raised many more questions.

Humans cells contain 46 chromosomes and the genome has a size of around 3.3 giga base pairs. The initial number of genes was estimated to be around 100.000, which was an astonishing low number, taking into account the diversity and amount of the identified protein isoforms (Moraes and Góes 2016). The number of protein-coding genes was even lower, only around 2% of the total gene pool (20.000). These numbers are increasing to date, with increasing numbers of deep sequencing studies. Some proteincoding genes are still being identified and annotated, but the major proportion of novel genes are transcribed into non-coding RNAs (Salzberg 2018). Considering the amount of protein-coding genes, the human proteome complexity can only be achieved when more than one protein is encoded from one gene. From transcription of a messenger RNA (mRNA) in the nucleus until its export to the cytoplasm, several processing steps take place, such as splicing and alternative splicing (AS) (Ben-Yishay and Shav-Tal 2019). In the next sections these steps will be introduced to illustrate how they lead to the formation of different protein isoforms and how they control gene expression post transcriptionally.

1.2. The messenger RNA (mRNA) life cycle

During transcription from DNA to RNA, many processing steps take place to ensure that the mRNA is mature and can be exported to the cytoplasm and translated (McKee and Silver 2007). An overview of the pre-mRNA processing steps is shown on Figure 1.

Pre-mRNA is transcribed by RNA Polymerase II (RNA Pol II), which moves from the 3' end of the DNA template to the 5' end. The RNA is then synthetized in the 5' to 3' direction. The first pre-mRNA processing step is 5' capping. The cap structure protects the nascent RNA from degradation by exonucleases. RNA 5'-triphosphatase (RT), guanylyl-transferase (GT) and methyl transferase enzymes remove the 5'-end γphosphate of the nascent transcript leading to the generation of a pre-mRNA with a diphosphate at its 5'end. Afterwards, a monophosphate guanosine is transferred to the diphosphate terminus and is methylated (Lee and Tarn 2013). After the cap is added, the cap-binding complex (CBP) binds to the cap and protects the RNA from degradation.

RNA Pol II continues to transcribe the pre-mRNA and during transcription the noncoding sequences (introns) are removed and the coding sequences (exons) are ligated together in a process called pre-mRNA splicing (Manning and Cooper 2016). The nascent pre-mRNA contains specific sequences and regions, which are recognized by the splicing machinery and splicing factors that aid in the definition and recognition of exons and introns. The 5' and 3' ends of introns contain conserved consensus sequences, which are bound by the spliceosome components U1 and U2, called 5' and 3' splice sites (5'ss and 3'ss). The canonical consensus sequence in the 5'ss is a GU and at the 3'ss a AG (Gregory A. and Zefeng 2014). Aside from the splice sites, a motif consisting of two uracil and one adenine called branch point (located 20-40 nt away of the 3'ss) and a polypyrimidine-rich region named polypyrimidine tract (PPT) are also important for premRNA splicing (Wahl et al. 2009). A detailed overview of the splicing reaction, the factors and proteins, which recognize these sequences and promote splicing will be presented in the next section.

The next processing step is 3'end processing, which consists of two tightly connected reactions: RNA cleavage and PolyA-tail synthesis. Cleavage of the pre-mRNA releases it from the DNA and is promoted by a protein complex that recognizes sequences

in the last exons of the pre-mRNAs. This cleavage and polyadenylation complex includes the cleavage and polyadenylation specificity factor (CPSF) that binds to U or GU-rich sequence elements around 30nt downstream of the PolyA site (PAS) and which cleaves the pre-mRNA. Subsequently, the PolyA polymerase (PAP) binds to the PolyA sites and adds a PolyA-tail of about 150 nt (Millevoi and Vagner 2010). Cleavage and polyadenylation are the final steps of pre-mRNA processing. Afterwards the nuclear export factor 1 (NXF1) is recruited to the mature mRNA, the mRNA is packed and exported to the cytoplasm through interactions between NXF1 and the nuclear pore complex (NPC) (Müller-McNicoll and Neugebauer 2013).

In the cytoplasm, the CBC still bound to the 5' cap recruits translation initiation factors such as EIF4G, cap-binding protein CBP80/20-dependent translation initiation factor (CTIF), eIF3G and eIF4III. These factors promote the assembly of the ribosome and mRNA translation (Ramanathan et al. 2016).

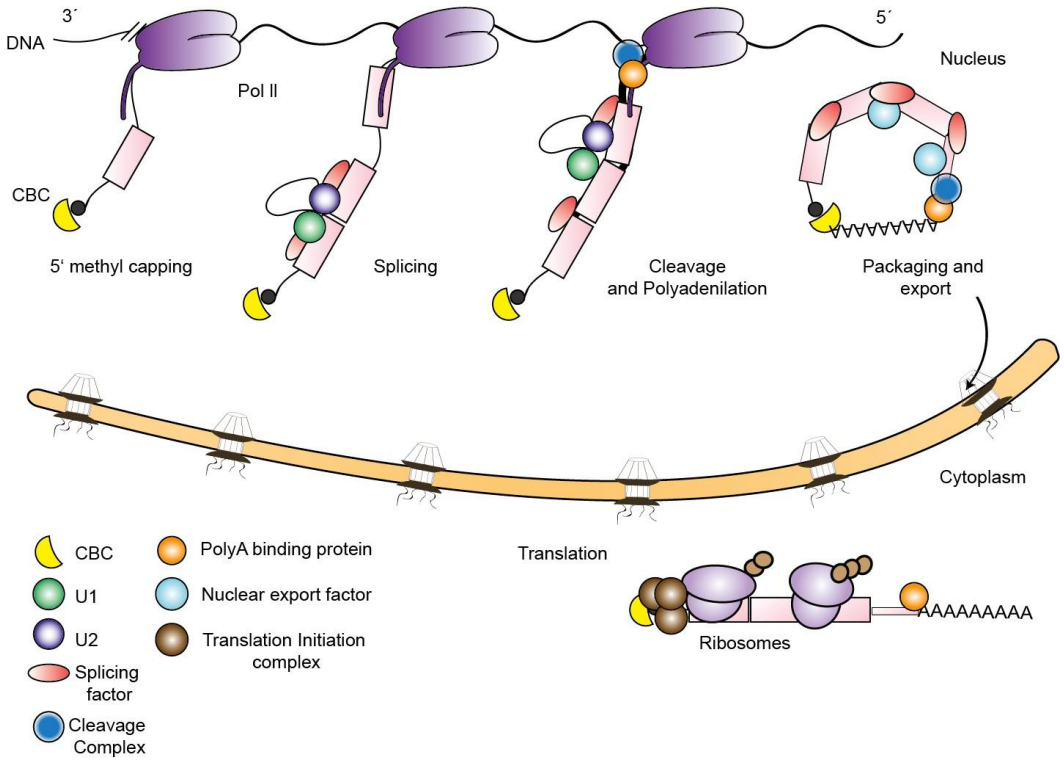

Figure 1. Simplified mRNA life cycle. mRNA processing steps from transcription to nuclear export and translation. CBC: cap binding complex. Figure adapted from (Müller-McNicoll and Neugebauer 2013).

1.3. Pre-mRNA splicing

In this study, we focus on the second processing step - pre-mRNA splicing. As soon as splice sites are transcribed, the splicing machinery (spliceosome) assembles cotranscriptionally at each intron-exon boundary of the pre-mRNA *de novo*. The spliceosome consists of five small nuclear RNAs (snRNAs) and about 200 proteins forming a mega-Dalton RNA-protein (RNP) complex, which catalyzes the splicing reaction to remove introns and ligate exons (Figure 2) (Will and Lührmann 2011; Gregory A. and Zefeng 2014).

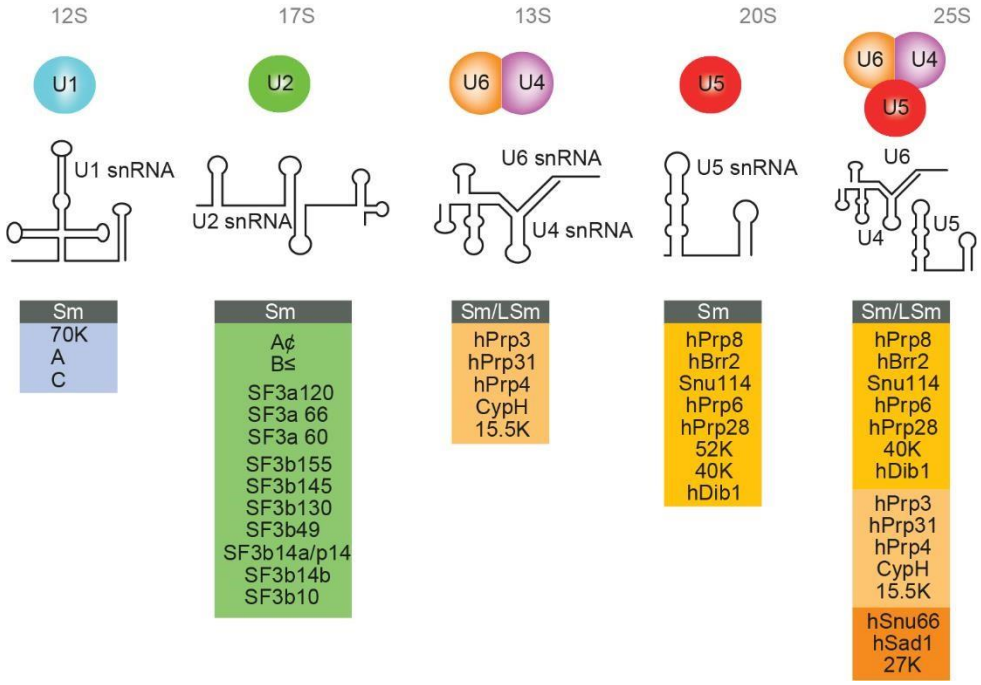

Figure 2. Protein composition of human spliceosomal snRNPs. Secondary structure of human spliceosomal snRNAs (U1, U2, U4-U6, U5 and U4-U5-U6 tri-snRNP). Below are the common and snRNPspecific proteins (Will and Lührmann 2011).

Figure 3 shows an overview of the pre-mRNA, the two splicing reaction steps and the assembly of snRNPs, which promote these steps. The first catalytic step of the reaction is a nucleophilic attack at the 5'ss by the 2'OH group of the adenosine at the branch point. In the second step, the 3′ss is attacked by the free 3′OH group of the 5′ exon. This leads to the ligation of the 2 exons and release of the intron in form of a lariat

structure (Figure 3A) (Will and Lührmann 2011). The assembly of the spliceosome starts with the recognition of the splice sites, branch point and polypyrimidine tract (Figure 3B). The U1 snRNP binds to the 5'ss and promotes binding of U2AF to the polypyrimidine tract upstream of the 3'ss and the splicing factor 1 (SF1) protein to the branch point, forming the complex E. This culminates the recruitment of the U2 snRNP to the 3'ss. The interaction between U1 and U2 is dependent on the helicases PRP5 and UAP56 and this interaction forms the pre-spliceosome complex A. Next, the pre-assembled U4/U6•U5 trisnRNP complex is recruited and the pre-catalytic complex B is formed. Through a series of ATP-dependent rearrangements U1 and U4 leave the spliceosome, while nineteen complex (NTC) joins and afterwards the catalytic complex B* and C is formed, which performs the first and second step of the splicing reaction. After the second step, both exons are ligated and the intron forms a lariat (post-spliceosomal P complex). After the splicing reaction is completed, the ligated exons and intron lariat are released from the spliceosome by the PRP22 helicase. Finally U2, U5 and U6 disassemble from the spliced mRNA and are recycled for the next round of splicing (Gregory A. and Zefeng 2014; Shi 2017; Papasaikas and Valcárcel 2016).

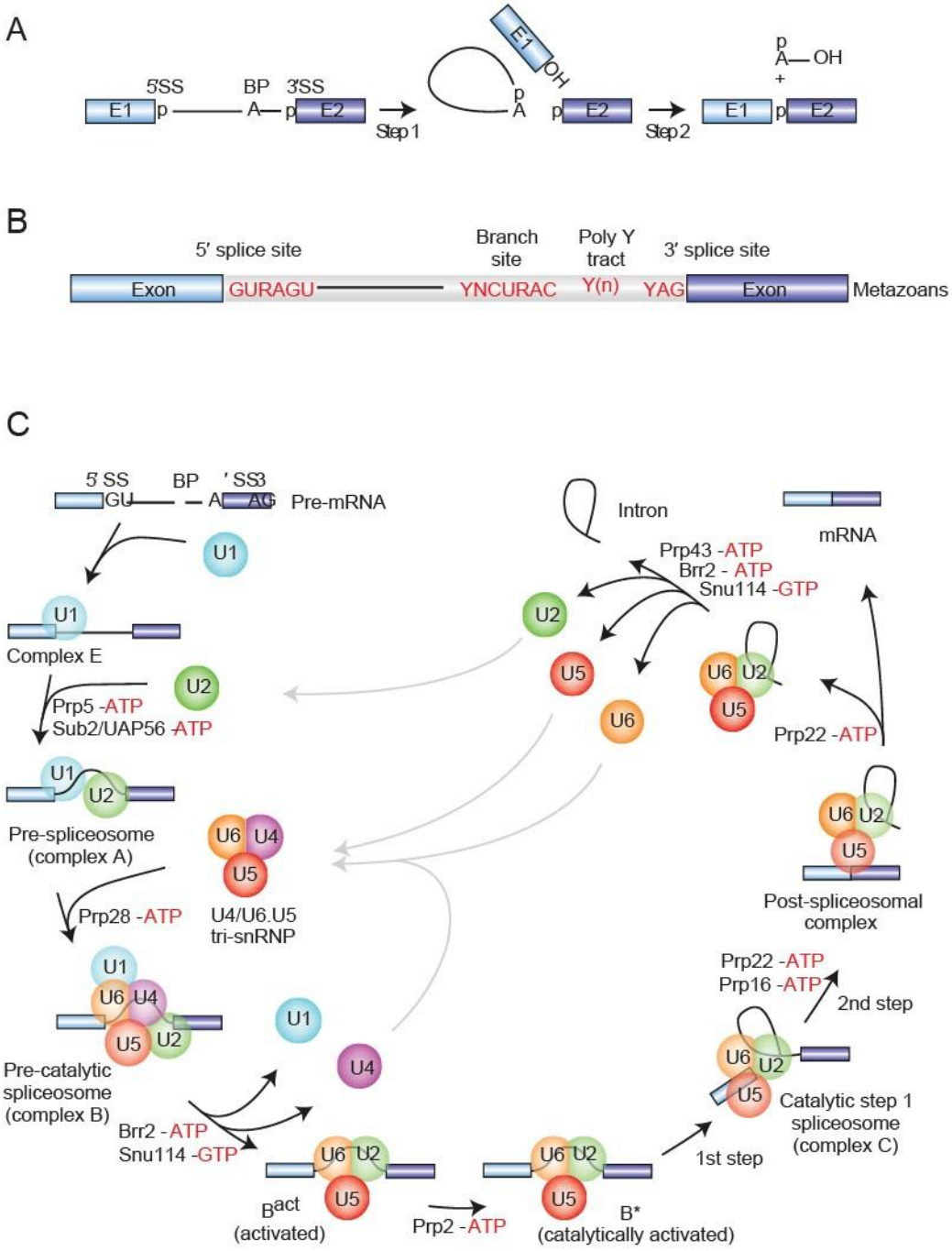

Figure 3.Overview of pre-mRNA splicing. A) Two splicing reaction steps. **B)** Scheme of a pre-mRNA with conserved sequences recognized by the spliceosome. **C)** Assembly of the different spliceosome complexes, which are conserved in metazoans. U1 snRNP recognizes the 5'ss of the exon and recruits the splicing factor 1 (SF1) and U2AF. Assembly of these proteins lead to formation of the complex E. Next, the U2 snRNP joins the complex and SF1 leaves. Complex A now associates with the pre-assembled U4, U5 and U6 tri-snRNP complex leading to the formation of the pre-catalytic complex B. Complex B undergoes different conformational changes though actions of the indicated helicases, such as Prp8 and Prp2. In this step U1 and U4 are released from the complex. The activated complex B can then perform the catalytic splicing reaction. It undergoes more conformational changes during the first step of splicing (branching).

Complex C is responsible for the second step of splicing (exon ligation). After this step the complex P is formed containing the ligated exons and the intron lariat still bound by U2, U5 and U6. When the intron lariat is released, snRNPs are recycled and join a new round of splicing (Will and Lührmann 2011).

1.4. Alternative Splicing (AS)

In humans, 95% of genes are alternatively spliced (Kornblihtt et al. 2013; Manning and Cooper 2016). Alternative splicing (AS) of transcripts can be differentially regulated in cell types and can be essential for cellular stress response by regulating the expression of specific protein isoforms, which have specific functions. The recognition of splice sites is the initial and an essential step during the splicing process. This defines whether exons will be included or excluded in the transcript. There are different mechanisms, which lead to exon recognition and inclusion. Constitutive exons are predominantly included in transcripts by conservative splicing. They contain highly conserved and strong 5' splice signals, which are more efficiently recognized and bound by the spliceosome. Alternative exons contain weaker splice signals whose recognition and usage is regulated by splicing factors (ROCA et al. 2005). Splicing factors can bind to specific sequences called exonic and intronic splicing enhancers or silencers (ESE, ESS, ISE and ISS) in the pre-mRNA and enhance or inhibit the usage of weak alternative splice sites through a regulated recruitment of the spliceosome (Roy et al. 20; Wang et al. 2015). Another factor, which plays a role in recognition of weak splice sites is the transcription rate. During normal transcription elongation the spliceosome assembles preferentially at strong splice sites. When transcriptional elongation is slow and the DNA Polymerase pauses, the spliceosome can bind to the weak splice sites and include alternative exons (Kornblihtt 2006).

Figure 4 shows the different categories of AS events, which have been described so far. When splicing factors bind to alternative cassette exons, they can promote either their inclusion or their skipping. Some transcripts contain neighboring exons, which are spliced in a mutually exclusive manner. In this case the mRNA isoforms will only contain either one exon or the other. There can be several alternative splice sites in exons and their differential recognition leads to alternative 3' or 5' splice site usage. Introns can also be retained in transcripts, e.g. through binding of splicing factors to ISS sites. AS can also

lead to alternative first and last exon usage (Baralle and Giudice 2017). AS events, which alter the coding sequence of the mRNA will lead to translation of different protein isoforms with a different amino acid content and different protein domains. These protein isoforms can have alternative functions and/or a dominant negative effect on the main isoform (Wang et al. 2008). AS in the 3' untranslated region (3'UTR) does not influence the protein coding potential of the mRNAs, however, in this case the stability and localization of the mRNA might be affected. For example, alternative Poly(A) sites can be recognized, which leads to transcripts with longer or shorter 3'UTRs (Feng et al. 2015). mRNAs with longer 3'UTRs have been shown to be less stable, e.g. due to an increased amount of potential micro-RNA binding sites or other instability elements, such as AU-rich elements. In turn, mRNAs containing shorter 3'UTRs are more stable and also more efficiently exported to the cytoplasm. Therefore, alternative last exon usage can influence in protein expression levels by influencing mRNA available for translation (Matoulkova et al. 2012; Moore 2005). For a long time, the importance of AS has not be fully appreciated. However, in the last decade AS and the generation of different protein isoforms have been shown to be essential for cellular differentiation, stress responses, disease development and cancer cell survival (Coltri et al. 2019; Harries 2019; Scherrer 2018; Tam and Stirling 2019; Yamazaki et al. 2018; Yin and Rogge 2019).

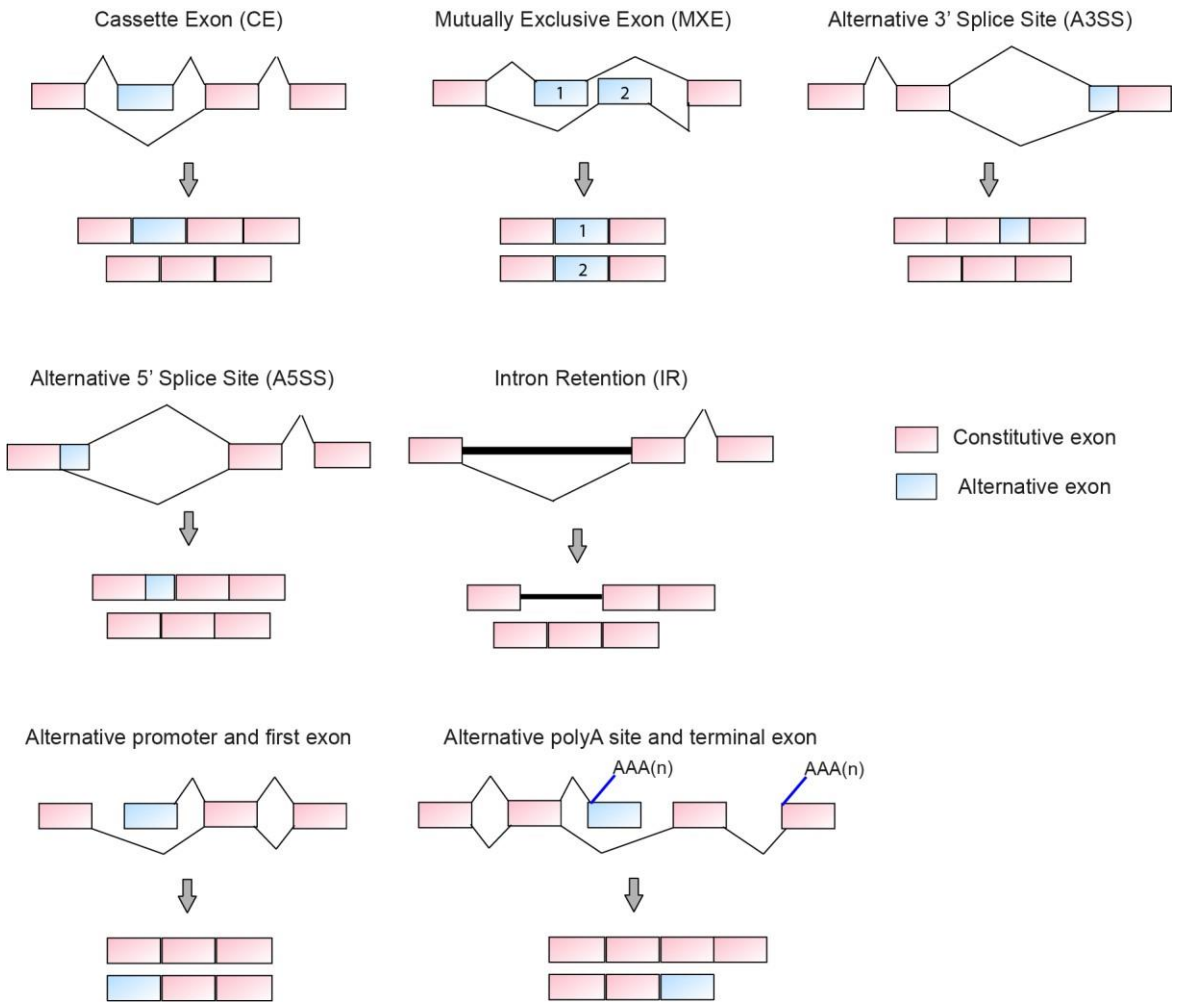

Figure 4. The different categories of AS events. Constitutive exons are shown in pink, alternative exons in blue. Different transcripts generated through the AS event are depicted below the splicing scheme.

1.4.1. Backsplicing and the formation of circular RNAs (circRNAs)

During splicing, the 5'ss of one exon is ligated to the 3'ss of a downstream exon. However, one type of AS event involves the ligation of a 5'ss to the 3'ss of an upstream exon. This process is called backsplicing and leads to the formation of a circular RNA transcript (circRNA). CircRNAs have been already described in the early 70s, but only recently with the development of high throughput sequencing techniques and bioinformatics tools specifically developed for the detection of circRNAs, their abundance and expression levels have been thoroughly recognized (Wilusz 2018; Hansen 2018) . Due to their formation by backsplicing, circRNAs do not contain PolyA-tails as most linear

RNAs do. Their circularity and lack of free 3' ends makes them further resistant to degradation by exonucleases such as RNase I and R. Therefore, circRNAs are highly stable transcripts and have longer half-life times than linear transcripts, such as mRNAs. Many studies have shown that circRNAs are abundantly cell type-specifically expressed, with neurons having the highest abundance of circRNAs (Bartsch et al. 2018; Rybak-Wolf et al. 2015; Werfel et al. 2016).

Backsplicing and circRNA biogenesis can be regulated through different mechanisms (Figure 5). For exons to be backspliced, their splice sites need to be in close proximity. One mechanism promoting backsplicing is the base-pairing between complementary sequences in flanking introns. During transcription, complementary sequences in the introns can base-pair and form secondary structures that allow distant exons to come together. Introns often contain *Alu* repeats, which can also base-pair and the form long double-stranded RNA regions. Indeed, exons that are circularized have an enrichment in *Alu* repeats in their flanking introns and their presence can be used to predict circRNA formation (Jeck and Sharpless 2014; Ivanov et al. 2015). A second mechanism promoting circRNA formation is the binding of RNA binding proteins (RBPs) to introns upstream and downstream of the splice sites. This mechanism has been shown for the RBP Quaking (QKI). When two QKI proteins bind to introns and interact, they can bring the introns together and the exons in close proximity allowing backsplice events to occur (Conn et al. 2015). As a third mechanism, circRNA formation can be coupled to canonical splicing and AS. CircRNAs are spliced by the canonical splicing machinery, since knockdown of different splicing factors affects linear splicing as well as circRNA formation (Starke et al. 2015). When splicing is efficient, introns are quickly removed, impairing their interaction and backsplicing. In this way linear splicing competes with backsplicing (Ashwal-Fluss et al. 2014). In addition, exon skipping can lead to formation of exonic lariat structures, which in turn can result in backsplicing of the skipped exons. In these cases circRNAs can be formed at the expense of the linear isoforms leading to a decrease in the levels of linear mRNAs or the formation of alternative mRNA isoforms lacking the circularized exons (Suzuki and Tsukahara 2014; Ashwal-Fluss et al. 2014).

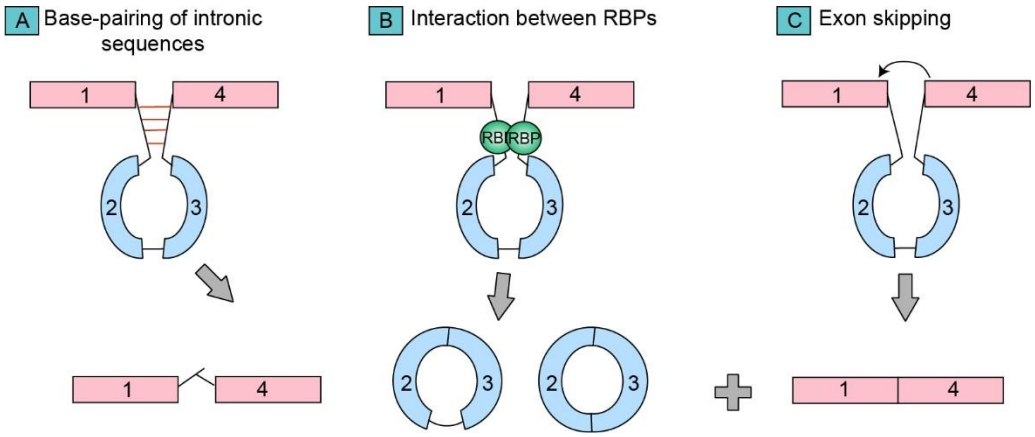

Figure 5. Three mechanisms of circRNA formation. CircRNA formation mechanisms require that the ends of circularized exons are brought in close proximity for backsplicing to occur. **A)** Base-pairing of complementary sequences within flanking introns. **B)** Interaction between RBPs that bind to introns. **C)** Lariat formation during exon skipping. For all three mechanisms introns can be either partially kept in the transcript (eIcRNAs) or they can be completely spliced (exonic circRNAs). Figure adapted from (Ebbesen et al. 2016).

CircRNAs have been intensively studied in the last years. An ever increasing amount of circular transcripts has been identified that are differentially expressed in cancer cells, during differentiation, during cellular stress such as hypoxia or related to diseases (Boeckel et al. 2015; Lei et al. 2018; Zhao et al. 2018; van Rossum et al. 2016). Many functions of circRNAs have been described; e.g. they can act as microRNA sponges, form complexes with RBPs and regulate transcription and translation, have functions in cellular stress response or regulate important cell signaling pathways (Figure 6 and Table 1). Although circRNAs are generally considered as long non-coding RNAs (lncRNAs), recent studies suggested that they can contain internal ribosome entry sites (IRES) and can be translated via cap-independent translation (Pamudurti et al. 2017; Zhang et al. 2018a) . Most circRNAs studies focused on their identification and potential functions and very little is known on how these transcripts are induced or differentially regulated in different cellular conditions or as part of a stress response.

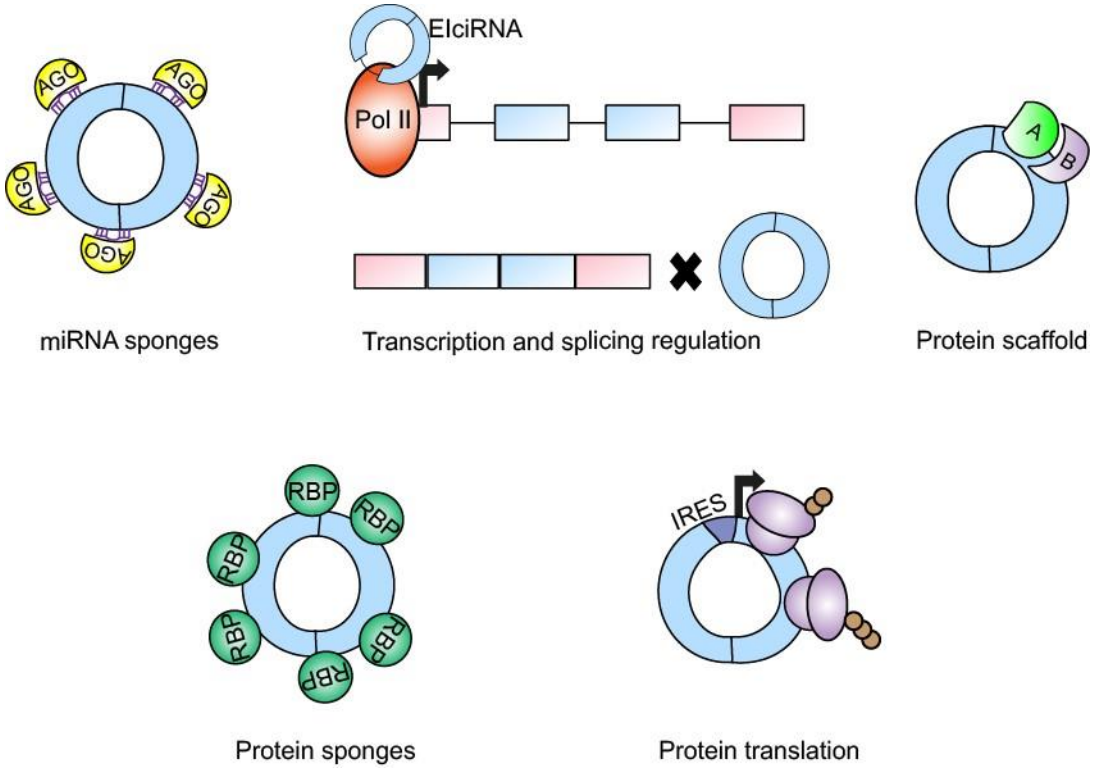

Figure 6. CircRNA functions. CircRNAs can act as microRNA sponges. MicroRNAs with complementary sequences base-pair with the circRNA instead of the mRNA target transcripts thereby impairing mRNA degradation and promoting increase in protein translation. Since circRNAs contain the same sequences as the linearized exons, RBPs can bind to the circle. The circRNA can function as scaffold for protein – protein interactions. CircRNAs can regulate RNA and protein expression. EIciRNAs can interact with the DNA Pol II and enhance transcription of their host genes. Additionally, circRNA formation can directly compete with linear splicing and mRNA formation, decreasing protein levels. CircRNAs can impair activity of the RBPs through sponging and sequestering. Some circRNAs contain IRES, which can be bound by ribosomes leading to translation of circRNA proteins. Figure adapted from (Kristensen et al. 2018).

Table 1. Overview of circRNA functions.

Function	circRNA	Target	Cell Type/Origin	Reference
miRNA sponge	*CiRS-7*	miR-7	Total Brain, HEK293	(Hansen et al. 2013)
	circSry	miR-138		
	CircPVT1	miR-125	Gastric cancer tissue	(Chen et al. 2017a)
	CircMYLK	miR-29a	Bladder cancer cells	(Zhong et al. 2017)
	CircCDR1	miR-7	Zebrafish, HEK293, mouse embryo brain	(Memczak et al. 2013)
	CircRNA_100290	miR-29b	Human oral squamous cell carcinoma	(Chen et al. 2017b)
	CircMTO1	miR-9	Human hepatocarcinoma	(Han et al. 2017a)
	CircABCB10	miR-1271	Human breast cancer	(Liang et al. 2017)
	CircP4HB	miR-133a-5p	Non-small cell lung carcinoma	(Wang et al. 2019b)
	hsa_circ_0005105	miR-26a	Chondrocytes	(Wu et al. 2017)
	circUBAP2	miR-143	Osteosarcoma	(Zhang et al. 2017)
Protein scaffold	*circNFATC3, circANKRD17*	IMP3 protein	Human hepatocarcinoma	(Schneider et al. 2016)
	circFoxo3	p21 and CDK2 proteins	NIH3T3, mouse cardiac fibroblast	(Du et al. 2016)
Transcription regulation	*circEIF3J, circPAIP2*	*EIF3J, PAIP2* genes	HeLa	(Li et al. 2015)
Splicing regulation through protein sponging	*circSMARCA5*	SRSF1 sponge-> *VEGFA* splicing regulation	U87-MG; glioblastoma multiforme	(Barbagallo et al. 2018)
	circMBL1	MBL1 sponge ->*MBL1* splicing regulation	Drosophila S2, HeLa	(Ashwal-Fluss et al. 2014)
Translation regulation through protein sponging	*circPABN1*	HuR sponge -> *PABN1* translation regulation	HeLa	(Abdelmohsen et al. 2017)
Protein translation	*CircSHPRH*	SHPRH-146aa	Glioblastoma	(Begum et al. 2018) 2018)
	CircZNF609		Myoblast	(Legnini et al. 2017)

1.4.2. Alternative splicing and nonsense-mediated decay (NMD)

AS can also result in the generation of mRNA isoforms that contain premature termination codons (PTCs). PTCs can either appear due to the inclusion of an alternative exon or the retention of introns. Translation of mRNAs containing PTCs could give rise to truncated protein isoforms, which can be toxic for the cell or have a dominant negative function on the main isoform (Hwang and Maquat 2011). To prevent the synthesis of such truncated proteins, the nonsense-mediated decay pathway (NMD) degrades mRNAs containing PTCs during the first round of translation (Lloyd 2018). When the ribosome translates an mRNA and encounters a stop codon it pauses for termination. Ribosome pausing occurs usually at the end of the coding region and at the beginning of the 3'UTR. Interaction of the ribosome with the cytoplasmic PolyA binding protein (PABPC1), which binds to the polyA-tail of the transcript, leads to polypeptide release and translation termination. When the ribosome encounters a PTC the distance to the 3'end of the transcript is elevated and the interaction with PABPC1 is impaired. Instead the regulator of nonsense transcripts 1 (UPF1) binds to the mRNA next to the ribosome. This interaction leads to the release of the mRNA from the ribosome and target it for degradation (Mühlemann et al. 2008; Nicholson and Mühlemann 2010).

Splicing is also coupled to the regulation of the NMD pathway. During splicing exon junction complexes (EJC) are deposited ~24nt upstream of every splice junction. The presence of EJCs downstream of stop codons marks them as PTCs and assists in the recruitment of NMD factors (Figure 7) (Nicholson and Mühlemann 2010). In a similar mechanism, splicing factors such as SRSF1 have been shown to recruit the NMD factor UPF1 when they remain bound to the mRNA in the cytoplasm due to ribosome pausing in a upstream stop codon (Aznarez et al. 2018). Translation inhibitors such as cyclohexamide (CHX) and knockdown of NMD factors such as UPF1 causes an inactivation of the NMD pathway and the accumulation of mRNAs with PTCs. Using this approach, studies have shown that AS of NMD target transcripts is a conserved mechanism for the regulation of protein levels (Lareau and Brenner 2015). During transcription, inclusion of exons containing PTCs, also called 'poison cassette exons' (PCEs), lead to the formation of transcript isoforms that are NMD-targets at the expense

of the main protein-coding mRNA isoform, which ultimately results in decreased protein levels. Many RBPs, spliceosome components and splicing factors, such as SR proteins, are regulated by PCE inclusion to maintain protein homeostasis (Saltzman et al. 2008).

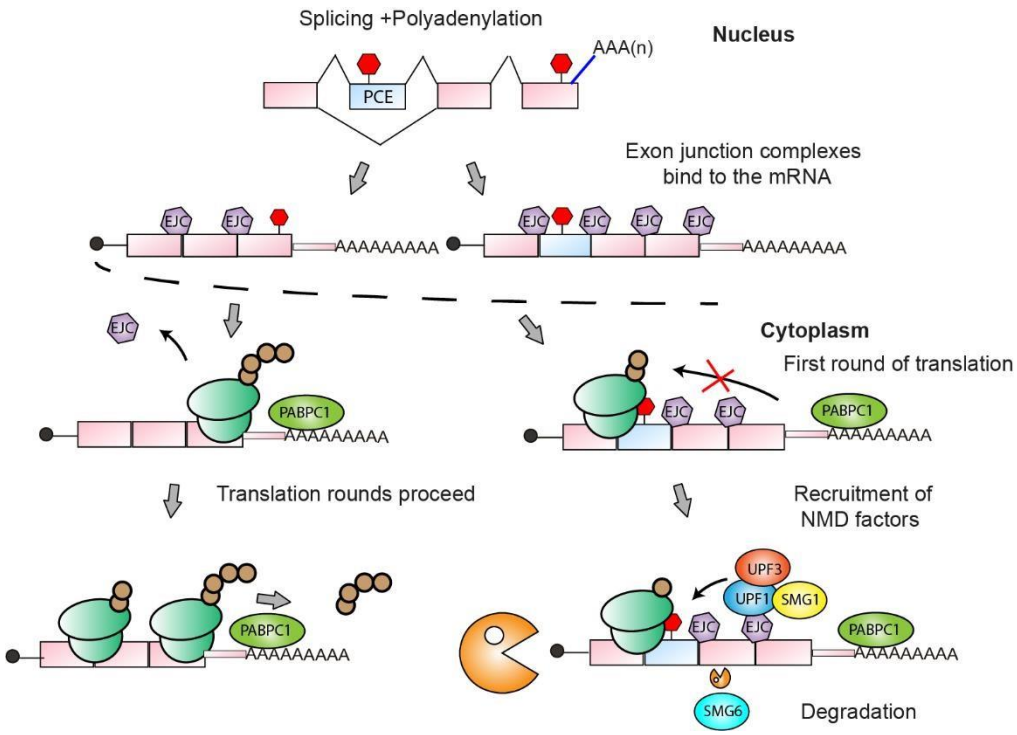

Figure 7. Simplified NMD pathway. During splicing, exon junction complexes (EJCs) are deposited at most splice junctions. Alternative exons with premature termination codons (PTC - indicated by red hexagons), named 'poison cassette exons' (PCE) can be included during AS. After transcription terminates, polyA-tails are added to the mRNAs. The mature mRNA is exported to the cytoplasm for translation. In the cytoplasm the cytoplasmic PolyA binding protein 1 (PABPC1) binds to the polyA-tail. During the first round of translation the ribosome moves along the transcript and EJCs are displaced. When the ribosome encounters a stop codon it stalls. Stalling of the ribosome at stop codons at the end of the coding region allows interaction with PABPC1. This interaction leads to translation termination and protein release. Further rounds of translation can be initiated. In the second scenario the ribosome encounters a PTC and stalls. EJCs further downstream remain on the mRNA and interaction with PABPC1 does not occur. In this case, NMD factors and the endonuclease SMG6 are recruited and the mRNA and truncated protein are targeted for degradation, preventing further translation rounds.

1.5. SR proteins – essential alternative splicing regulators

Serine-, arginine-rich proteins (SR proteins) are essential splicing factors that regulate constitutive and alternative splicing. SR proteins act mostly as splicing enhancers and bind preferentially to exons within ESEs. They assist in the splice site recognition and can recruit the spliceosome (Howard and Sanford 2015). Although SR proteins binding to exonic sequences rather promotes exon inclusion, multiple examples have been reported in which SR proteins binding to adjacent exons can also promote exon skipping. In this case the downstream and upstream exons are ligated while the alternative exon(s) in the middle are skipped (Figure 8) (Twyffels et al. 2011). Furthermore, SR proteins can inhibit binding of hnRNP proteins to ESS and ISS, which inhibit spliceosome assembly (Zhou and Fu 2013; Shepard and Hertel 2009).

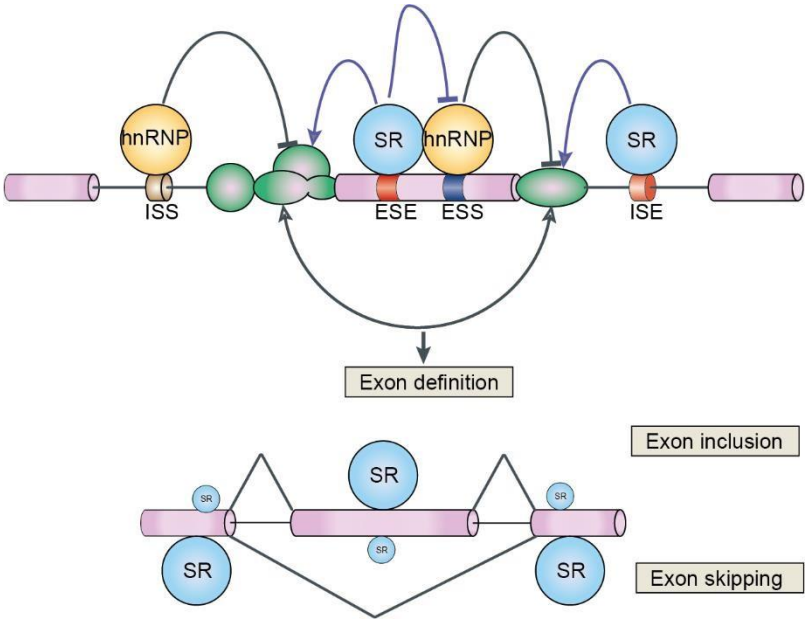

Figure 8. SR proteins functions in constitutive splicing and AS. SR proteins can bind to exonic or intronic splicing enhancers (ESS, ISE). They promote exon recognition and recruitment of the spliceosome (green) to the splice sites. In addition, SR protein can inhibit binding of hnRNPs to exonic and intronic splicing silencer sequences (ESS, ISS) counteracting their inhibitory functions. When SR proteins bind to an exon they promote exon inclusion. When they bind to flanking exons they can promote exon skipping. Figure adapted from (Kornblihtt et al. 2013; Zhou and Fu 2013).

The SR protein family contains twelve canonical SR proteins named SRSF1-12 (Manley and Krainer 2010). They contain one or two RNA recognition domains (RRM and RRMH) at their N-terminus and a C-terminal arginine-, serine-rich domain (RS domain), which varies in length. Beside these highly conserved domains, SR proteins can have additional protein domains. For example, SRSF7 contains a zinc knuckle domain between the RRM and RS domains (Figure 9) (Cavaloc et al. 1999). The RRMs bind to pre-mRNA during transcription to promote co-transcriptional splicing (Sapra et al. 2009). Although the structure and sequences within the RRMs are similar between SR protein family members, they have different binding motifs and target exons (Ankö et al. 2010). The RS domain serves as a proteins interaction platform and has been shown to interact with many RNA processing factors. Phosphorylation of the serine residues within the RS domain determines the activities of SR proteins (Ghosh and Adams 2011).

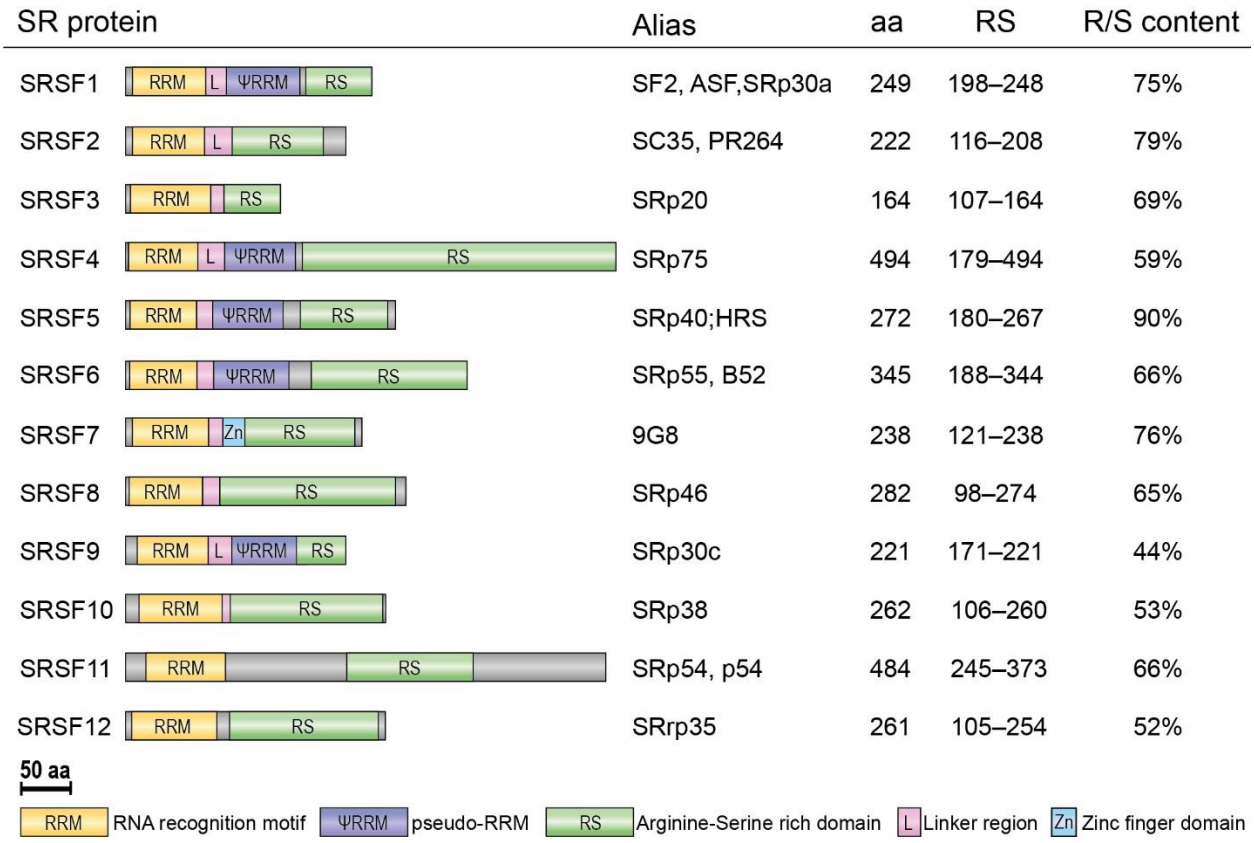

Figure 9. Overview of the domain structure of canonical SR proteins (SRSF1-12). Indicated are the names, the domain structure, other known names, the total number of amino acids, the position where the RS domain is in the protein and the percentage of RS direpeats within the RS domain (Wegener and Müller-McNicoll M. 2019).

The phosphorylation state of the RS domain is highly dynamic and is regulated by a complex interplay between phosphatases and SR protein specific kinases. Different phosphorylation states stimulate conformational changes within the SR proteins. These conformational changes allow interactions with the spliceosome and other proteins partners and regulate the SR proteins activity and localization (Aubol et al. 2017). The SR protein phosphorylation cycle is illustrated in Figure 10. In the nucleus, they are hyperphosphorylated by the nuclear CDC2 like kinases 1-4 (CLKs). In this form they are recruited to nascent pre-mRNAs, they bind to their target RNA sequences and recruit the U1 and U2 snRNP and promote spliceosome assembly. During splicing, SR proteins become dephosphorylated by protein phosphatase 1 (PP1) and in this form they are able to recruit the nuclear export factor 1 (NXF1) (Novoyatleva et al. 2008; Müller-McNicoll et al. 2016). Recruitment of NXF1 leads to the nuclear export of mature mRNAs to the cytoplasm. Most SR proteins remain bound to the exported mRNA and shuttle as part of the mRNP to the cytoplasm. In the cytoplasm, SR-specific protein kinases (SRPK1-2) rephosphorylate the RS domain to an intermediate state, which promotes SR protein reimport to the nucleus via Transportin-SR and their targeting to nuclear speckles (Aubol et al. 2018; Saitoh et al. 2012; Zhong et al. 2009). In the nuclear speckles, SR proteins are stored and interact with other nuclear speckle proteins and polyadenylated RNAs, such as the lncRNA *MALAT1*. SR proteins remain in nuclear speckles until they are reactivated by hyper-phosphorylation and participate in a new round of splicing (Corkery et al. 2015).

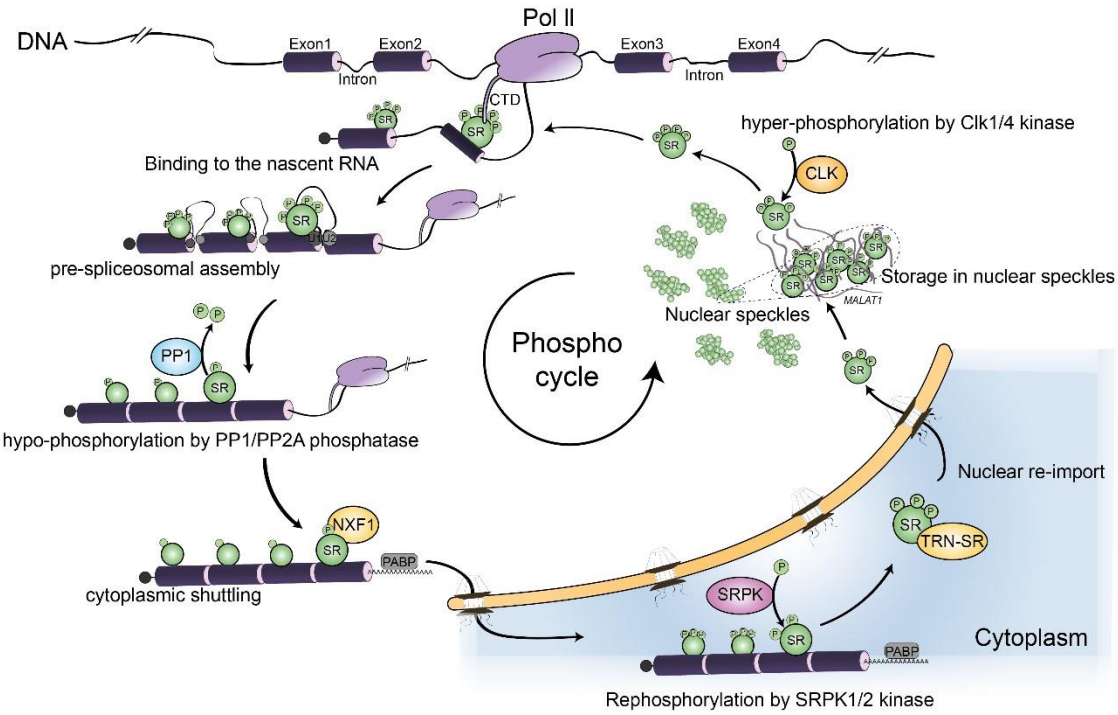

Figure 10. The SR protein phosphorylation cycle. The SR protein phosphorylation state determines their localization and activity. The CLKs 1/4 hyper-phosphorylate SR proteins and in this state they bind to premRNA during transcription and promote spliceosome assembly and splicing. During splicing they are dephosphorylated by protein phosphate 1 (PP1) and remain bound to the mature RNA. In this state, SR protein recruit the export factor NXF1 and promote mRNA export to the cytoplasm. SR protein shuttle to the cytoplasm with the bound mRNA. In the cytoplasm, they are removed from the mRNA by the ribosome during the first round of translation. Subsequently, they become re-phosphorylated by SRPK1/2 kinases and are re-imported into the nucleus. In this intermediate phosphorylation state, they are stored within nuclear speckles were they bind to other splicing factors and *MALAT1* until being hyper-phosphorylated by CLKs and able to leave the speckles for new round of splicing (Wegener and Müller-McNicoll M. 2019)

1.5.1. Nuclear speckles (NS) and *MALAT1*

Nuclear speckles (NS) are membrane-less dynamic structures present in the interchromatin spaces within the nucleus. They are formed through the interactions between RBPs and are considered as storage compartments for splicing factors, spliceosomal components and the lncRNA *MALAT1* (Mao et al. 2011). High resolution images of NS have shown that splicing factors are mostly localized in the inner part of the speckle while *MALAT1* localizes to the periphery (Fei et al. 2017). NS are dynamic structures and their composition, morphology and localization can change in different cellular conditions. Upon transcription inhibition, NS can localize to transcription sites, which allows the rapid recruitment of splicing factors to these sites to promote

posttranscriptional splicing (Girard et al. 2012). NS also contain mature mRNAs and nuclear export factors and have been described as a quality control hub, where mRNAs have to transit through prior their cytoplasmic export (Wegener and Müller-McNicoll 2018; Wang et al. 2018). SR proteins are also stored in NS and they are released when they are hyperphosphorylated by CLKs (Aubol et al. 2017). Within NS, SR proteins bind to the lncRNA *MALAT1. MALAT1* has been shown to be a component of nuclear speckles, but it is also highly abundant in the nucleoplasm. Contrary to core nuclear speckle proteins such as SRSF2 (SC35) and SRm300, depletion of *MALAT1* or deletion of different regions of this lncRNA does not affect nuclear speckle assembly (Miyagawa et al. 2012; Nakagawa et al. 2012).

MALAT1 is up-regulated in many cancer cells and upon stress conditions, such as hypoxia, but its functions are not completely understood. Many studies suggested that *MALAT1* induction might be important for cell proliferation, migration and survival. In agreement with this proposal, knockdown of *MALAT1* in HeLa cells caused cell cycle arrest and nuclear fragmentation during replication. However, a recent study showed that *MALAT1* actually prevents metastasis and cellular migration in breast cancer cells (Hou et al. 2017; Brock et al. 2017; Kim et al. 2018; Liu et al. 2017; Liu et al. 2018; Tripathi et al. 2010). Although the functions of *MALAT1* seem to vary dependent on the cell type and cellular conditions, it is clear that its interaction with SR proteins represents one important mechanism of how *MALAT1* might be able to regulate splicing and transcription. So far, studies have investigated only the interplay of *MALAT1* with SRSF1 (Figure 11). It is unknown whether the interaction of *MALAT1* with other SR proteins might affect its activities in a different manner. For example, SRSF6 remains in NS upon cellular stress, while SRSF1 is released to the nucleoplasm, suggesting that these two SR proteins might have different functions upon stress (Hochberg-Laufer et al. 2019). Investigating the *MALAT1* interaction with other SR proteins could help to understand the function of this lncRNA in different cell types and stress conditions.

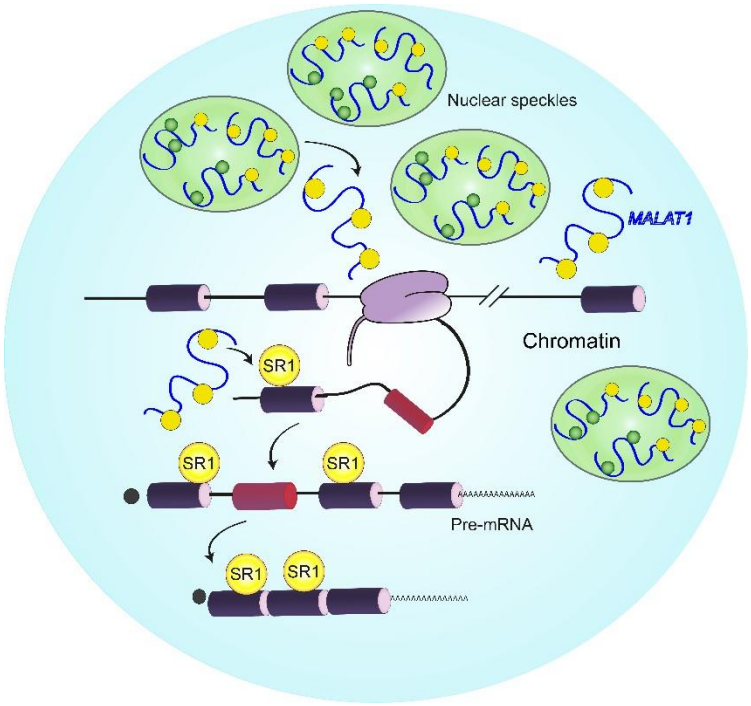

Figure 11. *MALAT1* regulates splicing by moving SRSF1 from speckles to the chromatin. *MALAT1* is a lncRNA present in nuclear speckles (NS) and in the nucleoplasm. It contains many binding sites for SRSF1 and other RBPs (yellow and green circles). *MALAT1*-SRSF1 complexes can leave NS and move together to the chromatin during transcription. *MALAT1* binds to chromatin and brings SRSF1 in close proximity to nascent pre-mRNA facilitating its binding to target sequences and promoting the inclusion of SRSF1 target exons.

1.5.2. Serine-, arginine-rich splicing factor 6 (SRSF6)

SRSF6 is a member of the canonical SR protein family. It contains one RRM and one RRMH domain and is very similar to SRSF4 in sequence and domain structure (Figure 9). Accordingly, SRSF6 and SRSF4 share a similar binding motif and can bind to the same target RNAs, but they often regulate splicing in opposite directions and might rather compete for binding sites (Müller-McNicoll et al. 2016). For example, it has been shown that splicing of exon 5 of the coagulation factor TF in monocytes is regulated by SRSF6 and SRSF4 in an opposing manner (Chandradas et al. 2010).

SRSF6 was shown to play an important role in in pancreatic cells, where it regulates splicing of the anti-apoptotic isoform of Bim and assures cell proliferation and survival (Hara et al. 2013; Juan-Mateu et al. 2018). SRSF6 also regulates splicing of the vascular endothelial growth factor *VEGFA*, which is important for the response of tumor

cells to hypoxia (see chapters below) (Nowak et al. 2008). SRSF6 also emerged as oncogene, since it is overexpressed in different cancer cells and promotes tumor progression and aggressiveness (Chandradas et al. 2010; Iborra et al. 2013; Wan et al. 2017). Moreover, these studies provided compelling evidence that SRSF6 is an important splicing regulator in tumors that regulates the proliferation and migration capacities of cancer cells. Most likely, overexpression of SRSF6 will lead to aberrant AS of many genes, but so far only very few SRSF6 target transcripts have been identified and characterized. Furthermore, the regulation of SRSF6 levels in the hypoxia response and adaptation of tumor cells has not been explored yet.

1.6. The role of AS in stress conditions and upon DNA damage

AS of transcripts can lead to the translation of protein isoforms with antagonistic functions, which can be essential to control the fate of a cell upon stress. For example, activation of the apoptosis signaling pathway upon DNA damage or mutation can impair the survival of carcinoma cells and block tumor progression. While the main isoform of Bim, a BCL2 family member, has pro-apoptotic functions, the alternatively spliced isoform Bim-S, which lacks exon 4, has anti-apoptotic functions (Juan-Mateu et al. 2018). Another example is MDM4, which is a negative regulator of the pro-apoptotic protein p53. An alternative spliced *MDM4* isoform lacking exon 6 leads to the translation of a protein isoform, which lacks the p53 inhibitory domain and causes activation of p53 and the apoptosis signaling pathway (Allende-Vega et al. 2013).

In addition to the modulation of the apoptotic pathway, AS of cell cycle regulators can also determine whether cell division is induced or if the cell cycle is arrested upon stress conditions and in cancer cells. For example, SRSF3 can be spliced into a truncated protein isoform, which has a dominant negative effect on the splicing of SRSF3 targets. When the truncated SRSF3 protein binds to the *Sororin* transcript, intron 1 and 2 are retained, which leads to creation of a NMD isoform. Consequently, Sororin protein levels are decreased culminating in cell cycle arrest (Jiménez et al. 2019).

The cellular response to DNA damage is essential to prevent accumulation of damaged cells and cancer development. In cancer cells and solid tumors, proliferation of cells with damaged DNA can further stimulate tumor progression and metastasis. Recent studies have shown that many transcripts undergo AS in response to DNA damage (Lenzken et al. 2013; Shkreta and Chabot 2015; Chen and Kastan 2017). For example, the Chk1 (checkpoint kinase 1) protein is essential for the DNA repair in DNA damaged cells. It promotes cell cycle arrest allowing the DNA to be repaired before division. Skipping of exon 18 of the *Chk1* transcripts results in the translation of a truncated protein isoform (Chk1-short), which interacts and antagonizes Chk1 impairing the cell cycle arrest and leading to proliferation of DNA damaged cells (Pabla et al. 2012).

DNA damage including mutations or double strand breaks (DSB) induce the DNA damage repair response (DDR), which triggers phosphorylation of the histone variant H2AX. Phosphorylated H2AX locates to sites of DSB and recruits ATM kinases (Burma et al. 2001; Ji et al. 2017; Huang et al. 2004; Podhorecka et al. 2010). ATM kinases activate downstream signaling pathways, which cause phosphorylation and regulation of splicing factors. This leads to AS of transcripts important for the DDR, involved in DNA repair, apoptosis activation and cell cycle regulation. Impaired DDR causes uncontrolled growth and additional genomic errors due to inefficient chromosome segregation and a lack of homologous repair. Errors during mitosis, especially during chromosome pairing and segregation can lead to the formation of micronuclei or abnormal shaped nuclei. Micronuclei have been shown to be an marker of DNA damage and an impaired DDR response (Fonseca et al. 2019; Zhu et al. 2011).

1.7. Hypoxia

The DDR is impaired in cancer cells and they tend to proliferate until they reach solid tumor stages. Cells in the middle of solid tumors are distant from blood vessels and oxygen (O_2) supply. In this condition, cancer cells can experience a stress condition named hypoxia. Hypoxia occurs when the oxygen (O_2) supply in cells and tissues is lower than the amount necessary for their normal metabolic functions. Hypoxia has been first described more than 50 years ago, when it was observed that cancer cells were resistant

to radiation therapy, when they were isolated from blood vessels and had low O_2 supply (Thomlinson & Gray 1955). Radiation of cells with normal oxygen levels causes DNA damage due to the generation of reactive oxygen species. Hypoxic cells are adapted to lower O_2 levels due to the hypoxia response, thus fewer reactive oxygen species are generated and they become resistant to DNA damage (Brown and Wilson 2004; Graham and Unger 2018).

In the last decades, hypoxia has been described to occur in several other physiological conditions such as ischemia, stroke and wound healing. Upon hypoxia, cells release growth factors which act on endothelial cells and promote growing of new blood vessels, a process called angiogenesis. Therefore, the hypoxia response is essential for the revascularization of the affected areas. (Yang et al. 2018; Simon and Keith 2008; Zhang and Zhang 2018). The level of oxygen supply in the human body varies considerably between tissues, which is mainly due to the localization and amount of blood vessels which supply the respective tissue or cells in the body. O_2 levels can vary from 19% in the tracheas, where the atmospheric air enters, to 4% in muscle tissue and 1% in superficial layers of the skin (Carreau et al. 2011; Wenger et al. 2015; Esteban et al. 2019). Therefore, the percentage of O_2 that induces the hypoxia response can vary between tissues and cell types. Cancer cells can grow excessively and form tumors in all tissues. Studies have shown that due to the cellular organization and the lack of blood vessels, 90% of solid tumors display hypoxic conditions in their microenvironment (Vaupel et al. 2001; Muz et al. 2015).

Cells that are under hypoxia need to respond to this stress in order to survive. The mechanisms, which allow cellular survival on low or insufficient O_2 levels have been intensively studied through the last years. Adaptation occurs at many levels and the hypoxia response comprises global changes in gene expression and cellular processes. However, due to this major reprogramming that cells experience and the induction of various signaling pathways, the hypoxia response is still far from being understood.

Wenger and colleagues discussed the question of what is considered a hypoxic condition *in vivo* and *in vitro* (Wenger et al. 2015). Depending on the cell type from which the tumor originated, the relative decrease in O_2 compared to the normal tissue can vary from 20-90%, with less than 1% O_2 in some cases. *In vitro*, cells are cultivated with 20%

O_2 (21% O_2 with 5% CO_2, which results in 19,95% total O_2). Therefore, for most of the hypoxia studies the O_2 levels used, are between 0.2-1.5%. This decrease in O_2 supply mimics the physiological hypoxic conditions and can induce the hypoxia response in cells *in vitro* (Vordermark and Brown 2003).

1.7.1. Hypoxia inducible factor pathway

One of the most important signaling pathways for the hypoxia response is the hypoxia inducible factor (HIF) pathway. HIFs are a family of transcription factors, which bind to promoter regions and induce expression of genes associated with the hypoxia response. The function of HIFs in promoting the expression of hypoxia-inducible genes has been described in the early 90s (Guang l et al. 1995) and since then, many studies have shown the importance of these transcription factors for cellular adaptation and survival upon hypoxia.

HIF1 and HIF2 are the most studied HIF transcription factors and they have common and differential functions in the hypoxia response. These transcription factors contain 2 subunits, alpha and beta. Only when both subunits are dimerized they can bind to the promoter regions of the DNA and promote transcription (Bartoszewski et al. 2019; Schito and Semenza 2016). In normal conditions, HIF1 and HIF2 alpha subunits are translated and rapidly degraded in the cytoplasm by the proteasome (half-life ~5 minutes, Figure 10). Rapid degradation occurs upon ubiquitination by the von Hippel-Lindau tumor (pVHL) suppressor protein, an E3 ubiquitin ligase. The recognition of HIF1/2 alpha by pVHL is dependent on the hydroxylation of proline residues within HIF1/2 alpha, catalyzed by prolyl-4-hydroxylases (PHDs) or HIF1/2 prolyl hydroxylases (HPHs). At low oxygen levels, PHDs and HPHs are no longer able to hydroxylate HIF1/2 alpha and the proteins are consequently stabilized. Upon stabilization, HIF1/2 alpha translocate to the nucleus, form heterodimers with the constitutively expressed HIF1 beta subunit and bind to other cofactors such as the CREB-binding protein (p300/CBP). Subsequently, HIF1/2 alpha bind to specific promoter sequences called E-box-like hypoxia response elements (HREs) and induce the transcription of thousands of genes important for the cellular hypoxia response (Salceda and Caro 1997; Kazuhiro et al. 1999; Masoud and Li 2015).

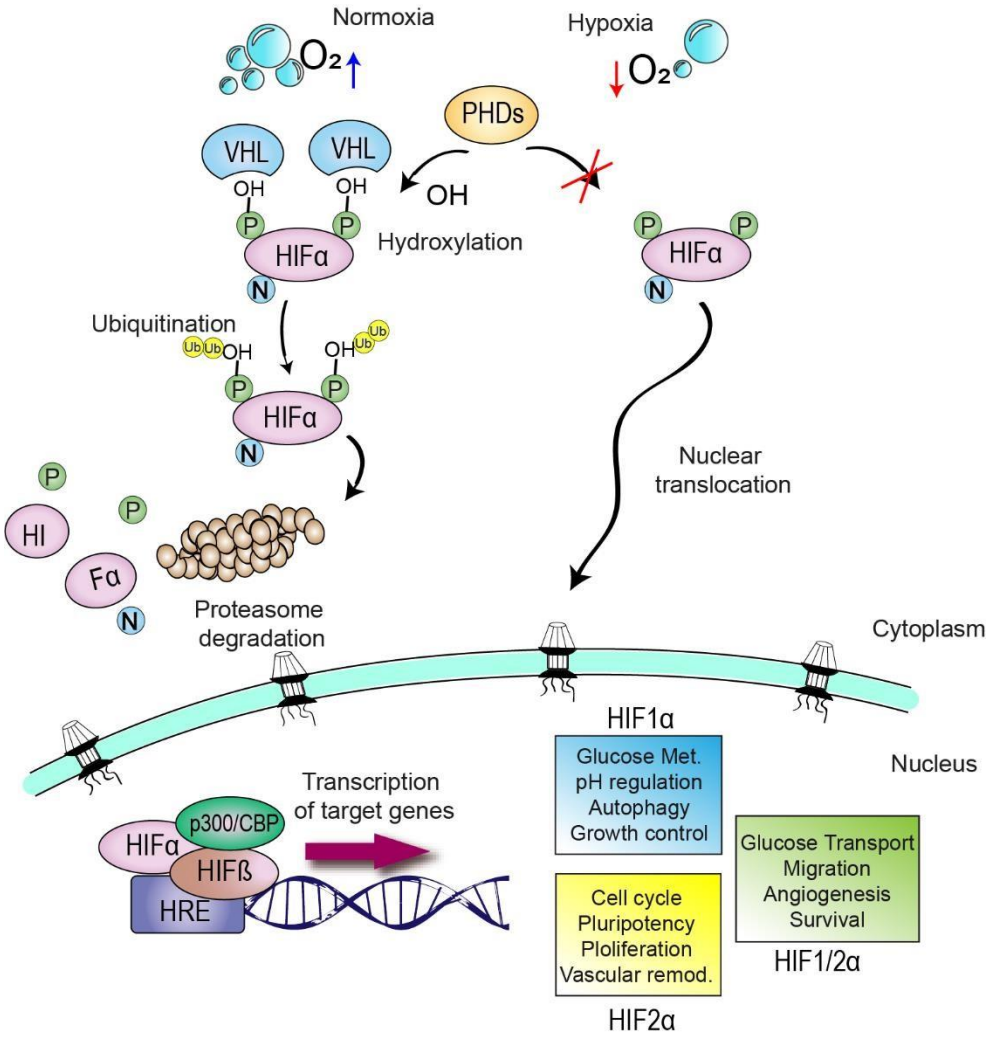

Figure 12. HIF1α signaling pathway. HIF1/2 transcription factors have two subunits, the alpha subunit stays in the cytoplasm and is rapidly degraded, while the beta subunit is stable and imported to the nucleus. When cells have high O_2 levels, PHDs hydroxylate HIF1/2 alpha in the cytoplasm. Hydroxylated HIF1/2 alpha are recognized and bound by VHL, which ubiquitinates HIF1/2 alpha. Ubiquitinated HIFs are rapidly degraded by the proteasome. In hypoxia conditions, low O_2 levels impair the hydroxylation of HIF1/2 alpha. In this case, HIF1/2 alpha are not recognized by VHL and stabilized and translocate to the nucleus. In the nucleus they dimerize with the HIF1 beta subunit and bind to DNA sequences named hypoxia response elements and promote transcription of genes involved in the hypoxia response.

Genes induced by the HIF1a pathway act in diverse cellular processes. In the early hypoxia response, mitochondrial genes are down-regulated and genes involved in anaerobic metabolism and glycogenesis are induced by HIF1 alpha (Singh et al. 2017). Another target of HIF1 alpha and important hypoxia marker is the vascular endothelial growth factor (VEGFA). *VEGFA* expression and induction in hypoxic cells is pivotal for

tumor and ischemic tissue survival (Shibuya 2011). This growth factor is produced and secreted by hypoxic cells and stimulates growth and migration of endothelial cells towards a VEGFA gradient, leading to blood vessel growth in a process called angiogenesis, which allows reoxygenation of the hypoxic cells and tissues (Figure 13). When tumor cells are provided with blood vessels, cancer cells tend to detach from the tumor and fall into the blood vessel. This allows tumor cells to reach other tissues and become metastatic (Schito and Semenza 2016). Furthermore, HIF1 alpha target genes have been shown to regulate cellular proliferation, migration and cell survival through regulation of the apoptosis pathway (Mori et al. 2016; Bai et al. 2013; Greijer and van der Wall 2004).

HIF2 alpha acts in the same way as HIF1 alpha and binds to HREs promoting expression of genes involved in the hypoxia response. Although less studied than HIF1 alpha, HIF2 alpha also induces expression of *VEGFA* (Hu et al. 2003; Lee and Simon 2015; Franke et al. 2013). HIF2 alpha is also important in the regulation of selective protein translation in hypoxia (Uniacke et al. 2012). It forms a complex with the RBP RBM4 and the cap-binding protein eIF4E2 that binds to sequences in the mRNAs 5'end denominated rHREs (RNA hypoxia response elements), which in turn promotes ribosome recruitment and translation.

The stabilization of the Hypoxia Inducible Factors (HIF) is a main characteristic of the hypoxia response. HIF target genes, such as *VEGFA* and *CA9* are highly induced in different cell types and are considered as hypoxia markers (Simon 2016).

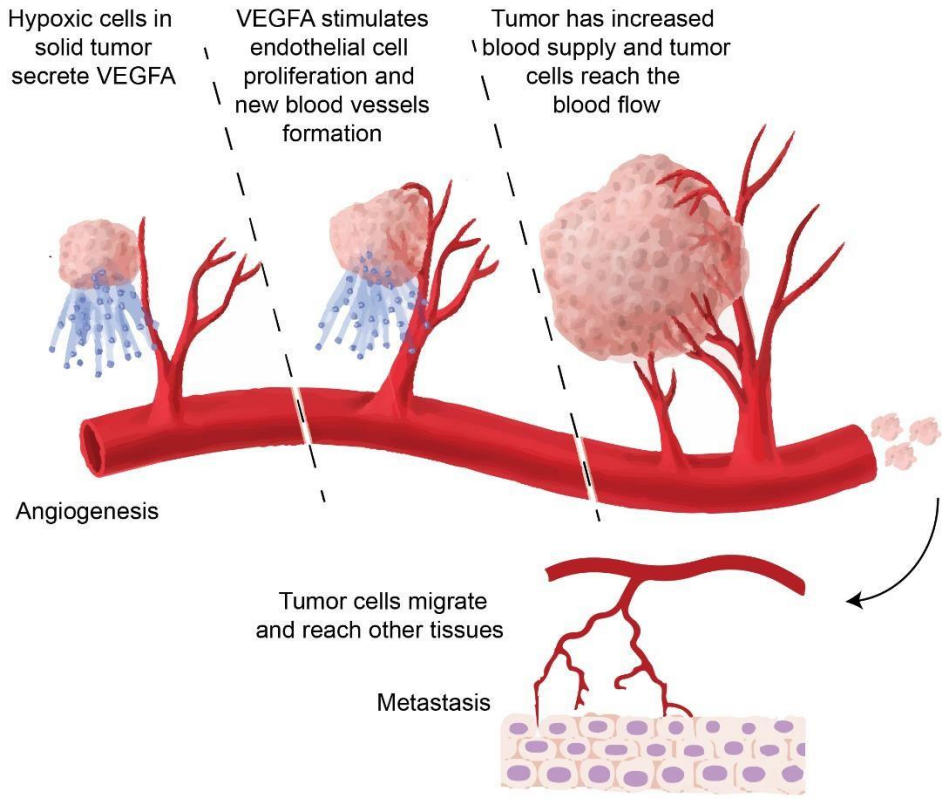

Figure 13. Angiogenesis and tumor metastasis. Figure modified from LUNGevity foundation website (https://lungevity.org/)

1.7.2. HIF independent hypoxia response pathways

Hypoxia and oxidative stress lead to the activation of other HIF-independent signaling pathways that also increase the cellular hypoxia response and cell survival. For example, in hypoxia the amount of produced cellular ATP and energy is reduced. Cells switch from oxidative phosphorylation to glycogenesis, which maintains cellular ATP production but is not as efficient to produce energy. Therefore, processes which demand large amounts of energy are down-regulated (Gonzalez et al. 2018). One of the most energy consuming cellular processes is protein translation. In hypoxia, global protein synthesis is reduced through the activation of different signaling pathways while selective translation of proteins required for the hypoxia response is induced (Chipurupalli et al. 2019; Chee et al. 2019).

At physiological conditions many proteins are synthesized at the Endoplasmic reticulum (ER). Hypoxia and oxidative stress can lead to disturbances in protein synthesis and folding at the ER and consequently cause ER stress. To alleviate ER stress, cells activate the unfolded protein response (UPR) pathway, which leads to a decrease in

global protein synthesis due to the inhibition of the mTOR signaling pathway, and reestablishes proper folding and processing of proteins at the ER (Bonnet-Magnaval et al. 2016). Hypoxia induced ER stress also leads to activation of the endoplasmic reticulum (ER)-resident kinase (PERK). This kinase phosphorylates the eukaryotic initiation factor 2 alpha (eIF2α) which inhibits the activity of the initiation factor 2B, responsible for loading mRNAs in the ribosome for translation initiation (Chipurupalli et al. 2019; Koumenis et al. 2002).

The Akt pathway, which is mainly regulated by Akt and PI3K kinases, is also activated in hypoxia. These kinases are able to phosphorylate the kinase mTOR, which activates it. Activation of the mTOR signalling pathway leads to phosphorylation and activation of its targets, 4E-binding protein-1 (4EBP1) and ribosomal protein S6 kinases (S6K), which promotes cellular proliferation and survival through ehnhanced translation and inhibition of apoptosis (Zhang et al. 2018b). In hypoxia, the Akt/PI3K pathway can be activated due to the binding of growth factors which are released from neighboring hypoxic cells. On the other hand, the micro-RNA miR-21, which is highly expressed in hypoxia, targets PTEN, a suppressor of Akt phosphorylation and activation (Polytarchou et al. 2011). Activation of this signaling pathway can enhance the hypoxia response and has been suggested to be part of a chronic hypoxia feedback loop, in which activation of mTOR and protein synthesis is necessary. In addition, the Akt/PIK3 pathway has also been shown to stabilize and increase HIF1 alpha protein levels. Although the mechanism for this regulation is not clear, it has been proposed that PI3K kinases can influence the activity of the proteasome and promote HIF alpha stabilization (Zhang and Zhang 2018).

Other than HIF-induced transcription, differential gene expression in hypoxia is also regulated by the NF-kB transcription factor family. Under physiological conditions NF-kB is bound to the IkB protein and remains in the cytoplasm. During certain stress conditions or inflammation, IkB is degraded by the proteasome and NF-kB is released (Cartwright et al. 2016; Lawrence 2009). NF-kB translocates to the nucleus where it binds to promoter regions in the DNA and induces gene expression. In hypoxia, NF-kB has been shown to be activated by the Akt kinase. Additionally, some studies have explored the effects of VHL inactivity and NF-Kb activation, although the mechanisms leading to this activation are not clear. NF-kB induced transcription activates the anti-apoptotic pathway

and promotes cell survival and proliferation. Furthermore, NF-kB has been shown to be important for tumor metastasis and drug resistance (Bedogni et al. 2008; Zhang and Zhang 2018).

1.8. Hypoxia mimic

Activation of the HIF1/2 alpha pathway in response to hypoxia has a major importance for cellular reprogramming and adaptation to this condition. HIF1 alpha stabilization can be also chemically achieved by treating cells with cobalt (II) chloride ($CoCl_2$), which mimics the hypoxia transcriptional response in normoxic conditions. Cobalt ions replace the iron in the active sites of PHDs leading to the inhibition of their hydroxylase activity. In addition, cobalt ions can bind to hydroxylated HIF1/2 alpha preventing binding of VHL and their ubiquitination (Muñoz-Sánchez and Chánez-Cárdenas 2019). Indeed, the chemical induced hypoxia response by $CoCl_2$ has been shown to mimic induction of *VEGFA* expression, activation of the PI3K/Akt and mTOR pathway and induction of glycolytic gene expression (Chen et al. 2017c; Osera et al. 2015; Zimmerman et al. 2018; Gregg L. et al. 1994).

However, while stabilization of HIF1/2 alpha normally decreases after longer times of hypoxia exposure, CoCl2 stabilizes HIF1/2 alpha during the entire time of supply. Furthermore, although HIF1/2 alpha are stabilized, cells still have sufficient O_2 and different signaling pathways are active, thus a prolonged hypoxia response cannot be fully mimicked by $CoCl_2$ treatment.

1.9. Hypoxia and AS

Upon hypoxia, thousands of genes are induced or differentially regulated. In addition to the differential gene expression in hypoxia, AS has recently emerged as an important regulation mechanism to respond and adapt to hypoxia in different cell types (Bowler et al. 2018). Sena and colleagues have published a comprehensive analysis of genes, which are alternatively spliced in hypoxia. This indicated that a large proportion of genes that are alternatively spliced are not transcriptionally induced in hypoxia (Sena et

al. 2014). These results are evidence for the potential importance of AS as an additional layer of gene regulation during the hypoxia response. Although some studies have shown the general importance of AS in cancer cells, chondrogenic differentiation or endothelial cells in hypoxia (Gonçalves et al. 2017; Han et al. 2017b; Yao et al. 2016; Kemmerer and Weigand 2014), the splicing factors, which are responsible for the AS regulation in this condition remained elusive. Interestingly, recently it was shown that the SR proteinspecific kinases CLKs are high expressed in hypoxia and contribute to the phosphorylation and activation of splicing factors in this condition (Bowler et al. 2018). Moreover, Jakubauskiene and colleagues showed that CLKs and SRPK1 are activated upon hypoxia and influence the splicing outcome (Jakubauskiene et al. 2015). Regarding the functions of alternatively spliced isoforms in hypoxia very little is known. Some isoforms have been described and validated but functional studies are scarce. Brady and colleagues showed that intron retention in the transcript encoding eukaryotic translation initiation factor 2B5 (*EIF2B5*) leads to the generation of a truncated protein isoform, which has a dominant negative effect on the main isoform and inhibits translation (Brady et al. 2017)). *VEGFA*, which plays an important role in the hypoxic response, has several alternatively spliced isoforms and alternative splicing has been shown to play an important role in angiogenesis induced by hypoxia in different cell types. The isoforms have differential effects on the angiogenesis promoting potential of *VEGFA* (Guyot et al. 2017; Biselli-Chicote et al. 2017). There are pro- and anti-angiogenic *VEGFA* isoforms and their generation can be regulated by the inclusion of exon 8a and 8b, respectively (Figure 21C). The switch in splicing from the anti- (exon8b) to the proangiogenic (exon8a) isoform in hypoxia is modulated by the activation of the SR protein SRSF1 in hypoxia. SRSF1 binds to exon 8a and favors its inclusion. In contrast, the antiangiogenic isoform is generated by binding of SRSF6, which promotes inclusion of the exon 8b (Nowak et al. 2010; Nowak et al. 2008).

1.10. Hypoxia and HeLa cells

In this study, we use HeLa cells as a model to study the hypoxia response and adaptation of cancer cells. HeLa cells are the first immortal cell lineage used for laboratory studies. They were isolated from Henrietta Lacks in 1950. Henrietta had an advanced cervical carcinoma and when she sought treatment, some of her carcinoma cells were collected and cultivated by George Grey. Surprisingly, he realized that unlike other cells, HeLa cells could grow for many passages without dying or getting old (Masters 2002). Later, it was shown that Henrietta Lacks had a human papillomaviruses (HPV) infection and the virus genome integrated in the healthy cells causing mutation and deactivation of p53. HeLa cells are immortal because the apoptosis pathway is compromised and upon DNA mutations and damage the cells can still divide and proliferate. Activation of p53 transcription in HeLa and other cancer cell lines has been shown to revert their continuous growth (Hoppe-Seyler and Butz 1993; Leroy et al. 2014). HeLa cells have been used for research since their discovery and many mechanisms leading to cell survival and tumor progression have been elucidated using them as experimental model. Although some studies have shown that primary tumor cells and cancer cell lines can vary in their genomic expression, their continuous growth and ability to generate tumors *in vivo* indicate that many cellular processes, signaling pathways activation and stress responses reflect the physiological tumor response (Gillet et al. 2013). As previously described, tumor cells such as HeLa cells, are resistant to DNA damage and able to adapt to cellular stresses such as hypoxia. When submitted to hypoxia conditions, HeLa cells respond to this stress *in vitro* similar to other cancer cell lines. They express and secret growth factors, which mimic angiogenesis induction by tumors. Hypoxia also induces the proliferation and migration of HeLa cells similarly to primary cancer cell tumors (Vaupel and Harrison 2004; Edwald et al. 2014; Fu et al. 2015; Setty et al. 2017).

2. Objectives

The hypoxia response induces global changes in cellular gene expression and alternative splicing is essential for the stress response and cell survival. The factors that regulate the AS response to hypoxia are poorly understood. SR proteins are essential splicing regulators, but their role in the AS hypoxia response has not yet been studied.

The objectives of this thesis were the following:

1) Characterize global AS and backsplicing events in HeLa cells in hypoxia!
2) Elucidate the functions of SRSF6 in the regulation of the AS response in hypoxia!
3) Investigate the role of SRSF6-*MALAT1* interactions for the regulation of hypoxia AS!

3. Material and Methods

3.1. Materials

3.1.1. List of chemicals, solutions, reagents and enzymes

Table 2. List of chemicals, solutions, enzymes and reagents.

Product	Company
Solutions	
1 M Magnesium chloride	Life Technologies
1 M Tris, pH 7.0	Life Technologies
1 M Tris, pH 8.0	Life Technologies
10X TBE	Thermo Fisher Scientific
Dimethyl sulfoxide hybri-max sterile (DMSO)	Sigma-Aldrich
1x Dulbecco's phosphate buffered saline	Sigma-Aldrich
2-Mercaptoethanol,>=99.0%	Sigma-Aldrich
2-Propanol	Sigma-Aldrich
3M Sodium acetate pH 5.5	Life Technologies
5M Sodium chloride	Life Technologies
Chloramphenicol,>=98% (TLC)	Sigma-Aldrich
Cobalt chloride 0.1 M solution	Sigma-Aldrich
Cycloheximide,from microbial, >=94% (TLC)	Sigma-Aldrich
DMEM, high glucose, GlutaMAX™ Supplement, pyruvate	Life Technologies
EDTA (0.5 M), pH 8.0	Life Technologies
Ethanol, 70%	Carl Roth
Fetal Bovine Serum	Thermo Fisher Scientific
Formaldehyde solution 37 %	Carl Roth
Geneticin® Selective Antibiotic (G418 Sulfate)	Life Technologies
Igepal® CA-630	Sigma-Aldrich
Methanol	Sigma-Aldrich
NuPAGE® MOPS SDS Running Buffer (20X)	Thermo Fisher Scientific
Penicillin-Streptomycin (10,000 U/mL)	Life Technologies
Phenol:Chloroform:Isoamyl Alcohol 25:24:1, Saturated with 10mM Tris, pH 8.0, 1mM EDTA	Sigma-Aldrich
Phosphate buffered saline,10x concentrate	Sigma-Aldrich
Pierce 16% Formaldehyde (w/v), Methanol-free	Thermo Fisher Scientific

Ponceau S, 500mL	Amresco
ProLong® Diamond Antifade Mountant	Invitrogen
Roitpuran >99,8%, Ethanol	Carl Roth

Rotiphorese - Acrylamide 30% solution 37.5:1	Carl Roth
SDS Solution	Bio-Rad
Sodium deoxycholate bioxtra, 98%	Sigma-Aldrich
Stellaris® RNA FISH Hybridisation Buffer	BioCat
Stellaris® RNA FISH Wash Buffer A	BioCat
Stellaris® RNA FISH Wash Buffer B	BioCat
TBE buffer dry tris-borate-edta, 40L	Amresco
Trichlormethan/Chloroform, ROTISOLV® ≥99,8 %, Pestilyse	Carl Roth
Tris-EDTA buffer solution, BioUltra, for molecular biology, pH 7.4	Sigma-Aldrich
Triton X 100	Carl Roth
TRIzol® Reagent	Thermo Fisher Scientific
Tween 20, 1L	Amresco
Water, Molecular Biology Reagent	Sigma-Aldrich
Enzymes and reagents	
2x RNA Loading Dye	Fermentas
50 bp DNA Ladder	Invitrogen
ACCUPRIME SUPERMIX I 200 RX	Life Technologies
BamHI-HF - 50,000 units	New England Biolabs (NEB)
CircLigase™ II ssDNA Ligase	Lucigen
cOmplete(TM) Protease Inhibitor Cocktail	Sigma-Aldrich
dNTP Set, 100mM Solutions	Thermo Fisher Scientific
Dynabeads® Protein G for Immunoprecipitation	Thermo Fisher Scientific
GlycoBlue™ Coprecipitant (15 mg/mL)	Invitrogen
Hexanucleotide Mix	Sigma-Aldrich
Hoechst 34580	Sigma-Aldrich
O'GeneRuler 50 bp DNA Ladder, ready-to-use	Thermo Fisher Scientific
Oligo dT25 Magnetic Beads - 25 mg	New England Biolabs (NEB)
ORA™ qPCR Green ROX L Mix, 2X	highQu
PageRuler™ Prestained Protein Ladder, 10 to 180 kDa	Life Technologies
Redsafe staining solution	Hiss Diagnostics GmbH

RiboLock RNase Inhibitor (40 U/µL)	Thermo Fisher Scientific
RNase I (Cloned)	Invitrogen
RNaseOUT™ Recombinant Ribonuclease Inhibitor	Thermo Fisher Scientific
SuperScript® III Reverse Transcriptase	Life Technologies
SuperScript® IV Reverse Transcriptase	Life Technologies
SYBR® Gold	Thermo Fisher Scientific
T4 Polynucleotide Kinase	New England Biolabs (NEB)
Taq DNA Polymerase with ThermoPol Buffer	New England Biolabs (NEB)
TURBODNase	Invitrogen
Powder	
Agar bacteriological, 1Kg	Amresco
Agarose	Sigma-Aldrich
Albumin from bovine serum	Sigma-Aldrich
Bicine,>=99% (titration)	Sigma-Aldrich
Bis-tris,>=98.0% (titration)	Sigma-Aldrich
Boric acid ~99%	Sigma-Aldrich
Calciumchlorid	Carl Roth
Ethylenediaminetetraacetic acid,ACS reagent, 99.4-100.06%	Sigma-Aldrich
Glycerin	Carl Roth
Glycin AnalaR NORMAPUR	VWR
Hepes free acid, 1kg	Amresco
LB Broth	Sigma-Aldrich
Milk Powder	Applichem
Sodium chloride, for molecular biology, >=98% (titration)	Sigma-Aldrich

3.1.2. List of Equipment

Table 3. List of equipment.

Equipment	Company
Herasafe KSP 1 biological safety cabinet	Thermo Fisher Scientific
Gel doc GENi	Syngene
VWR® Maxi 20 Electrophoresis System	VWR
VWR® Mini Horizontal Electrophoresis System	VWR
XCell SureLock® Mini-Cell	Novex - Thermo Fisher Scientific
Mini-PROTEAN Tetra Vertical Electrophoresis Cell	Biorad

PowerPac™ Basic Power Supply	Biorad
CL-1000 UV crosslinker	Analytic Jena
Microscope Motic AE31	Motic
Sonifier	Branson
Balance PCB	KERN
Centrifuge MICRO STAR 17R	VWR
Centrifuge SU1550	SunLab
ChemiDoc™ MP Imaging System	BioRad
Microscope (confocal) LSM 780	Zeiss
NanoDrop 1000 Photometer	Thermo Fisher Scientific
Rocking platform	VWR
Stackable shaker MAXQ 4450	Thermo Fisher Scientific
Stiring platform D-6010	NeoLab
Vortex mixer 7-2020	NeoLab
PikoReal96 Thermocycler	Thermo Fisher Scientific

3.1.3. Kits

Table 4. List of kits.

Kit	Company
DNA, RNA, and protein purification	Machery & Nagel
Effectene® Transfection Reagent	Qiagen
jetPRIME® Transfection Reagent	Polyplus
Amersham ECL Prime Western Blotting Detection Reagent	GE Healthcare
miRNeasy Mini kit	Qiagen

3.1.4. List of buffers and solutions recipes

Table 5. Buffers and solutions recipes.

Protein extraction/ Western Blot		
NET2 Buffer	5X Laemmli Buffer	10X SDS-Running Buffer
50 mM Tris-HCl, 150 mM NaCl 0,05% NP-40 H_20 Add Fresh 10 mM β-Phosphoglycerate 1x complete protease inhibitor cocktail	10% SDS 50% Glycerol 300 mM Tris pH 6.8 Bromophenol Blue	30g Tris-Base 144g Glycine 10g SDS H_2O to 1L
10X SDS-Transfer Buffer	10X TBST	Blocking Solution

15.14g Tris-Base 72.06g Glycine H_2O to 1L 20% Methanol for 1X	24g Tris-Base 88g NaCl H_2O to 1L 0,5Ml Tween 20 for 1XTBST	5% Milk / 1X TBST or 3% BSA / 1X TBST
DNA electrophoresis	Immunofluorescence	
TBE 10X	Fixation Buffer	Blocking/Permeabilizing Solution
108g Tris-Base 74g EDTA 55g Boric Acid H_2O to 1L	26mL H_2O 10mL 16% PFA 4mL 10X PBS	5% BSA 1X PBS 0.1% Triton X100

iCLIP		
Lysis Buffer	High-salt wash buffer	PNK wash buffer
RNase free H_2O 50 mM Tris- HCl, pH 7.5 100 mM NaCl 1% IGEPAL 0.1% SDS 0.5% Sodium deoxycholate	RNase free H_2O 50 mM Tris- HCl, pH 7.5 1 M NaCl 1 mM EDTA 0.1% SDS 0.5% Sodium deoxycholate 1% IGEPAL	RNase free H_2O 20 mM Tris- HCl pH 7.5 10 mM MgCl2 0.2% Tween- 20
5x PNK buffer; pH 6.5	Proteinase K buffer	Proteinase K buffer/Urea
RNase free H_2O 350 mM Tris- HCl pH 6.5 50 mM MgCl2 5 mM DTT	RNase free H_2O 100 mM Tris- Cl pH 7.5 50mM NaCl 10 mM EDTA	RNase free H_2O 7 M urea 100 mM Tris- Cl pH 7.5 50mM NaCl 10 mM EDTA
TE buffer		
RNase free H_2O 10 mM Tris-HCl pH 8.0 1 mM EDTA pH 8.0		

3.1.5. List of oligonucleotides

Table 6. Oligonucleotides used in PCR, qPCR and iCLIP assays.

Target	Primer	Sequence 5'-3'	Expected PCR product
BORA	hBORA_Exon2_fw	AACACCAGAAACTCCAGGAAGGA	334bp/ 181bp
	hBORA_Exon5_rev	AAGCTGTTTCCCTTCATGATCAGT	
CEP192	hCEP192_exon27_fw	TCAGTGGATCCAAAGAATCTACTCC	329bp /

	hCEP192_exon29_rev	AGCAGTCGTAAATGTTGAGTTGT	155bp
CSPP1	hCSPP1_Exon4_fw	TTGCGGCAAGATTACAGACGTT	323bp / 117bp
	hCSPP1_Exon5_rev	CACCTGCCTGAACTTTTCACTG	
EIF4A2	hEIFAE2_exon10_fw	TGTGCAACAAGTGTCTTTGGT	200bp / 114 bp
	hEIFAE2_exon11_rev	CAGCCACATTCATGGGCATC	
MDMD4	hMDM4_Exon4_fw	ACGTCAGAGCTTCTCCGTGA	248bp / 148bp
	hMDM4_Exon7_rev	CTCAAATCCAAGGTCCAGCCT	
SRSF3	hSRSF3_Exon3_fw	CACTATGTGGCTGCCGTGTA	696bp / 240bp
	hSRSF3_Exon5_rev	ATCGGGACGGCTTGTGATTT	
SRSF6	hSRSF6_exon2_fw	GACGCCGTTTACGAGCTGAA	498bp / 230bp
	hSRSF6_exon3_rev	AAATCTTGCCAACTGCACCG	
circGSE1	hcirc_GSE1_fw	CCAGCTTTGCCGCCGCGCTG	61bp
	hcirc_GSE1_rev	GTGGAAAGCATCCCTAGCG	
circHIPK3	hcirc_HIPK3_fw	TCGGCCAGTCATGTATCAAA	196bp
	hcirc_HIPK3_rev	CCCTTAGTGGGAGGATGAGA	
	hcirc_CAMSAP1_fw	CCCTGATGATGGCCTACACT	157bp
circCAMSAP1	hcirc_CAMSAP1_rev	TGTGCTCCTGCTCATACTGG	
circRICTOR	hcirc_RICTOR_fw	GAAAGAGACAGAATGGTCCGAGC	230bp
	hcirc_RICTOR_rev	ACCTCGTTGCTCTGTTGTATGTC	
circREV1	hcirc_REV1_fw	AGTTTCGATCAGATGCTGCTATGC	128bp
	hcirc_REV1_rev	ACCTTGGCAGCCATATACCCAC	
circGCN1	hcirc_GCN1_fw	GTGCTGGATGCTTTGGGACG	201bp
	hcirc_GCN1_rev	TCAATCAGCAAGGAGCAGAGGTC	
circSLTM	hcirc_SLTM_fw	AAGAGGACATCGAAAGTCAGG	118bp
	hcirc_SLTM_rev	GTGCCTCTTGATTCTCCAATTC	
circPLOD2	hcirc_PLOD2_fw	GAAGTCATGGAACACTATGCTG	132bp
	hcirc_PLOD2_rev	ACCTCTCCATTCTTCTCCTTGACC	
circCPSF6	m+hcirc_CPSF6_fw	TATTACAGAGAGAGAAGCAGAGAACGAGAGAG	245bp
	m+hcirc_CPSF6_rev	GCTCCTTTACCCACATCATCACCAACAG	
circAAGAB	hcirc_AAGAB_fw	GAGGAGTTGCCTGAGGAGGATG	116bp
	hcirc_AAGAB_rev	TCTCACAGCATCATTGGAAGTCAC	
circMAN1A2	hcirc_MAN1A2_2_fw	GGGCAAAGATGGATTGAAGACAACC	167bp
	hcirc_MAN1A2_2_rev	TTGCTTCTTCCAAGGCCTTCTCATG	
circexoZNF292	hcirc_exonicZNF292_fw	ACCCGGTACTGTGCACTATTCTTTC	151bp
	hcirc_exonicZNF292_rev	GGTCGGGCTTTAACATAACTTTGG	

circintZNF292	hcirc_intronicZNF292_fw	GCTCAAGAGACTGGGGTGTG	97bp
	hcirc_intronicZNF292_rev	AGTGTGTGTTCTGGGGCAAG	
circSRSF4	hcirc_SRSF4_fw	AAGACAAGCCAGGTTCCAGA	116bp
	hcirc_SRSF4_rev	TTTTGCGTCCCTTGTGAGC	
circCDYL	hcirc_CDYL_fw	CAGGCTTAGCTGTTAACGGG	60bp
	hcirc_CDYL_rev	TGTCATAGCCTTTCCACCGA	
circMTCL1	circMTCL1_fw	GCTTATTCGAAGCCTGGAGCAG	147bp
	circMTCL1_rev	CTCTAAATAACTGTCTCTCATCTCTTCCATCTC	
circRTN4	circRTN4_fw	TCTTATTGCCTCCAGATGTTTCTGCTTT	223bp
	circRTN4_rev	GCAGAGGAGCGTATCACAGG	
circSPECC1	circSPECC1_fw	AAATGTTGAAAGTAGCCCGAGCAG	162bp
	circSPECC1_rev	CGTGGGGCTGGAATGCC	
PLOD2	hlin_PLOD2_fw	CTCGAGCATCCCCACAGATAAA	282bp
	hlin_PLOD2_rev	ACTTCTTCTGGACCACCAGC	
U6	qPCR_U6-1_fw	GCTCGCTTCGGCAGC	103bp
	qPCR_U6-1_rev	AAATATGGAACGCTTCACGAATT	
	qPCR_SRSF1-3_fw	ATCTCATGAGGGAGAAACTGCC	
SRSF1	qPCR_SRSF1-3_rev	CGAGATCTGCTATGACGGGG	192bp
SRSF2	qPCR_SRSF2-5_fw	AATCCAGGTCGCGATCGAAG	188bp
	qPCR_SRSF2-5_rev	CTCCGAGCAGCACTCCTAAT	
SRSF3	qPCR_SRSF3-1_fw	CACTATGTGGCTGCCGTGTA	141bp
	qPCR_SRSF3-1_rev	TTGGAGATCTGCGACGAGGT	
SRSF4	qPCR_SRSF4-10_fw	GAGTCATTCAAGGTCTCGCTCT	104bp
	qPCR_SRSF4-10_rev	ACCTGGACCGAGATCTACTCTTA	
SRSF5	qPCR_SRSF5-5_fw	CTCACTTTGAGGGCAAGCCT	131bp
	qPCR_SRSF5-5_rev	CCGGCTAGTACTTCCTCGAAT	
SRSF6	qPCR_SRSF6-5_fw	AAAAATGGGTACGGCTTCGT	196bp
	qPCR_SRSF6-5_rev	TGCCAGATGTTCTCCGACTG	
SRSF7	qPCR_SRSF7-3_fw	CGATCCAGAGGAAGGCGATAC	237bp
	qPCR_SRSF7-3_rev	AGATCTGGACTTTGATCGGCTG	
VEGFA	hVEGFA-fw	ATCTGCATGGTGATGTTGGA	218bp
	hVEGFA-rev	GGGCAGAATCATCACGAAGT	
VEGFA165a	hVEGFA165a_ fw	AAGGGGCAAAAACGAAAGCGCA	186bp
	hVEGFA165a_ rev	TCACCGCCTCGGCTTGTCACAT	
MALAT1	hMALAT1_2_fw	TGAGTGTATGAGACCTTGCAGT	202bp
	hMALAT1_2_rev	GCAGCGGGATCAGAACAGTA	

CA9	hCA9_fw	CATCCTAGCCCTGGTTTTTGG	103bp
	hCA9_rev	GCTCACACCCCCTTTGGTT	
SNAP25	hSNAP25exon4_5junction_fw	GGATGAACAAGGAGAACAACTCGAT	223bp
	hSNAP25_exon6_rev	CCGTTCGTCCACTACACGAG	
CHAF1A	hCHAF1A_exon3_fw	TGTGAGACCACCGCAAATCA	231bp
	hCHAF1A_exonjunctio3-5_rev	CGCTCCTGATCTCTGCGGA	
PAPOLA	hPAPOLA_exon19_fw	ACACAACCAGCCATTTCTCCA	219bp
	hPAPOLA_hypjunction_19-21_rev	ATCAAGTTGTTCCTCTTCTGTTTTGGT	
SRSF6_NMD	hSRSF6-5_fw	AAAAATGGGTACGGCTTCGT	168bp
	hSRSF6_poisonexon_rev	CCCATTGGTCATGCGGCTT	
iCLIP oligonucleotides			
Preadenylated DNA adapter L3-App:		rAppAGATCGGAAGAGCGGTTCAG/ddC/	
Rt1clip	X33NN**AACC**NNNAGATCGGAAGAGCGTCGTGgatcCTGAACCGC		
Rt2clip	X33NNACAANNNAGATCGGAAGAGCGTCGTGgatcCTGAACCGC		
Rt9clip	X33NNGCCANNNAGATCGGAAGAGCGTCGTGgatcCTGAACCGC		

3.1.6. List of Antibodies

Table 7. Antibodies used in Western Blot and Immunofluorescence assays.

Western Blot				
Primary Antibody	Target	Company	Dilution	Blocking
mAb104	SR epitope of SR proteins	provided by Karla Neugebauer	1:3	3%BSA
SRSF6	SRSF6 (aa250300)	LS Biosciences (LSC290327)	1:2000	5% milk
HIF1alpha	HIF1a (aa400450)	Novus Biosciences (NB100-134)	1:1000	5% milk
Alpha-tubulin	Alpha-tubulin (aa400-C terminus)	Abcam (ab176560)	1:1000	3%BSA
Secondary Antibody		Company	Dilution	
Donkey Anti-Mouse IgG Antibody, HRP conjugate		Sigma Aldrich (AP192P)	1:10000	
Peroxidase-AffiniPure Donkey AntiMouse IgM, µ Chain Specific		Jackson ImmunoResearch (715035-020)	1:10000	

Donkey Anti-Rabbit IgG Antibody, HRP conjugate		Sigma Aldrich (AP182P)	1:10000	
Immunofluorescence				
Primary Antibody	Target	Company	Dilution	
SC35	phospho-epitope of the SC35	Abcam (ab11826)	1:200	
H2A.X	Phospho-Ser 139 of H2A.X histone	Biolegend (2F3)	2µg/mL	
Secondary Antibody		Company	Dilution	
anti-Mouse alexa fluor 555		Abcam (ab150110)	1:500	

3.2. Programs and Databases

3.2.1. Adobe Illustrator

Adobe Illustrator CC 2018 (www.adobe.com) is a software for design and illustration. All figures from this thesis were created with this software.

3.2.2. GraphPad Prism

GraphPad Prism, version 8 (www.graphpad.com/scientific-software/prism/) is a scientific software, which allows the generation of graphics and plots and performs statistical analyses. GraphPad Prism was used to generate all graphics and perform all statistical tests described in the Methods section.

3.2.3. Pubmed NCBI

The Pubmed database of the National Center for Biotechnology Information (NCBI, https://www.ncbi.nlm.nih.gov/pubmed/) contains millions of articles and citations. This database was used for the bibliographic review of this thesis.

3.2.4 Citavi

Citavi, version 6.0 (Swiss Academic Software GmbH, www.citavi.com) is a reference manager software. It was used to insert and manage the citations and reference section.

3.2.5. Refseq NCBI

The Refseq database of the NCBI (O'Leary et al. 2016), contains annotations of human transcripts. Annotations contain millions of transcripts and protein sequences from

human and other organisms. Refseq transcripts of interest were imported from NCBI to SnapGene. Refseq proteins were also acquired from this database.

3.2.6. SnapGene

SnapGene software, (from GSL Biotech; available at snapgene.com) was used to design primers. NCBI reference sequence IDs were imported to the program with features (exons, start codons and stop codons). For designing specific circRNA primers, the sequences of the circularized exons were copied and edited to generate the circular transcripts. *In silico* prediction of proteins were performed with this software for the analyses of putative alternative spliced protein isoforms.

3.2.7. Primer Blast NCBI

Primer-Blast (Ye et al. 2012) is an online available on www.ncbi.nlm.nih.gov/tools/primer-blast. This tool was used to design specific primers and predict binding to unintended targets using the Refseq human genome annotation.

3.2.7. Clustal Omega

Clustal Omega, www.ebi.ac.uk/Tools/msa/clustalo, (Sievers et al. 2011) is an online tool to perform protein, DNA and RNA sequence alignments. This tool was used to align SRSF4 and SRSF6 proteins sequences.

3.2.8. Fiji and Biovoxxel plug-in

Fiji software (Schindelin et al. 2012) available on https://imagej.net/, is an open source software to process and analyze images. It was used to quantify splicing PCR band ratios and intensities. Immunofluorescence and FISH images were also processed with Fiji to crop whole images into one cell zooms. Signal intensity profiles were plotted with the Fiji "Plot Profile" tool. The Biovoxxel tool box (Brocher 2015) available at http://www.biovoxxel.de, was used to create nuclear regions of interest (ROI) with the "Analyze Particle" tool. Fluorescence intensity as well as the solidity values from nucleus were measured using ROIs.

3.2.9. UCSC

The UCSC database (Kent et al. 2002) was used to visualize transcripts. Browser shots from iCLIP cross link sites were takes with the View-> pdf option.

3.2.10. iCount

The iCount software (Müller-McNicoll et al. 2016) was used to process RNA-protein iCLIP interaction data. Reads from iCLIP deep sequencing libraries were mapped to the Human genome assembly GRCh37 (hg19), crosslink maps were generated by keeping only the first nucleotide from each uniquely mapping read and peak calling was performed with iCount. Browser shots from SRSF6 binding sites were acquired by visualizing the grouped peaks from iCount as bed.files in the UCSC genome browser.

3.2.11. FastQC

FastQC (https://www.bioinformatics.babraham.ac.uk/projects/fastqc/) was used to perform the first quality check of RNAseq reads.

3.2.12. DESeq2

DESeq2 (Love et al. 2014) was used to calculate differential expression of genes and circRNAs from the RNAseq dataset of HeLa cells in normoxia and hypoxia conditions.

3.2.13. clusterProfiler

The clusterProfiler package from R (Yu et al. 2012) was used to analyze enrichment of differential expressed genes involved in biological processes.

3.2.14. Bowtie and STAR

The Bowtie2 (Langmead and Salzberg 2012) and STAR (Dobin et al. 2013) alignment tools were used to map RNAseq reads to the human genome (version GRCh38/hg38).

3.2.15. rMATS rMATS (Shen et al. 2014) tool was used to analyze alternative splicing in the RNAseq dataset of HeLa cells in normoxia and hypoxia conditions.

3.2.16. Find_circ and CIRCexplorer.

Find_circ (Memczak et al. 2015) and CIRCexplorer (Zhang et al. 2014) were used to identify circRNA candidates in the RNAseq dataset.

3.3. Methods

3.3.1. Cell Culture

3.3.1.1. Thawing cells

HeLa cells were frozen and kept in vials at -80°C or in liquid nitrogen. To thaw and cultivate the cells, one vial containing 500µl of frozen HeLa cells was thawed in a water bath at 37°C until only a small ice block was visible in the cell suspension. The 500µl cell suspension was transferred into a 15mL Falcon tube containing 4mL of culture medium: Dulbecco's Modified Eagle Medium (DMEM), GlutaMAX™ (Thermo Fisher Scientific) supplemented with 10% heat inactivated Fetal Bovine Serum (Thermo Fisher Scientific), 100 U/ml penicillin and 100 µg/ml streptomycin (Thermo Fisher Scientific). Cells were pelleted by centrifugation (1000xg for 5 min at 4°C). The supernatant was removed, cells were ressuspended in 1mL medium by pipetting up and down with a 1mL pipet and transferred to 10cm culture dishes containing 10mL of culture medium.

3.3.1.2. Seeding cells

When cells reached confluence, they were seeded into new 10cm plates for experiments or to maintain in culture when necessary. For seeding, the culture medium was removed and cells were washed 1x with 3mL PBS (Dulbecco's Phosphate Buffered Saline, Sigma-Aldrich). 1.5mL of Trypsin-EDTA (0.05%), phenol red (Thermo Fisher Scientific) was added to the cells and the plate was incubated for 5 min at room temperature (RT) until cells were detached. After cells were detached, Trypsin was inactivated with 3mL of fresh culture medium, cells were ressuspended by pipetting up and down with a 1mL pipet and 400µl of cell suspension were transferred to new 10cm plates containing 10mL of fresh culture medium.

3.3.1.3. Freezing cells

To freeze cells, confluent 10cm plates were trypsinized as described above. Detached cells in suspension were transferred into 15mL Falcon tubes and pelleted by centrifugation (1000xg for 5 min at 4°C). After centrifugation, the supernatant was removed

and cells were ressuspended in 2mL freezing medium: 10% DMSO (99.7% Dimethyl sulfoxide, Sigma-Aldrich) diluted in culture medium. After resuspension, 500µl of cell suspension was transferred to four cryovials. Cryovials were placed in the Mr. Frosty freezing container (Thermo Fisher Scientific) containing Isopropanol (2-Propanol, VWR) and transferred to -80°C for 24h. After 24h inside the Mr. Frosty, cells were stored in boxes at -80°C for short-term storage or in a liquid nitrogen tank for long-term storage.

3.3.2 Generation of SRSF4-GFP and SRSF6-GFP cell lines

Glycerol stocks of *E. coli* DH10 cells containing the BACs with complete *SRSF4* and *SRSF6* genes, green fluorescent protein (GFP) sequence, kanamycin and chloramphenicol resistance genes sequences were stably inserted in HeLa wild type cells as previously described (Poser et al. 2008). In the next subsections a brief description of the method is provided.

3.3.2.1. Bacterial artificial chromosome (BAC) Isolation

To isolate BACs, *E. coli* DH10 cells were streaked on Lysogeny broth (LB) plates containing 50µg/mL of kanamycin (Sigma-Aldrich) and chloramphenicol (Sigma-Aldrich) and incubated at 37°C overnight. Single colonies were picked and transferred to 2mL tubes containing LB medium supplemented with kanamycin and chloramphenicol (50µg/mL) and incubated at 37°C on thermomixer for 6 hours. From this culture, 20µL were transferred to 100mL Erlenmeyer flasks containing 20mL LB medium supplemented with kanamycin and chloramphenicol (50µg/mL) and let grow overnight on a shaker at 37°C. BACs were then isolated using the BAC prep kit (Macherey & Nagel) following the manufacture´s protocol. After isolation, BAC DNA was ressuspended in Tris-EDTA buffer and the concentration was measured with a NanoDrop (Thermo Fisher Scientific).

3.2.2. BAC transfection

For transfection, 50 µl of HeLa wild type (WT) cells were seeded from a confluent 10cm plate into 6 well plates. The next day, cells were transfected with 1µg of isolated BAC plasmid DNA using Effectene transfection kit (Qiagen) following the manufacture’s

protocol. After 24h, the medium containing transfection reagent was removed and replaced with new medium supplemented with 4.5mg/ml of Geneticin (Thermo Fisher Scientific). Cells with the BAC integrated into their genome carry a Geneticin resistance gene and are thereby selected upon Geneticin treatment. WT cells were kept as control, which should not survive in medium containing Geneticin. After cells reached confluence, they were transferred to 10cm plates and cultured as previously described.

The resulting cells that contain the BAC express GFP-tagged proteins at different levels. To obtain cell lines with homogenous GFP expression levels, SRSF4- and SRSF6GFP expressing cell pools were sorted by FACS (Fluorescence activated cell sorting of live cells) into low and high expresser pools (SRSF6(L)-GFP, SRSF6(H)-GFP and SRSF4(H)-GFP). After sorting, the pools were expanded and cultured as previously described for the experiments.

3.3.3. Hypoxia treatment

For hypoxia experiments, HeLa WT and GFP-tagged cell lines were seeded in 10cm plates 24h prior to hypoxia incubation. Due to the observed fast growth of HeLa cells upon hypoxia conditions, for the 24h hypoxia treatment 30% less cells were seeded than for the normoxia and 4h hypoxia treatment plates. After 24h, cells were either left in a normal incubator for normoxia and 4h hypoxia treatment (21% O_2 , 5% CO_2, 37°C) or transferred to an hypoxia station (0.2% O_2, 5% CO_2, 37°C) (Hypoxiastation H35, Don Whitely Scientific Limited). For the 4h treatment, cells were transferred to the hypoxia station 4h before the 24h hypoxia treatment finished. When the 4h and 24h treatment was complete, hypoxic cells were harvested inside the chamber. Normoxic cells were harvested beforehand using the same procedures, described in the topic cell harvesting.

3.3.4. Cobalt chloride treatment

To induce HIF1a stabilization in normal O_2 conditions, cells were treated with Cobalt chloride ($CoCl_2$) (Sigma-Aldrich). Cells were seeded in 10 cm plates and let grown until 60-80% confluence was reached. New medium was then added to the cells with 250 µM of $CoCl_2$ (24h $CoCl_2$) or without (control and 4h $CoCl_2$). 4 hours before the 24h treatment was

finished, new medium with 250 µM of $CoCl_2$ was added to the 4h treatment plate. All cell plates were harvested at the same time (by the end of the 24h treatment).

3.3.5. Cycloheximide treatment

To inhibit translation and study nonsense-mediated decay target transcripts, a cycloheximide (CHX) treatment was performed in cells in hypoxia and normoxia conditions. For that, cells were seeded and incubated in normoxic and hypoxic conditions as previously described. 2 hours prior harvesting, 100 µg/ml of CHX (Sigma-Aldrich) or DMSO (99.7% Dimethyl sulfoxide, Sigma-Aldrich) was added to the culture medium.

3.3.6. *Knock down*

3.3.6.1. *SRSF6* knock down

SRSF6 knock down (KD) was performed in WT HeLa cells in normoxic conditions. Cells were cultivated in 10cm dishes and seeded 24h prior to the KD into 6-cm dishes (as described in 3.2.1.2). 150µl of cells from a confluent 10cm dish were seeded. Two siRNAs targeting two different sequences of the *SRSF6* transcript were used for the KD (siRNA sequences are listed on Table 8). The two siRNAs were pooled and transfected into HeLa cells in a total concentration of 66nM. The mission universal negative control siRNA (Sigma Aldrich) was used as control. The transfection was performed using jetPRIME® Transfection Reagent (Polyplus) as recommended by the manufacturer. After 48h KD, cells were harvested as described in 3.3.7.

3.3.6.2. *MALAT1* knock down

MALAT1 KD was performed in HeLa WT cells in normoxia and hypoxia conditions. A scheme of the KD strategy is illustrated on Figure 14. For the KD, 350µl and 500µl of cell suspension were seeded into 10cm dishes 24h before the experiment (as described in 3.3.1.2). The next day, two antisense oligonucleotides containing five 2′-Omethoxyethyl nucleotides at the 5′ and 3′ ends to support RNase H activity (ASOs) complementary to two different regions of *MALAT1* were transfected into HeLa cells (sequences were acquired from Tripathi et. al, 2010, Table 8). ASOs containing a sequence complementary

to the Luciferase mRNA were used as control. The transfection was performed as described by the manufacturer. A total concentration of 12.5nM of ASOs was used for the KD and control.

After transfection, cells were kept in normal incubator (21% O_2) for 8h. After 8h, medium containing the ASOs was removed and new medium was added to the cells. The less confluent dishes were transferred to the hypoxia chamber (0.2% O_2) for 24h hypoxia treatment. After 24h, normoxic and hypoxic KD and control cells were harvested as described in 3.3.7.

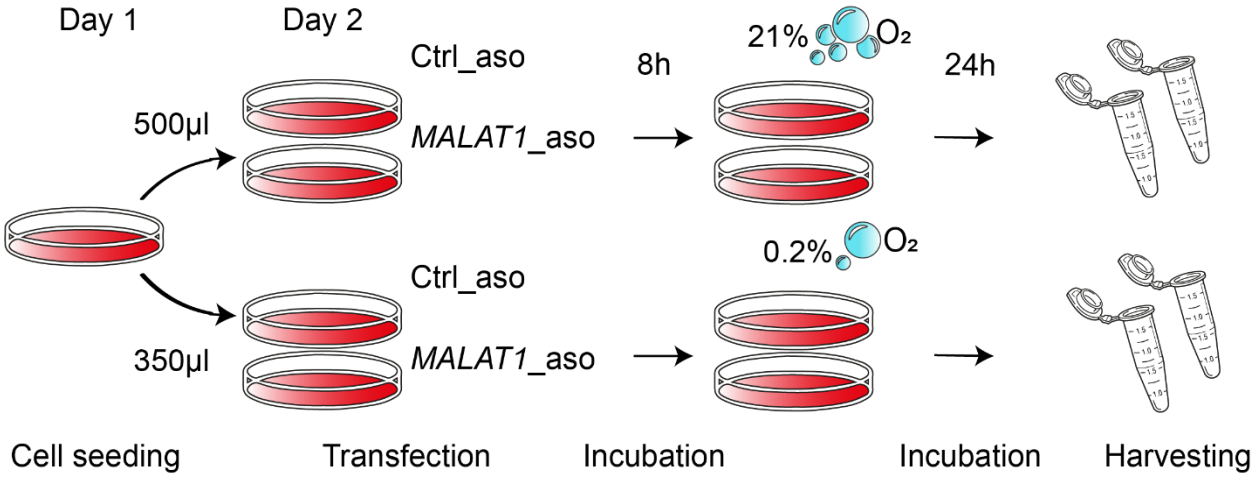

Figure 14. Schematic of *MALAT1* KD experiment in normoxia and hypoxia.

Table 8. siRNAs and ASOs information.siRNAs were predesigned and acquired from Sigma. Sequence start indicates the first base number from the transcript were the siRNA was designed (NM_006275). Complete sequence is not offered by the company.

Name	Target	Sequence	Company
MISSION® siRNA Universal Negative Control	No target	Unknown	Sigma-Aldrich
SASI_Hs02_00341239	*SRSF6*	Seq. start: 1235	
SASI_Hs02_00341240	*SRSF6*	Seq. start: 1129	
Luc_ASO	Luciferase	TCGAAATGTCCGTTCGGTTG	Integrated DNA technologies
*MALAT1*_ASO_1	*MALAT1*	GGGAGTTACTTGCCAACTTG	
*MALAT1*_ASO_2	*MALAT1*	ATGGAGGTATGACATATAAT	

3.3.7. Cell Harvesting

After experiments were performed, cells were harvest for protein and RNA extraction. Culture medium was removed and cells were washed 2x with 1xPBS (Phosphate buffered saline, 10x; Sigma-Aldrich, diluted in distilled water). For hypoxia experiments, cells were harvested inside the hypoxia station, which has a temperature of 37°C, to maintain hypoxia response transcripts and protein levels. Normoxic cells were harvested at room temperature, but washed with pre-warmed PBS at 37°C to increase comparability. After washing, 1mL of PBS was added to the plate and cells were scraped and collected in 1.5mL tubes. Tubes were centrifuged for 5 min at 1000xg, 4°C and the supernatant was removed from the cells. Cell pellets were either snap-frozen in liquid nitrogen for subsequent protein extraction or ressuspended in TRIzol (Thermo Fisher Scientific) for RNA extraction. Pellets and TRIzol suspension were stored at -80°C.

3.3.8. RNA extraction

Total RNA was extracted from cells using TRIzol. After performing the experiments in 10cm plates and harvesting the cells as previously described (3.3.7), pellets were ressuspended and lysed in TRIzol (Thermo Fisher Scientific) (500ul for half a 10 cm plate and 1 mL for an entire 10cm plate) and placed in the freezer (-80°C) for at least 2 hours prior to extraction. Lysates in TRIzol were thawed on ice and 100ul of chloroform (Carl

Roth) was added per 500ul of TRIzol. RNA/DNA were phase separated from proteins by centrifugation (17000xg for 15 min at 4°C) and transferred to a new tube.

RNA was precipitated with isopropanol (Sigma Aldrich) (1:1) for at least 30 min on ice. After precipitation, RNA was pelleted by centrifugation (17000xg for 25 min at 4°C) and pellets were washed with 440ul of 70% ethanol (100% ethanol - VWR - diluted in RNase free water – Sigma Aldrich) (12000xg for 5min at 4°C). A DNase treatment was then performed with 4U of TurboDNase (Thermo Fisher Scientific) for 30 min at 37°C to clean the RNA from genomic DNA. A second precipitation was performed with 100% ethanol (VWR) and 3M sodium acetate pH 5.5 (Life Technologies) overnight at -80°C. On the next day, RNA was pelleted (17000xg for 25 min at 4°C) and washed with 70% ethanol (12000xg for 5min at 4°C). After removing ethanol and drying the RNA pellets, they were ressuspended in RNase free water by pipetting up and down and 5 min incubation at 37°C. RNA was then quantified using a Nanodrop and stored at -80°C.

3.3.9. RNA sequencing samples preparation

HeLa cells were cultured in normoxic (21%O_2) and hypoxic (0.2%O_2) conditions for 24h. Cells were harvested and total RNA was extracted using the miRNeasy Mini kit (Qiagen), according to manufacturer instructions. 500 ng RNA were quality checked on a 1% agarose gel. rRNA was depleted using the RiboZero kit (Zymo). Libraries were prepared and sequenced on an Illumina NextSeq500 sequencer with HighOutput (75-nt single-end reads). The sequencing resulted in ca. 100 Mio reads per sample.

3.3.10. UV Cross-linking and ImmunoPrecipitation (iCLIP)

HeLa SRSF6(L)-GFP cells were grown in normoxia and hypoxia conditions (4h and 24h) as described in section 3.3.3. Before harvesting, cells were UV-irradiated one time with 150mJ/cm^2 at 254nm. Two 10cm dishes were pooled per sample, and one noncross-linked sample was kept as negative control. Cells were harvested and pellets were snap-frozen in liquid nitrogen. The iCLIP experiment and the library preparation was performed by Francois McNicoll according to (Huppertz et al. 2014). All buffers and reagents used for the iCLIP experiment are listed in Table 5. In brief, cells were lysed in 1mL lysis buffer and RNA was partially digested to lengths of 80-200 nucleotides with RNase I (Invitrogen) for 5 min at 37°C. After digestion, SRSF6-GFP protein was immunoprecipitated using Protein

G Dynabeads® (ThermoFisher Scientific) coupled with an anti-GFP antibody (12µg, provided by D. Drechsel, MPI-CBG, Dresden) for 2 hours at 4°C on a rotating wheel. Bound RNA fragments were dephosphorylated using T4 polynucleotide kinase (PNK) (New England Biolabs) and an L3 linker (IDT) was ligated to the 3'end of the RNAs overnight using T4 ssRNA ligase (New Englands Biolabs). Ligated RNA fragments were radioactively labeled with P^{32} at their 5'end and a Western Blot was performed to stringently purify and size select all RNA fragments that were cross-linked to SRSF6. Cross-linked RNA was extracted from the membrane by degrading all proteins with Proteinase K (Thermo Fisher Scientific). Isolated RNA fragments were reverse transcribed with Superscript IV (ThermoFisher Scientific) and barcoded RT-primers that anneal to the L3 linker (sequences on Table 6). cDNA fragments were resolved on a 6% TBU acrylamide gel (Invitrogen) and fragments of 150 to 300 bp were cut from the gel. After purification, cDNA fragments were circularized using CircLigaseTM (Epicentre) and re-linearized by *Bam*HI (NEB). The final cDNA libraries containing now 5' and 3' adapters were amplified using AccuPrime (ThermoFisher Scientific) and sequenced on an Illumina HiSeq2000 machine (single-end 75 nucleotide reads, 20 million reads per replicate).

3.3.11. Analysis of RNA-Seq and iCLIP data

RNAseq data analysis were performed by Antonella Di Liddo.

RNAseq reads were quality controlled using FastQC. Reads with Phred score >20 and with more than 20 nucleotide length were filtered using Flexbar (version 2.5). Reads were mapped to the human genome (version hg38/GRCh38) based on GENCODE annotation (release 24). Reads were mapped with STAR (Dobin et al. 2013) a spliceaware mapper, which can predict linear and chimeric junctions. Differential expression analysis was performed with DESeq2 (Love et al. 2014), and an adjusted P-value of 0.05 was considered for the differentially expressed genes (DEGs). Splicing analyses were performed with rMATS version 3.2.5 (Shen et al. 2014). Significant alternative splicing events were considered above a false discovery rate (FDR)<0.05 and change in percentage splice in ($|\Delta PSI|$) ≥ 10%. Chimeric junctions from STAR were used for the circular RNA prediction tool CIRCexplorer (Zhang et al., 2014). Reads were also mapped

with the alignment tool Bowtie2 (Langmead and Salzberg, 2012) and unmapped reads were used with the Find_circ tool (Memczak et al., 2015) to predict circRNAs.

Analysis of the iCLIP sequencing data was performed using the iCOUNT package (http://icount.biolab.si) with default options by Michaela Müller-McNicoll and Igor Ruiz de Los Mozos. Briefly, adapters and barcodes were removed from all iCLIP reads before mapping to the human genome (version hg19/GRCh19) based on GENCODE annotation. After analysis of reproducibility, replicates were pooled to allow determination of statistically significant cross-link events (X-links). For this, all uniquely mapping reads were used, PCR duplicates were removed using the random barcodes within the 3'adapter, X-link sites were extracted (1st nucleotide of the read) and randomized within co-transcribed regions. Significant X-links (false discovery rate [FDR] <0.05) were calculated using normalized numbers of input X-links as previously described (König et al., 2010). The entire iCOUNT script for the analysis is available on github: https://github.com/tomazc/iCount.

For quantification of significant X-links in genes and genic regions, significant Xlinks were counted into transcript regions using human hg19 transcript coordinates using the iCount annotate and segment functions respectively.

All unique X-link events were used to generate the RNA maps. Bedgraph files were downloaded from iCOUNT and imported into R using import.bedGraph and corrected for score and strand. The rMATs output table including the genomic coordinates of the regulated and flanking exons were loaded into R and converted into a Granges object. The region around regulated exons (and upstream and downstream constitutive exons) was extended by 300 nt in both directions using flank. Crosslink sites were counted in the extended regions using countOverlaps and attributed to the 5'ss or 3'ss. RNA maps were plotted with R plot.

For motif searching, a z-score analysis for enriched k-mers was performed as described previously (König et al., 2010). Sequences surrounding significant X-links were extended in both directions by 30 nucleotides (windows: -30 to -5 nt and 5-30 nt). All occurring k-mers within the evaluated interval were counted and weighed. Then a control dataset was generated by 100x randomly shuffling significant X-links within the same genes, and a Z-score was calculated relative to the randomized genomic positions. The

top 20 k-mers were aligned to determine the *in vivo* binding consensus motif. Sequence logos were produced using WebLogo (http://weblogo.berkeley.edu/logo.cgi).

3.3.12. Reverse Transcription

To perform splicing analyses and quantitative PCRs (qPCR), cDNA was synthetized from total RNA by reverse transcription. For reverse transcription, 2ug of total RNA were diluted in water in a final volume of 10ul. Reverse transcription primers (random hexanucleotide mix and oligodT; Sigma Aldrich) were mixed with dNTPs (Thermo Fisher Scientific) (1:1 ratio) and added to the RNA dilution. RNA was denatured at 65°C for 5 minutes and cooled down to 4°C until the mastermix was added. The master mix was prepared (1X First Strand buffer, 0.1M DTT and 40U of Ribolock RNase Inhibitor- Thermo Fisher Scientific) and added to the samples together with 200U of SuperScript III (Thermo Fisher Scientific). As a control one of the samples was prepared with only the master mix and no Superscript was added (RT- control). The program was resumed and reverse transcription was performed for 60 min at 50°C. Reaction was inactivated by incubation at 75°C for 15 min. After reverse transcription, cDNA was stored at -20°C until use.

3.3.13. Splicing analyses

For splicing PCRs, cDNA was obtained as described above. To detect cassette exon (CE) inclusion/skipping events, primers were designed to anneal on the upstream and downstream exons flanking the CE. Primers were designed using SnapGene and the sequences were blasted to the human Refseq database using PrimerBlast. PCR was performed using Taq DNA polymerase (New England Biolabs). Protocol and concentrations are described in Table 9. Primers used for splicing analyses are listed in Table 6. DNA loading dye (Orange DNA loading dye 6X - Thermo Fisher Scientific) was added to PCR products and these were resolved on agarose gels (2% agarose, dissolved in 0.7X TBE). A 50bp DNA ladder (O' GeneRuler 50bp DNA Ladder; Thermo Fisher Scientific) was used to estimate the PCR products size. Gels were stained with RedSafe staining solution (Hiss Diagnostics) and images were acquired with a GelDoc station (Syngene). Quantification of the isoforms and isoform fractions was performed with Fiji and graphics/statistics with GraphPad Prism (Figure 15).

Table 9. Taq PCR protocol and program.

Taq PCR Protocol	Taq PCR program		
20.9 µl water	95°C	30 sec	
2.5 µl 10x Taq buffer	95°C	30 sec	
0.5 µl 10 mM dNTPs Mix 0.125 µl Taq	60°C	30sec	**30 cycles**
0.5 µl 10mM forward primer	68°C	(1min per kb)	
0.5 µl 10mM reverse primer	68°C	5 min	
1µ cDNA	4°C	Infinite hold	

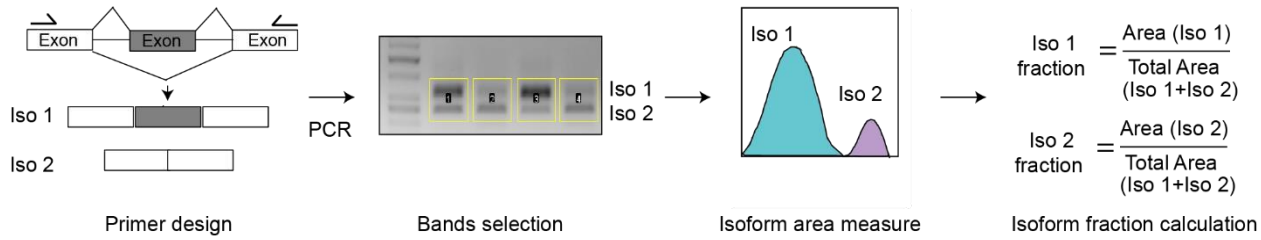

Figure 15. Quantification and calculation of isoform fractions. Primers were designed to anneal at exons flanking the cassette exons. Primers are indicated as black arrows over the exons. Splicing PCRs were performed and isoform fractions calculated with Fiji.

3.3.14. Real time PCR

For real time PCRs (qPCRs), cDNAs were diluted 1:8. The ORA^{TM} SEE qPCR Green ROX L kit (highQu) diluted to 1X was mixed with the forward and reverse primers of interest. Primers were designed using SnapGene and the sequences were blasted to the human Refseq database using PrimerBlast to avoid unspecific amplification (primer sequences are listed on Table 6). A melting curve step was added to check primer specificity in each experiment. Table 10 shows the qPCR protocol and program.

Table 10. qPCR protocol and program. A melting curve was added after the final elongation step, going from 60 to 95 degrees.

qPCR Protocol	Taq PCR program
2.5 µl ORA qPCR Master mix 1.5 µl forward and reverse primer (0.5-2µM) 1µ cDNA (1:8 dilution)	95°C 2 min 95°C 20 sec 60°C 20sec } **30 cycles** 72°C 30sec 72°C 5 min 60°C → 95°C Hold 1sec; temperature increase after hold 0.2°C 25°C Infinite hold

3.3.15. Circular RNA validation

To validate the circularity of the selected circRNAs, three methods were chosen. PolyA+ selection, RNase R treatment and PCR amplification of backsplice junctions with divergent primers. CircRNAs should be enriched in the non-polyadenylated RNA (Poly A-) fractions since they do not contain PolyA-tails, they should be resistant to exonuclease treatment with RNase R and only amplifiable with divergent primer pairs that amplify the backsplicing junctions. After PolyA selection and RNase R treatment, RNA was reverse transcribed into cDNA as described in 3.3.9. PCRs with divergent (circRNAs-specific) and convergent (linear RNA-specific) primers were performed to estimate the circRNA abundance in the respective samples. Linear isoforms (linRNA) cannot be amplified with circRNA junction primers. PCR with Taq DNA polymerase was performed as described in 3.3.10, circRNA and linRNA primers are listed in Table 6.

3.3.15.1. PolyA+ selection

Total RNA was extracted from HeLa cells as previously described (3.2.8). For PolyA+ selection, Oligod$(T)_{25}$ magnetic beads (New England Biolabs) were used following the manufacturer protocol with slight modifications. In brief, 10µg of total RNA were incubated with binding buffer for 5 minutes. Next, RNA solution was added to 100µl beads (pre-washed with binding buffer) and incubated for 10min at RT. After incubation, the

supernatant was transferred to a new tube as PolyA- fraction. PolyA+ RNA bound to the beads was washed and eluted as described in the manufacturer protocol. To thoroughly clean the PolyA- fraction from the remaining PolyA+ RNA, the PolyA- supernatant was incubated one more time with fresh beads. In the end, both PolyA+ fractions were pooled. PolyA- and A+ fractions were precipitated overnight with 100% ethanol and 3M NaAc pH 5.5. On the next day, RNA was pelleted (17000xg for 25 min at 4°C) and washed with 70% ethanol (12000xg for 5min at 4°C). PolyA+ and PolyA- RNA were ressuspended in 15µl of RNase-free water and stored at -80°C until reverse transcription was performed.

3.3.15.2. RNase R treatment

For RNase R treatment 10µg of total RNA was incubated with or without 10 units of RNase R (Epicentre), 1x RNase R buffer and RNase-free water to a final volume of 20µl. Incubation was performed for 40min at 37°C in a thermomixer at 1100 RPM. Next, samples were incubated at 95°C for 3min to inactivate the RNase R. After treatment, RNA was precipitated overnight. On the next day, RNA was pelleted (17000xg for 25 min at 4°C), washed with 70% ethanol (12000xg for 5min at 4°C), ressuspended in 20µl of RNase-free water and stored at -80°C until reverse transcription was performed.

3.3.16. Protein Extraction

Cell pellets were thawed on ice for 10 min, then NET2 buffer with 25X cOmplete™ Protease Inhibitor Cocktail (Roche) and 1M B-phosphoglycerate was added to the pellets to lyse the cells (NET2 buffer receipt on Table 5). Lysates were sonicated for 30 sec at 20% amplitude and cleared by centrifugation for 10 min, 13000 RPM at 4°C. Supernatants were transferred to new tubes and protein concentration was quantified with Quick Start™ Bradford 1x Dye Reagent (Biorad) on a Nanodrop. After quantification, samples were diluted so all the samples had same amount of protein as the less concentrated sample. Laemmli buffer (receipt on Table 5) was added to the lysates and protein denaturation was performed by incubating the samples at 95°C for 5 min. Samples were stored at 20°C until loaded onto SDS gels.

3.3.17. Western Blot

Around 30ug of protein were loaded onto an home-made SDS gel (receipt in Table 11) or pre-cast gradient gels (NuPAGE™ 4-12% Bis-Tris Protein Gels; Thermo Fisher Scientific). Gels were run at 150V for around 45 min and transferred onto nitrocellulose membranes (0.1um pore size) according to the recommendations of the used system (BioRad for home-made gels and NOVEX for pre-cast gels). After blotting, the membranes were blocked for 2 hours with either 3% BSA or 5% milk solution diluted in TBST, depending on the antibody (Buffers and solutions receipts are listed on Table 5). Primary antibodies were added to the membranes and these were incubated overnight at 4°C or for 2 hours at RT. After primary antibody incubation, membranes were washed 2 times with TBST for 15 min and secondary antibody was added (1:10000 dilution) for 4560 min. All antibodies and dilutions used on this study are listed on Table 7. Membranes were washed two more times with TBST and developed on Chemiluminescent Imager (Biorad) using ECL Prime detection reagent (GE Healthcare). Multiple exposure time pictures were acquired and saved. Images were subsequently processed and protein quantification was performed with Imagelab software (Biorad).

Table 11. SDS-PAGE gel receipt

Solution	Separation Gel (8%)	Stacking Gel (4%)
Water	2.05 ml	1.22 ml
30% Bis-Acrylamide	1.6 ml	260 µl
1M Tris-HCl pH 8.8	2.25 ml	-
1M Tris-HCl pH 6.8	-	500 µl
10% SDS	60 µl	20 µl
10 % APS	30 µl	25 µl
TEMED	10 µl	2.5 µl

3.3.18. Fluorescence and Immunofluorescence microscopy

To acquire fluorescent images of the GFP-tagged proteins in the SRSF6-GFP and SRSF4-GFP cell lines, coverslips were added to the dishes before cells were seeded for experiments. After experiments were performed, the cells were harvested as described on 3.3.7. During cell harvesting, after the first wash with 1X PBS, coverslips were removed

from the dishes and transferred to 24 well plates. Cells grown on the coverslips were fixated with 4% Paraformaldehyde solution (PFA) (diluted from 16% Paraformaldehyde; Sigma-Aldrich) for 15 minutes. For visualization of GFP-tagged proteins (fluorescence assay), cells were washed two times with 1X PBS and then incubated with Hoechst nuclear staining solution (1:4000) for 15 min. Coverslips were then washed one time with 1X PBS and placed on a paper towel for 15 min to dry. After drying, coverslips were mounted on microscopy slides with ProLong® Diamond Antifade Mountant (Invitrogen). Slides were left to dry overnight at RT and on the next day they were transferred to 4°C until imaging. For immunofluorescence, after fixation and washing, cells were incubated with blocking/permeabilizing solution (receipt on Table 5) for 30 min. After blocking/permeabilization, cells were incubated with a primary antibody diluted in 3% BSA in 1X PBS for 2 hours at RT. After primary antibody incubation, cells were washed two times with PBS. Next, cells were incubated with a secondary antibody diluted in 3% BSA in 1X PBS for 1 hour at RT. Nuclear staining and slides preparation were performed as described above for the fluorescence assay.

3.3.19. RNA Fluorescence in Situ Hybridization (FISH) and Immunofluorescence

For FISH-IF experiments, 12mm diameter coverslips were placed inside 10cm plates used for the experiments. After removing the medium and washing the cells with 1X PBS, the coverslips were collected using tweezers and transferred to 24-well plates. FISH was performed using Stellaris probes and buffers (LG Bioserch Technologies) following the manufacturer protocol with modifications for the Immunofluorescence – FISH combination. Briefly, cells were fixated with 4% Paraformaldehyde solution (diluted from 16% Paraformaldehyde; Sigma-Aldrich) for 15 minutes. After fixation, cells were washed with PBS and permeabilized with 70% ethanol for at least one hour. Next, cells were washed with Wash Buffer A and coverslips were placed in a humidified chamber and were hybridized for 16 hours at 37°C in the dark. *MALAT1* probes (Stellaris FISH Probes, Premade: Human *MALAT1* with Quasar 670 Dye) were diluted 1:100 in hybridization buffer together with the anti-SC35 antibody [SC-35] - Nuclear Speckle Marker (Abcam). After hybridization, cells were incubated for 30 min at 37°C with Wash Buffer A solution

containing 1:500 dilution of the secondary antibody (Donkey anti-Mouse alexa fluor 555, Abcam). A second incubation at 37 degrees for 30 min with Wash Buffer A was performed and Hoechst 34580 (Sigma-Aldrich) was added to the buffer for nuclear staining. Coverslips were washed for 2-5 min with Wash Buffer B and then dried for 15 minutes at RT in the dark and subsequently mounted in slides as previously described in 3.3.18.

3.3.20. Cell imaging

Cell images were acquired with a confocal laser-scanning microscope (LSM780; Zeiss) with a Plan-Apochromat 63x objective with a numeral aperture of 1.4, using immersion oil. The Zen 2012 software was used to acquire images. Images from the same experiment were acquired in the same day with the same settings for all conditions (laser power, gain, pin hole size and offset).

3.3.21. Image processing and quantification

Fiji software was used to process and analyze the acquired images of fluorescence, FISH and immunofluorescence experiments. Pictures were cropped with Image crop function and scale bars were added. Below the strategies for quantification and image processing are detailed.

3.3.21.1. Fluorescence quantification

For fluorescence quantification fields with similar numbers of cells were captured until at least 100 cells were obtained. Pictures were opened in Fiji (Schindelin et al. 2012) and the channel corresponding to Hoechst (nuclear staining) was used to acquire a threshold image (“Threshold Li”). The “Particle analyzer” plug in from the Biovoxxel toolbox (Brocher 2015) was used to obtain the nuclear Regions of interest (ROI). was used to obtain the ‘nuclear regions of interest’ (ROI). Next, nuclear ROIs were transferred to the GFP channel image and fluorescence was quantified using the ‘integrated density value’ (mean gray value per pixel x area) (Figure 16). Fluorescence values were plotted in GraphPad Prism.

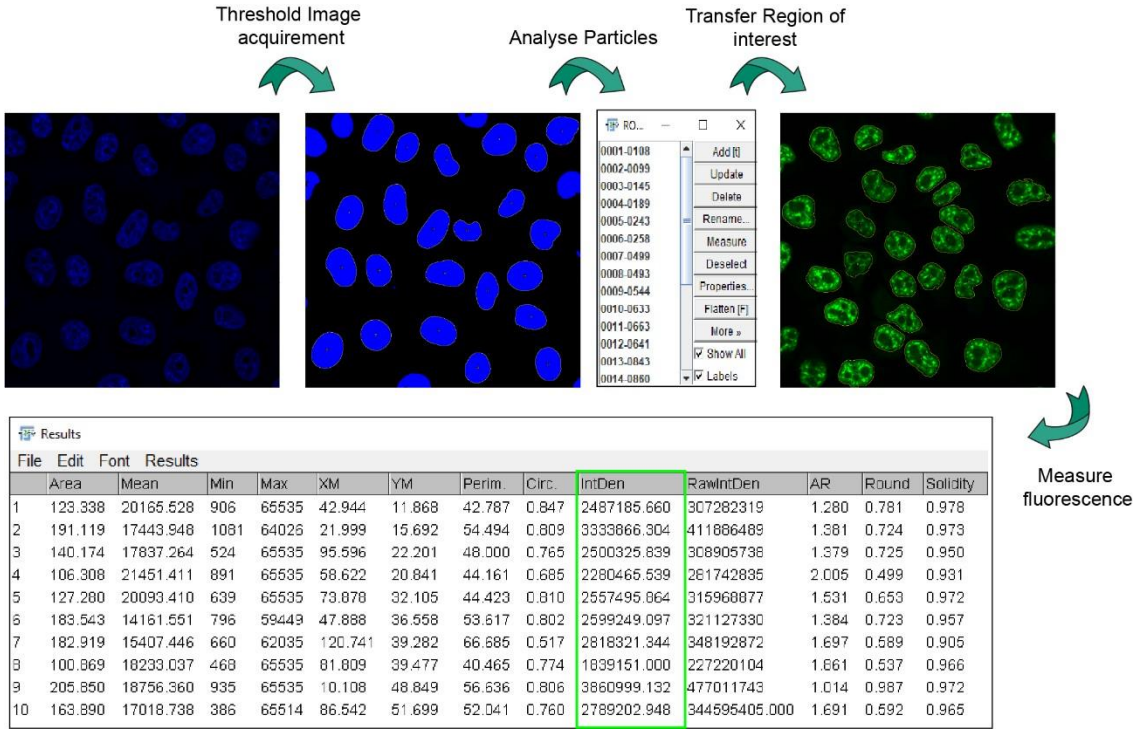

	Area	Mean	Min	Max	XM	YM	Perim.	Circ.	IntDen	RawIntDen	AR	Round	Solidity
1	123.338	20165.528	906	65535	42.944	11.868	42.787	0.847	2487185.660	307282319	1.280	0.781	0.978
2	191.119	17443.948	1081	64026	21.999	15.692	54.494	0.809	3333866.304	411886489	1.381	0.724	0.973
3	140.174	17837.264	524	65535	95.596	22.201	48.000	0.765	2500325.839	308905738	1.379	0.725	0.950
4	106.308	21451.411	891	65535	58.622	20.841	44.161	0.685	2280465.539	281742835	2.005	0.499	0.931
5	127.280	20093.410	639	65535	73.878	32.105	44.423	0.810	2557495.864	315968877	1.531	0.653	0.972
6	183.543	14161.551	796	59449	47.888	36.558	53.617	0.802	2599249.097	321127330	1.384	0.723	0.957
7	182.919	15407.446	660	62035	120.741	39.282	66.685	0.517	2818321.344	348192872	1.697	0.589	0.905
8	100.869	18233.037	468	65535	81.809	39.477	40.465	0.774	1839151.000	227220104	1.661	0.537	0.966
9	205.850	18756.360	935	65535	10.108	48.849	56.636	0.806	3860999.132	477011743	1.014	0.987	0.972
10	163.890	17018.738	386	65514	86.542	51.699	52.041	0.760	2789202.948	344595405.000	1.691	0.592	0.965

Figure 16. Quantification of GFP fluorescence with Fiji. The cell nucleus was used to acquire a threshold image. The plug in “Analyze Particle” identifies the cell number and saves the nuclear region (ROI). ROIs are transferred to the image of interest and fluorescence intensity per pixel is acquired (IntDen).

3.3.21.2. Micronuclei, DNA damage foci and nuclear shape quantification

For micronuclei quantification, fields with similar amount of cells were captured until at least 100 cells were obtained. Threshold images of the cell nuclei were acquired as described above. For each picture, the number of cells containing micronuclei were counted and the percentage relative to the total number of cells in the field was calculated. The same procedure was used for counting cells with positive phosphorylated histone H2A.x foci. The nuclear ROIs were transferred to the pH2A.x channel and cells containing pH2A.x foci were counted. Percentage of cells containing micronuclei and pH2A.x foci were plotted in GraphPad Prism. For solidity values, nuclear ROIs were measured and the solidity value was acquired from the Fiji results table, solidity values of at least 200 cells per condition were plotted in GraphPad Prism.

3.3.21.3. Line scans

To acquire the fluorescence intensity per pixel in a cell area and visualize nucleoplasm and speckle fluorescence, a straight line was drawn across the cell nucleus.

To obtain the maximum nucleoplasm and speckle signal, this line was draw from one extremity to another of the cell nucleus without going through the nucleolus. The line scans were performed in one-cell zooms to increase resolution. A straight line was traced in one channel of interest and the profile was acquired from Fiji (Analyze – Plot profile). The same line was transferred to the other channels and the fluorescence of each channel was plotted in the line area. The values of each graphic were saved and a profile for all the channels was plotted in GraphPad Prism.

3.3.22. Statistical analyses

To quantify differences between controls and treatments, isoform fractions, relative RNA levels and fluorescence intensity values were analyzed using the GraphPad Prism software. One-way ANOVA followed by Dunnett's multiple comparisons test was performed using GraphPad Prism version 8.00 for Windows, GraphPad Software, La Jolla California USA, www.graphpad.com. The same test was used to compare percentage of cells containing micronuclei in different cells lines as indicated in the results figure legends. Significance is indicated by asterisks.

4. Results

4.1. Hypoxia causes differential expression of thousands of transcripts in HeLa cells

To identify global changes of the HeLa cell transcriptome upon hypoxia stress, we performed total RNAseq of cells grown in normoxia or hypoxia conditions (24h; 0.2%). Using DESeq2 (Love et al. 2014) we quantified changes in expression and identified 7962 differential expressed genes (DEGs; padj<0.05), approximately half of them were downregulated (n: 3862, 49%) and the other half up-regulated (n: 4100, 51%) (Figure 17A). When we applied a more stringent cut-off (Log2-fold change > or < 1) we still acquired 2495 DEGs (padj<0.05). Of those, 66% were up-regulated upon hypoxia (1653) and 34% (842) down-regulated (Figure 17B). We subsequently performed a Gene Ontology (GO) analysis using GOenrich (Yu et al. 2012) to investigate in which biological processes DEGs are enriched. We found that biological processes known to be important for the response to hypoxia, such as angiogenesis and positive regulation of epithelial cell proliferation were significantly enriched among the up-regulated DEGs (Figure 17C). Confirming the efficiency of the hypoxia treatment, genes involved in aerobic metabolism and mitochondrial gene expression were mostly down-regulated. Furthermore, we found that hypoxia likely affects cell cycle progression, as genes responsible for cell cycle arrest were up-regulated and genes involved in the transition from G2 phase to mitosis were down regulated (Figure 17D). Interestingly, down-regulated genes were also highly enriched in the GO-term categories ‘mRNA splicing’ and ‘mRNA processing’ (Figure 17D). A down-regulation of splicing factors should lead to major changes in alternative splicing, such as exon skipping and inclusion, alternative 3’ and 5´UTR splice site usage or intron retention.

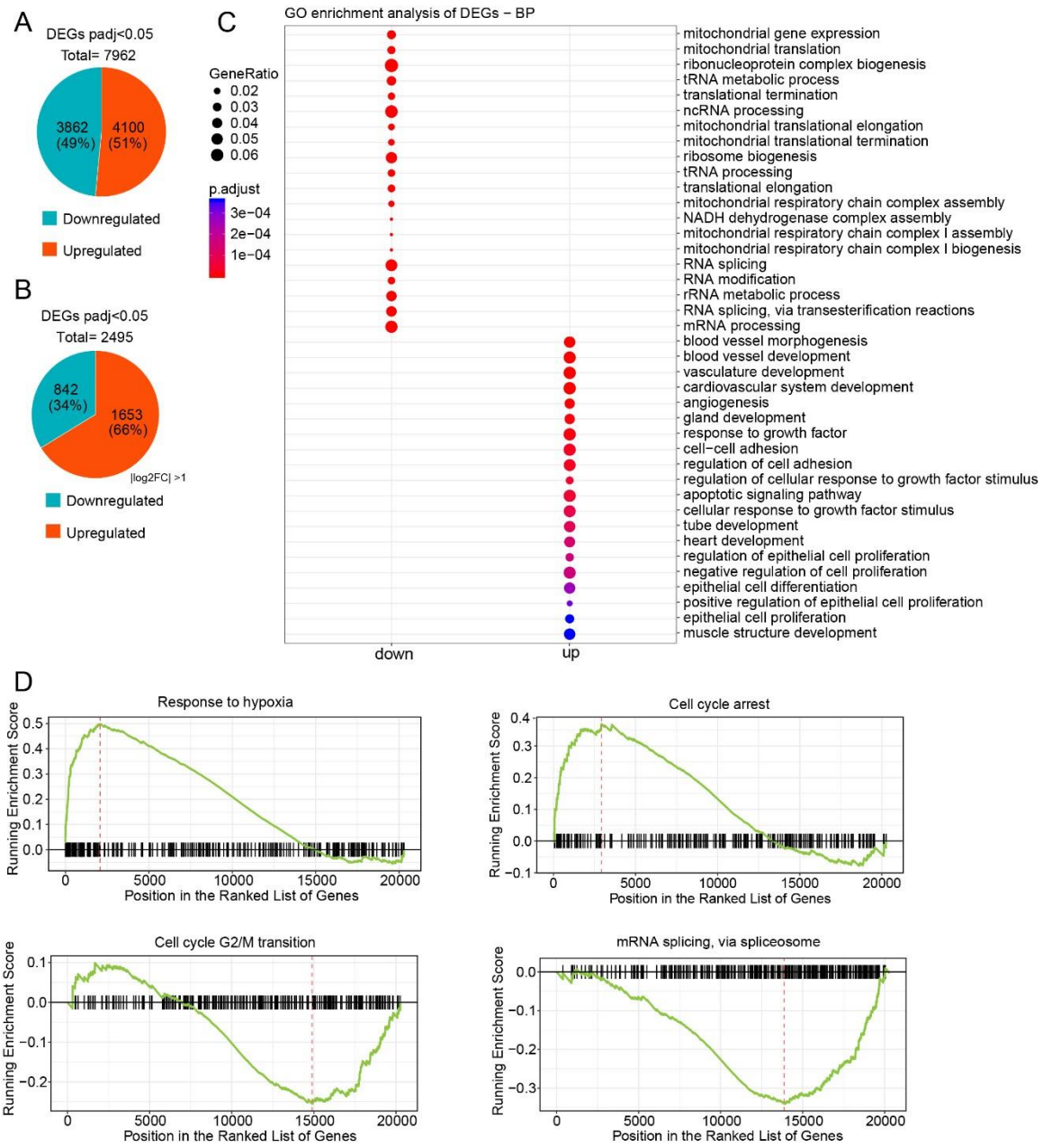

Figure 17. **Hypoxia leads to global changes in gene expression. A)** Pie chart displaying the total number of significantly differentially expressed genes (DEGs) (up and down regulated, padj<0.05) quantified using DESeq2 on RNA-Seq data comparing HeLa hypoxic (0.2% O_2) and normoxic cells (21% O_2). n= 3 replicates per condition. **B)** Pie chart displaying DEGs with Log2 fold change > or < 1.0 (up and down regulated, padj<0.05). **C)** GO-term analysis for biological processes (BP) that are enriched among DEGs (from A, padj<0.05) using GOenrich (GO). The point color represents the degree of enrichment and the point size represents the gene ratio compared to all genes annotated for the respective BP. **D)** Plots showing enrichment score profiles of DEGs assigned to 4 enriched BPs upon hypoxia. The black lines represent the genes, the X-axis indicates their ranking in the list of DEGs and the Y-axis shows their enrichment score in the GO analysis.

4.2. Hypoxia causes global changes in alternative splicing

In order to investigate changes in alternative splicing (AS) occurring upon hypoxia, we used the replicate multivariate analyses of transcript splicing (rMATs) tool (Shen et al. 2014) and applied it to the RNAseq dataset. The following splice events were analyzed: cassette exons (CE), alternative 3' and 5' splice site usage (A3SS, A5SS), mutually exclusive exons (MXE) and retained introns (IR) (Figure 18A). We identified 4434 transcripts that were alternatively spliced after 24h hypoxia. The majority of events that changed were CEs (2912 events, padj<0.05), including exon skipping or inclusion, whereby exon skipping was the most frequent splicing event in hypoxia (1783 events) (Figure 18B). Alternatively spliced isoforms were enriched in 3 BPs, related to microtubule and centrosome localization (Figure 18C). This might indicate that AS in hypoxia plays a role in the generation or expression of different protein isoforms that are involved in centrosome and microtubule organization or the regulation of the cell cycle.

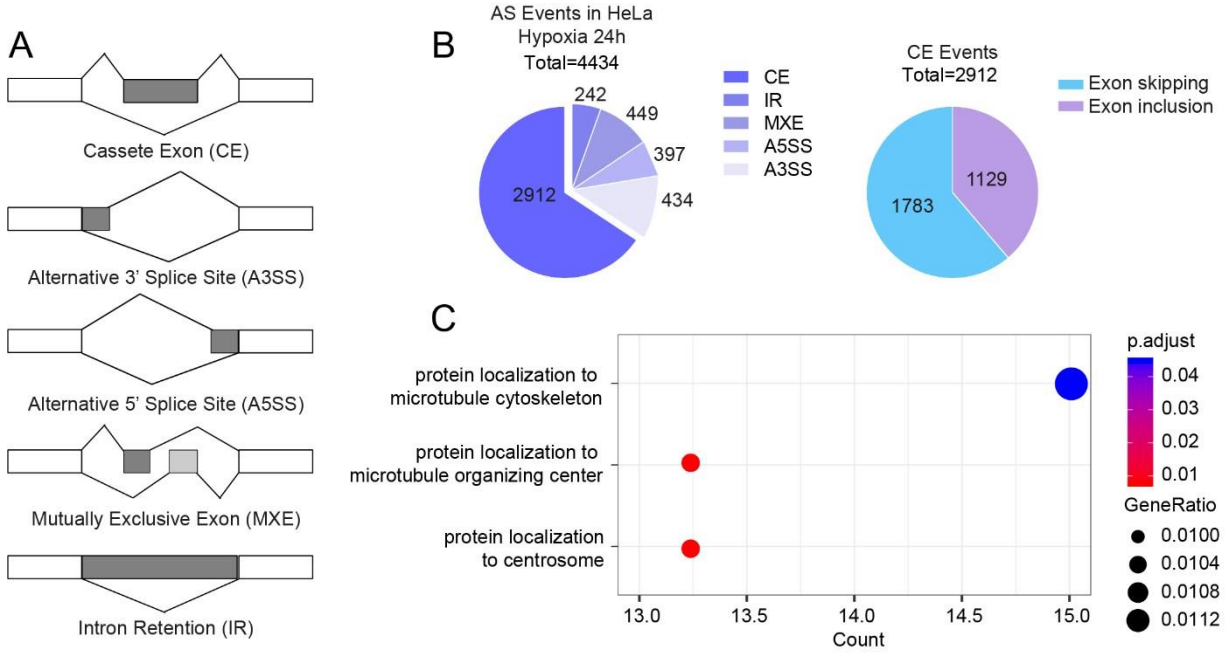

Figure 18. **Thousands of transcripts are alternatively spliced upon hypoxia**. **A)** Alternative Splicing (AS) events identified with rMATS. **B) Left panel:** Pie chart displaying significantly changed AS events (padj<0.05) comparing RNAseq data from HeLa hypoxic (0.2% O_2) and normoxic cells (21% O_2). n=3 replicates per condition. **Right panel:** Pie chart displaying all significantly changed cassette exon (CE) events, divided into exon skipping and inclusion events. **C)** GO-term analysis (BP) for AS events (from B, padj<0.05) acquired using GOenrich. The point color represents the degree of enrichment and the point size represents the gene ratio compared to all genes annotated for the respective BP.

We selected five CE splice events for validation by RT-PCR (Figure 17A). All 5 affected transcript isoforms are protein-coding genes. *BORA* (aurora kinase A activator), *CEP192* (centrosomal Protein 192) and *CSPP1* (centrosome and spindle pole associated protein 1) code for proteins associated with centrosome organization and cell cycle progression. *EIF4A2* (eukaryotic translation initiation factor 4A 2) encodes a translation initiation factor, involved in the regulation of cap-dependent translation initiation, and *MDM4* (MDM4 regulator of p53) encodes a protein involved in the regulation of apoptosis signaling. For *BORA,* exons 3 and 4 are skipped, in the *CEP192* transcript exon 28 is more included in hypoxia. *CSSP1* has an alternative exon inclusion between exon 4 and 5 in normoxia and this exon is skipped in hypoxia. *EIF4A2* AS event results in the inclusion of exons in the 3'UTR in hypoxia. Skipping of exon 6 of *MDM4* has been previously described in tumor cells; it leads to translation of a truncated protein. This truncated protein has a repressive effect on p53 and apoptosis pathway activation (Rallapalli et al. 1999). We designed primers that anneal to the upstream and downstream exons, flanking the hypoxia-skipped/included exons, and analyzed three replicates from normoxic and 24h hypoxic HeLa samples (Figure 19B). To test whether the alternative transcript isoforms generated by exon skipping or inclusion are targets of the NMD pathway, we treated normoxic and hypoxic cells with cycloheximide (CHX), which inhibits the translation-dependent NMD pathway. DMSO was used as control. Figure 19C-G shows splicing gels for the 5 selected targets as well as the calculated ratio between the isoforms.

For all targets we could validate significant differences in the isoform fraction between normoxia and hypoxia (Pvalue<0.05). Moreover, with the exception of *EIF4A2*, no significant stabilization of the alternative isoforms was detectable upon CHX treatment. This indicates that alternative isoforms generated during hypoxia are generally not targeted for degradation by NMD and should be translated into functional protein isoforms.

A

GeneID	Gene	Inclusion level hyp/norm	PValue	Gene type	log2FC Gene hyp/norm	padj Gene
ENSG00000136122	*BORA*	-0.512	2.81E-11	protein coding	0.06	0.79
ENSG00000101639	*CEP192*	0.205	2.74E-06	protein coding	0.08	0.54
ENSG00000104218	*CSPP1*	-0.29	2.20E-03	protein coding	0.13	0.46
ENSG00000156976	*EIF4A2*	-0.248	1.11E-09	protein coding	0.44	0.00
ENSG00000198625	*MDM4*	-0.304	8.00E-06	protein coding	0.27	0.02

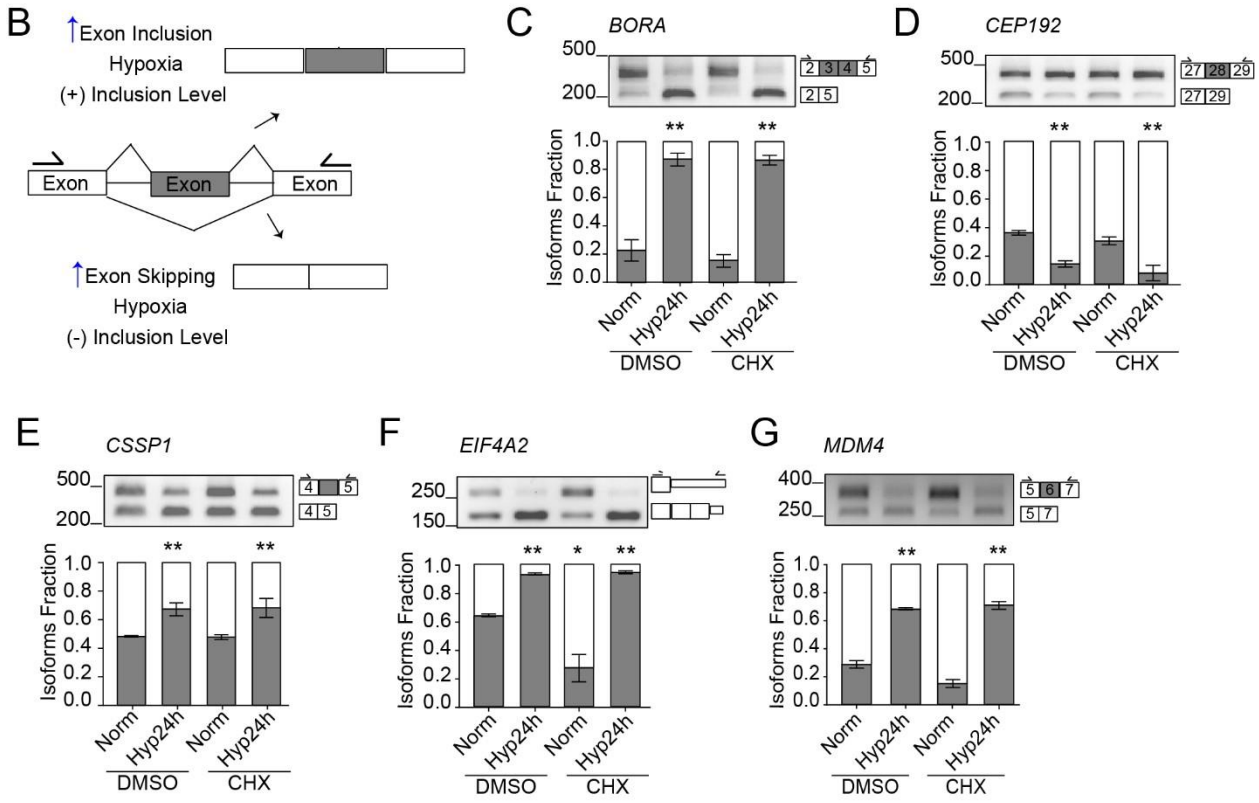

Figure 19. Validation of cassette exon (CE) events in hypoxia. A) Table showing five CE events selected for validation, including transcript IDs, gene names, inclusion level differences in hypoxia relative to normoxia, calculated Pvalues, the gene type from which the alternatively spliced transcript is transcribed, log2 fold changes of the corresponding gene quantified by DESeq2 and the respective adjusted Pvalues. **B)** Scheme of validated CE events. Black arrows above the exons indicate the primers that were designed for exons flanking the regulated CE. **C-G)** RT-PCR splicing agarose gels (2% concentration) for the five AS events. Exons which are skipped or included in hypoxia are represented in gray beside the gel. Black arrows above the exons indicate the primer position. A 50bp ladder was used for every gel. The sizes are indicated on the left side of the picture. Below the gels, the relative isoform fraction quantification is shown (n=3). The normoxic isoform is depicted in white and the alternative isoform, which is increased upon hypoxia, in grey. A T-test was performed to test for differences between the isoform ratios. Significant changes between normoxia DMSO control and each sample is shown by asterisks (*p<0.05, **p<0.01).

4.3. Hypoxia changes the abundance of several circular RNAs (circRNAs)

Our results so far show that upon hypoxia mRNA splicing is reduced and that thousands of transcripts undergo AS, particularly exon skipping, in this condition. It was recently shown that under conditions of reduced splicing also the formation of circular RNAs (circRNAs) increases through enhanced backsplicing (Liang et al. 2017). To test whether this is also true in hypoxia, we searched our RNAseq dataset for backsplicing events to identify all circRNAs that are generated in HeLa cells in normoxic and hypoxic conditions (Figure 20A). In collaboration with Antonella DiLiddo (AK Zarnack) we set up a computational pipeline and combined two circRNA prediction tools, Find_circ (Memczak et al., 2015) and CIRCexplorer (Zhang et al., 2014) to predict and quantify circRNAs (DiLiddo et al., 2019). For a high confidence set of circRNA candidates, we considered only the overlap between both tools and required at least 2 unique reads mapping to the backsplice junction. Using this approach, we identified 3,926 circRNAs that were expressed in HeLa normoxia and hypoxia cells.

We selected 9 highly expressed circRNA candidates for validation of expression and circularity using three different methods. First, we designed divergent PCR primers flanking the backsplice junction that can only amplify a PCR product from the circular transcript but not from the corresponding linear transcript (Figure 20B). Since circRNAs do not contain PolyA tails, we separated polyadenylated (PolyA+) from nonpolyadenylated (PolyA-) RNAs and verified the abundance of circRNAs and linear RNAs in these fractions by RT-PCR (Figure 20C, upper panel). Finally, due to the lack of free transcript ends, circRNAs are resistant to exonuclease activity. We performed an RNase R treatment on total RNA samples and verified whether our selected circRNAs candidates were resistant to degradation by this exonuclease (Figure 20C, lower panel). Indeed, all selected circRNA candidates were amplified with the divergent primers, enriched in the PolyA- fraction and resistant to exonuclease RNase R treatment confirming their circularity. The linear *PLOD2* transcript was used as control; it was enriched in the PolyA+ fraction and was degraded by RNase R treatment (Figure 20C).

To investigate whether circRNAs are differentially expressed upon hypoxia, we used the DESeq2 tool with slight modifications for the analysis of circRNAs (DiLiddo et. al, 2019).

We identified 22 circRNAs that were differentially expressed between normoxia and hypoxia in HeLa cells (Figure 20D). We selected 7 circRNAs (*exoZNF292, PLOD2, intZNF292, MTCL1, MAN1A2, SPECC1 and RTN4*) that were up-regulated in hypoxia, and 8 circRNAs (*SLTM, CAMSAP1, SRSF4, HIPK3, AAGAB, RICTOR, REV1* and *CPSF6*) that did not show significant differences in abundance to validate their expression changes by RT-qPCR. We could validate the differential expression of all 7 circRNAs (100%; Figure 20E), indicating that our circRNA identification pipeline works very robustly and avoids false positives. Furthermore, our results indicate that backsplicing is regulated upon hypoxia and the splicing balance is shifted to the enhanced formation of some circRNAs. In line with our previous results, these circRNAs could be formed either by enhanced exon skipping or due to decreased linear splicing activities through the downregulation of splicing factors that promote linear splicing.

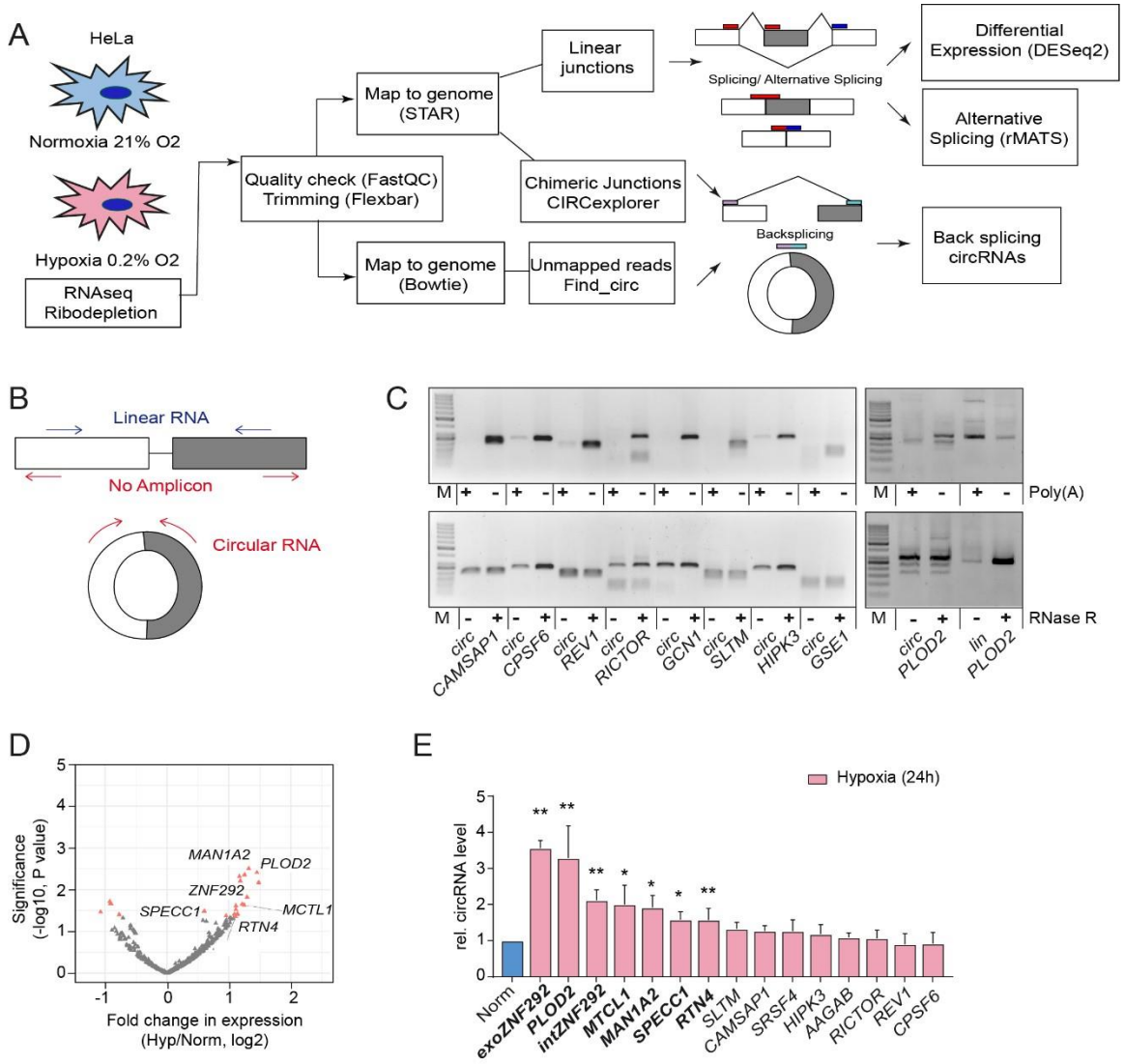

Figure 20. circRNA formation is regulated in hypoxia. A) Pipeline used for the identification and quantification of circRNAs candidates from RNAseq data of HeLa normoxic and hypoxic cells. Linear mapped reads were used for differential expression and alternative splicing analyses. Non-linear reads were used to identify circRNAs with two different tools. **B)** Scheme showing the primer design strategy for the amplification of circular and linear RNAs. Convergent primers (red) flank the backsplicing junction and amplify only circular RNAs. Convergent primers (blue) amplify only the linear spliced transcripts. **C) Upper panel:** RT-PCR using convergent and divergent primers validate the enrichment of circRNAs in the PolyA-fraction. **Lower panel:** RT-PCR from RNase R treated samples validate the resistance of circRNAs to RNase R treatment. **D)** Volcano plot showing differentially expressed circRNAs in hypoxia relative to normoxia samples. All tested circRNAs were from the high confidence dataset and had at least 5 reads mapping to the backsplice junction in at least two samples (n=3 replicates per condition). Differentially expressed circRNAs (FDR<0.05) are marked in red. Labeled circRNAs were selected for validation by RTqPCR. **E)** RT-qPCR analysis comparing the levels of 15 circRNAs in normoxia and hypoxia. Divergent qPCR primers flank the backsplice junction. CircRNAs predicted to be up-regulated in hypoxia are indicated in bold. Levels are normalized to *U6* expression and calculated relative to normoxia. All samples were (n=3, *p<0.05, **p<0.01). Figures are adapted from DiLiddo et. al, 2019.

4.4. Transcripts encoding SR proteins are differentially regulated in hypoxia

AS can be pivotal for the hypoxia response, either by promoting the expression of different protein isoforms or by regulating the levels of proteins through the expression of non-functional transcript isoforms (Sena et. al, 2014). Because of their well-known function as regulators of AS, we next investigated changes in the expression level of SR proteins upon 24h hypoxia. Our RNAseq data indicated that SR protein transcripts (*SRSF1* to *SRSR7)* are indeed differentially regulated upon hypoxia. While *SRSF2* and *SRSF4* show a significant up-regulation in hypoxia, most SR protein transcripts are downregulated, with *SRSF6* showing the strongest decrease among the SR protein family members (almost 4-fold down regulated). We validated the differential expression of SR protein transcripts by RT-qPCR (Figure 21A). The efficiency of the hypoxia treatment was confirmed using the hypoxia markers *CA9*, which is only expressed in hypoxic and oxidative stress conditions, and *VEGFA,* the vascular endothelial growth factor transcript, a known and important marker for the hypoxia response (Figure 21A).

To test whether the differential expression of SR protein transcripts is part of the transcriptional response to hypoxia via HIF1, we treated cells with $CoCl_2$, a commonly used compound that promotes HIF1 stabilization and mimics the HIF1-dependent hypoxia response. Interestingly, we did not detect a significant differential expression for any SR protein transcript after 24h $CoCl_2$ treatment, with the exception of *SRSF3,* which was slightly down-regulated (Figure 21B). This suggests that the differential expression of SR protein transcripts and particularly the down-regulation of *SRSF6* are not caused by HIF1a stabilization. *VEGFA* and *CA9* induction after 24h hours was controlled by RTqPCR to confirm the efficacy of the $CoCl_2$ treatment (Figure 21B).

It is known that SRSF6 binds to exon 8b of the *VEGFA* transcript and promotes its inclusion (Nowak et al. 2010), which favors the expression of the anti-angiogenic isoform of *VEGFA* (*VEGFA165b*). SRSF6 binding also counteracts the inclusion of exon 8a, which is bound by SRSF1, and the production of the pro-angiogenic isoform *VEGFA165a* (Figure 21C). In hypoxia, the pro-angiogenic isoform *VEGFA165a* increases, which we confirmed by RT-qPCR with primers that anneal to exon 8a (Figure 21D). *VEGFA165a* is essential for the hypoxia response in cancer cells. It is expressed and secreted by tumor

cells and promotes their migration as well as angiogenesis of endothelial cells to supply growing tumors with blood vessels (Biselli-Chicote et al. 2017). Since expression of *VEGFA165a* transcripts is inhibited by SRSF6 and SRSF6 is the most down-regulated SR protein in hypoxia, we decided to investigate the importance of this SR protein in regulating/suppressing the adaptation of cells to hypoxia conditions.

We first studied how SRSF6 down-regulation in hypoxia is achieved. Quantification of junction reads from the RNAseq data revealed that exon 3 of *SRSF6* is more included in hypoxia (3-fold; Figure 21E). This exon is called 'poison cassette exon' (PCE) as it contains a premature termination codon (PTC), and its inclusion generates *SRSF6* isoforms that should be degraded by NMD. Generation of NMD isoforms was shown to be an important mechanism for the regulation of SR protein levels, e.g. SRSF3 and SRSF1 (Jumaa and Nielsen, 1997; Shying et. al, 2010). Indeed, *SRSF3,* which is downregulated in hypoxia as well, also showed an increased inclusion of its PCE (2-fold; Figure 21F). Enhanced PCE inclusion in *SRSF6* and *SRSF3* transcripts was confirmed by RTPCR, using primers that anneal to exons upstream and downstream of the PCE (Figures
21G-H). NMD inhibition by CHX treatment confirmed the accumulation of *SRSF6* and *SRSF3* NMD isoforms in normoxic cells (Figures 21G-H). However, NMD isoforms were readily detectable in hypoxic cells, at the expense of the normal isoform, and did not accumulate further upon CHX treatment (Figures 21G-H).

These data suggest that the levels of normal protein-coding *SRSF3* and *SRSF6* transcript isoforms decrease in hypoxia due the increased generation of NMD isoforms, but their degradation is inhibited in hypoxia, likely due to a general NMD inactivation. Indeed, it has been shown that NMD is inhibited in different stress conditions including hypoxia (Gardner, 2008). The stable presence of PTC-containing transcripts and their translation could give rise to truncated protein isoforms that might fulfill specific functions in the hypoxia adaptation. Indeed it was recently shown that a truncated form of the translation initiation factor EIF2B5 contributed to the inhibition of translation in hypoxia (Ref Brady, 2017). Unfortunately, due to the lack of antibodies specific for the N-terminus of the proteins, we were not able to detect truncated protein isoforms for SRSF6 or SRSF3 in hypoxia samples. 24h $CoCl_2$ treatment did not accumulate *SRSF3* and *SRSF6* NMD

isoforms (Figure 21I), which could explain why *SRSF3* and *SRSF6* transcripts were not down-regulated in this treatment condition, and suggest the requirement of a cellular stress response.

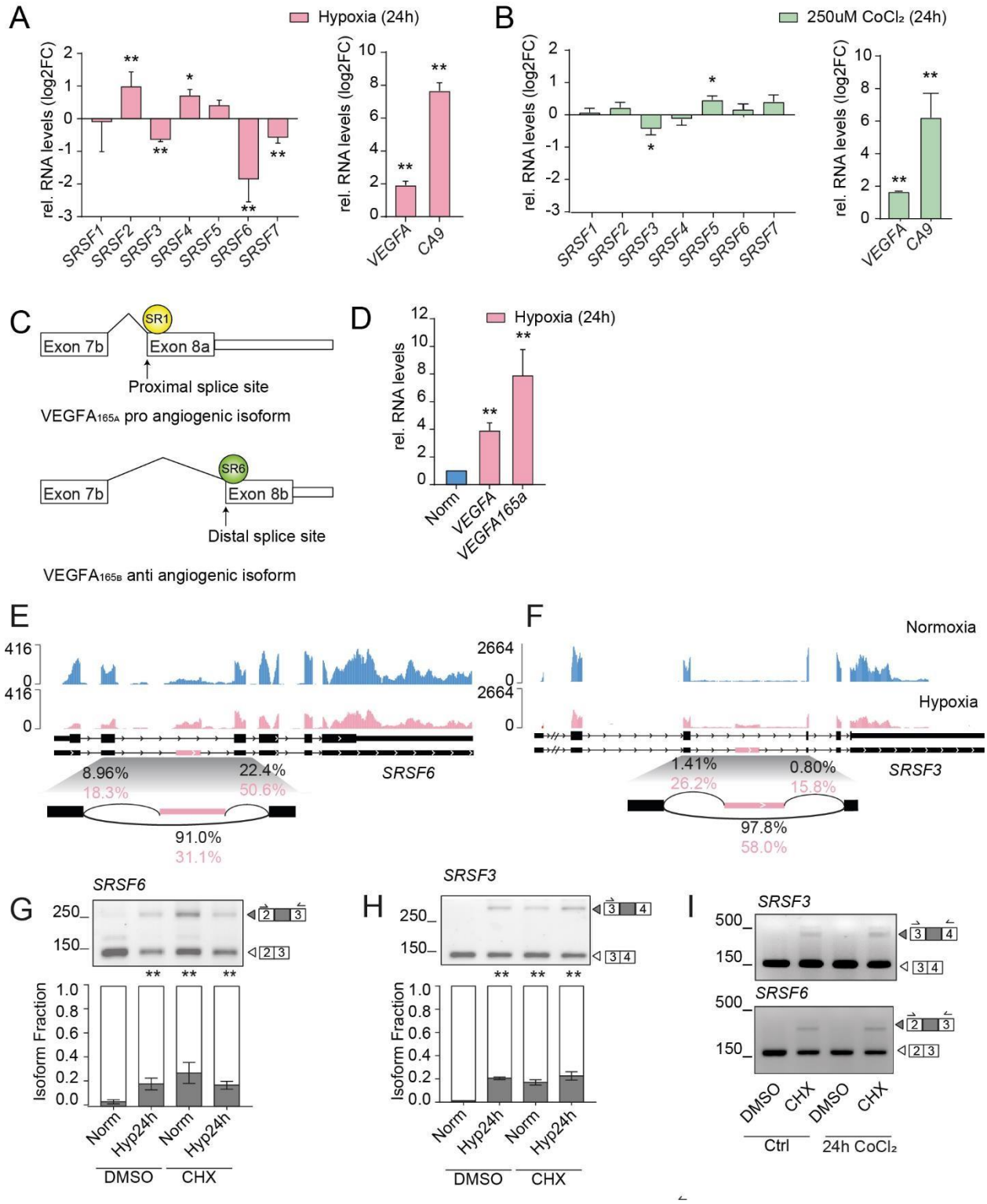
A
Hypoxia (24h)
rel. RNA levels (log2FC)
SRSF1
SRSF2
SRSF3
SRSF4
SRSF5
SRSF6
SRSF7
VEGFA
CA9
B
250uM CoCl₂ (24h)
C
SR1
Exon 7b
Exon 8a
Proximal splice site
VEGFA165A pro angiogenic isoform
SR6
Exon 8b
Distal splice site
VEGFA165B anti angiogenic isoform
D
rel. RNA levels
Norm
VEGFA
VEGFA165a
E
SRSF6
8.96%
18.3%
22.4%
50.6%
91.0%
31.1%
F
Normoxia
Hypoxia
SRSF3
1.41%
26.2%
0.80%
15.8%
97.8%
58.0%
G
H
I
Isoform Fraction
DMSO
CHX
Ctrl
24h CoCl₂

Figure 21.*SRSF6* and *SRSF3* transcript levels are strongly decreased in hypoxia. A) Left panel: RTqPCR validation of changes in SR protein transcripts (*SRSF1-7*) levels upon 24h hypoxia treatment. **Right panel:** RT-qPCR of hypoxia induced transcripts *VEGFA* and *CA9* as control for efficient hypoxia treatment. *U6* transcript was used for normalization of all samples. Log2 fold changes in hypoxia relative to normoxia were calculated (n=3, T-test *p<0.05, **p<0.01). **B) Left panel:** RT-qPCR to quantify changes in SR protein transcript levels (*SRSF1-7*) after 24h 250µM $CoCl_2$ treatment. **Right panel:** RT-qPCR of HIF1α-induced transcripts *VEGFA* and *CA9* as control for HIF1α stabilization upon $CoCl_2$ treatment. Log2 fold changes of $CoCl_2$ treated samples relative to control (H_2O) were calculated (n=3, T-test: *p<0.05, **p<0.01). **C)** Schematic representation of the *VEGFA* transcript and its two splice isoforms (*VEGFA165a and VEGFA165b*) regulated by SRSF1 and SRSF6. SRSF1 binds to exon 8a and promotes splicing of the proangiogenic isoform *VEGFA165a*. SRSF6 binds to exon 8b, counteracts SRSF1 and promotes inclusion of exon 8b and expression of the anti-angiogenic isoform *VEGFA165b*. **D)** RT-qPCR validation of hypoxia induced transcripts *VEGFA* and the *VEGFA165a* isoform. Primers were design to anneal to exon 8a to specifically amplify *VEGFA165a*. Changes in RNA levels in hypoxia relative to normoxia samples was calculated (n=3, T-test **p<0.01). **E-F)** Browser shots showing the RNA-Seq read coverage on the *SRSF6* and *SRSF3* genes in normoxic and hypoxia samples using IGV. Constitutive exons of the main protein coding isoform are shown as black boxes. The PCE is indicated in pink. Splicing junction usage in percent in normoxia (black) compared to hypoxia (pink) is shown for the PCE and its flanking exons. Values were acquired using Sashimi Plot in IGV. The scale represents the maximum number of reads per nucleotide position. **G-H) Upper panels:** Representative RT-PCR splicing gels validating *SRSF6* and *SRSF3* PCE inclusion upon 24h hypoxia and 2 hours CHX treatment (100µM) in normoxic and hypoxic samples. DMSO (100µM) was used as control. Primers were designed to anneal to the exons flanking the PCE (indicated by black arrows). **Lower panels:** Plots showing the fraction of isoforms (white - main isoform, grey - isoform with PCE inclusion). All samples were compared to the normoxia DMSO control and significance was tested using T-test, (n=3, **p<0.01). **I)** RT-PCR splicing gels to test PCE inclusion into *SRSF3* and *SRSF6* transcripts upon 24h $CoCl_2$ treatment and 2 hours CHX treatment (100µM). DMSO (100µM) was used as control. Primers are indicated by black arrows.

4.5. Hypoxia decreases SRSF6 protein level and alters its subnuclear localization

Since *SRSF6* transcripts are strongly decreased in hypoxia, we next investigated whether its protein and phosphorylation levels are also decreased, both of which determine its splicing activity. To determine changes in SRSF6 phosphorylation in initial and late stages of hypoxia, HeLa cells were incubated in hypoxia conditions for 4h or 24h. Western Blots probed with mAb104 antibodies that recognize phosphorylated RS domains, did not show any difference in phosphorylated SRSF6 levels upon hypoxia (Figure 22A). In contrast, total SRSF6 protein levels were decreased by 40% (n=3, p<0.05) after 24h hour hypoxia. As a control for the hypoxia response, we re-probed the membranes with an antibody specific for HIF1α and confirmed its stabilization after 4h and 24 hours (Figure 22B). In agreement with the mRNA expression data, 24h $CoCl_2$ treatment did not alter SRSF6 protein nor phosphorylation levels, despite a strong stabilization of HIF1α (Figure 22C). Altogether this suggests that SRSF6 protein levels are also decreased in 24h hypoxia, which is surprising, as SR proteins are highly stable

proteins. Moreover, since we detected no change in the levels of phosphorylated SRSF6 in hypoxia, the residual SRSF6 proteins must be hyper-phosphorylated. Indeed, it has been previously shown that most SR proteins are hyper-phosphorylated in hypoxia due to an increase in the expression of SR protein kinase 1 (SRPK1) (Jakubauskiene et. al, 2015).

To better quantify changes in SRSF6 protein levels and visualize changes in its cellular localization upon hypoxia, we generated HeLa cell lines stably expressing SRSF6-GFP from genomic loci using bacterial artificial chromosomes (BAC). The BAC contains the entire *SRSF6* gene fused to a C-terminal GFP-tag and randomly integrates into the genome (Poser, 2008) (Figure 22D,. We sorted GFP-positive cells in two different pools with low (SRSF6(L)) and high SRSF6-GFP expression (SRSF6(H)) levels (Figure S1A-B). The transgenes contain all regulatory sequences including introns and exons, and are alternatively spliced in hypoxia to generate more NMD isoforms, similar to the endogenous *SRSF6* gene (Figure 22E). Quantification of GFP fluorescence indicated that SRSF6(L)-GFP is also down-regulated by 35% after 24h hypoxia, similar to endogenous SRSF6 ($n>100$ cells, $p>0.01$; Figure 22F, S2A-B). Interestingly, in normoxic cells we observed a high SRSF6(L)-GFP fluorescence signal in the nucleoplasm (Figure 22G, blue arrows), but in hypoxia, residual SRSF6(L)-GFP protein localized exclusively to nuclear speckles (evidenced by a more condensed GFP signal and well-defined peaks in the line scans) (Figure 22G, red arrows). In line with our previous results, 24h $CoCl_2$ treatment did not decrease the fluorescence intensity of SRSF6(L)-GFP nor alter its localization ($n>100$ cells) (Figure 22H, S2C-D), underlining important differences between $CoCl_2$ and hypoxia in the splicing response.

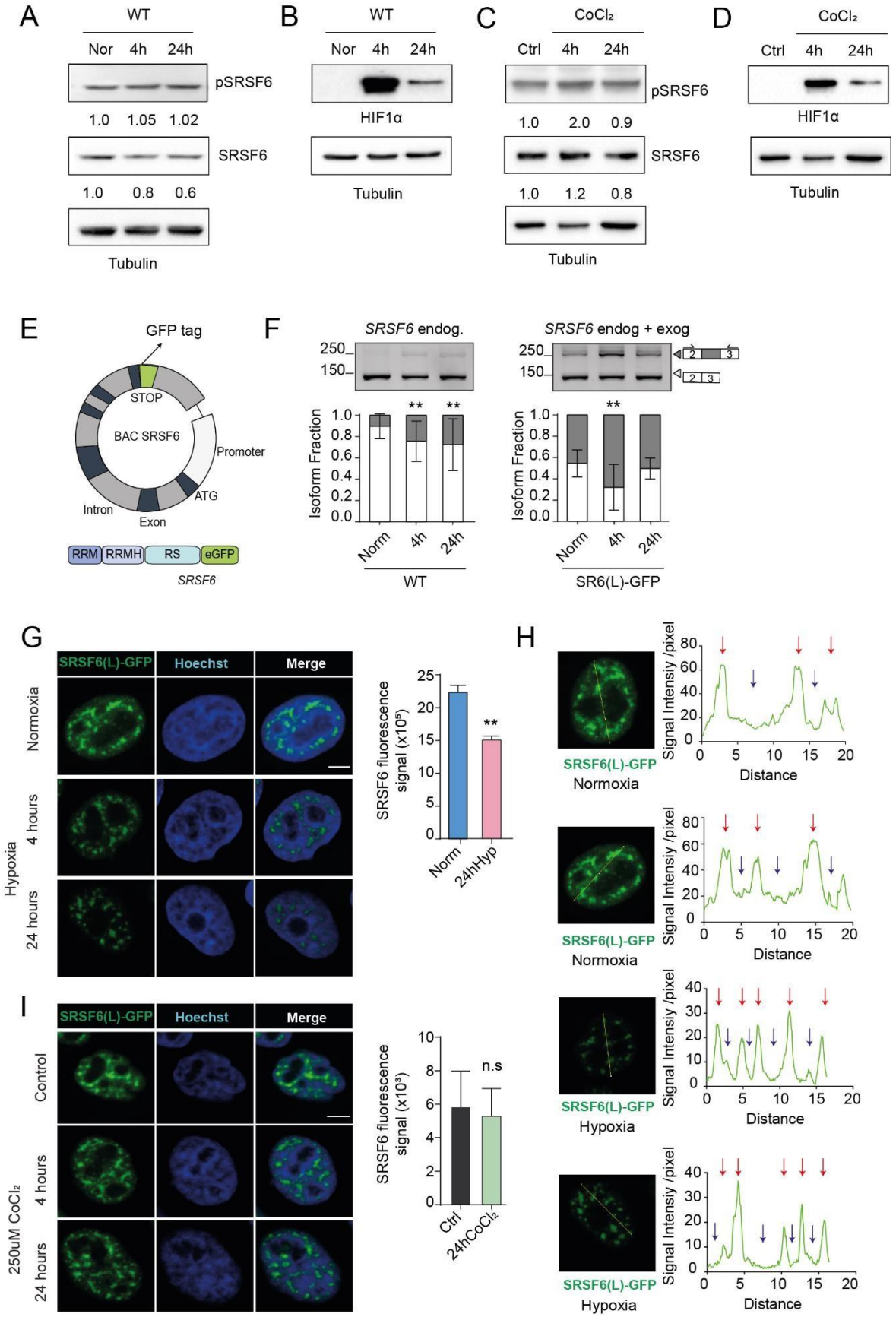
A
WT
Nor 4h 24h
pSRSF6
1.0 1.05 1.02
SRSF6
1.0 0.8 0.6
Tubulin
B
WT
Nor 4h 24h
HIF1α
Tubulin
C
CoCl₂
Ctrl 4h 24h
pSRSF6
1.0 2.0 0.9
SRSF6
1.0 1.2 0.8
Tubulin
D
CoCl₂
Ctrl 4h 24h
HIF1α
Tubulin
E
GFP tag
STOP
BAC SRSF6
Promoter
ATG
Exon
Intron
RRM RRMH RS eGFP
SRSF6
F
SRSF6 endog.
SRSF6 endog + exog
250
150
Isoform Fraction
Norm 4h 24h
WT
SR6(L)-GFP
G
SRSF6(L)-GFP
Hoechst
Merge
Normoxia
Hypoxia
4 hours
24 hours
SRSF6 fluorescence signal (x10⁵)
Norm
24hHyp
H
SRSF6(L)-GFP
Normoxia
Hypoxia
Signal Intensiy /pixel
Distance
I
Control
250uM CoCl₂
SRSF6 fluorescence signal (x10³)
n.s
Ctrl
24hCoCl₂

Figure 22. Hypoxia decreases SRSF6 protein levels and alters its nuclear localization. A) WB showing SRSF6 phosphorylation (pSRSF6 – anti-mAB104 antibody) and total protein levels (SRSF6 – anti-SRSF6 antibody) at 4h and 24h hypoxia. Tubulin was used as loading control. Protein levels were normalized and calculated relative to the normoxia control (representative picture from 3 experiments). **B)** HIF1α stabilization was confirmed by WB (anti-HIF1α antibody). **C)** WB showing SRSF6 phosphorylation and total protein levels at 4h and 24h $CoCl_2$ treatment Tubulin was used as loading control. Protein levels were normalized and calculated relative to the control. **D)** HIF1α stabilization at 4h and 24h $CoCl_2$ treatment was verified by WB. **E)** Scheme of the bacterial artificial chromosome (BAC) stably integrated into WT HeLa cells. The green boxes represent introns and the black boxes exons of the *SRSF6* gene. A GFP-tag is inserted before the STOP codon (indicated in green). The SRSF6-GFP protein domains derived from the BAC gene are shown below. **F)** Representative splice RT-PCR gels showing increased *SRSF6* PCE inclusion at 4h and 24h hypoxia in WT and SRSF6(L)-GFP cell lines. Primers anneal to exons flanking the PCE (indicated by black arrows) and amplify endogenous and exogenous *SRSF6* transcript isoforms. Plots below the gels show the fractions of isoforms (white – main isoform, grey – isoform with PCE inclusion). All samples were compared to normoxia (n=3, **p<0.01) and significance was tested using a T-test. **G) Left panel:** Representative fluorescence microscopy images of SRSF6(L)-GFP cells line in normoxia, 4h and 24h hypoxia, showing the GFP signal (green), nuclear staining with Hoechst (blue) and the merge of both channels. **Right panel:** Quantification of GFP fluorescence intensity in normoxia and 24h using FIJI (n>100 cells, 2 replicates, **p<0.01; scale bar = 5μm). **H)** Line profiles from SRSF6(L)-GFP cells line in normoxia and 24h hypoxia. Lines are shown in the micrograph (left) and the corresponding plots with signal intensity per pixel and line distance are shown on the right. Red arrows indicate GFP peaks, which correspond to nuclear speckle localization in the image. Blue arrows indicate nucleoplasmic SRSF6-GFP localization. **I) Left panel:** Representative fluorescence microscopy images of SRSF6(L)-GFP cells treated with 250μM $CoCl_2$ for 0h (control), 4h and 24h showing the GFP signal (green), nuclear staining Hoechst (blue) and the merge of both channels. **Right panel:** Quantification of GFP fluorescence intensity in control and 24h $CoCl_2$ treated cells using FIJI (n>100 cells, 2 replicates, n.s: non-significant; scale bar = 5μm).

4.6. SRSF6 overexpression in hypoxia promotes formation of micronuclei and DNA damage

Our data so far indicate that SRSF6 is down-regulated at the RNA and protein level upon 24h hypoxia. To test the importance of SRSF6 down-regulation for hypoxia adaptation we used the high-expressing SRSF6(H)-GFP cells and investigated their response to hypoxia. As a control, we generated cell lines expressing SRSF4-GFP and also sorted for high GFP levels (SRSF4(H)-GFP) (Figure S1A). SRSF4 is closely related to SRSF6 and has a high structural similarity (83% identity) (Lareau and Brenner 2015) (Figure S1C-D), but it is up-regulated in hypoxia (Figure 21A). Using WB and confocal microscopy, we validated the presence of GFP-tagged proteins in SRSF6(L)-GFP, SRSF6(H)-GFP and SRSF4(H)-GFP cell lines (Figures S1B).

We then subjected WT, SRSF4(H)-GFP and SRSF6(H)-GFP cell lines to hypoxia for 4 and 24h and investigated SRSF6 phosphorylation and total protein levels (Figure 23A). Similar to SRSF6(L)-GFP cells, transgenic SRSF6(H)-GFP and endogenous

SRSF6 protein was down-regulated by 35% after 24h hypoxia. Despite this decrease, SRSF6(H)-GFP cells still expressed 4-fold more SRSF6 than WT cells in normoxic and hypoxic conditions (n=3, p<0.05). In both, SRSF6(H)-GFP and SRSF4(H)-GFP cell lines, endogenous SRSF6 protein levels were decreased in comparison to WT (1.3-fold in normoxia and -4-fold in 24h hypoxia). This result is in agreement with studies performed in our lab showing that both, SRSF4 and SRSF6, regulate SRSF6 levels (data not published) (Figure 23B).

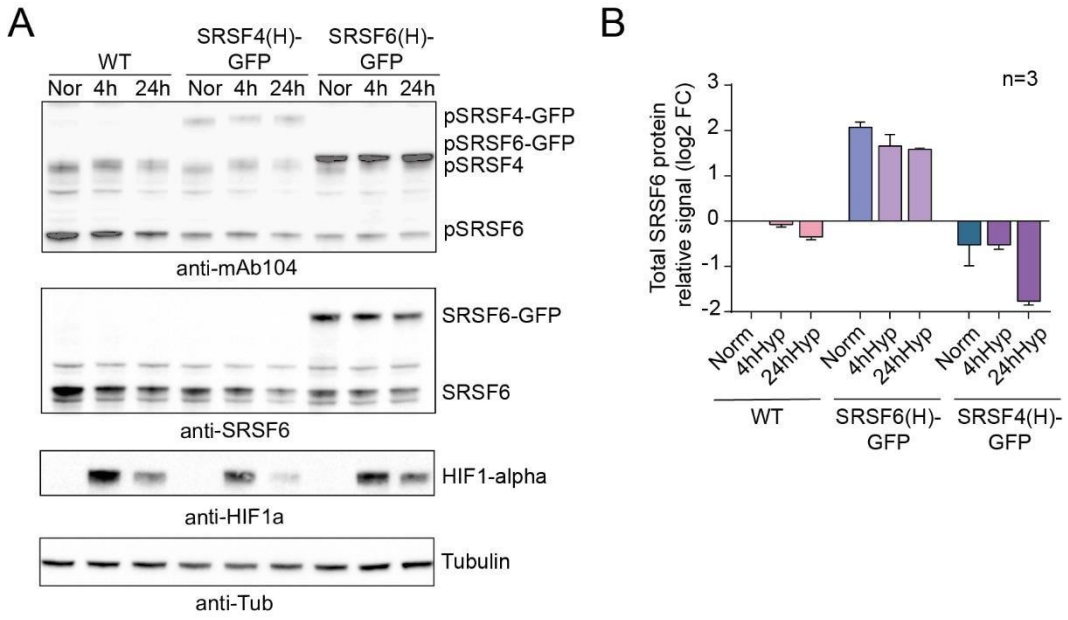

Figure 23. SRSF6 regulation in overexpressing cell lines in normoxia and hypoxia.

A) Representative WB from WT, SRSF6(H)-GFP and SRSF4(H)-GFP cell lines in normoxia, 4h and 24h hypoxia. mAb104 antibody was used to detect phosphorylated SRSF6 and SRSF4 endogenous proteins..Anti-SRSF6 antibody was used to detect total SRSF6 protein levels. Anti-HIF1α antibody was used as a control for hypoxia treatment efficiency. Tubulin was used as loading control. **B)** Quantification of total SRSF6 protein levels in all cell lines using ImageLab. SRSF6 signal was normalized and Log2-fold changes (log2FC) were calculated relative to WT normoxia values (n=3).

To identify phenotypic changes due to SRSF6 overexpression, we first analyzed cells by confocal microscopy. Interestingly, we observed that SRSF6(H)-GFP cells showed a significant increase in micronuclei abundance (Figures 24A-B, S3A). Micronuclei are small fragments of nuclei, which, due to errors during mitosis, become separated from the main cell nucleus. The presence of micronuclei and aberrant nuclei shapes are general indicators of inefficient DNA replication and errors in the assembly of

mitotic spindles and chromosomal segregation (Fonseca et. al 2019). Figure 24C shows different nuclei shapes and their respective solidity values measured using Fiji. In hypoxia, HeLa cells show generally higher solidity values, which might be explained by their increased proliferation and migration under these conditions (Figure 24D). SRSF4(H)-GFP cells show higher solidity values than the WT cells, which might be due to lower SRSF6 levels in this cell line. Most interestingly, SRSF6(H)-GFP cells display much lower solidity values in normoxic and hypoxic conditions compared to WT and SRSF4(H)-GFP cells (Figure 24D).

Cells, which display disturbances in chromosome segregation and homologous repair during cellular division, usually show higher DNA damage due to double strand breaks (DSBs). We therefore tested whether SRSF6(H)-GFP cells present higher number of DSB events than WT cells. DSBs can be detected by the presence of phosphorylated Serine139 in Histone H2Ax (yH2A.x). We performed Immunofluorescence (IF) experiments with normoxic and hypoxic cells (24h) and indeed, SRSF6(H)-GFP cells showed significantly higher numbers of pH2A.x nuclear foci compared to WT in normoxic and hypoxic cells (Figures 24E-F, S3B). Taking together, these results suggest that low SRSF6 levels are crucial for the proper regulation of DNA damage repair and chromosome segregation during cellular division and cell cycle progression under hypoxic conditions. Higher amount of cells with DNA damage might indicate that the apoptosis triggered by the DNA damage repair pathway is not active and these cells can still survive and divide.

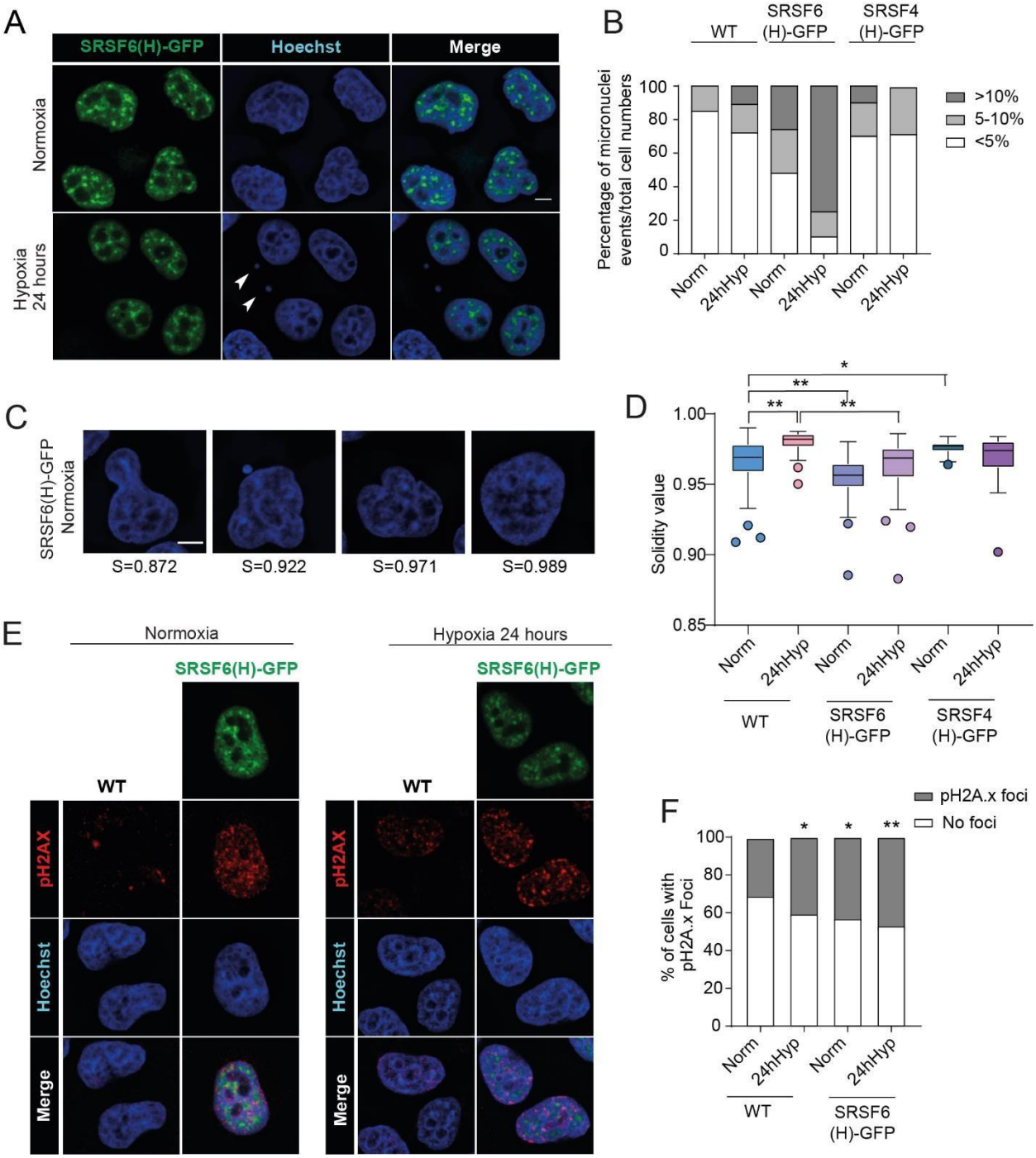

Figure 24. SRSF6 overexpression promotes micronuclei formation and DNA damage. A) Fluorescence images of SRSF6(H)-GFP cells in normoxia and 24h hypoxia showing increased formation of micronuclei (white arrows). **B)** Quantification of micronuclei events in WT, SRSF6(H)-GFP and SRSF4(H)-GFP cell lines in normoxia and 24h hypoxia. (n=2; >100 cells per experiment). **C)** Representative images of SRSF6(H)-GFP cell nuclei and the respective solidity (S) values analyzed by FIJI. Nuclei are stained with Hoechst. **D)** Mean solidity values of WT, SRSF6(H)-GFP and SRSF4(H)-GFP HeLa nuclei in normoxia and 24h hypoxia. (n=2; >200 cells per condition). Differences of nuclei solidity were

calculated for every cell line relative to WT in normoxia and hypoxia (T-test, *p<0.05, **p<0.01). **E)** Representative IF images of WT and SRSF6(H)-GFP cells in normoxia and 24h hypoxia stained with antiphospho Ser139 histone H2Ax (yH2A.x) antibody (red). GFP signal is shown in green, Hoechst nuclear staining in blue. **F)** Quantification of WT and SRSF6(H)-GFP cells with positive pH2A.x signal in normoxia and 24h hypoxia. The percentage of positive yH2A.x cells was calculated, plotted (n>100 cells) and tested for significant differences relative to the WT normoxia (T- test, *p<0.05, **p<0.01).

4.7. Identification of mis-regulated transcripts by SRSF6 overexpression in hypoxia using iCLIP

Our data indicate that SRSF6 overexpression in hypoxia negatively affects cell division and DNA stability. One reason for the observed phenotype could be alterations in AS of hypoxia-induced transcripts caused by sustained high SRSF6 level. SRSF6 binding usually promotes the inclusion of alternative exons (Shepard and Hertel 2009) and its decrease during hypoxia should in principle cause their skipping. SRSF6 overexpression might impair exon skipping in hypoxia due to sustained SRSF6 binding, and instead promotes exon inclusion (Figure 25A). On the other hand, SRSF6 could also promote exon skipping in hypoxia through enhanced binding to upstream and downstream exons flanking alternative exons, which are included in normoxia. To test these expectations and compare exons and transcripts that are bound by SRSF6 in normoxia and hypoxia at a transcriptome-wide level, we performed UV Cross-Linking and ImmunoPrecipitation (iCLIP) experiments, with SRSF6(L)-GFP cells grown in normoxic, 4h and 24 hours hypoxic conditions in three replicates (Figure 25B). After UV crosslinking, the cells were lysed and an RNaseI treatment was performed. RNA fragments (50-300nt) bound by SRSF6(L)-GFP were immunoprecipitated using an α-GFP antibody and stringently purified by SDS-PAGE (Figure 25C). SRSF6-bound RNAs were isolated and RT-PCR was performed to generate iCLIP libraries for Deep Sequencing (Figure 25D). Non cross-linked samples were used as control (Figures 25B-D).

After mapping the iCLIP reads to the human genome (hg19) we obtained 3,285,995, 4,178,237, 3,127,338 and 3,141 unique crosslinks (X-links) for the pooled replicates in normoxia, 4h, 24 hypoxia and controls, respectively. Peak calling derived 379,097, 611,391, 405,278 and 123 significant X-links (FDR<0.05) that were merged into 42,685, 52,388, 38,414 and 59 binding sites (Figure 25E). In general, there was a similar number of SRSF6 X-links and binding sites, which allowed for a direct comparison of the

data. Analyses of enriched 5-mers around significant X-links revealed the consensusbinding motif of SRSF6. This purine-rich binding motif (GARGAR) is the same in normoxia and hypoxia and similar to the one obtained with mouse P19 cells (Müller-McNicoll et. al, 2016) (Figure 25F). In agreement with SRSF6 binding preferentially to exons, significant X-links are enriched in coding regions including ORFs, 3´UTRs and 5´UTRs, with negligible binding to intronic regions (Figure 25G). There was also a high overlap of genes that were bound by SRSF6 in all three conditions, which allowed us to compare differential binding within genes and exons in normoxic and hypoxic conditions (Figure 25H).

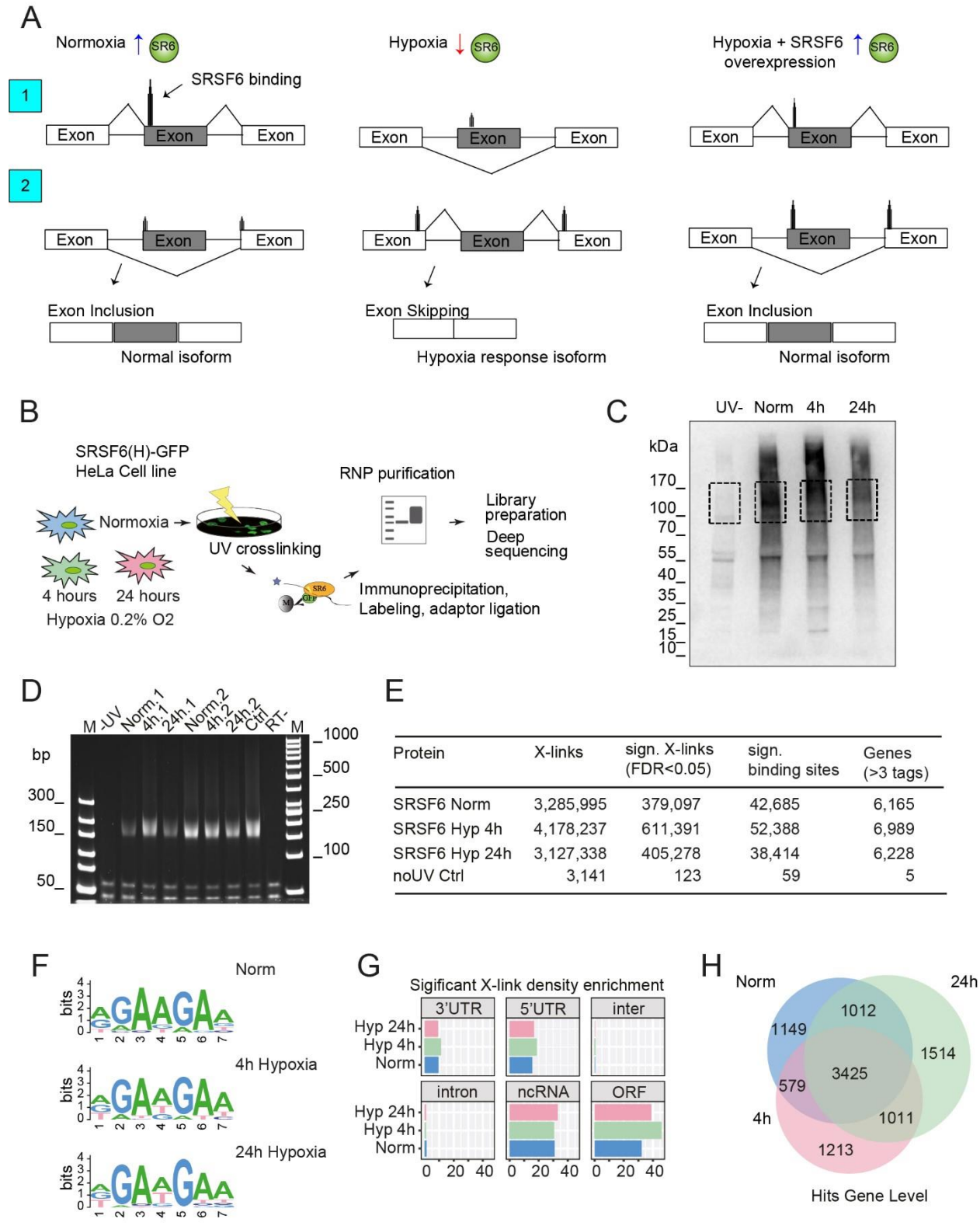

Protein	X-links	sign. X-links (FDR<0.05)	sign. binding sites	Genes (>3 tags)
SRSF6 Norm	3,285,995	379,097	42,685	6,165
SRSF6 Hyp 4h	4,178,237	611,391	52,388	6,989
SRSF6 Hyp 24h	3,127,338	405,278	38,414	6,228
noUV Ctrl	3,141	123	59	5

Figure 25. **Transcriptome-wide SRSF6 binding landscape in normoxia and hypoxia. A)** Schema of SRSF6 binding and potential splicing outcome in normoxia, hypoxia and SRSF6 overexpression in hypoxia.

Scenario 1. In normoxia SRSF6 protein binds to alternative exons and promotes their inclusion. In hypoxia, SRSF6 levels are decreased and less binding to target exons causes their skipping. Upon SRSF6 overexpression, binding to target exons persists, promoting the inclusion of exons, which are normally skipped in hypoxia. Scenario 2. SRSF6 binds weakly to flanking exons in normoxia and promotes inclusion of the regulated exons. In hypoxia the binding to flanking exons could be increased due to increase in RNA expression of induced genes and the regulated exons are skipped. Skipping could be reversed in hypoxia when upon SRSF6 overexpression binding in alternative exons is also increased. **B)** Workflow of the iCLIP experiment using SRSF6(H)-GFP cells subjected to normoxia, 4h and 24h hypoxia. **C)** Autoradiograph showing RNA cross-linked to purified SRSF6-GFP protein labeled with P^{32}. Squares indicate where the RNA was cut and purified. UV- represent control samples where no cross-linking was performed. **D)** 6% TBE-Urea gel stained with SYBR Gold showing the final iCLIP library amplified by RT-PCR (22 cycles). **E)** SRSF6 iCLIP mapping statistics from pooled replicates (n=3); tags – sign. X-links. **F)** Consensus binding motifs of SRSF6 in normoxia, 4h and 24h hypoxia treatment. **G)** Significant X-link enrichment in different genomic regions. ncRNA – non-coding RNA; inter – intergenic regions. **H)** Venn diagram showing the overlap of genes bound by SRSF6 in the three conditions.

We first analyzed changes in the binding of SRSF6 to exons that were alternatively spliced in hypoxia according to our RNAseq data. For this we separated all regulated exons into more included or less included and derived their genomic coordinates. We excluded exons whose transcripts increased significantly in abundance in hypoxia (log2fold-change>0.7). Exonic regions were extended by 100 nt in both directions to include X-links within intronic regions and around the splice sites. Then all X-links that mapped to this extended region were counted and their patterns compared between normoxia and hypoxia samples (see Material and Methods).

We observed that exons that are skipped in hypoxia are indeed more bound by SRSF6 in normoxia compared to up-regulated exons (Figure 26A), suggesting that SRSF6 binding promotes the inclusion of those exons under normal conditions. SRSF6 also bound more to skipped exons in hypoxia, however, binding is high at 4h and declines after 24h hypoxia (Figure 26B). This is probably because at 4h, hypoxia-induced premRNAs are more available for splicing by SRSF6 since SRSF6 levels are not decreased yet. But after 24h, when SRSF6 levels are reduced, apparent binding also decreases.

We next compared SRSF6 binding in exons upstream and downstream of hypoxiaskipped exons. Interestingly we observed a strong increase in SRSF6 binding within upstream exons in both hypoxic samples compared to normoxia, whereas in downstream exons this increase was less apparent (Figure 26C). These data suggest that in normoxia, weak SRSF6 binding to flanking exons and strong binding to alternative

exons promotes their inclusion, while in hypoxia decreased binding to alternative exons and enhanced binding to flanking regions enhances their skipping.

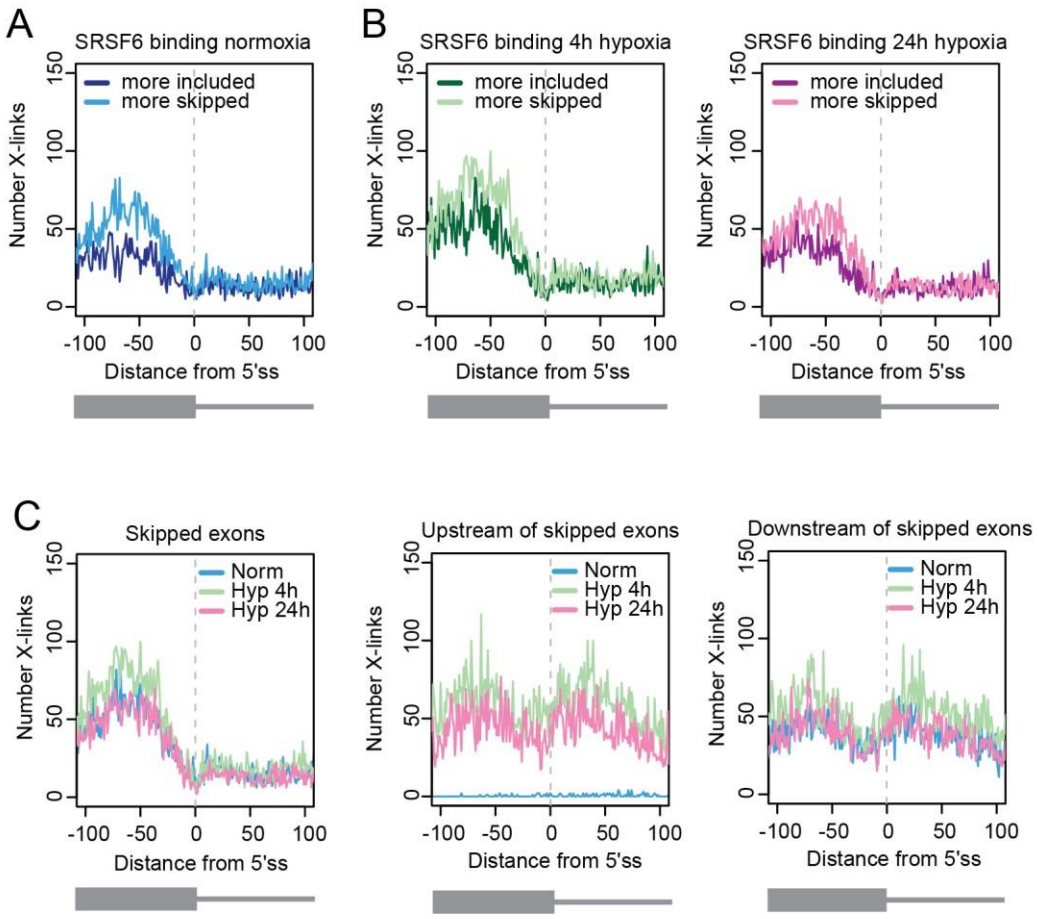

Figure 26. Changes in SRSF6 binding to regulated and flanking exons in hypoxia. A-B) SRSF6 Xlinks mapping to regulated exons that are more included and skipped upon 24h hypoxia treatment. X-link patterns were compared in normoxia, 4h and 24h hypoxia around the 5' splice site (5'ss) in a window of +/- 100nt upstream and downstream. **C)** SRSF6 X-links mapping to skipped exons and upstream and downstream flanking exons around the 5'ss in a window of +/- 100 nt.

To test these assumptions and identify SRSF6-regulated target exons, we visually inspected the binding patterns of SRSF6 around selected skipped exons. We considered only transcripts that had at least 2 significant X-links within the regulated and/or downstream and upstream exons and chose four transcripts that displayed differential SRSF6 binding for validation by RT-qPCR and RT-PCR.

In *SNAP25* (Synaptosome associated protein 25), both, exon 5 and 6 are skipped in hypoxia. SRSF6 binds to both exons, as well as to flanking exons in normoxia. In hypoxia, SRSF6 binding to the alternative exons decreases while binding to the upstream exon increases, which should promote exon skipping (Figure 27A). In the case of *PAPOLA* (Poly(A) polymerase alpha), SRSF6 also binds to the skipped exon 19 and upstream of it in normoxia, but in hypoxia binding to the skipped exon is lost (Figure 27B). In *MDM4,* SRSF6 binds to the skipped exon 6 in normoxia, but binding is lost in hypoxia, which should lead to exon skipping (Figure 27C). In *CHAF1A* (chromatin assembly factor 1 subunit A) SRSF6 binding to the skipped exon 4 and to upstream and downstream exon decreases in hypoxia (Figure 27D). We designed primers specific for the exon junction generated by the skipped isoforms of *SNAP25* and *PAPOLA* to quantify their expression by RT-qPCR (Figures 27E-F). This confirmed that in WT cells exons 5/6 of *SNAP25* are indeed more skipped in hypoxia, however in SRSF6 overexpressing cells (SRSF6(H)GFP), exons 5/6 are more included in normoxia and there is no change in hypoxia (Figure 27E). Exon 19 of *PAPOLA* is also more skipped in WT cells, but much more included in SRSF6(H)-GFP cells in hypoxia. Skipping of this exon in hypoxia was not significant due to high replicate variation (Figure 27F). *MDM4* exon 6 skipping in hypoxia was already validated by RT-PCR (Figure 27G), but in SRSF6(H)-GFP cells this exon is significantly more included in normoxia and hypoxia conditions (Figure 25G). We also quantified *CHAF1A* skipped isoform levels and indeed, in WT cells the skipped isoform increases in hypoxia, but upon SRSF6 overexpression it decreases, indicating that skipping of this exon also depends on low SRSF6 levels (Figure 27H). In conclusion, we positively validated 100% (4 out of 4) exons whose inclusion seems to be regulated by SRSF6. Given these promising results, we next performed RNA-Seq on WT and SRSF6(H)-GFP cells in normoxia and hypoxia to identify all SRSF6 splicing targets and test isoforms for impaired exon skipping (experiment ongoing). Analysis of these data will enable us to identify transcript isoforms that are important for hypoxia adaptation and further strengthen the importance of SRSF6 down-regulation for the alternative splicing response to hypoxia.

Finally, we wanted to investigate whether SRSF6 might regulate the decrease of its own protein levels in hypoxia through unproductive splicing. As shown before, SRSF6

transcripts display an increased inclusion of the PCE in hypoxia, but the resulting NMD isoforms are not degraded (Figure 21G). Using our iCLIP dataset, we investigated whether SRSF6 binds to the PCE and promotes its inclusion in hypoxia. Indeed, we found that SRSF6 binds strongly to the PCE in normal and hypoxic conditions, much more than to the other exons, suggesting it promotes its inclusion. In 4h and 24h hypoxia, although SRSF6 binding to flanking exons decreases, binding to the PCE remains high with a very pronounced peak at its 3'ss (Figure 27I). To validate inclusion of the PCE by RT-qPCR we used primers that bind to the PCE. Indeed, we observed higher PCE inclusion in SRSF6(H)-GFP cells compared to WT cells in hypoxia (Figure 27J). Altogether, this suggests that SRSF6 binds to its own PCE in normoxia and hypoxia, promotes its inclusion and thereby controls the amounts of functional SRSF6 protein levels.

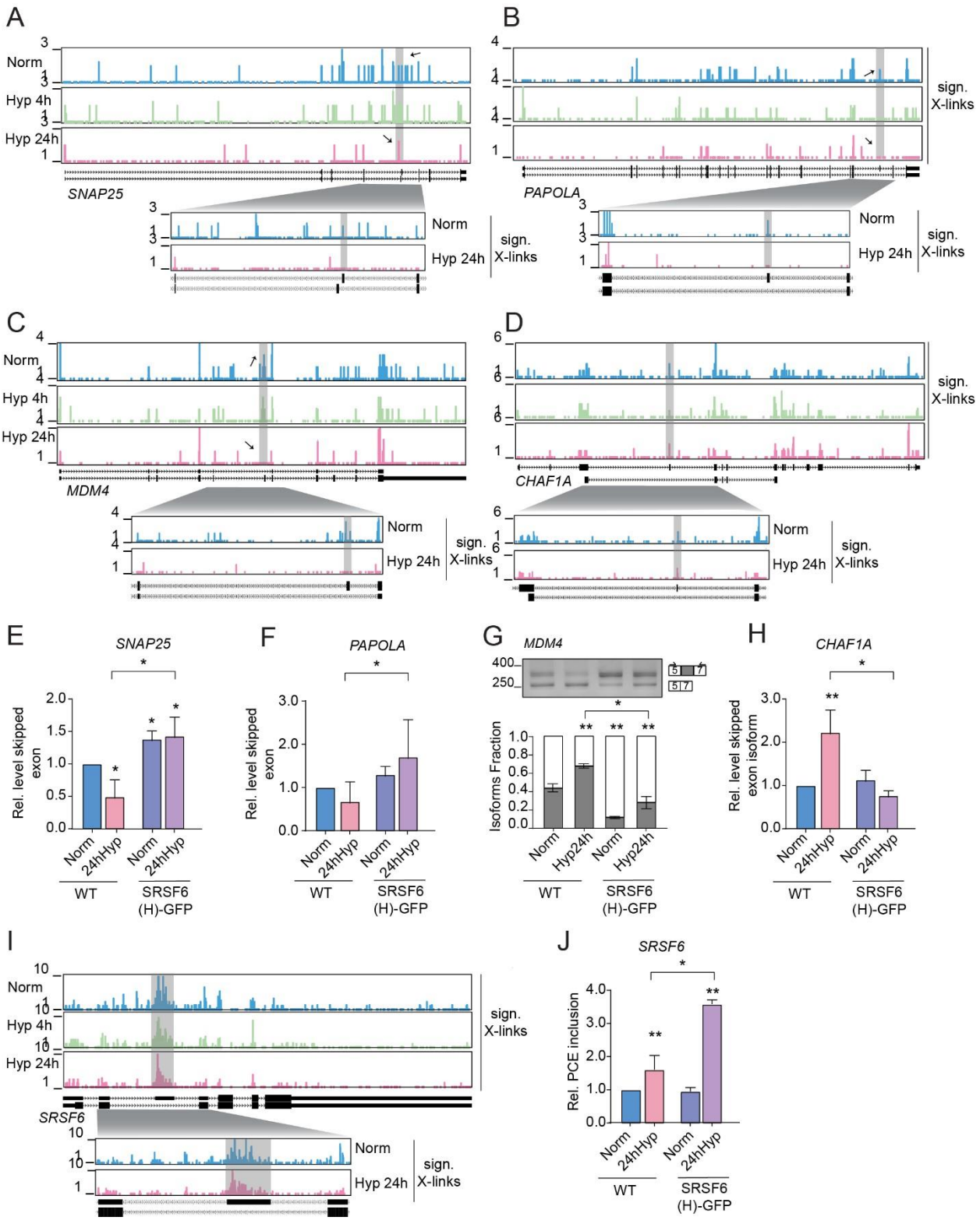
A
Norm
Hyp 4h
Hyp 24h
SNAP25
sign. X-links
B
PAPOLA
C
MDM4
D
CHAF1A
E
SNAP25
Rel. level skipped exon
F
PAPOLA
G
MDM4
Isoforms Fraction
H
CHAF1A
Rel. level skipped exon isoform
Norm
24hHyp
Hyp24h
WT
SRSF6 (H)-GFP
I
SRSF6
J
SRSF6
Rel. PCE inclusion

Figure 27. SRSF6 downregulation in hypoxia promotes exon skipping. A-D). Upper panel: Browser shots showing the distribution of significant SRSF6 X-links on 4 genes, which undergo exon skipping in hypoxia. Both isoforms with included and skipped exons are shown below. Grey boxes indicate the skipped exons for each transcript. **Lower panel:** Zoom into the region of the skipped exons and flanking exons upstream and downstream with significant SRSF6 X-links on normoxia and 24h hypoxia. **E-F)** RT-qPCR quantification of skipped exon levels in *SNAP25* and *PAPOLA* transcripts in normoxia and hypoxia comparing WT and SRSF6(H)-GFP cells. **G)** RT-PCR splicing gel showing skipping of exon 6 in the *MDM4* transcript in WT and SRSF6(H)-GFP cells in normoxia and hypoxia. Quantification of skipped and excluded isoforms in all conditions is shown below. **H)** RT-qPCR quantification of skipped exon levels in *CHAF1A* transcripts in normoxia and hypoxia comparing WT and SRSF6(H)-GFP cells.T-tests were performed to test for significance. (n=3 replicates, *p<0.05, **p<0.01). **I) Upper panel:** Browser shots showing the distribution of significant SRSF6 X-links on the *SRSF6* gene in normoxia, 4h and 24h hypoxia. The main isoform and the isoform with included PCE are shown below.Grey boxes indicate the PCE. **Lower panel:** Zoom into the PCE and flanking upstream and downstream exons with significant SRSF6 X-links in normoxia and 24h hypoxia. **J)** RT-qPCR quantification of PCE inclusion levels in WT and SRSF6(H)-GFP cell lines in normoxia and hypoxia.

4.8. SRSF6 inhibits circRNA formation in normoxia and hypoxia

Our results so far indicate that SRSF6 down-regulation is important for appropriate AS in response to hypoxia. Decreased SRSF6 levels leads to exon skipping and the formation of transcript isoforms that might fulfill specific functions in hypoxia adaptation. Decreased splicing activity and exon skipping is also one of the mechanisms that leads to enhanced circRNA formation (Liang et al. 2017; Ragan et al. 2018). Since some circRNAs show increased levels in hypoxia (Figure 20E), we next wanted to investigate whether reduced SRSF6 levels and exon binding are responsible for their formation (Figure 28A). To test this, we depleted SRSF6 in normoxic conditions and quantified the levels of 15 circRNAs that we had previously validated. Using 2 pooled siRNAs we successfully achieved an 80% KD at the RNA and protein level (Figure 28B). Indeed, 7 out of 15 circRNAs were significantly increased after SRSF6 KD: *circPLOD2, circMTCL1, circMAN1A2, circRTN4, circHIPK3, circSRSF4* and *circCPSF6* (Figure 26C). Out of these, 4 circRNAs were also up regulated in hypoxia: *circPLOD2, circMTCL1, circMAN1A2* and *circRTN4* (Figure 28C).

If SRSF6 depletion leads to enhanced circRNA formation due to increased exon skipping (Figure 28A), circularized exons should be bound by SRSF6 in normoxia. To investigate this, we interrogated our normoxia SRSF6(L)-GFP iCLIP data and compared SRSF6 X-links on circularized exons to neighboring linear exons of circRNA host transcripts. We did not consider hypoxia iCLIP data, since most circRNAs host transcripts

were up regulated in hypoxia, which confounds comparative binding analyses. Indeed, exons that can be circularized are strongly bound by SRSF6 in normoxia (Figure 28D). Thus, SRSF6 might promote inclusion of these exons into linear mRNAs, this way inhibiting circRNA formation by backsplicing. To test this, we quantified the levels of *circPLOD2, circMAN1A2* and *circRTN4* levels in WT and overexpresser (SRSF6(H)-GFP) cells in normoxia and 24h hypoxia by RT-qPCR. In WT cells, all circRNAs were significantly increased upon hypoxia. However, in SRSF6(H)-GFP cells, circRNAs levels did not increase, instead some circRNAs, e.g. *circRTN4,* even decreased in normoxia and hypoxia (Figure 28E). These results show that SRSF6 depletion in normoxia and hypoxia conditions leads to skipping of target exons and enhances the formation of circRNAs by backsplicing.

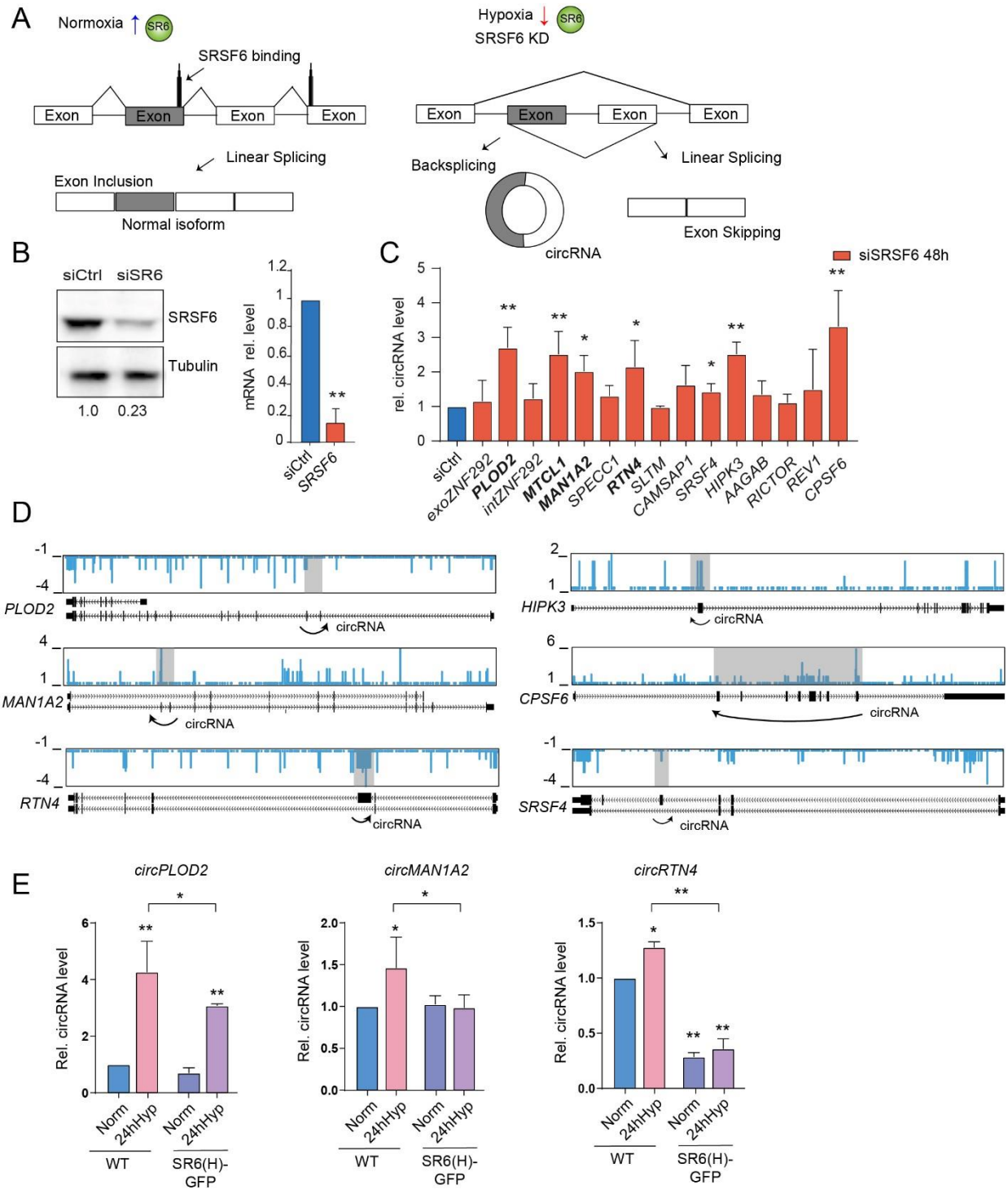
A
Normoxia
SR6
SRSF6 binding
Exon
Exon
Exon
Exon
Linear Splicing
Exon Inclusion
Normal isoform
Hypoxia
SR6
SRSF6 KD
Exon
Exon
Exon
Exon
Backsplicing
Linear Splicing
circRNA
Exon Skipping
B
siCtrl
siSR6
SRSF6
Tubulin
1.0
0.23
mRNA rel. level
siCtrl
SRSF6
C
siSRSF6 48h
rel. circRNA level
siCtrl
exoZNF292
PLOD2
intZNF292
MTCL1
MAN1A2
SPECC1
RTN4
SLTM
CAMSAP1
SRSF4
HIPK3
AAGAB
RICTOR
REV1
CPSF6
D
PLOD2
circRNA
MAN1A2
circRNA
RTN4
circRNA
HIPK3
circRNA
CPSF6
circRNA
SRSF4
circRNA
E
circPLOD2
circMAN1A2
circRTN4
Rel. circRNA level
Norm
24hHyp
Norm
24hHyp
WT
SR6(H)-GFP

Figure 28. SRSF6 overexpression inhibits circRNA formation. A) Schematic of potential circRNA formation mechanism upon SRSF6 depletion. SRSF6 is highly expressed in normoxia and can bind to exons promoting their inclusion and linear splicing. Upon SRSF6 depletion (KD or hypoxia), SRSF6 binds less to its target exons, which can cause exon skipping and circularization of the skipped exons by backsplicing resulting in formation of circRNAs and skipped transcript isoforms. **B)** Validation of SRSF6 KD with 2 pooled siRNAs at the protein and RNA levels. **Left panel:** WBs were probed with anti-SRSF6 antibody to investigate total SRSF6 levels in control and 48h KD samples. Tubulin was used as loading control. SRSF6 protein levels were quantified and normalized and are shown relative to the control. **Right panel:** SRSF6 mRNA levels were quantified by RT-qPCR relative to the control after normalization with *U6* (n=3, **p<0.01). **C)** RT-qPCR quantification of 15 circRNAs in control and SRSF6 KD samples. All qPCR primers amplify the backsplice junction. Four circRNAs up-regulated in hypoxia are indicated in bold. Levels of circRNAs were normalized to *U6* and calculated relative to control samples. (n=3, *p<0.05, **p<0.01). **D)** Browser shots of circRNAs host genes where circRNAs were up-regulated upon SRSF6 KD. Significant Xlinks of SRSF6 in normoxia are shown on each gene. Circularized exons are indicated by grey boxes and circularization is indicated with arrows. Isoforms containing or lacking circularized exons are shown below (when annotated). **E)** RT-qPCR quantification of circRNA levels in WT and SRSF6(H)-GFP cells in normoxia and 24h hypoxia. T-tests were performed to compare circRNA levels in SRSF6(H)-GFP cells in 24h hypoxia relative to WT 24h hypoxia (n=3 replicates, *p<0.05, **p<0.01).

4.9. SRSF6 overexpression impairs *MALAT1* induction and *VEGFA165* splicing in hypoxia

Our iCLIP data also detected strong binding of SRSF6(L)-GFP to non-coding RNAs (ncRNA) (Figure 25G). Two of the most SRSF6-bound ncRNAs were *NEAT1* and *MALAT1* (Figures 29A). Both, SRSF6 and *MALAT1* are known to localize to nuclear speckles. *MALAT1* is induced in hypoxia and was shown to repress splicing of the antiangiogenic *VEGFA165b* isoform (Pruszko et. al, 2017). In contrast, we show here that SRSF6, which promotes splicing of *VEGFA165b,* is down-regulated in hypoxia and the remaining SRSF6 localizes exclusively to nuclear speckles. In line with this localization, iCLIP binding profiles and quantification of significant X-links revealed that *MALAT1* is densely coated by SRSF6 and binding increases at least 2-fold in hypoxia despite decreased SRSF6 levels (Figures 29A and 29B).

MALAT1 was previously shown to regulate the phosphorylation, protein levels and localization of some SR proteins (Tripathi et al. 2010). Therefore, we decided to investigate whether *MALAT1* induction in hypoxia might regulate *SRSF6* activities and in turn hypoxia adaptation. We first confirmed by RT-qPCR that *MALAT1* is indeed 2.5-fold up-regulated in HeLa WT cells after 24h hypoxia treatment (Figure 29C). Since SRSF6 and *MALAT1* display anti-correlated expression changes upon hypoxia, we next tested

whether depletion of SRSF6 induces *MALAT1* expression also in normoxia. Indeed, depletion of SRSF6 increased *MALAT1* expression by 3.8-fold (Figure 29D). Interestingly, although no hypoxia treatment was performed, we also observed a slight increase (1.5fold) in *VEGFA* levels upon *SRSF6* KD. Even more strikingly, the pro-angiogenic *VEGFA165a* isoform increased by 2.7-fold compared to the control (Figure 29E). These results confirmed that SRSF6 is an important suppressor of *VEGFA165a* splicing in normal conditions.

These data suggested that SRSF6 depletion in hypoxia might induce *MALAT1* expression. To test this, we submitted WT and SRSF6(H)-GFP cells to hypoxia for 4h and 24h. Indeed, SRSF6 overexpression significantly impaired *MALAT1* induction after 24h hypoxia (Figure 29F). Moreover, inclusion of exon 8a and expression of the *VEGFA165a* isoform was also decreased in SRSF6(H)-GFP cells. The transcriptional hypoxia response was unchanged in both cell types confirmed by the similar induction of the hypoxia marker *CA9* (Figure 29G). These data indicate that a failure to down-regulate SRSF6 in hypoxia impairs the generation of pro-angiogenic *VEGFA165a* isoforms and *MALAT1* induction.

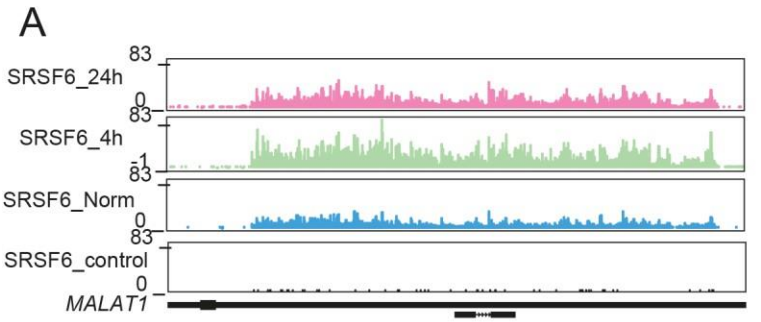

B

Changes target binding

Gene	Norm	4h Hyp	24h Hyp
NEAT1 (%)	3.271	2.928	4.806
MALAT1 (%)	1.615	2.243	2.914
VEGFA (%)	0.004	0.033	0.082
SRSF6 (%)	0.116	0.113	0.138

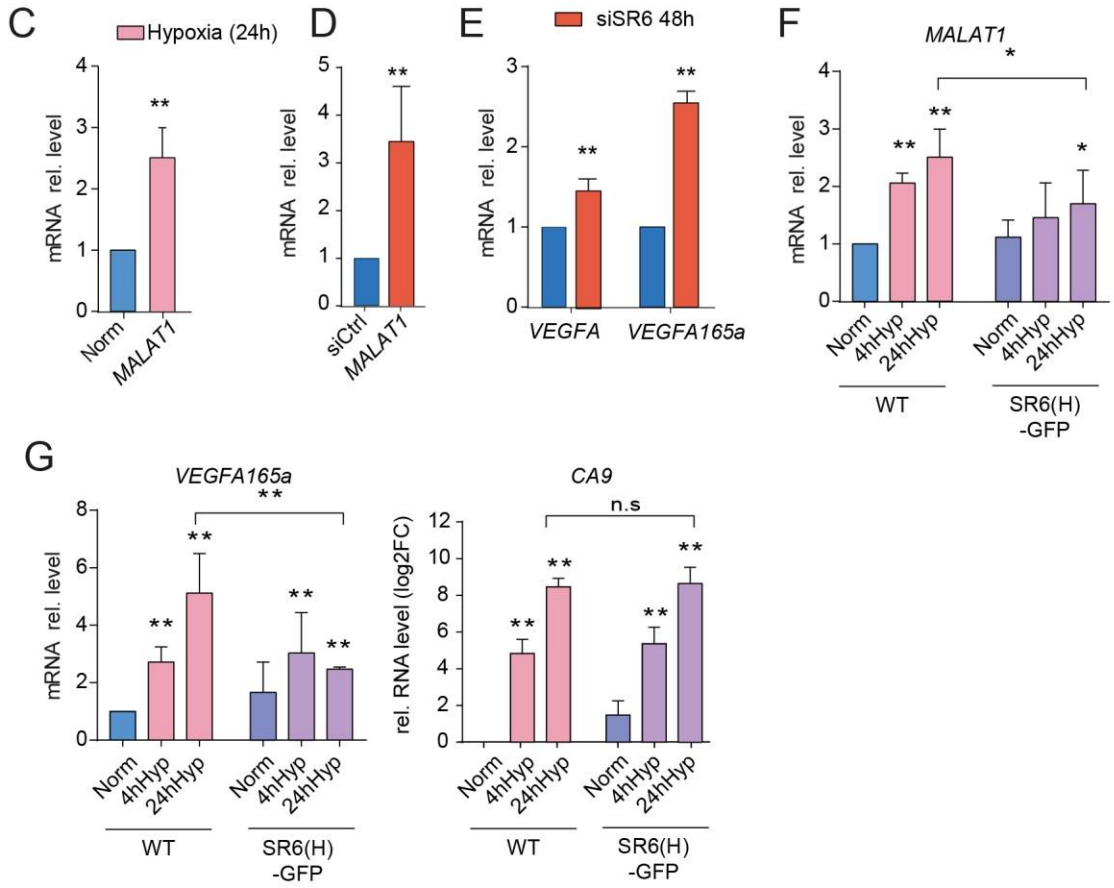

Figure 29. SRSF6 regulates *MALAT1* expression in normoxia and hypoxia. A) Browser shots of significant SRSF6 X-links on the *MALAT1* transcript in normoxia, 4h and 24h hypoxia. **B)** Number of SRSF6 X-links mapping to the indicated transcripts in percent compared to all X-links in normoxia, 4h and 24h hypoxia. **C-G)** RT-qPCR analyses to quantify expression levels of the indicated transcripts in hypoxia and SRSF6 KD. T-tests were performed to compare the levels of the indicated transcripts in all conditions relative to normoxia or control siRNA samples. T-tests were performed to compare transcript levels in SRSF6(H)-GFP cells in 24h hypoxia to WT cells in 24h hypoxia (n=3 replicates, *p<0.05, **p<0.01).

4.10. SRSF6 overexpression in hypoxia increases *MALAT1* accumulation in nuclear speckles

To compare the localization of *MALAT1* in normoxia and hypoxia and study the effect of SRSF6 overexpression we performed RNA FISH coupled with immunofluorescence (IF) in WT and SRSF6(H)-GFP cells. In normoxia, *MALAT1* localized mostly to the nucleoplasm of both cell lines (Figure 30A). In hypoxia, there is a general increase in *MALAT1* signal in both cell types, in line with *MALAT1* induction, however, SRSF6(H)-GFP cells show a different localization pattern compared to WT cells. While *MALAT1* signal increases similarly in the nucleoplasm and nuclear speckles in WT cells, in SRSF6(H)-GFP cells *MALAT1* signal increases only in nuclear speckles with a concomitant decrease in nucleoplasmic signal (Figure 30B).

In order to better compare the *MALAT1* distributions we generated line scan profiles and determined the signal intensity per pixel of *MALAT1*, SRSF6 and the nuclear speckle marker SC35 throughout the cell (Figure 30C). These profiles revealed that accumulations of *MALAT1* signal coincide precisely with SC35 signal confirming the localization of *MALAT1* to nuclear speckles. Defining a threshold for the nucleoplasmic signal (signal intensity per pixel < 50; dashed lines), we observed that in normoxia most *MALAT1* signal is nucleoplasmic with minor fluctuations, independent of the cell line (Figure 30C). In hypoxia, the profile shows multiple high peaks exceeding the threshold indicative of increased co-localization with SC35 and nuclear speckle localization. Although an increase in speckle related peaks (red arrows) is apparent for both cell lines, in SRSF6(H)-GFP cells the nucleoplasmic signal is much lower (Figure 30C). SRSF6 and *MALAT1* also co-localize in nuclear speckles, as indicated by the SRSF6 profile (Figure 30C; green). These data suggest that SRSF6 overexpression also decreases the nuclear mobility of *MALAT1* by sequestering it in nuclear speckles, and thus may impair its cotranscriptional splicing activities in hypoxia. In line with this, SRSF6 was recently identified as a core nuclear speckle component, while *MALAT1* is not required for speckle integrity (Hochberg-Laufer, 2019).

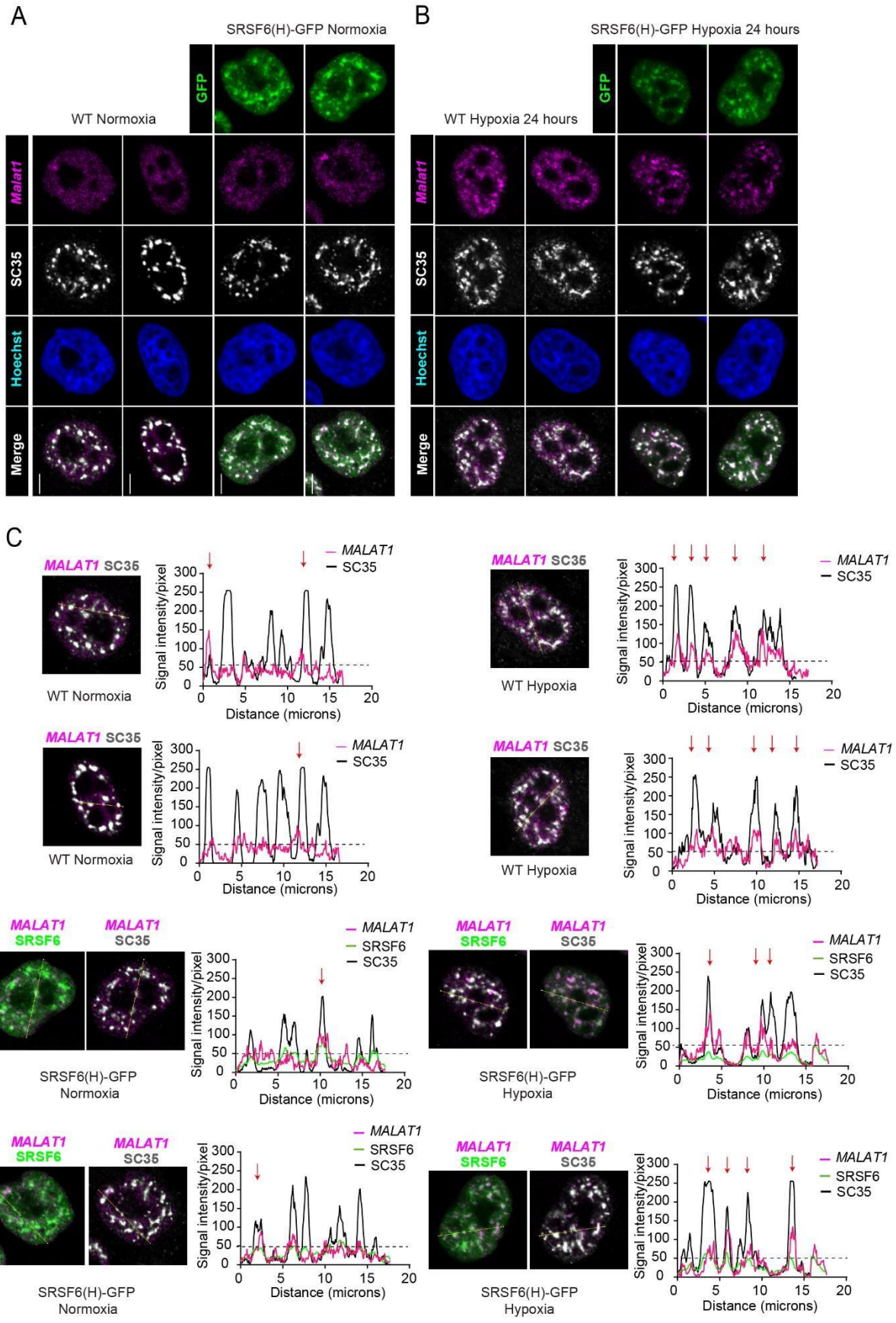
A
SRSF6(H)-GFP Normoxia
WT Normoxia
GFP
Malat1
SC35
Hoechst
Merge
B
SRSF6(H)-GFP Hypoxia 24 hours
WT Hypoxia 24 hours
C
MALAT1 SC35
WT Normoxia
WT Hypoxia
MALAT1
SC35
Signal intensity/pixel
Distance (microns)
MALAT1 SRSF6
SRSF6(H)-GFP Normoxia
SRSF6(H)-GFP Hypoxia
SRSF6

Figure 30. SRSF6 overexpression sequesters *MALAT1* in nuclear speckles upon hypoxia. A-B) Panel of *MALAT1* FISH-IF images of WT and SRSF6(H)-GFP cells line in normoxia (A) and 24h hypoxia (B). Representative images show the GFP signal (green), *MALAT1* (magenta), SC35 (grey), nuclear staining Hoechst (blue) and the merge of the *MALAT1*-SC35-SRSF6 channels. **C)** Line profiles from WT and SRSF6(H)-GFP cells in normoxia and 24h hypoxia. A line was traced in diagonal through the cell nucleus to acquire the longest distance containing nucleoplasm and speckle signal without crossing the nucleolus. The signal intensity per pixel in the line area was measured on Fiji and plotted on GraphPad Prism. Red arrows indicate speckle localization based on speckle marker SC35 signal. Dashed line represents the threshold for nucleoplasmic signal (Scale bars = 5µm).

4.11. *MALAT1* depletion in hypoxia phenocopies SRSF6 overexpression and causes formation of micronuclei

We hypothesized that impaired co-transcriptional splicing activities of *MALAT1* upon SRSF6 overexpression may have contributed to the phenotype we have observed in hypoxia – the formation of micronuclei. Indeed, *MALAT1* depletion was shown to cause cell cycle arrest and replication errors (Vidisha et. al, 2010). To test this, we depleted *MALAT1* in normoxic and hypoxic conditions using antisense oligonucleotides (ASOs) targeting two different regions of the *MALAT1* transcript. KD efficiency and hypoxia response were confirmed by RT-qPCR using *MALAT1*- and *CA9*-specific primers (Figure 31A). *VEGFA165a* levels were decreased upon *MALAT1* KD in hypoxia, confirming that *MALAT1* normally promotes splicing of this isoform antagonizing SRSF6 (Figure 31B). *MALAT1* KD did not affect *SRSF6* transcript levels in both conditions (Figure 31C).

We next inspected micronuclei abundance and nuclei shape aberrations upon *MALAT1* KD in normoxia and hypoxia. As shown in Figures 31D-E and Figure S4B, *MALAT1* depleted cells showed an increase in micronuclei formation in normoxia and this effect is even more pronounced in hypoxia (10% to 20% of cells containing micronuclei). Furthermore, solidity of *MALAT1* depleted nuclei is significantly lower than control cells in normoxia and hypoxia (Figure 31F).

Since *MALAT1* KD displayed a similar phenotype as SRSF6 overexpression with regard to cell division errors, we postulate that SRSF6 depletion during hypoxia serves a dual purpose; on the one hand it allows exon skipping of direct SRSF6 target exons, and on the other hand it allows boosting of *MALAT1* expression and enhances its nuclear mobility to allow co-transcriptional splicing of non-SRSF6 target isoforms that are also required for hypoxia adaptation.

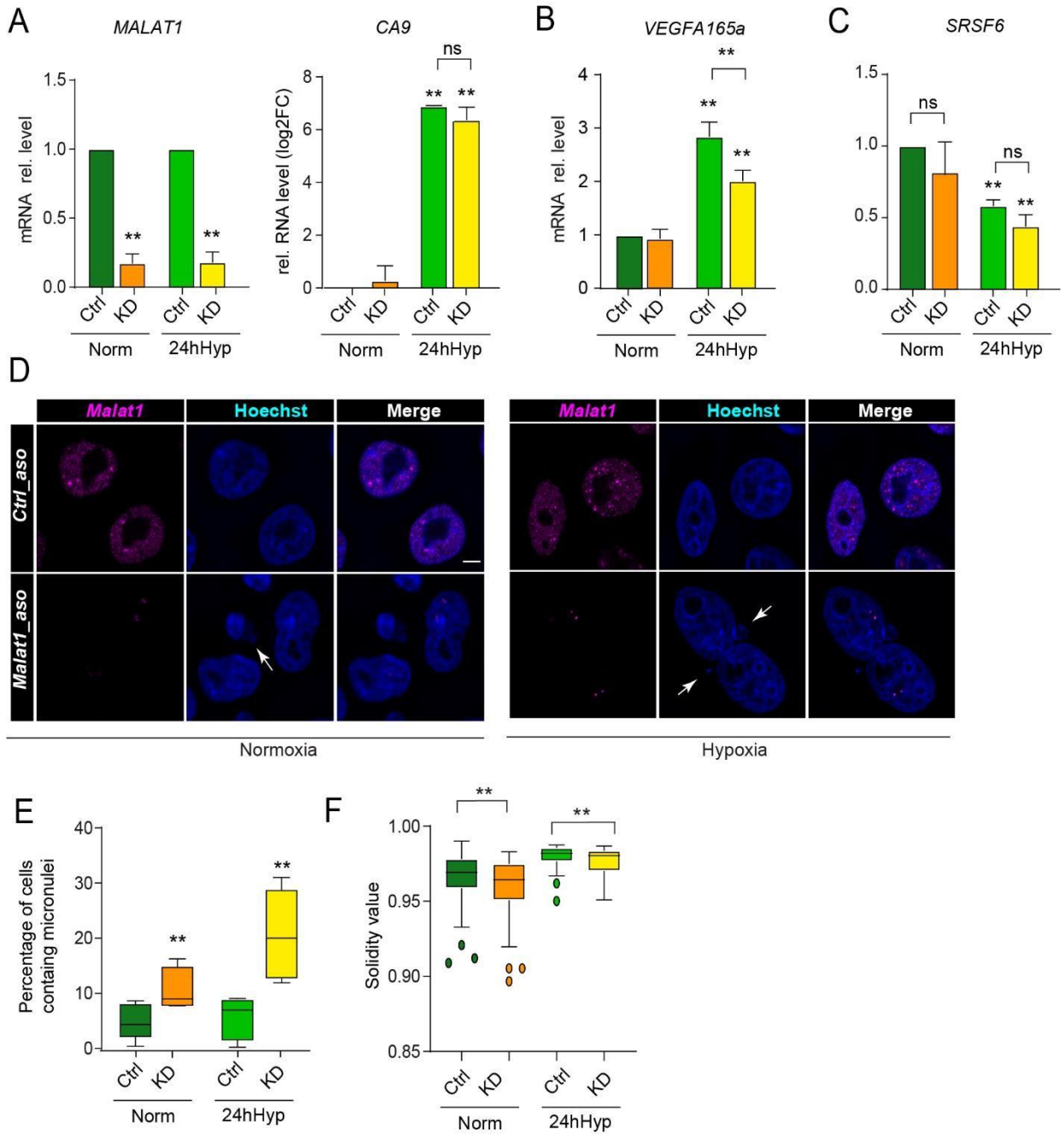

Figure 31. *MALAT1* KD phenocopies SRSF6 overexpression in the formation of micronuclei and aberrant nuclei shapes. A-C) RT-qPCR quantification of expression levels of the indicated transcripts in *MALAT1* KD in normoxia and 24h hypoxia. T-tests were performed to compare the levels of the indicated transcripts in all conditions relative to the normoxia control ASOs. A second T-test was performed to compare transcript levels on *MALAT1* KD cells relative to ASO control in 24h hypoxia (n=3 replicates, *p<0.05, **p<0.01). **D)** Fluorescence images of *MALAT1* control and KD cells in normoxia and 24h hypoxia showing micronuclei (white arrows). **E)** Quantification of micronuclei events in *MALAT1* control and KD cells in normoxia and 24h hypoxia. Images containing ca. 20 cells were acquired and the number of micronuclei was counted. The percentage of cells containing micronuclei per field was calculated and plotted using

GraphPad Prism (n=2, >100 cells per experiment). **F)** Solidity values of cell nuclei from *MALAT1* control and KD cells in normoxia and 24h hypoxia. (n=2; >200 cells per condition). Differences in nuclei solidity were tested relative to control cells in both conditions (T-test, *p<0.05, **p<0.01).

Based on our data, we propose that SRSF6 is an important regulator of the alternative splicing response to hypoxia. It binds to exons in normal conditions and promotes their inclusion. Upon hypoxia, SRSF6 depletion allows exon skipping and expression of isoforms, which are important for the hypoxia response. Skipping of SRSF6 exons might also allow their circularization and promotes circRNA formation in hypoxia. In addition to regulation of its direct targets, SRSF6 controls *MALAT1* expression level and its nuclear mobility/splicing availability to ensure splicing of anti-angiogenic *VEGFA* isoforms and likely many other target transcripts. SRSF6 overexpression in hypoxia, however, impairs *MALAT1* activities and splicing of pro-angiogenic isoforms, thereby resulting in abnormal splicing and cell division errors. This could lead to increased DNA damage and mutagenesis culminating in a more aggressive and metastatic tumor phenotype. The DNA damage repair response pathway leads to activation of cellular apoptosis. This response prevents survival and accumulation of cancer cells. Thus SRSF6 represents an interesting target for cancer intervention, it acts as an oncogene and higher expression levels might increase tumor metastasis and aggressiveness upon hypoxia. As an example, we show that SRSF6 can promote splicing of the anti-apoptotic isoform of *MDMD4*.

5. Discussion

In this study we investigated changes in gene expression and alternative splicing (AS) in response to hypoxia in HeLa cells as a model for cancer cells and demonstrated that down-regulation of the splicing factor SRSF6 is crucial for an appropriate AS response to hypoxia. A failure to down-regulate SRSF6 in hypoxia causes a misregulation of several alternative isoforms and results in DNA damage, aberrant chromosome segregation and abnormal cancer cell growth.

Specifically we show that hypoxia induces changes in expression and AS of thousands of transcripts, many of which are involved in cell cycle regulation, mitotic spindle assembly and chromosomal segregation. In addition to AS of mRNAs, backsplicing and circRNA formation is induced in hypoxia. We further show that SRSF6 is strongly down-regulated in hypoxia and this down-regulation is essential for an appropriate hypoxia response at the level of AS. SRSF6 down-regulation promotes I) the skipping of many SRSF6 target exons, II) splicing of the pro-angiogenic isoform of *VEGFA*, an essential hypoxia response factor, III) the formation of circRNAs, which might fulfill specific functions in hypoxia, IV) *MALAT1* induction in hypoxia, and V) the nuclear mobility and availability of *MALAT1* for co-transcriptional splicing. Failure to downregulate SRSF6 prevents exon skipping, *VEGFA165a* splicing and the formation of circRNAs, and sequesters *MALAT1* in nuclear speckles (NS). As a consequence, SRSF6 overexpressing cells present higher numbers of micronuclei and DNA damage sites, a phenotype that is mimicked by *MALAT1* depletion.

We propose a mechanism whereby SRSF6 down-regulation in hypoxia serves a dual purpose. On the one hand it allows AS of direct SRSF6 targets, and on the other hand it regulates the mobility and availability of *MALAT1*. Normally, SRSF6 competes with SRSF1 for binding sites within *MALAT1*. During hypoxia, SRSF6 levels decrease, the nuclear mobility of *MALAT1* increases and SRSF1-*MALAT1* complexes leave the NS and move to the transcription sites to splice SRSF1 target exons co-transcriptionally. In contrast, SRSF6 overexpression replaces SRSF1 from *MALAT1* and sequesters it instead within NS, impairing the splicing of SRSF1 targets in hypoxia (Figure 30).

Finally, we present here the first comparative iCLIP experiment in normoxic and hypoxic cells and identified and validated several novel targets of SRSF6. These targets show exon skipping or circularization in hypoxia and upon SRSF6 depletion, but exon inclusion and linear splicing upon SRSF6 overexpression. A model of mechanism of AS splicing regulation in hypoxia by SRSF6 and *MALAT1* is shown in Figure 30.

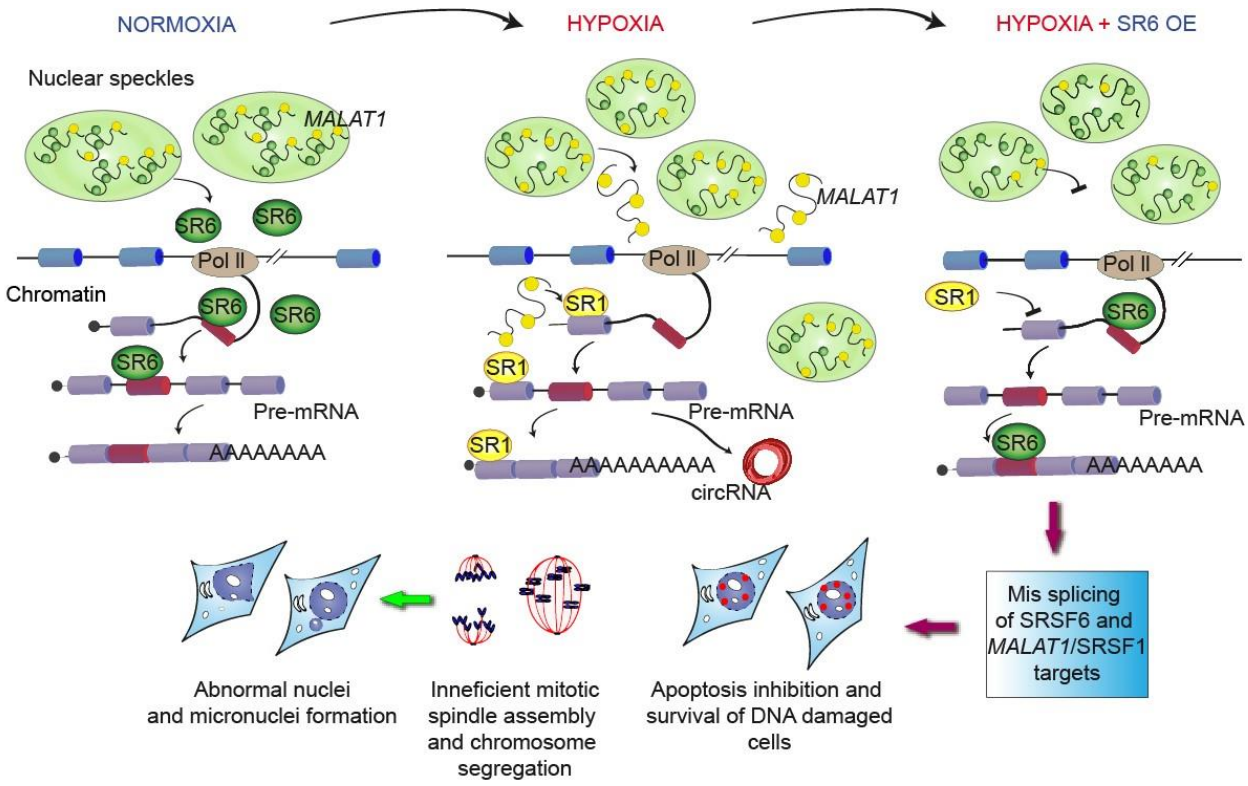

Figure 32. Mechanism of AS regulation by SRSF6 in hypoxia. In normal conditions SRSF6 is expressed at high levels and promotes inclusion of its target exons. SRSF6 is present in the nucleoplasm and within nuclear speckles (NS) where it binds to *MALAT1*. In hypoxia, *MALAT1* levels increase and SRSF6 protein decreases. Remaining SRSF6 is concentrated in speckles. *MALAT1* is now bound by SRSF1, which is activated in hypoxia and leaves the NS and relocates to the chromatin. SRSF6 target exons are skipped and SRSF1-*MALAT1* targets are alternatively spliced. This leads to the generation of pro-apoptotic and pro-angiogenic isoforms, AS of chromatin assemblers and cells cycle regulators, cell survival and adaptation to hypoxia. Upon SRSF6 overexpression in hypoxia, SRSF6 remain high and on the one side, SRSF6 can still bind to its target exons promoting the splicing of anti-angiogenic and anti-apoptotic isoforms. On the other side, it binds more to *MALAT1* in NS and impairs *MALAT1*-SRSF1 complexes from moving to the transcription sites, which prevents AS of *MALAT1/SRSF1* targets. SRSF6 overexpression leads to the survival of DNA damaged cells, inefficient mitotic spindle assembly and chromosome segregation. Cells show increased numbers of micronuclei and abnormal nuclei formation.

5.1. Gene expression and alternative splicing regulation in hypoxia

5.1.1 Identification of differential expressed genes and regulated biological processes in hypoxia

In this study, we identified 7962 differentially expressed genes (DEGs) in HeLa cells after 24h hypoxia (0.2% O_2). Previous studies have also shown that hypoxia induces global changes in gene expression in human cancer cells. Highly expressed genes in hypoxia have been investigated as potential markers in cancer development and

progression (Chi et al. 2006; El Guerrab et al. 2017; Favaro et al. 2011). Up-regulation of genes in hypoxia is mostly caused through enhanced transcription by the hypoxiainducible transcription factor (HIFs) family. We performed gene ontology analyses, which showed that the hypoxia conditions used in this study confirm previously described changes in gene expression and induction of biological pathway processes. Genes induced by HIFs were involved in the metabolic response to hypoxia, such as exchange from aerobic ATP production to glycolysis, cell migration, apoptosis and induction of endothelial cell growth (Hu et al. 2003; Bartoszewski et al. 2019). We confirmed in our data that HIF1α is stabilized and target genes such as CA9, VEGFA, PLOD2 and GAPDH were induced.

Our results also show that half of the DEGs (3862 genes) are down-regulated in hypoxia. This is consistent with previous studies that showed that an important part of the hypoxia response is the down-regulation of energy-consuming processes. We found that genes assigned to biological processes such as mitotic cell cycle progression, RNA metabolism, RNA splicing and ribosome biogenesis were down-regulated. The same processes were also down-regulated in in hypoxia in 16 different breast cancer cell lines (Abu-Jamous et al. 2017). In normal conditions, transcription of some genes involved in these processes is induced by the transcription factor MYC. It has been shown that in hypoxia, HIF1α stabilization leads to inhibition of MYC target genes (Dang et al. 2008). One mechanism for this inhibition is the HIF1α induced transcription of MIX, which binds to MYC and impairs is activities. In addition, HIF1 alpha also competes with MYC for binding to the cofactor MAX leading to MYC inactivity and down-regulation of its target genes (Corn et al. 2005; Gordan et al. 2007; Koshiji et al. 2004). In line with these previous studies, in our dataset we identified MYC target genes, such as the Ribosomal protein L3 (*RPL3*), the splicing factor *SRSF7* and cell cycle regulators *CDC25A* and *CDC25C* to be down-regulated in 24h hypoxia (Zeller et al. 2003).

5.1.2 AS as a hypoxia response mechanism

AS is an important mechanism for the post-transcriptional regulation of gene expression. In hypoxia, thousands of transcripts are alternatively spliced (Bowler et al. 2018). We found in our analyses that 4434 transcripts undergo AS and the most occurring AS event is exon skipping. A previous study in MCF7 cell lines has identified intron retention as the most common AS event (Han et al. 2017). This contrasting result could be due to the different cell line and hypoxia conditions used in the study (1% O_2). Indeed, the number of DEGs identified was also smaller (<1000 genes) as well as total AS events (1684) (Han et al. 2017). In agreement with our data, Sena and colleagues showed that in Hep3B cells, exon skipping was also the most common AS event in hypoxia (1.5%O_2 for 16h) predicted by two different AS analysis tools (Sena et al. 2014). Furthermore, they reported that most AS events occur in transcripts whose transcription is not induced in hypoxia. These results highlight the importance of AS as an additional layer of gene expression regulation in hypoxia. We also performed a gene ontology analysis for splice isoforms, and interestingly, we found three biological processes enriched in our dataset, all related to centrosome and microtubule protein localization. The findings are in line with previous findings which show that transcripts many alternatively spliced transcripts in cancer cells are involved in cell cycle progression and regulation (Dominguez et al. 2016; Moore 2005; Oltean and Bates 2014).

5.1.3 Putative functions of newly identified splice isoforms in hypoxia

From our splicing analysis, we have chosen 5 transcripts and successfully validated the predicted AS events. With the exception of *EIF4A2*, NMD inhibition did not cause an accumulation of these alternative isoforms in normoxic or hypoxic conditions. This indicates that these alternative isoforms are not unstable NMD targets, but are rather translated into protein isoforms with altered functionalities. AS of *BORA* (aurora kinase A activator) leads to skipping of exons 3 and 5. *BORA* is an important cell cycle regulator. Its phosphorylation leads to the activation of aurora protein kinase and recruitment of the polo like kinase 1 (PLK1). This complex has an important function in promoting cell cycle progression after mitotic arrest due to the DNA damage repair response (Parrilla et al.

2016; Zheng and Yu 2018). Mutations in *BORA,* which impair its phosphorylation were shown to inhibit its activity and cause cell cycle arrest (Bruinsma et al. 2017; Vigneron et al. 2018). Although the phosphorylated amino acids are not encoded by the skipped exons, *In silico* prediction indicates that this exon skipping event could lead to translation of an altered protein isoform which lacks 50 amino acids (aa) at the protein N-terminal (full length isoforms: 620aa; skipped isoform: Δaa112-162). This isoform might either not interact with its partners or not be phosphorylated. However, this alternative protein isoform has not been characterized so far. Further studies are required to understand the effects of the missing exons on the final transcript and the encoded protein.

In silico translation indicates that skipping of exon 28 of the centrosomal protein 192 (*CEP192*) leads to a deletion of 56 amino acids from the full length protein. Previous studies have shown that CEP192 interacts with Aurora kinase A and PLK1 regulating centrosome and spindle assembly during mitosis (Gomez-Ferreria and Sharp 2008; Gomez-Ferreria et al. 2007; Joukov et al. 2014). Deletions in CEP192 showed that interactions with Aurora kinase A and PLK1 occurs in different protein domains. However, deletion of the region containing the amino acids that are lacking in the putative alternative isoform of *CEP192* did not show any effects on these interactions (Meng et al. 2015). CEP192 can be highly phosphorylated and this phosphorylation leads to interaction and recruitment of cell cycle regulators and centrosome components (Nasa et al. 2017). Based on the *in silico* translation prediction, the protein derived from the skipped isoform would have less serine and tyrosine amino acids as the full-length isoform. Thereby, this could potentially affect the phosphorylation state of CEP192 and thereby its function. AS of Centrosome and Spindle Pole Associated Protein 1 *CSSP1* results in the formation of a large long isoform denominated *CSSP-L*. Here we show that this isoform is down-regulated in hypoxia, while the shorter *CSSP1-S* isoform is increased. CSSP1 protein is involved in the regulation of cell cycle progression from S-phase into G1 phase by promoting mitotic spindle assembly. In contrast, CSSP1-L overexpression induced formation of protein aggregates and impairment of cell cycle progression (Patzke et al. 2006). In light of these results, in hypoxia, higher expression of CSSP1-S might be important to induce cellular division and proliferation.

We further show that in normal conditions an intron-retained isoform of the eukaryotic initiation factor A2 (*EIF4A2)* is expressed in addition to the canonical proteincoding isoform. This alternative isoform seemed to be a NMD target, since it was accumulated upon CHX treatment in normoxia. However, in hypoxia, the NMD target isoform decreased and the main protein-coding isoform increased. There are not many studies on EIFA2 and its functions, but it has been reported that EIFA2 protein has helicase activity, which is important for the translation of pro-oncogenic mRNAs with more structured 5'UTRs (Raza et al. 2015). Furthermore, a recent study has shown that EIFA2 has a role in stress granule formation upon cellular stress (Jongjitwimol et al. 2016). Our results show that the protein-coding isoform of *EIF4A2* is increased upon hypoxia suggesting that EIF4A2 might be important for the translation of hypoxia-induced mRNAs or stress granule formation in this condition.

Finally, we show that the short isoform of the MDM4 regulator of p53 mRNA (*MDM4-S*) lacking exon 6 is increased upon hypoxia. This splice event leads to the formation of a shorter protein isoform (MDM4-S). The role of the two protein variants of MDM4 (MDM4-FL and MDM4-S) has been previously described in cancer cells. MDM4FL represses p53 transcriptional activity by interacting with the DNA binding domain of p53 (Rallapalli et al. 1999). The MDM4-S isoform lacks the p53 interaction domain and does not suppress its activity. This isoform has been shown to be up-regulated in cancer cells as a mechanism to activate the apoptosis signaling pathway (Pant et al. 2017). Here we show that upon hypoxia the MDM4-S isoform is increased. In HeLa cells, p53 is not expressed, however regulation of this splicing event in hypoxia could indicate that MDM4 has other functions in these cells. Indeed, recent studies have shown that apart from its role in suppressing p53 activity, MDM4 is involved in mitotic multipole spindle formation and inhibits the kinase mTOR (Matijasevic et al. 2007; Mancini et al. 2017). Although MDM4-S counteracts MDM4 function as p53 repressor, it has not yet been shown if it can also impair its other functions. Our results suggest that this protein might have functions in HeLa cells in response to hypoxia, which are probably unrelated to p53 activation. Further studies are necessary to understand the importance of MDM4S isoform in response to stress.

In conclusion, we have identified and validated novel hypoxia-induced splicing events, which, with the exception of *EIF4A2*, culminate in the translation of different protein isoforms. All proteins are involved in cell cycle regulation, either by promoting assembly of centrosomes and mitotic spindles (*CEP192, CSPP1, MDM4*), or by interacting with key cell cycle regulators (*BORA*). Taken together, these results support the importance of AS for cell cycle regulation in hypoxia.

5.1.4 Backsplicing and generation of circRNAs is induced in hypoxia

In this study we identified 3,926 circRNAs expressed in HeLa cells in normoxia and hypoxia conditions, using a combination of two different circRNA identification tools, Find_circ and CIRCexplorer (Memczak et al. 2015; Zhang et al. 2014). This tools take reads which are not linear mapped to the genome to predict circRNA transcripts based on their backsplice junctions. Previous studies in different cell lines have also shown that circRNAs can be highly abundant. For example, 5500 circRNAs were identified in gastric cancer tissues with the find_circ pipeline and 7388 circRNAs were found in Human umbilical vein endothelial cells (HUVECs) in normoxia and hypoxia conditions (Chen et al. 2017a; Boeckel et al. 2015). It is important to emphasize that a big portion of predicted circRNAs can be false positives. Recently, it has been shown that different circRNA predictions tools have a small overlap of the final predicted circRNAs (Hansen 2018). Therefore, combining tools and more stringent filter strategies can improve the prediction of true circRNAs. Here, we combined two different tools and filtered for circRNA candidates, which had at least 2 unique reads supporting the backsplice junction. Using this approach, we were able to validate the circularity of all tested circRNAs.

Our results show that some circRNAs were up-regulated in hypoxia in HeLa cells. In HUVECs, circRNAs were also induced in hypoxia, although the up-regulated circles were not identical (Boeckel et al. 2015). We found 22 circRNAs that were differentially expressed in HeLa hypoxic cells. Only one circRNA, *circZNF292*, was up regulated in hypoxia in both, HUVECs and HeLa cells. *circZNF292* is generated through circularization of the alternative exon 1a and exon 2 of the *ZNF292* transcript. We identified an alternative isoform of *circZNF292* in HeLa cells, which contains the exons 2 and 3. We denominated these isoforms intronic and exonic *circZNF292* (*intZNF292* and *exoZNF292*), respectively.

Boeckel and colleagues performed a knockdown (KD) of *circintZNF292* in HUVECs in normoxia and hypoxia and showed that this circRNA promotes angiogenesis and sprouting of HUVECs in in hypoxia (Boeckel et. al, 2015). It is not known whether the exonic isoform, identified in this study, has a similar function. We tested five other circRNAs that were predicted to be up-regulated in hypoxia (*circRTN4, circMTCL1, circSPECC1, circMAN1A2* and *circPLOD2*). For all of them we were able to confirm their up-regulation. These circular RNAs have been previously identified in different cell types, but their potential functions remain unknown (Li et al. 2017; Kaur et al. 2018; Maass et al. 2017; Nan et al. 2017; Mo et al. 2018; Okholm et al. 2017).

5.2. SRSF6 is downregulated in hypoxia through NMD

We found that mRNA processing and splicing by the canonical splicing machinery is one of the biological processes down-regulated in hypoxia. SR proteins are essential splicing factors involved in conservative and alternative splicing regulation (Wegener and Müller-McNicoll M. 2019; Twyffels et al. 2011; Zhou and Fu 2013), prompting us to investigate the expression levels of the canonical members of the SR protein family (*SRSF1-7*) in hypoxia. Indeed, we found that most of SR protein transcripts were downregulated. *SRSF6* was the most affected, with a 4-fold down-regulation in hypoxia. This effect was not mimicked by $CoCl_2$ treatment and HIF1α stabilization, indicating that other mechanisms induced by hypoxia stress are responsible for the regulation of SR protein level. Supporting this observation, recent studies have also shown that $CoCl_2$ does not mimic several layers of the hypoxia response (Muñoz-Sánchez and Chánez-Cárdenas 2019).

SRSF6 is an interesting but not well-studied member of the SR protein family. It has been shown to be an oncogene, since its up-regulation in cancer cells is associated with tumor progression (Chandradas et al. 2010; Iborra et al. 2013; Wan et al. 2017). Moreover, SRSF6 has been shown to promote splicing of the anti-angiogenic isoform of *VEGFA* (*VEGFA165b*) by counteracting the exon 8a inclusion by SRSF1 (Juan-Mateu et al. 2018; Nowak et al. 2008b). We confirmed AS of *VEGFA* in hypoxia, showing that while total levels of *VEGFA* increase 4-fold in hypoxia, *VEGFA165a* increases 8-fold. In light of

these results and previous studies, we hypothesized that down-regulation of SRSF6 might be important for the hypoxia response and cell survival through the regulation of *VEGFA* splicing and potentially other transcripts.

Interrogation of RNAseq data showed that in hypoxia, an alternative exon containing a premature stop codon (PTC) is included in the *SRSF6* transcript. We validated this exon inclusion event and demonstrated that this NMD isoform is generated in expense of the main protein-coding isoform. NMD isoforms are usually not detectable in normal conditions. They are rapidly degraded by the NMD pathway in the first round of translation (Hwang and Maquat 2011). However, the NMD isoforms of *SRSF6* and *SRSF3* are readily detectable in hypoxia without NMD inhibition. Two mechanisms could explain this observation. First, the NMD signaling pathway has been shown to be less active in hypoxia. It was shown that NMD factors are localized into stress granules in the cytoplasm and cannot perform their function (Gardner 2008). Second, previous studies have shown that global translation is reduced in hypoxia while selective translation is increased. mRNAs containing hypoxia regulated elements are recognized and translated while other mRNAs are not translated due to inhibition of the canonical translation pathway (Uniacke et al. 2012; Chipurupalli et al. 2019). If NMD target RNAs are not bound by ribosomes for the pioneer round of translation, they would not be detected by the NMD machinery. This could also contribute to the accumulation of these isoforms.

Previous studies have shown that *SRSF1, SRSF2* and *SRSF3* levels can be regulated through generation of NMD isoforms (Sun et al. 2010; Sureau et al. 2001; Jumaa and Nielsen 1997). Here we show for the first time that higher expression of the *SRSF6* NMD isoform decreases the level of the main protein-coding *SRSF6* isoform. Furthermore, we show that *SRSF3* is down-regulated in a similar manner in hypoxia. Supporting this mechanism, we did not detect the NMD isoform induction in the $CoCl_2$ treatment where *SRSF6* levels remain constant.

Decrease in expression of the main *SRSF6* isoform in expense of the NMD isoform up-regulation correlated with depletion of SRSF6 protein. We observed that phosphorylated SRSF6 levels remain constant in 24h hours hypoxia but a 40% depletion of SRSF6 was observed in total protein levels. This suggests that SRSF6 is downregulated in hypoxia, but the remaining SRSF6 pool is hyper-phosphorylated. In

agreement with this, previous studies have shown that SR proteins are highly phosphorylated in hypoxia due to the up-regulation of SR protein kinases (SRPK1-2) (Jakubauskiene et al. 2015). Phosphorylation of SR proteins by SRPK1 was shown to target them to NS were they are stored (Aubol et al. 2017; Aubol et al. 2018; MüllerMcNicoll and Neugebauer 2013). In agreement with that, using stable cell lines expressing low levels of SRSF6-GFP tagged protein we show that SRSF6 protein depletion in hypoxia affects mostly SRSF6 protein present in the nucleoplasm. The remaining detectable SRSF6 protein is exclusively localized to NS.

SRSF6 hyper-phosphorylation could increase specific binding to its targets. Our iCLIP data showed that SRSF6 binds strongly to its own PCE, this binding likely promotes the inclusion of this exon and generation of the NMD isoform. In this mechanism, SRSF6 hyper-phosphorylation could lead to increase binding to his own exon in an autoregulatory mechanism. It is very likely that regulation of SRSF6 protein levels occurs in the transcriptional level, since inhibition of the proteasome in normoxia and hypoxia conditions did not result in increased SRSF6 protein levels (data not shown).

Another mechanism in which SRSF6 could be down-regulated in hypoxia in the transcriptional level is the up regulation of SRSF4 in hypoxia. Previous work performed in our lab showed that upon SRSF4 overexpression SRSF6 is down-regulated. This down-regulation is likely due to strong binding of SRSF4 to the *SRSF6* PCE which leads to accumulation of the *SRSF6 NMD* isoform and down regulation of the protein-coding isoform (data not published).

Taken together, this results have shown that SRSF6 protein levels are down regulated in hypoxia due to induction of the *SRSF6* NMD isoform. Furthermore, remaining SRSF6 is higher phosphorylated and localizes to nuclear speckles which could impair SRSF6 binding to most of his target exons.

5.3. SRSF6 down regulation is essential for AS in hypoxia

5.3.1 SRSF6 splicing targets and their potential functions in hypoxia

In this study we have for the first time used comparative iCLIP as a method to compare RNA-binding profiles of an RBP in normoxia and hypoxia. Since SRSF6 levels

are down-regulated in hypoxia, we used cell lines with low SRSF6-GFP levels to acquire a dataset of SRSF6 binding sites, close to physiological conditions. We integrated the iCLIP data with the hypoxia AS data and found that SRSF6 binds more to exons that are skipped in hypoxia. This observation is in line with the proposed mechanism, whereby SRSF6 and other canonical members of the SR protein family enhance the inclusion of bound alternative exons (Zhou and Fu 2013; Shepard and Hertel 2009). Manual interrogation of the iCLIP data identified 4 alternatively spliced transcripts, which showed differential SRSF6 binding in normoxia and hypoxia. Loss of SRSF6 binding to exons correlated with their skipping in hypoxia. Using a stable SRSF6 overexpresser cell line we then showed that exon skipping of these 4 targets is impaired in hypoxia.

Moreover, splicing of the pro-angiogenic isoform of *VEGFA (VEGFA165a)* is impaired upon SRSF6 over-expression. These results showed that exon inclusion is regulated by SRSF6 and that too high SRSF6 levels impair proper AS of these exons in hypoxia.

Specifically, we found that inclusion of exon 6 of *MDM4* is regulated by SRSF6. Skipping of this exon results in the translation of a shorter protein isoform, which has opposite functions than the main isoform. Furthermore, we found that skipping of exon 4 of *CHAF1A* (chromatin assembly factor 1 subunit A), exon 5/6 of *SNAP25* (Synaptosome associated protein 25) and exon 19 of *PAPOLA* (PolyA polymerase alpha) was also impaired by SRSF6 overexpression in hypoxia. In the following paragraphs we explore potential functions of the alternative spliced transcripts based on the available literature. We have not tested whether protein isoforms encoded by the AS isoforms are more expressed in HeLa upon hypoxia. However, the hypothesis and putative functions put forward here allowed us to generate a model, which will help us to understand the importance of SRSF6 in counteracting the hypoxia response through an impairment of splicing of target exons.

CHAF1A has been described as an important chaperone and histone assembly factor. During DNA replication, CHAF1A interacts with histones H3/H4 and deposits them into newly replicated DNA. The longer subunit of CHAF1A has been shown to be essential for the interaction with nucleosome components and its activity. Furthermore, CHAF1A has also been described to be important for chromatin assembly and modulation during

the DNA repair response after DNA damage (Lechner et al. 2005; Moggs et al. 2000; Sauer et al. 2018; Xin et al. 2018). AS of *CHAF1A* can lead to generation of a proteincoding isoform, which does not contain the histone interaction domain of the main protein isoform. This alternative isoform has been annotated, but not yet studied. Exon skipping by SRSF6 could lead to the formation of this protein isoform and impair the DNA damage response and chromatin assembly in hypoxia.

SNAP25 is part of the SNARE (soluble N-ethylmaleimide-sensitive factor attachment protein receptor) complex and is essential for cellular communications through lysosome and vesicle trafficking. This protein has been mostly studied for its function in modulating synaptic vesicle trafficking (Irfan et al. 2018; Jiang et al. 2019; Ramos-Miguel et al. 2018). However, recent studies have demonstrated the importance of SNAP25 regulation in cancer cells (Mu et al. 2018). KD of SNAP25 suppresses the uptake of anti-angiogenic and pro-apoptotic proteins through endosomes in endothelial cells (Chen et al. 2018). Importantly, SNAP25 has been already shown to be regulated through AS. The alternatively spliced isoform *SNAP25b* is protein-coding and has a negative effect on the function of *SNAP25a* (Kádková et al. 2018). Here we show that *SNAP25* is alternatively spliced in hypoxia and the *SNAP25b* isoform is increased. In light of previous studies, we suggest that AS of *SNAP25* in hypoxia can be important to inhibit anti-angiogenic and pro-apoptotic protein traffic.

PAPOLA is a polyA polymerase, which binds to newly transcribed pre-mRNA and adds adenosines for the PolyA-tail. PAPOLA activity is essential for proper pre-mRNA processing and maturation. Addition of a PolyA tail recruits polyA binding proteins, can cause nuclear retention of transcripts or cause their degradation due to mis-splicing (Muniz et al. 2015). Fours isoforms are described for the PAPOLA transcript, which are protein-coding (Zhao and Manley 1996). Here we show that in hypoxia, the exon 20 skipped isoform *PAPOLA II* is up-regulated. This isoform encodes a protein that lacks 21 amino acids within the C terminal region. According to previous studies, loss of this domain might impair PAPOLA interaction with proteins of the 14-3-3 family. This interaction normally inhibits PAPOLA activity, therefore up-regulation of the *PAPOLA II* splicing isoform might lead to the translation of a constitutively active protein isoform (Colgan et al. 1998; Kim et al. 2003; Rapti et al. 2010). PAPOLA activation can lead to

an increase in number of adenosines added to the PolyA tails. It has been previously showed that longer Poly A tails can enhance translation (Rutledge et al. 2014; Fuke and Ohno 2007), or enhance nuclear retention and decay (Bresson and Conrad 2013).

Since in hypoxia, selective translation of hypoxia response transcripts is induced, one could propose that these transcripts might have longer Poly A tails as a mechanism to improve translation efficiency.

5.3.2 SRSF6 inhibits circRNA formation in hypoxia

In this study, we show that circRNA formation is induced in hypoxia. Furthermore, we show that SRSF6 down-regulation in this condition increases skipping of its target exons. Previous studies have shown that exon skipping is one of the mechanisms leading to circRNA formation (Starke et al. 2015). Here we show for the first time that SRSF6 depletion promotes circRNA formation in normoxia and hypoxia conditions. SRSF6 KD in normoxic cells induced the formation of 4 circRNAs, which were also up-regulated in hypoxia: *circPLOD2, circMTCL1, circMAN1A2* and *circRTN4*. Furthermore, 3 other circRNAs (*circHIPK3, circSRSF4* and *circCPSF6),* tested in this study, were up-regulated upon SRSF6 KD. Interrogation of the iCLIP data revealed that SRSF6 binds with high affinity to these circularized exons. In contrast, *circZNF292,* which was not up-regulated by SRSF6 KD, did not show binding of SRSF6 to the circularized exons (data not shown). This supports our hypothesis that SRSF6 might suppress circRNA formation by binding to circularized exons and promoting their linear splicing. Indeed, we showed that upon SRSF6 overexpression in hypoxia, the formation of *circPLOD2, circMAN1A2* and *circRTN4* was repressed.

Exon skipping and the formation of circRNAs can lead to generation of alternative splice isoforms, which do not contain the circularized exons (Suzuki and Tsukahara 2014; Ashwal-Fluss et al. 2014). We performed AS analyses but did not detect these events. One possible reason for this could be the lower stability of these exon-skipped isoforms. They might be rapidly degraded precluding their detection. It is possible that these alternative spliced isoforms could be generated as a consequence of increase in the main host expression. Transcriptional increase of the host gene, but decrease in SRSF6 available for splicing could lead to exon skipping and allows formation of circles.

5.4. SRSF6 modulates *MALAT1* levels and availability in hypoxia

MALAT1 is a highly abundant nuclear long non-coding RNA (lncRNA). Although it is up-regulated in many cancer cells and upon hypoxia, its functions are highly debated in the field. Some studies show that *MALAT1* is up-regulated in cancer cells and in hypoxia, promoting proliferation, cancer cell survival and migration (Wang et al. 2019a). However, latest evidence show that it might suppress cellular migration in endothelial cells and breast cancer metastasis (Kim et al. 2018; Michalik et al. 2014). We believe that *MALAT1* functions might depend of the availability and activity of its protein interactors. For example, on the one hand *MALAT1* was shown to interact with transcription factors and inhibits transcription of important cell cycle regulators and *VEGFA* and this way suppressed tumor metastasis (Kim et al. 2018). On the other hand, *MALAT1* interaction with SRSF1 has been shown to be important for splicing of the pro-angiogenic *VEGFA* isoform and other SRSF1 targets (Tripathi et al. 2010). It is possible that *MALAT1* is bound by different RBPs in different cell types, which in fact modulate its availability and consequently its functions. Supporting this hypothesis, previous studies have shown that binding of mutant p53 protein to *MALAT1* promotes its translocation to the nucleoplasm and to transcription sites (Pruszko et al. 2017). In a similar mechanism, *MALAT1* can modulate AS of SRSF1 transcripts. SRSF1-*MALAT1* complexes can relocate to transcription sites facilitating binding of SRSF1 to its target exons. Here we show that SRSF6 binds to *MALAT1* over the entire length of the transcript. SRSF6 overexpression leads to an accumulation of *MALAT1* in NS in hypoxia. These results suggest a mechanism in which, contrary to SRSF1, SRSF6 binds to *MALAT1* in the NS and prevents its mobilization to the nucleoplasm and transcription sites. In addition, we show that SRSF6 can further repress *MALAT1* functions by regulating its levels. In hypoxia and upon SRSF6 KD, low SRSF6 protein levels lead to an up-regulation of *MALAT1,* whereas overexpression of SRSF6 in hypoxia prevents *MALAT1* induction.

Taken together, our results suggest that SRSF6 overexpression in hypoxia might impair AS of SRSF6 direct target exons and of SRSF1/*MALAT1* target exons. SRSF1 and SRSF6 have a similar binding motif (GGAGGA and GAAGAA) share many binding sites over the entire *MALAT1* transcript (Müller-McNicoll, 2016). Competition for binding

between these splicing factors can modulate *MALAT1* localization and activity. In hypoxia, where SRSF6 levels are depleted, more SRSF1-*MALAT1* complexes can be formed to allow nuclear mobility and facilitate splicing of SRSF1 targets. In line with this hypothesis, it has been shown that SRSF6 is a core NS factor, which remains in NS during cellular stress (Hochberg-Laufer et al. 2019). Therefore, SRSF6 binding to *MALAT1* could lead to this lncRNA retention in NS.

While upon SRSF6 overexpression in hypoxia, SRSF6 binds more to *MALAT1* preventing its translocation and interaction with SRSF1 and suppresses splicing of SRSF1 target exons. Supporting this mechanism, we showed that upon SRSF6 KD inclusion of the exon 8a and up-regulation *VEGFA165a* is induced, while in SRSF6 overexpression this AS event, which is promoted by SRSF1 and *MALAT1* is repressed.

5.5 SRSF6 overexpression in hypoxia protects cells from death due to DNA damage leading to micronuclei formation

SRSF6 has been shown to be an oncogene. It is amplified in lung, colon and skin cancer and its up-regulation correlates with poor prognosis (Cohen-Eliav et al. 2013; Jensen et al. 2014). SRSF6 is also an important splicing regulator in ß-pancreatic cells. It promotes splicing of transcripts involved in chromatin remodeling, exocytosis and cell death (Alvelos et al. 2018). Upon SRSF6 depletion, exon skipping of *BIM, BAX* and *DIABLO* leads to formation of pro-apoptotic isoforms and cell death. SRSF6 up-regulation protects ß-cells from apoptosis by promoting inclusion of its target exons and translation of the anti-apoptotic proteins such as BIM-L (Juan-Mateu et al. 2018). The apoptosis signaling pathway when deregulated can be harmful and lead to death of healthy cells. However, upon DNA damage, activation of the apoptosis pathway prevents accumulation of mutated cells. Uncontrolled growth and division of DNA-damaged cells can lead to cancer and tumor development. SRSF6 normally protects cells from apoptosis, which strongly suggests that this might be the one of the mechanisms, which leads to tumor progression and aberrant cell growth upon SRSF6 up-regulation (Piekielko-Witkowska et al. 2010; Wan et al. 2017). In agreement with this, it was shown that after DNA damage,

SRSF6 is up-regulated and promotes cell proliferation in p53- deficient U2OS cells (Filippov et al. 2008) have shown that after DNA damage, SRSF6 is up-regulated and promotes cells proliferation. In hypoxia, the DNA damage repair pathway is less active, leading to higher numbers of cells with DNA damage and chromosomal instability (Riffle et al. 2017). Here we show an increase of cells containing pH2A.x nuclear foci, indicative of DNA damage, upon SRSF6 overexpression. This increase is already visible in normal condition, but is higher in hypoxia. In light of previous studies, we suggest that SRSF6 overexpression can impair apoptosis of cells after DNA damage. When these cells are submitted to hypoxia, they continue to divide and proliferate leading to chromosomal instability and replication errors.

The AS of anti-apoptotic isoforms by SRSF6 can explain why cells with DNA damage continue to grow, which can lead to further chromosomal instability (Fonseca et al. 2019). However, previous studies showed that KD of SRSF6 in DNA damaged cells only regulates AS of few targets (Filippov et al. 2011). This suggests that up-regulation of SRSF6 might affect proliferation and aggressiveness of cancer cells also by additional mechanisms. Here we show that in hypoxia, SRSF6 directly regulates splicing of genes associated with chromosomal assembly and cell cycle regulation. Interestingly, we also show for the first time that up-regulation of SRSF6 decreases *MALAT1* availability and levels. *MALAT1* regulation can be another mechanism to explain why SRSF6 upregulation has stronger effects on cancer progression than SRSF6 KD. Our results show that increase of SRSF6 binding to *MALAT1* might impair binding of SRSF1 and translocation of *MALAT1*-SRSF1 complexes to the transcription site. This can lead to inefficient splicing of SRSF1 and *MALAT1* targets and act as a second mechanism leading to micronuclei formation due to chromosomal instability and replication errors in cells with high levels of SRSF6. Indeed, previous studies have shown and we confirmed, that *MALAT1* depleted cells present a similar phenotype than the one observed in SRSF6 overexpressing cells ((Tripathi et al. 2010; Tripathi et al. 2013), namely increased number of micronuclei and abnormal nuclei formation.

Taken together our observations strongly suggest that SRSF6 up regulation directly and indirectly regulates AS in hypoxic cells. Mis-regulation of AS in response to

hypoxia my lead to increase in tumor cells growth and proliferation. Therefore, SRSF6 down-regulation is essential to prevent poor prognostics and metastasis in cancer.

6. Conclusions and outlook

In hypoxia thousands of transcripts undergo alternative splicing (AS). AS in hypoxia can lead to expression of different protein isoforms, which might have alternative or opposite functions. In order to survive, cells in hypoxia stress need to suppress energy consuming processes such as protein translation. Cell division is also regulated in hypoxia and apoptosis pathway is activated, likely to prevent cell overgrowth and competition for O_2 and allow survival of the remaining cells. AS of cell cycle regulator transcripts can be a mechanism to modulate cell division and down-regulation of the canonical splicing machinery could be a mechanism to allow global AS regulation and exon skipping. One AS event induced in hypoxia is circRNA formation. Exon circularization in hypoxia might be due to major exon skipping or to the down-regulation of canonical splicing machinery.

SRSF6 is down regulated in hypoxia, and this down-regulation occurs due to AS of the SRSF6 transcript and up-regulation of the non-coding protein isoform, which contains a poison exon cassette with a premature stop codon. SRSF6 promotes inclusion of this poison cassette exon in hypoxia, in an auto-regulatory mechanism. SRSF6 generally promotes exon inclusion when it binds to its target exons. Therefore, SRSF6 down-regulation is necessary for a proper AS of SRSF6 direct targets. SRSF6 depletion also leads to circRNA formation. It is unclear by which mechanism SRSF6-regulated circRNAs form, but we hypothese that circRNA formation could occur through exon skipping of SRSF6 target exons followed by backsplicing. Indeed, we showed that SRSF6 overexpression in hypoxia impairs exon skipping and circularization. To prove the hypothesis that circRNAs are formed through skipping of SRSF6 target exons, further investigation of the putative alternatively spliced isoforms is required.

SRSF6 might also regulate AS of transcripts indirectly. SRSF6 binds with high affinity to *MALAT1* and competes for binding sites with SRSF1. Upon SRSF6 depletion in hypoxia, SRSF1 can bind more to *MALAT1* and these complexes can move to the transcription sites, promoting splicing of SRSF1 target exons, such as exon 8a of *VEGFA*.

When SRSF6 is overexpressed in hypoxia, it represses *MALAT1* functions. On the one hand, it represses *MALAT1* induction. On the other hand, it binds to *MALAT1* and Conclusions and outlook

retains it in nuclear speckles, impairing its mobility and availability. *MALAT1* can no longer efficiently form complexes with SRSF1 and their target exons might not be properly spliced.

To prove these proposed mechanisms AS analyses from RNAseq data of SRSF6 overexpression and *MALAT1* KD in hypoxia will be analyzed in the near future. We expect to find in the overlap of regulated AS targets, genes that are responsible for cell survival and proliferation. To date very few direct SRSF6 AS targets have been identified. This might be due to the fact that KD of SRSF6 reveals only a subset of direct targets, while SRSF6 overexpression would affect a different subset. Investigating the overlap between *MALAT1* KD and SRSF6 overexpression targets might uncover many more AS events, which are causative for cancer development and poor prognosis. Our data will also give insights in the mechanisms that render SRSF6 a pro-oncogene. Targets for therapy in cases of SRSF6 up-regulation might need to be directed towards SRSF1 and *MALAT1* target genes and not only to direct SRSF6 targets. RNA splicing therapy such as antisense nucleotides, which could target alternatively spliced exons could be used to prevent cancer cells proliferation in SRSF6 up-regulated cells.

It remains unclear whether *MALAT1* forms also complexes with other splicing factors that are also impaired by SRSF6 overexpression. The increased localization of *MALAT1* in speckles is a good indicative that it is sequestered by SRSF6. To investigate this, *MALAT1* pull-downs and the Capture and Hybridization Analysis of RNA Targets (CHART) method (Simon et al. 2011) can be used to investigate whether upon SRSF6 overexpression *MALAT1* is less bound by its interactors, e.g. SRSF1 and less recruited to the chromatin.

7. References

Abdelmohsen, Kotb; Panda, Amaresh C.; Munk, Rachel; Grammatikakis, Ioannis; Dudekula, Dawood B.; De, Supriyo et al. (2017): Identification of HuR target circular RNAs uncovers suppression of PABPN1 translation by CircPABPN1. In *RNA biology* 14 (3), pp. 361–369. DOI: 10.1080/15476286.2017.1279788.

Abu-Jamous, Basel; Buffa, Francesca M.; Harris, Adrian L.; Nandi, Asoke K. (2017): In vitro downregulated hypoxia transcriptome is associated with poor prognosis in breast cancer. In *Molecular cancer* 16. DOI: 10.1186/s12943-017-0673-0.

Allende-Vega, N.; Dayal, S.; Agarwala, U.; Sparks, A.; Bourdon, J-C; Saville, M. K. (2013): p53 is activated in response to disruption of the pre-mRNA splicing machinery. In *Oncogene* 32 (1), pp. 1–14. DOI: 10.1038/onc.2012.38.

Alvelos, Maria Inês; Juan-Mateu, Jonàs; Colli, Maikel Luis; Turatsinze, Jean-Valéry; Eizirik, Décio L. (2018): When one becomes many-Alternative splicing in β-cell function and failure. In *Diabetes, obesity & metabolism* 20 Suppl 2, pp. 77–87. DOI: 10.1111/dom.13388.

Ankö, Minna-Liisa; Morales, Lucia; Henry, Ian; Beyer, Andreas; Neugebauer, Karla M. (2010): Global analysis reveals SRp20- and SRp75-specific mRNPs in cycling and neural cells. In *Nature structural & molecular biology* 17 (8), pp. 962–970. DOI: 10.1038/nsmb.1862.

Ashwal-Fluss, Reut; Meyer, Markus; Pamudurti, Nagarjuna Reddy; Ivanov, Andranik; Bartok, Osnat; Hanan, Mor et al. (2014): circRNA biogenesis competes with pre-mRNA splicing. In *Molecular cell* 56 (1), pp. 55–66. DOI: 10.1016/j.molcel.2014.08.019.

Aubol, Brandon E.; Hailey, Kendra L.; Fattet, Laurent; Jennings, Patricia A.; Adams, Joseph A. (2017): Redirecting SR Protein Nuclear Trafficking through an Allosteric Platform. In *Journal of molecular biology* 429 (14), pp. 2178–2191. DOI: 10.1016/j.jmb.2017.05.022.

Aubol, Brandon E.; Keshwani, Malik M.; Fattet, Laurent; Adams, Joseph A. (2018): Mobilization of a splicing factor through a nuclear kinase-kinase complex. In *The Biochemical journal* 475 (3), pp. 677–690. DOI: 10.1042/BCJ20170672.

Aznarez, Isabel; Nomakuchi, Tomoki T.; Tetenbaum-Novatt, Jaclyn; Rahman, Mohammad Alinoor; Fregoso, Oliver; Rees, Holly; Krainer, Adrian R. (2018): Mechanism of Nonsense-Mediated mRNA Decay Stimulation by Splicing Factor SRSF1. In *Cell reports* 23 (7), pp. 2186–2198. DOI: 10.1016/j.celrep.2018.04.039.

Bai, Haitao; Ge, Shengfang; Lu, Jian; Qian, Guanxiang; Xu, Rang (2013): Hypoxia inducible factor-1α-mediated activation of survivin in cervical cancer cells. In *The journal of obstetrics and gynaecology research* 39 (2), pp. 555–563. DOI: 10.1111/j.1447-0756.2012.01995.x.

Baralle, Francisco E.; Giudice, Jimena (2017): Alternative splicing as a regulator of development and tissue identity. In *Nature reviews. Molecular Biology*.

Barbagallo, Davide; Caponnetto, Angela; Cirnigliaro, Matilde; Brex, Duilia; Barbagallo, Cristina; D'Angeli, Floriana et al. (2018): CircSMARCA5 Inhibits Migration of Glioblastoma Multiforme Cells by Regulating a Molecular Axis Involving Splicing Factors SRSF1/SRSF3/PTB. In *International journal of molecular sciences* 19 (2). DOI: 10.3390/ijms19020480.

Bartoszewski, Rafal; Moszyńska, Adrianna; Serocki, Marcin; Cabaj, Aleksandra; Polten, Andreas; Ochocka, Renata et al. (2019): Primary endothelial-specific regulation of hypoxia-inducible factor (HIF)-1 and HIF-2 and their target gene expression profiles during hypoxia. In *FASEB journal : official publication of the Federation of American Societies for Experimental Biology*, fj201802650RR. DOI: 10.1096/fj.201802650RR.

Bartsch, Deniz; Zirkel, Anne; Kurian, Leo (2018): Characterization of Circular RNAs (circRNA) Associated with the Translation Machinery. In *Methods in molecular biology (Clifton, N.J.)* 1724, pp. 159–166. DOI: 10.1007/978-1-4939-7562-4_13.

Bedogni, Barbara; Warneke, James A.; Nickoloff, Brian J.; Giaccia, Amato J.; Powell, Marianne Broome (2008): Notch1 is an effector of Akt and hypoxia in melanoma development. In *The Journal of clinical investigation* 118 (11), pp. 3660–3670. DOI: 10.1172/JCI36157.

Begum, S.; Yiu, A.; Stebbing, J.; Castellano, L. (2018): Novel tumour suppressive protein encoded by circular RNA, circ-SHPRH, in glioblastomas. In *Oncogene*. DOI: 10.1038/s41388-018-0230-3.

Ben-Yishay, Rakefet; Shav-Tal, Yaron (2019): The dynamic lifecycle of mRNA in the nucleus. In *Current opinion in cell biology* 58, pp. 69–75. DOI: 10.1016/j.ceb.2019.02.007.

Bianconi, Eva; Piovesan, Allison; Facchin, Federica; Beraudi, Alina; Casadei, Raffaella; Frabetti, Flavia et al. (2013): An estimation of the number of cells in the human body. In *Annals of human biology* 40 (6), pp. 463–471. DOI: 10.3109/03014460.2013.807878.

Biselli-Chicote, Patrícia Matos; Biselli, Joice Matos; Cunha, Bianca R.; Castro, Rodrigo; Maniglia, José Victor; Neto, Dalísio de Santi et al. (2017): Overexpression of Antiangiogenic Vascular Endothelial Growth Factor Isoform and Splicing Regulatory Factors in Oral, Laryngeal and

Pharyngeal Squamous Cell Carcinomas. In *Asian Pacific journal of cancer prevention : APJCP* 18 (8), pp. 2171–2177. DOI: 10.22034/APJCP.2017.18.8.2171.

Boeckel, Jes-Niels; Jaé, Nicolas; Heumüller, Andreas W.; Chen, Wei; Boon, Reinier A.; Stellos, Konstantinos et al. (2015): Identification and Characterization of Hypoxia-Regulated Endothelial Circular RNA. In *Circulation research* 117 (10), pp. 884–890. DOI: 10.1161/CIRCRESAHA.115.306319.

Bonnet-Magnaval, Florence; Philippe, Céline; van den Berghe, Loïc; Prats, Hervé; Touriol, Christian; Lacazette, Eric (2016): Hypoxia and ER stress promote Staufen1 expression through an alternative translation mechanism. In *Biochemical and biophysical research communications* 479 (2), pp. 365–371. DOI: 10.1016/j.bbrc.2016.09.082.

Bowler, Elizabeth; Porazinski, Sean; Uzor, Simon; Thibault, Philippe; Durand, Mathieu; Lapointe, Elvy et al. (2018): Hypoxia leads to significant changes in alternative splicing and elevated expression of CLK splice factor kinases in PC3 prostate cancer cells. In *BMC cancer* 18 (1), p. 355. DOI: 10.1186/s12885-018-4227-7.

Brady, Lauren K.; Wang, Hejia; Radens, Caleb M.; Bi, Yue; Radovich, Milan; Maity, Amit et al. (2017): Transcriptome analysis of hypoxic cancer cells uncovers intron retention in EIF2B5 as a mechanism to inhibit translation. In *PLoS biology* 15 (9), e2002623. DOI: 10.1371/journal.pbio.2002623.

Bresson, Stefan M.; Conrad, Nicholas K. (2013): The human nuclear poly(a)-binding protein promotes RNA hyperadenylation and decay. In *PLoS genetics* 9 (10), e1003893. DOI: 10.1371/journal.pgen.1003893.

Brocher (2015): ImageJ User and Developer Conference, 2015.

Brock, Matthias; Schuoler, Claudio; Leuenberger, Caroline; Bühlmann, Carlo; Haider, Thomas J.; Vogel, Johannes et al. (2017): Analysis of hypoxia-induced noncoding RNAs reveals metastasis-associated lung adenocarcinoma transcript 1 as an important regulator of vascular smooth muscle cell proliferation. In *Experimental biology and medicine (Maywood, N.J.)* 242 (5), pp. 487–496. DOI: 10.1177/1535370216685434.

Brown, J. Martin; Wilson, William R. (2004): Exploiting tumour hypoxia in cancer treatment. In *Nature reviews. Cancer* 4 (6), pp. 437–447. DOI: 10.1038/nrc1367.

Bruinsma, W.; Aprelia, M.; García-Santisteban, I.; Kool, J.; Xu, Y. J.; Medema, R. H. (2017): Inhibition of Polo-like kinase 1 during the DNA damage response is mediated through loss of Aurora A recruitment by Bora. In *Oncogene* 36 (13), pp. 1840–1848. DOI: 10.1038/onc.2016.347.

Burma, S.; Chen, B. P.; Murphy, M.; Kurimasa, A.; Chen, D. J. (2001): ATM phosphorylates histone H2AX in response to DNA double-strand breaks. In *The Journal of biological chemistry* 276 (45), pp. 42462–42467. DOI: 10.1074/jbc.C100466200.

Carreau, Aude; El Hafny-Rahbi, Bouchra; Matejuk, Agata; Grillon, Catherine; Kieda, Claudine (2011): Why is the partial oxygen pressure of human tissues a crucial parameter? Small molecules and hypoxia. In *Journal of cellular and molecular medicine* 15 (6), pp. 1239–1253. DOI: 10.1111/j.1582-4934.2011.01258.x.

Cartwright, Tyrell; Perkins, Neil D.; L Wilson, Caroline (2016): NFKB1: a suppressor of inflammation, ageing and cancer. In *The FEBS journal* 283 (10), pp. 1812–1822. DOI: 10.1111/febs.13627.

Cavaloc, Y.; Bourgeois, C. F.; Kister, L.; Stévenin, J. (1999): The splicing factors 9G8 and SRp20 transactivate splicing through different and specific enhancers. In *RNA* 5 (3), pp. 468–483.

Chandradas, Sajiv; Deikus, Gintaras; Tardos, Jonathan G.; Bogdanov, Vladimir Y. (2010): Antagonistic roles of four SR proteins in the biosynthesis of alternatively spliced tissue factor transcripts in monocytic cells. In *Journal of leukocyte biology* 87 (1), pp. 147–152. DOI: 10.1189/jlb.0409252.

Chee, Nancy T.; Lohse, Ines; Brothers, Shaun P. (2019): mRNA-to-protein translation in hypoxia. In *Molecular cancer* 18 (1), p. 49. DOI: 10.1186/s12943-019-0968-4.

Chen, Jie; Li, Yan; Zheng, Qiupeng; Bao, Chunyang; He, Jian; Chen, Bin et al. (2017a): Circular RNA profile identifies circPVT1 as a proliferative factor and prognostic marker in gastric cancer. In *Cancer letters* 388, pp. 208–219. DOI: 10.1016/j.canlet.2016.12.006.

Chen, Jing; Kastan, Michael B. (2017): A novel DNA damage-induced alternative splicing pathway that regulates p53 and cellular senescence markers. In *Oncoscience* 4 (9-10), pp. 122–123. DOI: 10.18632/oncoscience.367.

Chen, L.; Zhang, S.; Wu, J.; Cui, J.; Zhong, L.; Zeng, L.; Ge, S. (2017b): circRNA_100290 plays a role in oral cancer by functioning as a sponge of the miR-29 family. In *Oncogene* 36 (32), pp. 4551–4561. DOI: 10.1038/onc.2017.89.

Chen, Linlin; Luo, Chunling; Shen, Lei; Liu, Yuguo; Wang, Qianqian; Zhang, Chang et al. (2017c): SRSF1 Prevents DNA Damage and Promotes Tumorigenesis through Regulation of DBF4B Pre-mRNA Splicing. In *Cell reports* 21 (12), pp. 3406–3413. DOI: 10.1016/j.celrep.2017.11.091.

Chen, Mo; Qiu, Tao; Wu, Jiajie; Yang, Yang; Wright, Graham D.; Wu, Min; Ge, Ruowen (2018): Extracellular anti-angiogenic proteins augment an endosomal protein trafficking pathway to reach mitochondria and execute apoptosis in HUVECs. In *Cell death and differentiation* 25 (11), pp. 1905–1920. DOI: 10.1038/s41418-018-0092-9.

Chi, Jen-Tsan; Wang, Zhen; Nuyten, Dimitry S. A.; Rodriguez, Edwin H.; Schaner, Marci E.; Salim, Ali et al. (2006): Gene expression programs in response to hypoxia: cell type specificity and prognostic significance in human cancers. In *PLoS medicine* 3 (3), e47. DOI: 10.1371/journal.pmed.0030047.

Chipurupalli, Sandhya; Kannan, Elango; Tergaonkar, Vinay; D'Andrea, Richard; Robinson, Nirmal (2019): Hypoxia Induced ER Stress Response as an Adaptive Mechanism in Cancer. In *International journal of molecular sciences* 20 (3). DOI: 10.3390/ijms20030749.

Cohen-Eliav, Michal; Golan-Gerstl, Regina; Siegfried, Zahava; Andersen, Claus L.; Thorsen, Kasper; Ørntoft, Torben F. et al. (2013): The splicing factor SRSF6 is amplified and is an oncoprotein in lung and colon cancers. In *The Journal of pathology* 229 (4), pp. 630–639. DOI: 10.1002/path.4129.

Colgan, D. F.; Murthy, K. G.; Zhao, W.; Prives, C.; Manley, J. L. (1998): Inhibition of poly(A) polymerase requires p34cdc2/cyclin B phosphorylation of multiple consensus and non-consensus sites. In *The EMBO journal* 17 (4), pp. 1053–1062. DOI: 10.1093/emboj/17.4.1053.

Coltri, Patricia P.; Dos Santos, Maria G. P.; da Silva, Guilherme H. G. (2019): Splicing and cancer: Challenges and opportunities. In *Wiley interdisciplinary reviews. RNA* 10 (3), e1527. DOI: 10.1002/wrna.1527.

Conn, Simon J.; Pillman, Katherine A.; Toubia, John; Conn, Vanessa M.; Salmanidis, Marika; Phillips, Caroline A. et al. (2015): The RNA binding protein quaking regulates formation of circRNAs. In *Cell* 160 (6), pp. 1125–1134. DOI: 10.1016/j.cell.2015.02.014.

Corkery, Dale P.; Holly, Alice C.; Lahsaee, Sara; Dellaire, Graham (2015): Connecting the speckles: Splicing kinases and their role in tumorigenesis and treatment response. In *Nucleus (Austin, Tex.)* 6 (4), pp. 279–288. DOI: 10.1080/19491034.2015.1062194.

Corn, Paul G.; Ricci, M. Stacey; Scata, Kimberly A.; Arsham, Andrew M.; Simon, M. Celeste; Dicker, David T.; El-Deiry, Wafik S. (2005): Mxi1 is induced by hypoxia in a HIF-1–dependent manner and protects cells from c-Myc-induced apoptosis. In *Cancer Biology & Therapy* 4 (11), pp. 1285–1294. DOI: 10.4161/cbt.4.11.2299.

Dang, Chi V.; Kim, Jung-whan; Gao, Ping; Yustein, Jason (2008): The interplay between MYC and HIF in cancer. In *Nature reviews. Cancer* 8 (1), pp. 51–56. DOI: 10.1038/nrc2274.

Dobin, Alexander; Davis, Carrie A.; Schlesinger, Felix; Drenkow, Jorg; Zaleski, Chris; Jha, Sonali et al. (2013): STAR: ultrafast universal RNA-seq aligner. In *Bioinformatics (Oxford, England)* 29 (1), pp. 15–21. DOI: 10.1093/bioinformatics/bts635.

Dominguez, Daniel; Tsai, Yi-Hsuan; Weatheritt, Robert; Wang, Yang; Blencowe, Benjamin J.; Wang, Zefeng (2016): An extensive program of periodic alternative splicing linked to cell cycle progression. In *eLife* 5. DOI: 10.7554/eLife.10288.

Du, William W.; Yang, Weining; Liu, Elizabeth; Yang, Zhenguo; Dhaliwal, Preet; Yang, Burton B. (2016): Foxo3 circular RNA retards cell cycle progression via forming ternary complexes with p21 and CDK2. In *Nucleic acids research* 44 (6), pp. 2846–2858. DOI: 10.1093/nar/gkw027.

Ebbesen, Karoline K.; Kjems, Jørgen; Hansen, Thomas B. (2016): Circular RNAs: Identification, biogenesis and function. In *Biochimica et biophysica acta* 1859 (1), pp. 163–168. DOI: 10.1016/j.bbagrm.2015.07.007.

Edwald, Elin; Stone, Matthew B.; Gray, Erin M.; Wu, Jing; Veatch, Sarah L. (2014): Oxygen depletion speeds and simplifies diffusion in HeLa cells. In *Biophysical journal* 107 (8), pp. 1873–1884. DOI: 10.1016/j.bpj.2014.08.023.

El Guerrab, Abderrahim; Cayre, Anne; Kwiatkowski, Fabrice; Privat, Maud; Rossignol, Jean-Marc; Rossignol, Fabrice et al. (2017): Quantification of hypoxia-related gene expression as a potential approach for clinical outcome prediction in breast cancer. In *PloS one* 12 (4), e0175960. DOI: 10.1371/journal.pone.0175960.

Esteban, Ortiz-Prado; Jeff F Dunn; Jorge Vasconez; Diana Castillo; Ginés, Viscor (2019): Partial pressure of oxygen in the human body: a general review. In *American journal of blood research*.

Favaro, Elena; Lord, Simon; Harris, Adrian L.; Buffa, Francesca M. (2011): Gene expression and hypoxia in breast cancer. In *Genome medicine* 3 (8), p. 55. DOI: 10.1186/gm271.

Fei, Jingyi; Jadaliha, Mahdieh; Harmon, Tyler S.; Li, Isaac T. S.; Hua, Boyang; Hao, Qinyu et al. (2017): Quantitative analysis of multilayer organization of proteins and RNA in nuclear speckles at super resolution. In *Journal of cell science* 130 (24), pp. 4180–4192. DOI: 10.1242/jcs.206854.

Feng, Dairong; Cheng, Yi; Meng, Yan; Zou, Liping; Huang, Shangzhi; Xie, Jiuyong (2015): Multiple effects of curcumin on promoting expression of the exon 7-containing SMN2 transcript. In *Genes & nutrition* 10 (6), p. 40. DOI: 10.1007/s12263-015-0486-y.

Filippov, Valery; Schmidt, Erin L.; Filippova, Maria; Duerksen-Hughes, Penelope J. (2008): Splicing and splice factor SRp55 participate in the response to DNA damage by changing isoform ratios of target genes. In *Gene* 420 (1), pp. 34–41. DOI: 10.1016/j.gene.2008.05.008.

Fonseca, Cindy L.; Malaby, Heidi L. H.; Sepaniac, Leslie A.; Martin, Whitney; Byers, Candice; Czechanski, Anne et al. (2019): Mitotic chromosome alignment ensures mitotic fidelity by promoting interchromosomal compaction during anaphase. In *The Journal of cell biology* 218 (4), pp. 1148–1163. DOI: 10.1083/jcb.201807228.

Franke, Kristin; Gassmann, Max; Wielockx, Ben (2013): Erythrocytosis: the HIF pathway in control. In *Blood* 122 (7), pp. 1122–1128. DOI: 10.1182/blood-2013-01-478065.

Fu, Zhichao; Chen, Dongsheng; Cheng, Huihua; Wang, Fengmei (2015): Hypoxia-inducible factor-1α protects cervical carcinoma cells from apoptosis induced by radiation via modulation of vascular endothelial growth factor and p53 under hypoxia. In *Medical science monitor : international medical journal of experimental and clinical research* 21, pp. 318–325. DOI: 10.12659/MSM.893265.

Fuke, Hiroyuki; Ohno, Mutsuhito (2007): Role of poly (A) tail as an identity element for mRNA nuclear export. In *Nucleic acids research* 36 (3), pp. 1037–1049. DOI: 10.1093/nar/gkm1120.

Gardner, Lawrence B. (2008): Hypoxic inhibition of nonsense-mediated RNA decay regulates gene expression and the integrated stress response. In *Molecular and Cellular Biology* 28 (11), pp. 3729–3741. DOI: 10.1128/MCB.02284-07.

Ghosh, Gourisankar; Adams, Joseph A. (2011): Phosphorylation mechanism and structure of serine-arginine protein kinases. In *The FEBS journal* 278 (4), pp. 587–597. DOI: 10.1111/j.1742-4658.2010.07992.x.

Gillet, Jean-Pierre; Varma, Sudhir; Gottesman, Michael M. (2013): The clinical relevance of cancer cell lines. In *Journal of the National Cancer Institute* 105 (7), pp. 452–458. DOI: 10.1093/jnci/djt007.

Girard, Cyrille; Will, Cindy L.; Peng, Jianhe; Makarov, Evgeny M.; Kastner, Berthold; Lemm, Ira et al. (2012): Post-transcriptional spliceosomes are retained in nuclear speckles until splicing completion. In *Nature communications* 3, p. 994. DOI: 10.1038/ncomms1998.

Gomez-Ferreria, Maria Ana; Rath, Uttama; Buster, Daniel W.; Chanda, Sumit K.; Caldwell, Jeremy S.; Rines, Daniel R.; Sharp, David J. (2007): Human Cep192 is required for mitotic centrosome and spindle assembly. In *Current biology : CB* 17 (22), pp. 1960–1966. DOI: 10.1016/j.cub.2007.10.019.

Gomez-Ferreria, Maria Ana; Sharp, David J. (2008): Cep192 and the generation of the mitotic spindle. In *Cell cycle (Georgetown, Tex.)* 7 (11), pp. 1507–1510. DOI: 10.4161/cc.7.11.5957.

Gonçalves, Vânia; Pereira, Joana F. S.; Jordan, Peter (2017): Signaling Pathways Driving Aberrant Splicing in Cancer Cells. In *Genes* 9 (1). DOI: 10.3390/genes9010009.

Gonzalez, Frank J.; Xie, Cen; Jiang, Changtao (2018): The role of hypoxia-inducible factors in metabolic diseases. In *Nature reviews. Endocrinology* 15 (1), pp. 21–32. DOI: 10.1038/s41574-018-0096-z.

Gordan, John D.; Thompson, Craig B.; Simon, M. Celeste (2007): HIF and c-Myc: sibling rivals for control of cancer cell metabolism and proliferation. In *Cancer cell* 12 (2), pp. 108–113. DOI: 10.1016/j.ccr.2007.07.006.

Graham, Kaitlin; Unger, Evan (2018): Overcoming tumor hypoxia as a barrier to radiotherapy, chemotherapy and immunotherapy in cancer treatment. In *International journal of nanomedicine* 13, pp. 6049–6058. DOI: 10.2147/IJN.S140462.

Gregg L., Semenza; Peter H., Roth; Hon-Ming, Fang; Guang L., Wang (1994): Transcriptional Regulation of Genes Encoding Glycolytic Enzymes by Hypoxia-inducible Factor l. In *The Journal of biological chemistry* 269.

Gregory A., Matera; Zefeng, Wang (2014): A day in the life of the spliceosome. In *Nature reviews. Molecular Biology* 15.

Greijer, A. E.; van der Wall, E. (2004): The role of hypoxia inducible factor 1 (HIF-1) in hypoxia induced apoptosis. In *Journal of clinical pathology* 57 (10), pp. 1009–1014. DOI: 10.1136/jcp.2003.015032.

Guang l, Wang; Bing-Hua, Jiang; Elizabeth A, Rue; Gregg I, Semenza (1995): Hypoxia-inducible factor 1 is a basic-helix-loop-helix-PAS heterodimer regulated by cellular 02 tension. In *Proc. Natl. Acad. Sci.* 90.

Guyot, Mélanie; Hilmi, Caroline; Ambrosetti, Damien; Merlano, Marco; Lo Nigro, Cristiana; Durivault, Jérôme et al. (2017): Targeting the pro-angiogenic forms of VEGF or inhibiting their expression as anti-cancer strategies. In *Oncotarget* 8 (6), pp. 9174–9188. DOI: 10.18632/oncotarget.13942.

Han, Dan; Li, Jiangxue; Wang, Huamin; Su, Xiaoping; Hou, Jin; Gu, Yan et al. (2017a): Circular RNA circMTO1 acts as the sponge of microRNA-9 to suppress hepatocellular carcinoma progression. In *Hepatology (Baltimore, Md.)* 66 (4), pp. 1151–1164. DOI: 10.1002/hep.29270.

Han, Jian; Li, Jia; Ho, Jolene Caifeng; Chia, Grace Sushin; Kato, Hiroyuki; Jha, Sudhakar et al. (2017b): Hypoxia is a Key Driver of Alternative Splicing in Human Breast Cancer Cells. In *Scientific reports* 7 (1), p. 4108. DOI: 10.1038/s41598-017-04333-0.

Hansen, Thomas B. (2018): Improved circRNA Identification by Combining Prediction Algorithms. In *Frontiers in cell and developmental biology* 6, p. 20. DOI: 10.3389/fcell.2018.00020.

Hansen, Thomas B.; Jensen, Trine I.; Clausen, Bettina H.; Bramsen, Jesper B.; Finsen, Bente; Damgaard, Christian K.; Kjems, Jørgen (2013): Natural RNA circles function as efficient microRNA sponges. In *Nature* 495 (7441), pp. 384–388. DOI: 10.1038/nature11993.

Hara, Hirokazu; Takeda, Tatsuya; Yamamoto, Nozomi; Furuya, Keisuke; Hirose, Kazuya; Kamiya, Tetsuro; Adachi, Tetsuo (2013): Zinc-induced modulation of SRSF6 activity alters Bim splicing to promote generation of the most potent apoptotic isoform BimS. In *The FEBS journal* 280 (14), pp. 3313–3327. DOI: 10.1111/febs.12318.

Harries, Lorna W. (2019): RNA Biology Provides New Therapeutic Targets for Human Disease. In *Frontiers in genetics* 10, p. 205. DOI: 10.3389/fgene.2019.00205.

Hochberg-Laufer, Hodaya; Neufeld, Noa; Brody, Yehuda; Nadav-Eliyahu, Shani; Ben-Yishay, Rakefet; Shav-Tal, Yaron (2019): Availability of splicing factors in the nucleoplasm can regulate the release of mRNA from the gene after transcription. In *PLoS genetics* 15 (11), e1008459. DOI: 10.1371/journal.pgen.1008459.

Hoppe-Seyler, F.; Butz, K. (1993): Repression of endogenous p53 transactivation function in HeLa cervical carcinoma cells by human papillomavirus type 16 E6, human mdm-2, and mutant p53. In *Journal of virology* 67 (6), pp. 3111–3117.

Hou, Zhouhua; Xu, Xuwen; Zhou, Ledu; Fu, Xiaoyu; Tao, Shuhui; Zhou, Jiebin et al. (2017): The long non-coding RNA MALAT1 promotes the migration and invasion of hepatocellular carcinoma by sponging miR-204 and releasing SIRT1. In *Tumour biology : the journal of the International Society for Oncodevelopmental Biology and Medicine* 39 (7), 1010428317718135. DOI: 10.1177/1010428317718135.

Howard, Jonathan M.; Sanford, Jeremy R. (2015): The RNAissance family: SR proteins as multifaceted regulators of gene expression. In *Wiley interdisciplinary reviews. RNA* 6 (1), pp. 93–110. DOI: 10.1002/wrna.1260.

Hu, C.-J.; Wang, L.-Y.; Chodosh, L. A.; Keith, B.; Simon, M. C. (2003): Differential Roles of Hypoxia-Inducible Factor 1 (HIF-1) and HIF-2 in Hypoxic Gene Regulation. In *Molecular and Cellular Biology* 23 (24), pp. 9361–9374. DOI: 10.1128/MCB.23.24.9361-9374.2003.

Huang, Xuan; Halicka, H. Dorota; Darzynkiewicz, Zbigniew (2004): Detection of histone H2AX phosphorylation on Ser-139 as an indicator of DNA damage (DNA double-strand breaks). In *Current protocols in cytometry* Chapter 7, Unit 7.27. DOI: 10.1002/0471142956.cy0727s30.

Hwang, Jungwook; Maquat, Lynne E. (2011): Nonsense-mediated mRNA decay (NMD) in animal embryogenesis: to die or not to die, that is the question. In *Current opinion in genetics & development* 21 (4), pp. 422–430. DOI: 10.1016/j.gde.2011.03.008.

Iborra, Severine; Hirschfeld, Marc; Jaeger, Markus; Zur Hausen, Axel; Braicu, Iona; Sehouli, Jalid et al. (2013): Alterations in expression pattern of splicing factors in epithelial ovarian cancer and its clinical impact. In *International journal of gynecological cancer : official journal of the International Gynecological Cancer Society* 23 (6), pp. 990–996. DOI: 10.1097/IGC.0b013e31829783e3.

Irfan, Muhammad; Daraio, Teresa; Bark, Christina (2018): SNAP-25 Puts SNAREs at Center Stage in Metabolic Disease. In *Neuroscience*. DOI: 10.1016/j.neuroscience.2018.07.035.

Ivanov, Andranik; Memczak, Sebastian; Wyler, Emanuel; Torti, Francesca; Porath, Hagit T.; Orejuela, Marta R. et al. (2015): Analysis of intron sequences reveals hallmarks of circular RNA biogenesis in animals. In *Cell reports* 10 (2), pp. 170–177. DOI: 10.1016/j.celrep.2014.12.019.

Jakubauskiene, Egle; Vilys, Laurynas; Makino, Yuichi; Poellinger, Lorenz; Kanopka, Arvydas (2015): Increased Serine-Arginine (SR) Protein Phosphorylation Changes Pre-mRNA Splicing in Hypoxia. In *The Journal of biological chemistry* 290 (29), pp. 18079–18089. DOI: 10.1074/jbc.M115.639690.

Jeck, William R.; Sharpless, Norman E. (2014): Detecting and characterizing circular RNAs. In *Nature biotechnology* 32 (5), pp. 453–461. DOI: 10.1038/nbt.2890.

Jensen, Mads A.; Wilkinson, John E.; Krainer, Adrian R. (2014): Splicing factor SRSF6 promotes hyperplasia of sensitized skin. In *Nature structural & molecular biology* 21 (2), pp. 189–197. DOI: 10.1038/nsmb.2756.

Ji, Jiuping; Zhang, Yiping; Redon, Christophe E.; Reinhold, William C.; Chen, Alice P.; Fogli, Laura K. et al. (2017): Phosphorylated fraction of H2AX as a measurement for DNA damage in cancer cells and potential applications of a novel assay. In *PloS one* 12 (2), e0171582. DOI: 10.1371/journal.pone.0171582.

Jiang, Xin; Zhang, Zeting; Cheng, Kai; Wu, Qiong; Jiang, Ling; Pielak, Gary J. et al. (2019): Membrane-mediated disorder-to-order transition of SNAP25 flexible linker facilitates its interaction with syntaxin-1 and SNARE-complex assembly. In *FASEB journal : official publication of the Federation of American Societies for Experimental Biology*, fj201802796R. DOI: 10.1096/fj.201802796R.

Jiménez, Maddalen; Urtasun, Raquel; Elizalde, María; Azkona, María; Latasa, M. Ujue; Uriarte, Iker et al. (2019): Splicing events in the control of genome integrity: role of SLU7 and truncated SRSF3 proteins. In *Nucleic acids research* 47 (7), pp. 3450–3466. DOI: 10.1093/nar/gkz014.

Jongjitwimol, Jirapas; Baldock, Robert A.; Morley, Simon J.; Watts, Felicity Z. (2016): Sumoylation of eIF4A2 affects stress granule formation. In *Journal of cell science* 129 (12), pp. 2407–2415. DOI: 10.1242/jcs.184614.

Joukov, Vladimir; Walter, Johannes C.; Nicolo, Arcangela de (2014): The Cep192-organized aurora A-Plk1 cascade is essential for centrosome cycle and bipolar spindle assembly. In *Molecular cell* 55 (4), pp. 578–591. DOI: 10.1016/j.molcel.2014.06.016.

Juan-Mateu, Jonàs; Alvelos, Maria Inês; Turatsinze, Jean-Valéry; Villate, Olatz; Lizarraga-Mollinedo, Esther; Grieco, Fabio Arturo et al. (2018): SRp55 Regulates a Splicing Network That Controls Human Pancreatic β-Cell Function and Survival. In *Diabetes* 67 (3), pp. 423–436. DOI: 10.2337/db17-0736.

Jumaa, H.; Nielsen, P. J. (1997): The splicing factor SRp20 modifies splicing of its own mRNA and ASF/SF2 antagonizes this regulation. In *The EMBO journal* 16 (16), pp. 5077–5085. DOI: 10.1093/emboj/16.16.5077.

Kádková, Anna; Radecke, Julika; Sørensen, Jakob B. (2018): The SNAP-25 Protein Family. In *Neuroscience*. DOI: 10.1016/j.neuroscience.2018.09.020.

Kaur, Simranjeet; Mirza, Aashiq H.; Pociot, Flemming (2018): Cell Type-Selective Expression of Circular RNAs in Human Pancreatic Islets. In *Non-coding RNA* 4 (4). DOI: 10.3390/ncrna4040038.

Kazuhiro, Iwai; Koji, Yamanaka; Takumi, Kamura; Nagahiro, Minato; Ronald C., Conaway; Joan W., Conaway et al. (1999): Identification of the von Hippel–Lindau tumor-suppressor protein as part of an active E3 ubiquitin ligase complex. In *PNAS* 96, pp. 12436–12441.

Kemmerer, Katrin; Weigand, Julia E. (2014): Hypoxia reduces MAX expression in endothelial cells by unproductive splicing. In *FEBS letters* 588 (24), pp. 4784–4790. DOI: 10.1016/j.febslet.2014.11.011.

Kent, W. James; Sugnet, Charles W.; Furey, Terrence S.; Roskin, Krishna M.; Pringle, Tom H.; Zahler, Alan M.; Haussler, David (2002): The human genome browser at UCSC. In *Genome research* 12 (6), pp. 996–1006. DOI: 10.1101/gr.229102.

Kim, Hana; Lee, June Hyung; Lee, Younghoon (2003): Regulation of poly(A) polymerase by 14-3-3epsilon. In *The EMBO journal* 22 (19), pp. 5208–5219. DOI: 10.1093/emboj/cdg486.

Kim, Jongchan; Piao, Hai-Long; Kim, Beom-Jun; Yao, Fan; Han, Zhenbo; Wang, Yumeng et al. (2018): Long noncoding RNA MALAT1 suppresses breast cancer metastasis. In *Nature genetics*. DOI: 10.1038/s41588-018-0252-3.

Kornblihtt, Alberto R.; Schor, Ignacio E.; Alló, Mariano; Dujardin, Gwendal; Petrillo, Ezequiel; Muñoz, Manuel J. (2013): Alternative splicing: a pivotal step between eukaryotic transcription and translation. In *Nature reviews. Molecular cell biology* 14 (3), pp. 153–165. DOI: 10.1038/nrm3525.

Koshiji, Minori; Kageyama, Yukio; Pete, Erin A.; Horikawa, Izumi; Barrett, J. Carl; Huang, L. Eric (2004): HIF-1alpha induces cell cycle arrest by functionally counteracting Myc. In *The EMBO journal* 23 (9), pp. 1949–1956. DOI: 10.1038/sj.emboj.7600196.

Koumenis, C.; Naczki, C.; Koritzinsky, M.; Rastani, S.; Diehl, A.; Sonenberg, N. et al. (2002): Regulation of Protein Synthesis by Hypoxia via Activation of the Endoplasmic Reticulum Kinase PERK and Phosphorylation of the Translation Initiation Factor eIF2. In *Molecular and Cellular Biology* 22 (21), pp. 7405–7416. DOI: 10.1128/MCB.22.21.7405-7416.2002.

Kristensen, L. S.; Hansen, T. B.; Venø, M. T.; Kjems, J. (2018): Circular RNAs in cancer: opportunities and challenges in the field. In *Oncogene* 37 (5), pp. 555–565. DOI: 10.1038/onc.2017.361.

Langmead, Ben; Salzberg, Steven L. (2012): Fast gapped-read alignment with Bowtie 2. In *Nature methods* 9 (4), pp. 357–359. DOI: 10.1038/nmeth.1923.

Lareau, Liana F.; Brenner, Steven E. (2015): Regulation of splicing factors by alternative splicing and NMD is conserved between kingdoms yet evolutionarily flexible. In *Molecular biology and evolution* 32 (4), pp. 1072–1079. DOI: 10.1093/molbev/msv002.

Lawrence, Toby (2009): The nuclear factor NF-kappaB pathway in inflammation. In *Cold Spring Harbor perspectives in biology* 1 (6), a001651. DOI: 10.1101/cshperspect.a001651.

Lechner, Mark S.; Schultz, David C.; Negorev, Dmitri; Maul, Gerd G.; Rauscher, Frank J. (2005): The mammalian heterochromatin protein 1 binds diverse nuclear proteins through a common motif that targets the chromoshadow domain. In *Biochemical and biophysical research communications* 331 (4), pp. 929–937. DOI: 10.1016/j.bbrc.2005.04.016.

Lee, Kuo-Ming; Tarn, Woan-Yuh (2013): Coupling pre-mRNA processing to transcription on the RNA factory assembly line. In *RNA biology* 10 (3), pp. 380–390. DOI: 10.4161/rna.23697.

Lee, Kyoung Eun; Simon, M. Celeste (2015): SnapShot: Hypoxia-Inducible Factors. In *Cell* 163 (5), 1288-1288.e1. DOI: 10.1016/j.cell.2015.11.011.

Legnini, Ivano; Di Timoteo, Gaia; Rossi, Francesca; Morlando, Mariangela; Briganti, Francesca; Sthandier, Olga et al. (2017): Circ-ZNF609 Is a Circular RNA that Can Be Translated and Functions in Myogenesis. In *Molecular cell* 66 (1), 22-37.e9. DOI: 10.1016/j.molcel.2017.02.017.

Lei, Wei; Feng, Tingting; Fang, Xing; Yu, You; Yang, Junjie; Zhao, Zhen-Ao et al. (2018): Signature of circular RNAs in human induced pluripotent stem cells and derived cardiomyocytes. In *Stem cell research & therapy* 9 (1), p. 56. DOI: 10.1186/s13287-018-0793-5.

Lenzken, Silvia C.; Loffreda, Alessia; Barabino, Silvia M. L. (2013): RNA splicing: a new player in the DNA damage response. In *International journal of cell biology* 2013, p. 153634. DOI: 10.1155/2013/153634.

Leroy, Bernard; Girard, Luc; Hollestelle, Antoinette; Minna, John D.; Gazdar, Adi F.; Soussi, Thierry (2014): Analysis of TP53 mutation status in human cancer cell lines: a reassessment. In *Human mutation* 35 (6), pp. 756–765. DOI: 10.1002/humu.22556.

Li, Lin; Zheng, Yong-Chang; Kayani, Masood Ur Rehman; Xu, Wen; Wang, Guan-Qun; Sun, Pei et al. (2017): Comprehensive analysis of circRNA expression profiles in humans by RAISE. In *International journal of oncology* 51 (6), pp. 1625–1638. DOI: 10.3892/ijo.2017.4162.

Li, Zhaoyong; Huang, Chuan; Bao, Chun; Chen, Liang; Lin, Mei; Wang, Xiaolin et al. (2015): Exon-intron circular RNAs regulate transcription in the nucleus. In *Nature structural & molecular biology* 22 (3), pp. 256–264. DOI: 10.1038/nsmb.2959.

Liang, Hai-Feng; Zhang, Xing-Zeng; Liu, Bao-Guo; Jia, Guo-Tao; Li, Wen-Lei (2017): Circular RNA circ-ABCB10 promotes breast cancer proliferation and progression through sponging miR-1271. In *American journal of cancer research* 7 (7), pp. 1566–1576.

Liu, Hengwei; Zhang, Zhibing; Xiong, Wenqian; Zhang, Ling; Du, Yu; Liu, Yi; Xiong, Xingao (2018): Long non-coding RNA MALAT1 mediates hypoxia-induced pro-survival autophagy of endometrial stromal cells in endometriosis. In *Journal of cellular and molecular medicine*. DOI: 10.1111/jcmm.13947.

Liu, Hui; Wang, Huihan; Wu, Bin; Yao, Kun; Liao, Aijun; Miao, Miao et al. (2017): Down-regulation of long non-coding RNA MALAT1 by RNA interference inhibits proliferation and induces apoptosis in multiple myeloma. In *Clinical and experimental pharmacology & physiology* 44 (10), pp. 1032–1041. DOI: 10.1111/1440-1681.12804.

Lloyd, James P. B. (2018): The evolution and diversity of the nonsense-mediated mRNA decay pathway. In *F1000Research* 7. DOI: 10.12688/f1000research.15872.2.

Love, Michael I.; Huber, Wolfgang; Anders, Simon (2014): Moderated estimation of fold change and dispersion for RNA-seq data with DESeq2. In *Genome biology* 15 (12), p. 550. DOI: 10.1186/s13059-014-0550-8.

Maass, Philipp G.; Glažar, Petar; Memczak, Sebastian; Dittmar, Gunnar; Hollfinger, Irene; Schreyer, Luisa et al. (2017): A map of human circular RNAs in clinically relevant tissues. In *Journal of molecular medicine (Berlin, Germany)* 95 (11), pp. 1179–1189. DOI: 10.1007/s00109-017-1582-9.

Mancini, Francesca; Teveroni, Emanuela; Di Conza, Giusy; Monteleone, Valentina; Arisi, Ivan; Pellegrino, Marsha et al. (2017): MDM4 actively restrains cytoplasmic mTORC1 by sensing nutrient availability. In *Molecular cancer* 16 (1), p. 55. DOI: 10.1186/s12943-017-0626-7.

Manley, James L.; Krainer, Adrian R. (2010): A rational nomenclature for serine/arginine-rich protein splicing factors (SR proteins). In *Genes & development* 24 (11), pp. 1073–1074. DOI: 10.1101/gad.1934910.

Manning, Kassie S.; Cooper, Thomas A. (2016): The roles of RNA processing in translating genotype to phenotype. In *Nature reviews. Molecular cell biology* 18 (2), pp. 102–114. DOI: 10.1038/nrm.2016.139.

Mao, Yuntao S.; Zhang, Bin; Spector, David L. (2011): Biogenesis and function of nuclear bodies. In *Trends in genetics : TIG* 27 (8), pp. 295–306. DOI: 10.1016/j.tig.2011.05.006.

Masoud, Georgina N.; Li, Wei (2015): HIF-1α pathway: role, regulation and intervention for cancer therapy. In *Acta pharmaceutica Sinica. B* 5 (5), pp. 378–389. DOI: 10.1016/j.apsb.2015.05.007.

Masters, John R. (2002): HeLa cells 50 years on: the good, the bad and the ugly. In *Nature reviews. Cancer* 2 (4), pp. 315–319. DOI: 10.1038/nrc775.

Matijasevic, Zdenka; Steinman, Heather A.; Hoover, Kathleen; Jones, Stephen N. (2007): MdmX Promotes Bipolar Mitosis To Suppress Transformation and Tumorigenesis in p53-Deficient Cells and Mice ▿ †. In *Molecular and Cellular Biology* 28 (4), pp. 1265–1273. DOI: 10.1128/MCB.01108-07.

Matoulkova, Eva; Michalova, Eva; Vojtesek, Borivoj; Hrstka, Roman (2012): The role of the 3' untranslated region in post-transcriptional regulation of protein expression in mammalian cells. In *RNA biology* 9 (5), pp. 563–576. DOI: 10.4161/rna.20231.

McKee, Adrienne E.; Silver, Pamela A. (2007): Systems perspectives on mRNA processing. In *Cell research* 17 (7), pp. 581–590. DOI: 10.1038/cr.2007.54.

Memczak, Sebastian; Jens, Marvin; Elefsinioti, Antigoni; Torti, Francesca; Krueger, Janna; Rybak, Agnieszka et al. (2013): Circular RNAs are a large class of animal RNAs with regulatory potency. In *Nature* 495 (7441), pp. 333–338. DOI: 10.1038/nature11928.

Memczak, Sebastian; Papavasileiou, Panagiotis; Peters, Oliver; Rajewsky, Nikolaus (2015): Identification and Characterization of Circular RNAs As a New Class of Putative Biomarkers in Human Blood. In *PloS one* 10 (10), e0141214. DOI: 10.1371/journal.pone.0141214.

Meng, Lingjun; Park, Jung-Eun; Kim, Tae-Sung; Lee, Eun Hye; Park, Suk-Youl; Zhou, Ming et al. (2015): Bimodal Interaction of Mammalian Polo-Like Kinase 1 and a Centrosomal Scaffold,

Cep192, in the Regulation of Bipolar Spindle Formation. In *Molecular and Cellular Biology* 35 (15), pp. 2626–2640. DOI: 10.1128/MCB.00068-15.

Millevoi, Stefania; Vagner, Stéphan (2010): Molecular mechanisms of eukaryotic pre-mRNA 3' end processing regulation. In *Nucleic acids research* 38 (9), pp. 2757–2774. DOI: 10.1093/nar/gkp1176.

Miyagawa, Ryu; Tano, Keiko; Mizuno, Rie; Nakamura, Yo; Ijiri, Kenichi; Rakwal, Randeep et al. (2012): Identification of cis- and trans-acting factors involved in the localization of MALAT-1 noncoding RNA to nuclear speckles. In *RNA (New York, N.Y.)* 18 (4), pp. 738–751. DOI: 10.1261/rna.028639.111.

Mo, Dingding; Li, Xinping; Cui, Di; Vollmar, Jeanne-Franca (2018): Intron-mediated enhancement boosts Rtn4 circRNA expression: A robust method for exploring circRNA function.

Moggs, Jonathan G.; Grandi, Paola; Quivy, Jean-Pierre; Jónsson, Zophonías O.; Hübscher, Ulrich; Becker, Peter B.; Almouzni, Geneviève (2000): A CAF-1–PCNA-Mediated Chromatin Assembly Pathway Triggered by Sensing DNA Damage. In *Molecular and Cellular Biology* 20 (4), pp. 1206–1218.

Moore, Melissa J. (2005): From birth to death: the complex lives of eukaryotic mRNAs. In *Science (New York, N.Y.)* 309 (5740), pp. 1514–1518. DOI: 10.1126/science.1111443.

Moraes, Fernanda; Góes, Andréa (2016): A decade of human genome project conclusion: Scientific diffusion about our genome knowledge. In *Biochemistry and molecular biology education : a bimonthly publication of the International Union of Biochemistry and Molecular Biology* 44 (3), pp. 215–223. DOI: 10.1002/bmb.20952.

Mori, Hiroyuki; Yao, Yao; Learman, Brian S.; Kurozumi, Kazuhiko; Ishida, Joji; Ramakrishnan, Sadeesh K. et al. (2016): Induction of WNT11 by hypoxia and hypoxia-inducible factor-1α regulates cell proliferation, migration and invasion. In *Scientific reports* 6, p. 21520. DOI: 10.1038/srep21520.

Mu, Yanchao; Yan, Xiaojie; Li, Ding; Zhao, Dan; Wang, Lingling; Wang, Xiaoyang et al. (2018): NUPR1 maintains autolysosomal efflux by activating SNAP25 transcription in cancer cells. In *Autophagy* 14 (4), pp. 654–670. DOI: 10.1080/15548627.2017.1338556.

Mühlemann, Oliver; Eberle, Andrea B.; Stalder, Lukas; Zamudio Orozco, Rodolfo (2008): Recognition and elimination of nonsense mRNA. In *Biochimica et biophysica acta* 1779 (9), pp. 538–549. DOI: 10.1016/j.bbagrm.2008.06.012.

Müller-McNicoll, Michaela; Botti, Valentina; Jesus Domingues, Antonio M. de; Brandl, Holger; Schwich, Oliver D.; Steiner, Michaela C. et al. (2016): SR proteins are NXF1 adaptors that link alternative RNA processing to mRNA export. In *Genes & development* 30 (5), pp. 553–566. DOI: 10.1101/gad.276477.115.

Müller-McNicoll, Michaela; Neugebauer, Karla M. (2013): How cells get the message: dynamic assembly and function of mRNA-protein complexes. In *Nature reviews. Genetics* 14 (4), pp. 275–287. DOI: 10.1038/nrg3434.

Muniz, Lisa; Davidson, Lee; West, Steven (2015): Poly(A) Polymerase and the Nuclear Poly(A) Binding Protein, PABPN1, Coordinate the Splicing and Degradation of a Subset of Human Pre-mRNAs. In *Molecular and Cellular Biology* 35 (13), pp. 2218–2230. DOI: 10.1128/MCB.00123-15.

Muñoz-Sánchez, Jorge; Chánez-Cárdenas, María E. (2019): The use of cobalt chloride as a chemical hypoxia model. In *Journal of applied toxicology : JAT* 39 (4), pp. 556–570. DOI: 10.1002/jat.3749.

Muz, Barbara; La Puente, Pilar de; Azab, Feda; Azab, Abdel Kareem (2015): The role of hypoxia in cancer progression, angiogenesis, metastasis, and resistance to therapy. In *Hypoxia (Auckland, N.Z.)* 3, pp. 83–92. DOI: 10.2147/HP.S93413.

Nakagawa, Shinichi; Ip, Joanna Y.; Shioi, Go; Tripathi, Vidisha; Zong, Xinying; Hirose, Tetsuro; Prasanth, Kannanganattu V. (2012): Malat1 is not an essential component of nuclear speckles in mice. In *RNA (New York, N.Y.)* 18 (8), pp. 1487–1499. DOI: 10.1261/rna.033217.112.

Nan, Aruo; Chen, Lijian; Zhang, Nan; Liu, Zhenzhong; Yang, Ti; Wang, Zhishan et al. (2017): A novel regulatory network among LncRpa, CircRar1, MiR-671 and apoptotic genes promotes lead-induced neuronal cell apoptosis. In *Archives of toxicology* 91 (4), pp. 1671–1684. DOI: 10.1007/s00204-016-1837-1.

Nasa, Isha; Trinkle-Mulcahy, Laura; Douglas, P.; Chaudhuri, Sibapriya; Lees-Miller, S. P.; Lee, Kyung S.; Moorhead, Greg B. (2017): Recruitment of PP1 to the centrosomal scaffold protein CEP192. In *Biochemical and biophysical research communications* 484 (4), pp. 864–870. DOI: 10.1016/j.bbrc.2017.02.004.

Nicholson, Pamela; Mühlemann, Oliver (2010): Cutting the nonsense: the degradation of PTC-containing mRNAs. In *Biochemical Society transactions* 38 (6), pp. 1615–1620. DOI: 10.1042/BST0381615.

Novoyatleva, Tatyana; Heinrich, Bettina; Tang, Yesheng; Benderska, Natalya; Butchbach, Matthew E. R.; Lorson, Christian L. et al. (2008): Protein phosphatase 1 binds to the RNA recognition motif of several splicing factors and regulates alternative pre-mRNA processing. In *Human molecular genetics* 17 (1), pp. 52–70. DOI: 10.1093/hmg/ddm284.

Nowak, Dawid G.; Amin, Elianna Mohamed; Rennel, Emma S.; Hoareau-Aveilla, Coralie; Gammons, Melissa; Damodoran, Gopinath et al. (2010): Regulation of vascular endothelial growth factor (VEGF) splicing from pro-angiogenic to anti-angiogenic isoforms: a novel therapeutic strategy for angiogenesis. In *The Journal of biological chemistry* 285 (8), pp. 5532–5540. DOI: 10.1074/jbc.M109.074930.

Nowak, Dawid G.; Woolard, Jeanette; Amin, Elianna Mohamed; Konopatskaya, Olga; Saleem, Moin A.; Churchill, Amanda J. et al. (2008): Expression of pro- and anti-angiogenic isoforms of VEGF is differentially regulated by splicing and growth factors. In *Journal of cell science* 121 (Pt 20), pp. 3487–3495. DOI: 10.1242/jcs.016410.

Okholm, Trine Line Hauge; Nielsen, Morten Muhlig; Hamilton, Mark P.; Christensen, Lise-Lotte; Vang, Søren; Hedegaard, Jakob et al. (2017): Circular RNA expression is abundant and correlated to aggressiveness in early-stage bladder cancer. In *NPJ Genomic Medicine* 2. DOI: 10.1038/s41525-017-0038-z.

Oltean, S.; Bates, D. O. (2014): Hallmarks of alternative splicing in cancer. In *Oncogene* 33 (46), pp. 5311–5318. DOI: 10.1038/onc.2013.533.

Osera, Cecilia; Martindale, Jennifer L.; Amadio, Marialaura; Kim, Jiyoung; Yang, Xiaoling; Moad, Christopher A. et al. (2015): Induction of VEGFA mRNA translation by CoCl2 mediated by HuR. In *RNA biology* 12 (10), pp. 1121–1130. DOI: 10.1080/15476286.2015.1085276.

Pabla, Navjotsingh; Bhatt, Kirti; Dong, Zheng (2012): Checkpoint kinase 1 (Chk1)-short is a splice variant and endogenous inhibitor of Chk1 that regulates cell cycle and DNA damage checkpoints. In *Proceedings of the National Academy of Sciences of the United States of America* 109 (1), pp. 197–202. DOI: 10.1073/pnas.1104767109.

Pamudurti, Nagarjuna Reddy; Bartok, Osnat; Jens, Marvin; Ashwal-Fluss, Reut; Stottmeister, Christin; Ruhe, Larissa et al. (2017): Translation of CircRNAs. In *Molecular cell* 66 (1), 9-21.e7. DOI: 10.1016/j.molcel.2017.02.021.

Pant, Vinod; Larsson, Connie A.; Aryal, Neeraj; Xiong, Shunbin; You, M. James; Quintas-Cardama, Alfonso; Lozano, Guillermina (2017): Tumorigenesis promotes Mdm4-S overexpression. In *Oncotarget* 8 (16), pp. 25837–25847. DOI: 10.18632/oncotarget.15552.

Papasaikas, Panagiotis; Valcárcel, Juan (2016): The Spliceosome: The Ultimate RNA Chaperone and Sculptor. In *Trends in biochemical sciences* 41 (1), pp. 33–45. DOI: 10.1016/j.tibs.2015.11.003.

Parrilla, Alfonso; Cirillo, Luca; Thomas, Yann; Gotta, Monica; Pintard, Lionel; Santamaria, Anna (2016): Mitotic entry: The interplay between Cdk1, Plk1 and Bora. In *Cell cycle (Georgetown, Tex.)* 15 (23), pp. 3177–3182. DOI: 10.1080/15384101.2016.1249544.

Patzke, Sebastian; Stokke, Trond; Aasheim, Hans-Christian (2006): CSPP and CSPP-L associate with centrosomes and microtubules and differently affect microtubule organization. In *Journal of cellular physiology* 209 (1), pp. 199–210. DOI: 10.1002/jcp.20725.

Piekielko-Witkowska, Agnieszka; Wiszomirska, Hanna; Wojcicka, Anna; Poplawski, Piotr; Boguslawska, Joanna; Tanski, Zbigniew; Nauman, Alicja (2010): Disturbed expression of splicing factors in renal cancer affects alternative splicing of apoptosis regulators, oncogenes, and tumor suppressors. In *PloS one* 5 (10), e13690. DOI: 10.1371/journal.pone.0013690.

Podhorecka, Monika; Skladanowski, Andrzej; Bozko, Przemyslaw (2010): H2AX Phosphorylation: Its Role in DNA Damage Response and Cancer Therapy. In *Journal of nucleic acids* 2010. DOI: 10.4061/2010/920161.

Polytarchou, Christos; Iliopoulos, Dimitrios; Hatziapostolou, Maria; Kottakis, Filippos; Maroulakou, Ioanna; Struhl, Kevin; Tsichlis, Philip N. (2011): Akt2 regulates all Akt isoforms and promotes resistance to hypoxia through induction of miR-21 upon oxygen deprivation. In *Cancer research* 71 (13), pp. 4720–4731. DOI: 10.1158/0008-5472.CAN-11-0365.

Pruszko, Magdalena; Milano, Elisa; Forcato, Mattia; Donzelli, Sara; Ganci, Federica; Di Agostino, Silvia et al. (2017): The mutant p53-ID4 complex controls VEGFA isoforms by recruiting lncRNA MALAT1. In *EMBO reports* 18 (8), pp. 1331–1351. DOI: 10.15252/embr.201643370.

Rallapalli, R.; Strachan, G.; Cho, B.; Mercer, W. E.; Hall, D. J. (1999): A novel MDMX transcript expressed in a variety of transformed cell lines encodes a truncated protein with potent p53 repressive activity. In *The Journal of biological chemistry* 274 (12), pp. 8299–8308.

Ramanathan, Anand; Robb, G. Brett; Chan, Siu-Hong (2016): mRNA capping: biological functions and applications. In *Nucleic acids research* 44 (16), pp. 7511–7526. DOI: 10.1093/nar/gkw551.

Ramos-Miguel, Alfredo; Gicas, Kristina; Alamri, Jehan; Beasley, Clare L.; Dwork, Andrew J.; Mann, J. John et al. (2018): Reduced SNAP25 Protein Fragmentation Contributes to SNARE Complex Dysregulation in Schizophrenia Postmortem Brain. In *Neuroscience*. DOI: 10.1016/j.neuroscience.2018.12.015.

Rapti, Aikaterini; Trangas, Theoni; Samiotaki, Martina; Ioannidis, Panayotis; Dimitriadis, Euthymios; Meristoudis, Christos et al. (2010): The structure of the 5'-untranslated region of mammalian poly(A) polymerase-alpha mRNA suggests a mechanism of translational regulation. In *Molecular and cellular biochemistry* 340 (1-2), pp. 91–96. DOI: 10.1007/s11010-010-0405-x.

Raza, Farheen; Waldron, Joseph Alexander; Le Quesne, John (2015): Translational dysregulation in cancer: eIF4A isoforms and sequence determinants of eIF4A dependence. In *Biochemical Society transactions* 43 (6), pp. 1227–1233. DOI: 10.1042/BST20150163.

Riffle, Stephen; Pandey, Ram Naresh; Albert, Morgan; Hegde, Rashmi S. (2017): Linking hypoxia, DNA damage and proliferation in multicellular tumor spheroids. In *BMC cancer* 17 (1), p. 338. DOI: 10.1186/s12885-017-3319-0.

ROCA, XAVIER; SACHIDANANDAM, RAVI; Krainer, Adrian R. (2005): Determinants of the inherent strength of human 5' splice sites. In *RNA* 11 (5), pp. 683–698.

Roy, Bishakha; Haupt, Larisa M.; Griffiths, Lyn R. (20): Review: Alternative Splicing (AS) of Genes As An Approach for Generating Protein Complexity. In *Current Genomics* 14 (3), pp. 182–194. DOI: 10.2174/1389202911314030004.

Rutledge, Charlotte E.; Lau, Ho-Tak; Mangan, Hazel; Hardy, Linda L.; Sunnotel, Olaf; Guo, Fan et al. (2014): Efficient translation of Dnmt1 requires cytoplasmic polyadenylation and Musashi binding elements. In *PloS one* 9 (2), e88385. DOI: 10.1371/journal.pone.0088385.

Rybak-Wolf, Agnieszka; Stottmeister, Christin; Glažar, Petar; Jens, Marvin; Pino, Natalia; Giusti, Sebastian et al. (2015): Circular RNAs in the Mammalian Brain Are Highly Abundant, Conserved, and Dynamically Expressed. In *Molecular cell* 58 (5), pp. 870–885. DOI: 10.1016/j.molcel.2015.03.027.

Saitoh, Noriko; Sakamoto, Chiyomi; Hagiwara, Masatoshi; Agredano-Moreno, Lourdes T.; Jiménez-García, Luis Felipe; Nakao, Mitsuyoshi (2012): The distribution of phosphorylated SR proteins and alternative splicing are regulated by RANBP2. In *Molecular biology of the cell* 23 (6), pp. 1115–1128. DOI: 10.1091/mbc.E11-09-0783.

Salceda, Susana; Caro, Jaime (1997): Hypoxia-inducible Factor 1 (HIF-1a) Protein Is Rapidly Degraded by the Ubiquitin-Proteasome System under Normoxic Conditions. In *The Journal of biological chemistry* 272.

Saltzman, Arneet L.; Kim, Yoon Ki; Pan, Qun; Fagnani, Matthew M.; Maquat, Lynne E.; Blencowe, Benjamin J. (2008): Regulation of multiple core spliceosomal proteins by alternative splicing-coupled nonsense-mediated mRNA decay. In *Molecular and Cellular Biology* 28 (13), pp. 4320–4330. DOI: 10.1128/MCB.00361-08.

Salzberg, Steven L. (2018): Open questions: How many genes do we have? In *BMC biology* 16 (1), p. 94. DOI: 10.1186/s12915-018-0564-x.

Sapra, Aparna K.; Ankö, Minna-Liisa; Grishina, Inna; Lorenz, Mike; Pabis, Marta; Poser, Ina et al. (2009): SR protein family members display diverse activities in the formation of nascent and mature mRNPs in vivo. In *Molecular cell* 34 (2), pp. 179–190. DOI: 10.1016/j.molcel.2009.02.031.

Sauer, Paul V.; Gu, Yajie; Liu, Wallace H.; Mattiroli, Francesca; Panne, Daniel; Luger, Karolin; Churchill, Mair Ea (2018): Mechanistic insights into histone deposition and nucleosome assembly by the chromatin assembly factor-1. In *Nucleic acids research* 46 (19), pp. 9907–9917. DOI: 10.1093/nar/gky823.

Scherrer, Klaus (2018): Primary transcripts: From the discovery of RNA processing to current concepts of gene expression - Review. In *Experimental cell research* 373 (1-2), pp. 1–33. DOI: 10.1016/j.yexcr.2018.09.011.

Schindelin, Johannes; Arganda-Carreras, Ignacio; Frise, Erwin; Kaynig, Verena; Longair, Mark; Pietzsch, Tobias et al. (2012): Fiji: an open-source platform for biological-image analysis. In *Nature methods* 9 (7), pp. 676–682. DOI: 10.1038/nmeth.2019.

Schito, Luana; Semenza, Gregg L. (2016): Hypoxia-Inducible Factors: Master Regulators of Cancer Progression. In *Trends in cancer* 2 (12), pp. 758–770. DOI: 10.1016/j.trecan.2016.10.016.

Schneider, Tim; Hung, Lee-Hsueh; Schreiner, Silke; Starke, Stefan; Eckhof, Heinrich; Rossbach, Oliver et al. (2016): CircRNA-protein complexes: IMP3 protein component defines subfamily of circRNPs. In *Scientific reports* 6, p. 31313. DOI: 10.1038/srep31313.

Sena, Johnny A.; Wang, Liyi; Heasley, Lynn E.; Hu, Cheng-Jun (2014): Hypoxia regulates alternative splicing of HIF and non-HIF target genes. In *Molecular cancer research : MCR* 12 (9), pp. 1233–1243. DOI: 10.1158/1541-7786.MCR-14-0149.

Setty, Bhuvana A.; Pillay Smiley, Natasha; Pool, Caitlyn M.; Jin, Yi; Liu, Yusen; Nelin, Leif D. (2017): Hypoxia-induced proliferation of HeLa cells depends on epidermal growth factor receptor-mediated arginase II induction. In *Physiological reports* 5 (6). DOI: 10.14814/phy2.13175.

Shen, Shihao; Park, Juw Won; Lu, Zhi-xiang; Lin, Lan; Henry, Michael D.; Wu, Ying Nian et al. (2014): rMATS: robust and flexible detection of differential alternative splicing from replicate RNA-Seq data. In *Proceedings of the National Academy of Sciences of the United States of America* 111 (51), E5593-601. DOI: 10.1073/pnas.1419161111.

Shepard, Peter J.; Hertel, Klemens J. (2009): The SR protein family. In *Genome biology* 10 (10), p. 242. DOI: 10.1186/gb-2009-10-10-242.

Shi, Yigong (2017): Mechanistic insights into precursor messenger RNA splicing by the spliceosome. In *Nature reviews. Molecular cell biology* 18 (11), pp. 655–670. DOI: 10.1038/nrm.2017.86.

Shibuya, Masabumi (2011): Vascular Endothelial Growth Factor (VEGF) and Its Receptor (VEGFR) Signaling in Angiogenesis: A Crucial Target for Anti- and Pro-Angiogenic Therapies. In *Genes & cancer* 2 (12), pp. 1097–1105. DOI: 10.1177/1947601911423031.

Shkreta, Lulzim; Chabot, Benoit (2015): The RNA Splicing Response to DNA Damage. In *Biomolecules* 5 (4), pp. 2935–2977. DOI: 10.3390/biom5042935.

Simon, M. Celeste (2016): The Hypoxia Response Pathways - Hats Off! In *The New England journal of medicine* 375 (17), pp. 1687–1689. DOI: 10.1056/NEJMcibr1610065.

Simon, M. Celeste; Keith, B. (2008): The role of oxygen availability in embryonic development and stem cell function. In *Nature reviews. Molecular Biology* volume 9, pp. 285–296.

Singh, Davinder; Arora, Rohit; Kaur, Pardeep; Singh, Balbir; Mannan, Rahul; Arora, Saroj (2017): Overexpression of hypoxia-inducible factor and metabolic pathways: possible targets of cancer. In *Cell & bioscience* 7, p. 62. DOI: 10.1186/s13578-017-0190-2.

Starke, Stefan; Jost, Isabelle; Rossbach, Oliver; Schneider, Tim; Schreiner, Silke; Hung, Lee-Hsueh; Bindereif, Albrecht (2015): Exon circularization requires canonical splice signals. In *Cell reports* 10 (1), pp. 103–111. DOI: 10.1016/j.celrep.2014.12.002.

Sun, Shuying; Zhang, Zuo; Sinha, Rahul; Karni, Rotem; Krainer, Adrian R. (2010): SF2/ASF autoregulation involves multiple layers of post-transcriptional and translational control. In *Nature structural & molecular biology* 17 (3), pp. 306–312. DOI: 10.1038/nsmb.1750.

Sureau, A.; Gattoni, R.; Dooghe, Y.; Stévenin, J.; Soret, J. (2001): SC35 autoregulates its expression by promoting splicing events that destabilize its mRNAs. In *The EMBO journal* 20 (7), pp. 1785–1796. DOI: 10.1093/emboj/20.7.1785.

Suzuki, Hitoshi; Tsukahara, Toshifumi (2014): A view of pre-mRNA splicing from RNase R resistant RNAs. In *International journal of molecular sciences* 15 (6), pp. 9331–9342. DOI: 10.3390/ijms15069331.

Tam, Annie S.; Stirling, Peter C. (2019): Splicing, genome stability and disease: splice like your genome depends on it! In *Current genetics*. DOI: 10.1007/s00294-019-00964-0.

Thomlinson & Gray (1955): The histological structure of some human luncg cancers and the possible implications for radio-therapy. In *Br. J. Cancer*.

Tripathi, Vidisha; Ellis, Jonathan D.; Shen, Zhen; Song, David Y.; Pan, Qun; Watt, Andrew T. et al. (2010): The nuclear-retained noncoding RNA MALAT1 regulates alternative splicing by modulating SR splicing factor phosphorylation. In *Molecular cell* 39 (6), pp. 925–938. DOI: 10.1016/j.molcel.2010.08.011.

Tripathi, Vidisha; Shen, Zhen; Chakraborty, Arindam; Giri, Sumanprava; Freier, Susan M.; Wu, Xiaolin et al. (2013): Long noncoding RNA MALAT1 controls cell cycle progression by regulating the expression of oncogenic transcription factor B-MYB. In *PLoS genetics* 9 (3), e1003368. DOI: 10.1371/journal.pgen.1003368.

Twyffels, Laure; Gueydan, Cyril; Kruys, Véronique (2011): Shuttling SR proteins: more than splicing factors. In *The FEBS journal* 278 (18), pp. 3246–3255. DOI: 10.1111/j.1742-4658.2011.08274.x.

Uniacke, James; Chet E. Holterman; Gabriel Lachance; Aleksandra Franovic; Mathieu D. Jacob; Marc R. Fabian et al. (2012): An oxygen-regulated switch in the protein synthesis machinery. In *Nature*.

van Rossum, Daniëlle; Verheijen, Bert M.; Pasterkamp, R. Jeroen (2016): Circular RNAs: Novel Regulators of Neuronal Development. In *Frontiers in molecular neuroscience* 9, p. 74. DOI: 10.3389/fnmol.2016.00074.

Vaupel, Peter; Harrison, Louis (2004): Tumor hypoxia: causative factors, compensatory mechanisms, and cellular response. In *The oncologist* 9 Suppl 5, pp. 4–9. DOI: 10.1634/theoncologist.9-90005-4.

Vaupel, Peter; Oliver Thews; Michael Hoeckel (2001): Treatment Resistance of Solid Tumors. In *Medical science monitor : international medical oncology* 18, pp. 243–259.

Vigneron, Suzanne; Sundermann, Lena; Labbé, Jean-Claude; Pintard, Lionel; Radulescu, Ovidiu; Castro, Anna; Lorca, Thierry (2018): Cyclin A-cdk1-Dependent Phosphorylation of Bora Is the Triggering Factor Promoting Mitotic Entry. In *Developmental cell* 45 (5), 637-650.e7. DOI: 10.1016/j.devcel.2018.05.005.

Vordermark, Dirk; Brown, J. Martin (2003): Endogenous markers of tumor hypoxia predictors of clinical radiation resistance? In *Strahlentherapie und Onkologie : Organ der Deutschen Rontgengesellschaft … [et al]* 179 (12), pp. 801–811. DOI: 10.1007/s00066-003-1150-9.

Wahl, Markus C.; Will, Cindy L.; Lührmann, Reinhard (2009): The spliceosome: design principles of a dynamic RNP machine. In *Cell* 136 (4), pp. 701–718. DOI: 10.1016/j.cell.2009.02.009.

Wan, Ledong; Yu, Wenying; Shen, Enhui; Sun, Wenjie; Liu, Yuan; Kong, Jianlu et al. (2017): SRSF6-regulated alternative splicing that promotes tumour progression offers a therapy target for colorectal cancer. In *Gut*. DOI: 10.1136/gutjnl-2017-314983.

Wang, Eric T.; Sandberg, Rickard; Luo, Shujun; Khrebtukova, Irina; Zhang, Lu; Mayr, Christine et al. (2008): Alternative isoform regulation in human tissue transcriptomes. In *Nature* 456 (7221), pp. 470–476. DOI: 10.1038/nature07509.

Wang, Ke; Wang, Lantian; Wang, Jianshu; Chen, Suli; Shi, Min; Cheng, Hong (2018): Intronless mRNAs transit through nuclear speckles to gain export competence. In *The Journal of cell biology* 217 (11), pp. 3912–3929. DOI: 10.1083/jcb.201801184.

Wang, Qiuyun; Lu, Guoping; Chen, Zhenyue (2019a): MALAT1 promoted cell proliferation and migration via MALAT1/miR-155/MEF2A pathway in hypoxia of cardiac stem cells. In *Journal of cellular biochemistry* 120 (4), pp. 6384–6394. DOI: 10.1002/jcb.27925.

Wang, Tao; Wang, Xiaoxu; Du, Qianyu; Wu, Nan; Liu, Xincheng; Chen, Yuqing; Wang, Xiaojing (2019b): The circRNA circP4HB promotes NSCLC aggressiveness and metastasis by sponging miR-133a-5p. In *Biochemical and biophysical research communications*. DOI: 10.1016/j.bbrc.2019.04.108.

Wang, Yan; Liu, Jing; Huang, B. O.; Xu, Yan-Mei; Li, Jing; Huang, Lin-Feng et al. (2015): Mechanism of alternative splicing and its regulation. In *Biomedical reports* 3 (2), pp. 152–158. DOI: 10.3892/br.2014.407.

Wegener, Marius; Müller-McNicoll, Michaela (2018): Nuclear retention of mRNAs - quality control, gene regulation and human disease. In *Seminars in cell & developmental biology* 79, pp. 131–142. DOI: 10.1016/j.semcdb.2017.11.001.

Wegener, Marius; Müller-McNicoll M. (2019): View from an mRNP - the roles of SR proteins in the assembly, maturation and turnover of mRNPs. The Biology of mRNA: Structure and Function.

Wenger, Roland H.; Kurtcuoglu, Vartan; Scholz, Carsten C.; Marti, Hugo H.; Hoogewijs, David (2015): Frequently asked questions in hypoxia research. In *Hypoxia (Auckland, N.Z.)* 3, pp. 35–43. DOI: 10.2147/HP.S92198.

Werfel, Stanislas; Nothjunge, Stephan; Schwarzmayr, Thomas; Strom, Tim-Matthias; Meitinger, Thomas; Engelhardt, Stefan (2016): Characterization of circular RNAs in human, mouse and rat hearts. In *Journal of molecular and cellular cardiology* 98, pp. 103–107. DOI: 10.1016/j.yjmcc.2016.07.007.

Will, Cindy L.; Lührmann, Reinhard (2011): Spliceosome structure and function. In *Cold Spring Harbor perspectives in biology* 3 (7). DOI: 10.1101/cshperspect.a003707.

Wilusz, Jeremy E. (2018): A 360° view of circular RNAs: From biogenesis to functions. In *Wiley interdisciplinary reviews. RNA*, e1478. DOI: 10.1002/wrna.1478.

Wu, You; Zhang, Ying; Zhang, Yu; Wang, Jia-Jia (2017): CircRNA hsa_circ_0005105 upregulates NAMPT expression and promotes chondrocyte extracellular matrix degradation by sponging miR-26a. In *Cell biology international* 41 (12), pp. 1283–1289. DOI: 10.1002/cbin.10761.

Xin, Liu; Fan, Wu; Du Tingting; Zuoming, Sun; Qiang, Zhang (2018): 4-phenylbutyric acid attenuates endoplasmic reticulum stress-mediated apoptosis and protects the hepatocytes from intermittent hypoxia-induced injury. In *Sleep & breathing = Schlaf & Atmung*. DOI: 10.1007/s11325-018-1739-y.

Yamazaki, Takashi; Liu, Lizhi; Lazarev, Denis; Al-Zain, Amr; Fomin, Vitalay; Yeung, Percy Luk et al. (2018): TCF3 alternative splicing controlled by hnRNP H/F regulates E-cadherin expression and hESC pluripotency. In *Genes & development* 32 (17-18), pp. 1161–1174. DOI: 10.1101/gad.316984.118.

Yang, Lei-Qing; Chen, Min; Zhang, Jun-Long; Ren, Da-Long; Hu, Bing (2018): Hypoxia Delays Oligodendrocyte Progenitor Cell Migration and Myelin Formation by Suppressing Bmp2b Signaling in Larval Zebrafish. In *Frontiers in cellular neuroscience* 12, p. 348. DOI: 10.3389/fncel.2018.00348.

Yao, Yuan; Shang, Jin; Song, Weilin; Deng, Qiyue; Liu, Huan; Zhou, Yue (2016): Global profiling of the gene expression and alternative splicing events during hypoxia-regulated chondrogenic differentiation in human cartilage endplate-derived stem cells. In *Genomics* 107 (5), pp. 170–177. DOI: 10.1016/j.ygeno.2016.03.003.

Yin, Wei; Rogge, Mark (2019): Targeting RNA: A Transformative Therapeutic Strategy. In *Clinical and translational science* 12 (2), pp. 98–112. DOI: 10.1111/cts.12624.

Yu, Guangchuang; Wang, Li-Gen; Han, Yanyan; He, Qing-Yu (2012): clusterProfiler: an R package for comparing biological themes among gene clusters. In *Omics : a journal of integrative biology* 16 (5), pp. 284–287. DOI: 10.1089/omi.2011.0118.

Zeller, Karen I.; Jegga, Anil G.; Aronow, Bruce J.; O'Donnell, Kathryn A.; Dang, Chi V. (2003): An integrated database of genes responsive to the Myc oncogenic transcription factor: identification of direct genomic targets. In *Genome biology* 4 (10), R69. DOI: 10.1186/gb-2003-4-10-r69.

Zhang, Hao; Wang, Guangchao; Ding, Chen; Liu, Peng; Wang, Renkai; Ding, Wenbin et al. (2017): Increased circular RNA UBAP2 acts as a sponge of miR-143 to promote osteosarcoma progression. In *Oncotarget* 8 (37), pp. 61687–61697. DOI: 10.18632/oncotarget.18671.

Zhang, Jing; Zhang, Qing (2018): VHL and Hypoxia Signaling: Beyond HIF in Cancer. In *Biomedicines* 6 (1). DOI: 10.3390/biomedicines6010035.

Zhang, Maolei; Huang, Nunu; Yang, Xuesong; Luo, Jingyan; Yan, Sheng; Xiao, Feizhe et al. (2018a): A novel protein encoded by the circular form of the SHPRH gene suppresses glioma tumorigenesis. In *Oncogene* 37 (13), pp. 1805–1814. DOI: 10.1038/s41388-017-0019-9.

Zhang, Xiao-Ou; Wang, Hai-Bin; Zhang, Yang; Lu, Xuhua; Chen, Ling-Ling; Yang, Li (2014): Complementary sequence-mediated exon circularization. In *Cell* 159 (1), pp. 134–147. DOI: 10.1016/j.cell.2014.09.001.

Zhang, Zhen; Yao, Li; Yang, Jinhua; Wang, Zhenkang; Du, Gang (2018b): PI3K/Akt and HIF-1 signaling pathway in hypoxia-ischemia (Review). In *Molecular medicine reports* 18 (4), pp. 3547–3554. DOI: 10.3892/mmr.2018.9375.

Zhao, W.; Manley, J. L. (1996): Complex alternative RNA processing generates an unexpected diversity of poly(A) polymerase isoforms. In *Molecular and Cellular Biology* 16 (5), pp. 2378–2386.

Zhao, Zheng; Wang, Kuanyu; Wu, Fan; Wang, Wen; Zhang, Kenan; Hu, Huimin et al. (2018): circRNA disease: a manually curated database of experimentally supported circRNA-disease associations. In *Cell death & disease* 9 (5), p. 475. DOI: 10.1038/s41419-018-0503-3.

Zheng, Ge; Yu, Hongtao (2018): Cyclin A Turns on Bora to Light the Path to Mitosis. In *Developmental cell* 45 (5), pp. 542–543. DOI: 10.1016/j.devcel.2018.05.017.

Zhong, Xiang-Yang; Ding, Jian-Hua; Adams, Joseph A.; Ghosh, Gourisankar; Fu, Xiang-Dong (2009): Regulation of SR protein phosphorylation and alternative splicing by modulating kinetic interactions of SRPK1 with molecular chaperones. In *Genes & development* 23 (4), pp. 482–495. DOI: 10.1101/gad.1752109.

Zhong, Zhenyu; Huang, Mengge; Lv, Mengxin; He, Yunfeng; Duan, Changzhu; Zhang, Luyu; Chen, Junxia (2017): Circular RNA MYLK as a competing endogenous RNA promotes bladder cancer progression through modulating VEGFA/VEGFR2 signaling pathway. In *Cancer letters* 403, pp. 305–317. DOI: 10.1016/j.canlet.2017.06.027.

Zhou, Zhihong; Fu, Xiang-Dong (2013): Regulation of splicing by SR proteins and SR protein-specific kinases. In *Chromosoma* 122 (3), pp. 191–207. DOI: 10.1007/s00412-013-0407-z.

Zhu, Feng; Zykova, Tatyana A.; Peng, Cong; Zhang, Jishuai; Cho, Yong-Yeon; Zheng, Duo et al. (2011): Phosphorylation of H2AX at Ser139 and a new phosphorylation site Ser16 by RSK2 decreases H2AX ubiquitination and inhibits cell transformation. In *Cancer research* 71 (2), pp. 393–403. DOI: 10.1158/0008-5472.CAN-10-2012.

Zimmerman, Mary A.; Biggers, Christan D.; Li, P. Andy (2018): Rapamycin treatment increases hippocampal cell viability in an mTOR-independent manner during exposure to hypoxia mimetic, cobalt chloride. In *BMC neuroscience* 19 (1), p. 82. DOI: 10.1186/s12868-018-0482-4.

8. Supplementary Figures

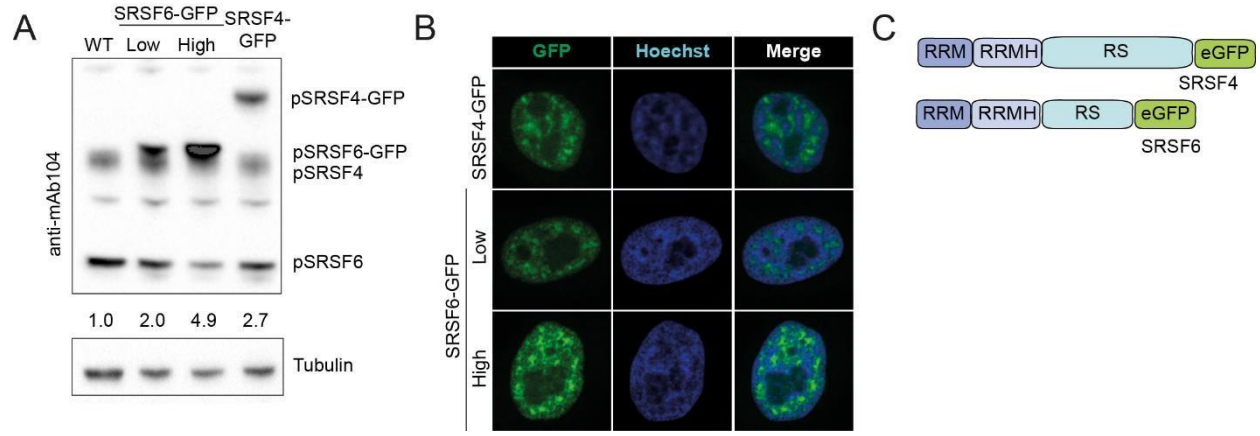

D

```
hSRSF6      MPRVYIGRLSYNVREKDIQRFFSGYGRLLEVDLKNGYGFVEFEDSRDADDAVYELNGKEL    60
hSRSF4      MPRVYIGRLSYQARERDVERFFKGYGKILEVDLKNGYGFVEFDDLRDADDAVYELNGKDL    60
***********:.**:*::***.***::**************:* *************:*
hSRSF6      CGERVIVEHARGPRRDRDGYSYGSRSGGGGYSSRRTSGRDKYGPPVRTEYRLIVENLSSR    120
hSRSF4      CGERVIVEHARGPRRDG---SYGSGRSGYGY---RRSGRDKYGPPTRTEYRLIVENLSSR    114
***************    ****  .* **   * *********.**************
hSRSF6      CSWQDLKDFMRQAGEVTYADAHKERTNEGVIEFRSYSDMKRALDKLDGTEINGRNIRLIE    180
hSRSF4      CSWQDLKDYMRQAGEVTYADAHKGRKNEGVIEFVSYSDMKRALEKLDGTEVNGRKIRLVE    174
********:************** *.******* *********:******:***:***:*
hSRSF6      DKPRTSHRRSYSGSRSRSRSRRRSRSRSRRSSRSRSRSISK----------SRSRSRSRS    230
hSRSF4      DKPGSRRRRSYSRSRSHSRSRSRSRHSRKSRSRSGSSKSSHSKSRSRSRSGSRSRSKSRS    234
*** : :***** ***:**** ***   :  *** * . *:          *****:***
hSRSF6      KGRSRSRSKGRKSRSKSKSKPKSDRGSHSH--SRSRSKDEYEKSRS-RSRSRSPKENGKG    287
hSRSF4      RSQSRSRSKKEKSRSPSKE--KSRSRSHSAGKSRSKSKDQAEEKIQNNDNVGKPKSRSPS    292
:.:****** .**** **.  **   ***   ***:***: *:. . ...  .**... .
hSRSF6      D--IKSKSRSRSQSRSNSPL-PVPPSKARSVSPPPKRATSRSRSRSRSKSRSRSRSSSRD    344
hSRSF4      RHKSKSKSRSRSQERRVEEEKRGSVSRGRSQEKSLRQSRSRSRSKGGSRSRSRSRSKSKD    352
*********.*  .       *:.** .   ::: *****:. *:*******.*:*
hSRSF6      ------------------------------------------------------------    344
                                                                hSRSF4      412
            KRKGRKRSREESRSRSRSRSKSERSRKRGSKRDSKAGSSKKKKKEDTDRSQSRSPSRSVS
hSRSF6      ------------------------------------------------------------    344
hSRSF4      KEREHAKSESSQREGRGESENAGTNQETRSRSRSNSKSKPNLPSESRSRSKSASKTRSRS    472


hSRSF6      ----------------------    344
hSRSF4      KSRSRSASRSPSRSRSRSHSRS    494
```

Figure S1. Validation of SRSF6 and SRSF4 cell lines. A) Western Blot with anti-mab104. The total amount of SRSF6 protein (exogenous + endogenous) in the SRSF6 (Low and High) relative to the WT SRSF6 is indicated below the lanes. Same calculation was performed for the SRSF4 cell line, indicated below the SRSF4–GFP lane. Values were normalized by tubulin loading control. **B)** Panel with fluorescence images of SRSF4 and SRSF6 cell lines. **C)** Representative scheme of SRSF4-GFP and SRSF6-GFP tagged proteins expressed in the stable cell lines. **D)** Alignment of SRSF6 and SRSF4 human protein sequences.

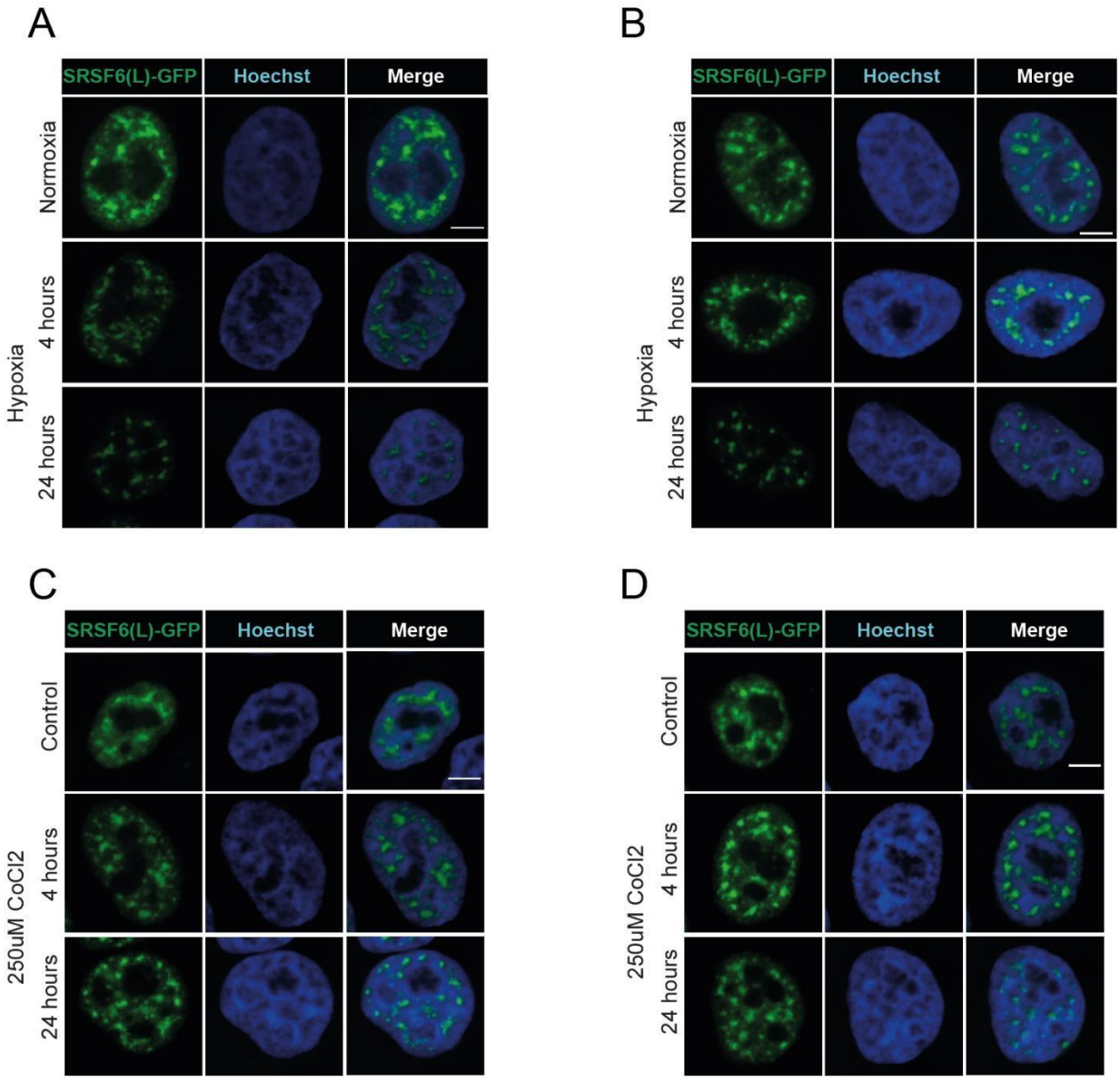

Figure S2. SRSF6 protein level decrease in hypoxia. A-B) Additional representative fluorescence microscopy images of SRSF6(L)-GFP cells line in normoxia, 4h and 24h hypoxia, showing the GFP signal (green), nuclear staining with Hoechst (blue) and the merge of both channels. **C-D)** Additional **r**epresentative fluorescence microscopy images of SRSF6(L)-GFP cells treated with 250µM $CoCl_2$ for 0h (control), 4h and 24h showing the GFP signal (green), nuclear staining Hoechst (blue) and the merge of both channels. Scale bar: 5µm.

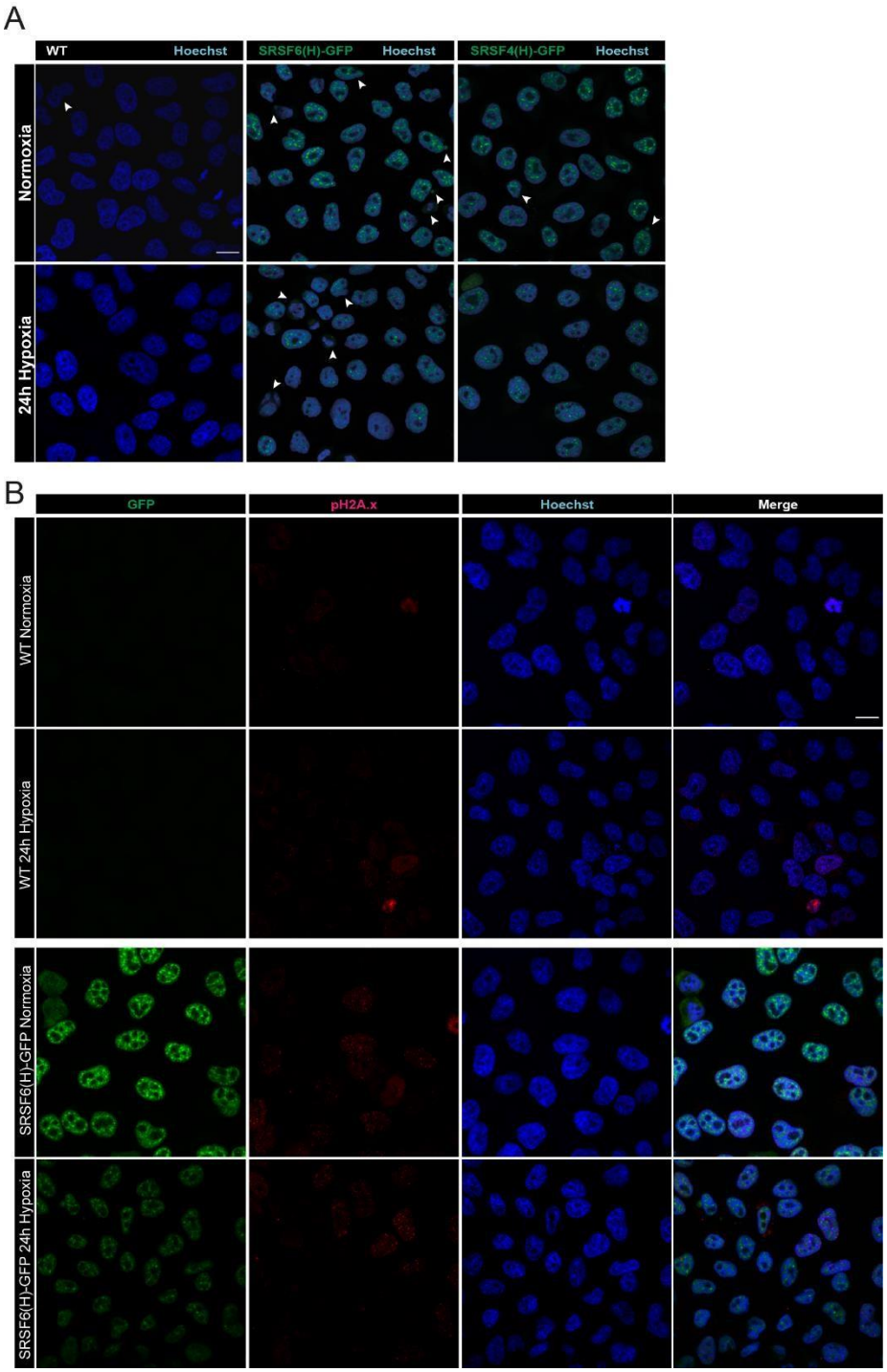

Figure S3. SRSF6 over expression leads to micronuclei formation and DNA damage. A) Fluorescence images of WT, SRSF4(H)-GFP and SRSF6(H)-GFP cell lines in normoxia and 24h hypoxia highlighting micronuclei formation **B)** IF images of WT and SRSF6(H)-GFP cells in normoxia and 24h hypoxia stained with anti-phospho Ser139 histone H2Ax (γH2A.x) antibody (red). GFP signal is shown in green, Hoechst nuclear staining in blue. Scale bar: 15µm.

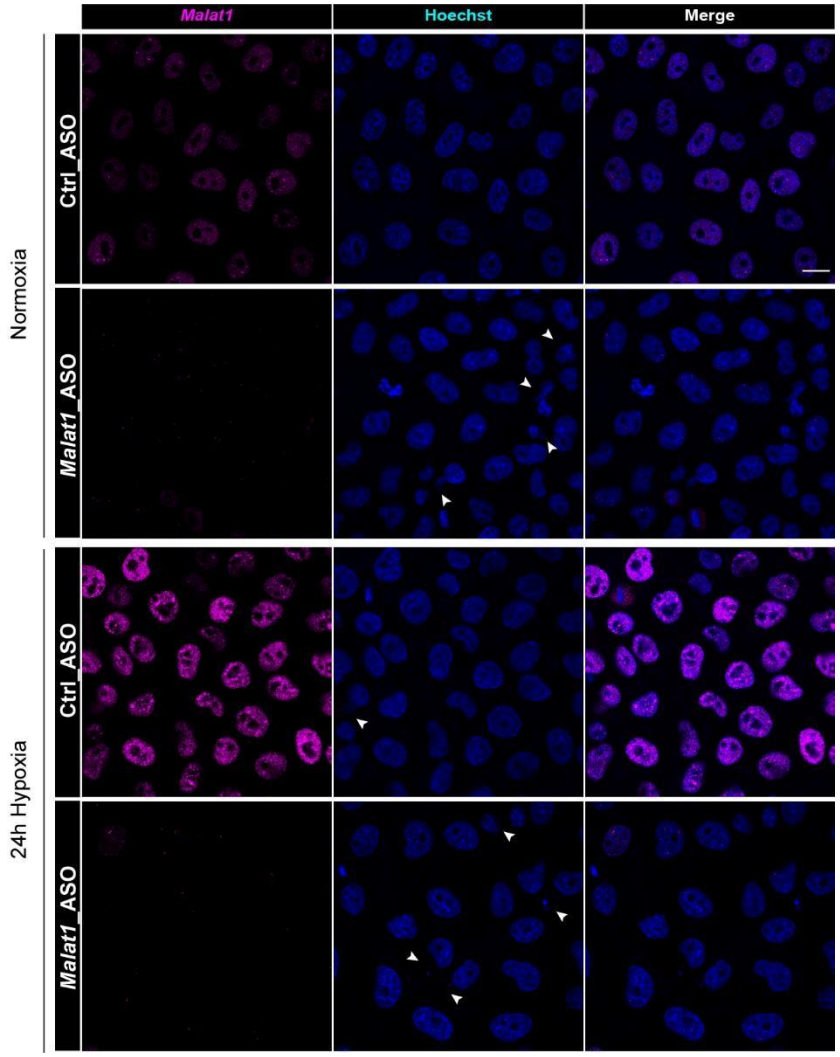

Figure S4.Micronuclei formation in *MALAT1* KD cells. Fluorescence in situ hybridization (FISH) images of *MALAT1* control and KD WT cells in normoxia and 24h hypoxia showing micronuclei (white arrows). Scale bar:15µm.

Acknowledgments

I would like to thank my main supervisor, JunProf. Michaela Müller-McNicoll, Ph.D. for giving me the opportunity to work on this project and in her group. Michi, you were an amazing supervisor and I thank you so much for all you did for me in these 4 years. For always going out of your way to help us, for all the talks, sharing ideas, for always being open and supportive, for always being there available for every kind of crisis… Your love and passion for science is very inspiring and I think I developed a lot under your supervision. Thank you!

Thank you also to Prof. Dr. Stefanie Dimmeler for giving me the opportunity to make this PhD and all the support during these years.

Thank you, Dr. Kathi Zarnack for your support, all the great meetings and discussions. Your nice input was always of great value to share new light over the project and experiments. Thank you for taking the time to be my second Gutachter.

Warm thanks to Antonella, from Kathi lab, for all the help with the bioinformatics part of this work. You are a great person and scientist, and was amazing to work together with you!

I want to thank all the members from the lab, because a fun and supportive working place is extremely important. Frank, Marius, Beni, Oli, Michal, who have been there this whole time with me… Frank thank you for your advices and borrowing your precious solutions! Thank you for the experiments and all the help. Special thank you for my student Michal, which has been with me since his Bachelor and helped me a lot. To my doctorand colleagues, thank you for sharing nice laughs, frustrations and stress, the good and the bad in these last years. Special thanks to Marius, for always being there for me, talks, experiments, scientific discussions and for your friendship. Thanks for the people who passed by and left their mark, in special Diana and Flavio, for helping me with the experiments. Thank you Sandra, you are an amazing friend and I am happy to have you in my life.

Thank you for all the members of my committee, for taking the time to read and judge this work.

Last but not least, I want to thank my family, in special my mom Rosa, brother Guilherme and grandpa Almiro. Minha familia, meu irmao, meu avo sao minha base e minha estrutura. Mae, voce sempre foi e sempre será a pessoa mais importante em minha vida. Sem voces eu nao seria quem sou hoje e nao estaria aqui. Voce e meu exemplo de vida, minha linda, guerreira. Eu te amo de todo meu coracao, obrigada por ser essa pessoa maravilhosa e por sempre me apoiar e estar ao meu lado mesmo de longe.

Erklärung und Versicherung

Erklärung

Ich erkläre hiermit, dass ich mich bisher keiner Doktorprüfung im mathematischnaturwissenschaftlichem Bereich unterzogen habe.

Frankfurt am Main, den _____

Camila Freitas Stahl

Versicherung

Ich versichere hiermit, dass die vorgelegte Doktorarbeit über „The roles of SRSF6 in the alternative splicing response to hypoxia“ selbständig und ohne unzulässige fremde Hilfe verfasst, andere als die in ihr angegebene Literatur nicht benutzt und, dass ich alle ganz oder annährend übernommenen Textstellen, sowie verwendete Grafiken, Tabellen und Auswertungsprogramme gekennzeichnet habe.

Außerdem versichere ich, dass die vorgelegte elektronische mit der schriftlichen Version der Doktorarbeit übereinstimmt.

Frankfurt am Main, den _____

Camila Freitas Stahl

Curriculum Vitae

CAMILA FREITAS STAHL

Master of Biology (Genetics)

Address: Heinrich-Becker-St, 17, Frankfurt am Main, Germany
Date of birth: 20/09/1989
Email: ofm.camila@gmail.com
Phone: +491737816817

Education

2015-Present PhD in Molecular Biology
Institute of Cellular Biology and Neuroscience, Goethe University of Frankfurt, Germany
Main Supervisor: Michaela Müller-McNicoll

Dissertation: The roles of SRSF6 in the alternative splicing response to hypoxia

2012-2014 Master in Biology (Genetics)
University of Sao Paulo, Brazil
Supervisor: Andrea Laurato Sertie
Scholarship from FAPESP (Fundação de Amparo à Pesquisa do Estado de São Paulo)

Thesis: Study of the protein Collybistin in Protein Syntheses Control

2007-2010 Bachelor in Biological Sciences Brazilian
Federal University of Mato Grosso do Sul, Campo Grade, MS, Brazil
Supervisor: Fabiane Siqueira and Yvelise Maria Possiede
Scholarship from: Council of Technological and Scientific Development

Project: Analyze of the association of SNPs on *CAPN1* and *CAST* genes with tenderness in bovines.

Work Experience

2011-2012 Research Assistant
Albert Einstein Jewish Hospital, Sao Paulo, Brazil Germany
Supervisor: Andrea Laurato Sertie
Scholarship from Albert Einstein Jewish Hospital

Project: mTOR Signaling pathway in patients with Autistic Spectrum Disorders

Publications

Altered mTORC1 signaling in multipotent stem cells from nearly 25% of patients with nonsyndromic autism spectrum disorders.
A M Suzuki, K Griesi-Oliveira, C de Oliveira Freitas Machado, E Vadasz, E C Zachi, M R PassosBueno, A L Sertie
Molecular Psychiatry 20, 551-552 (13th January 2015) doi:10.1038/mp.2014.175

Collybistin binds and inhibits mTORC1 signaling: a potential novel mechanism contributing to intellectual disability and autism.
Camila Oliveira Freitas Machado, Karina Griesi-Oliveira, Carla Rosenberg, Fernando Kok, Stephanie Martins, Maria Rita Passos-Bueno, Andrea Laurato Sertie
European Journal of Human Genetics (22nd April 2015) doi:10.1038/ejhg.2015.69

In review:
A combined computational pipeline to detect circRNAs in human cancer cells under hypoxic stress
Antonella Di Liddo,Camila Freitas Stahl, Sandra Fischer, Stefanie Ebersberger, Stefanie Dimmeler, Julia E. Weigand, Michaela Müller-McNicoll, Kathi Zarnack
Journal of Molecular Cell Biology

Selected work presented in scientific meetings

Regulation of circRNA formation by SR proteins and MALAT1 in hypoxia stress
Camila Freitas Stahl, Antonella Di Liddo, Nicolas Jaé, Kathi Zarnack, Stefanie Dimmeler, Michaela Müller-McNicoll
In: Splicing 2018, Caparica, Portugal, June 2018

Regulation of circRNA formation by SR proteins and MALAT1 in hypoxia stress
Camila Freitas Stahl, Antonella Di Liddo, Nicolas Jae, Kathi Zarnack, Stefanie Dimmeler, Michaela Müller-McNicoll
In: 22nd Annual Meeting of the RNA Society, Prag, May 2017

Altered cell growth and PI3K-mTOR signaling in idiopathic autism spectrum disorders
Suzuki, AM; Machado, COF; Oliveira KG; Vadasz E, Passos-Bueno, MR; Sertié, AL
In: American Society of Human Genetics Meeting; São Francisco, 06-10 November de 2012

Induced pluripotent stem cell (iPSC)-derived neurons from one patient with a deletion of the collybistin gene as a model system to study underlying cellular neuropathology Machado, COF; Oliveira, KG; Rosemberg, C; Kok, F; Passos-Bueno, MR; Sertié, AL In: XXI World Congress of Psychiatry Genetics, Boston, October 17- 21, 2013

Analysis of CAPN530/Psyl polymorphism in cattle from different genetic groups.
MACHADO, C. O. F., Flores, R.S, Siqueira, F, Torres, R.A.A, Medeiros,S.R, Feijó, G.L.D In: 56° Brazilian Genetics Congress, 2010, Guarujá.